Water Balance Dynamics of Cyprus

Actual State and Impacts of Climate Change

Dissertation

zur Erlangung des naturwissenschaftlichen Doktorgrades
der Bayerischen Julius-Maximilians-Universität Würzburg

vorgelegt von
Dipl.-Geol. Dipl.-Geogr.
Armin Dünkeloh
aus
Stuttgart

Würzburg 2011

Eingereicht am: 29.09.2011

1. Gutachter: Prof. Dr. Peter Udluft

2. Gutachter: Prof. Dr. Roland Baumhauer

der Dissertation

1. Prüfer: Prof. Dr. Peter Udluft

2. Prüfer: Prof. Dr. Heiko Paeth

der mündlichen Prüfung

Tag der mündlichen Prüfung: 07.11.2012

Abstract

A completely revised and enhanced version of the water balance model MODBIL of the regional water balance dynamics of Cyprus was developed for this study. The model is based on a physical, process-oriented, spatially distributed concept and is applied for the calculation of all important water balance components of the island for the time period of 1961-2004. The calibrated results are statistically analysed and visualised for the whole island area, and evaluated with respect to the renewability of natural water resources. Climate variability and changes of the past decades are analysed with regard to their influence on water balances. A further part of the study focusses on the simulation of impacts of potential climate change. The water balances are simulated under changing climatic conditions on the base of theoretical precipitation, temperature and relative humidity changes and the revealed impacts on the water balances and renewable resources are discussed. Furthermore, a first principal water balance scenario is developed for the assessment of the regional hydrological changes expected for Cyprus by the end of the 21st century. The scenarios are based on recently calculated climate change assessments for this part of the Mediterranean, under an assumed further increase of greenhouse gasses in the atmosphere.

Keywords: water balance model, groundwater recharge, renewable water resources, climate variability, climate change impacts, scenario modelling, sustainable water management, Cyprus

Kurzfassung

Eine vollständig überarbeitete und erweiterte Version des Wasserhaushaltsmodells MODBIL ist für die Untersuchung des Wasserhaushalts auf Zypern entwickelt worden. Auf der Basis dieses physikalischen, prozessorientierten und flächendifferenzierten Modells werden alle wesentlichen Wasserhaushaltskomponenten für die gesamte Insel im Zeitraum 1961-2004 berechnet, die Ergebnisse statistisch und visuell ausgewertet sowie hinsichtlich der Erneuerbarkeit der natürlichen Wasserressourcen bewertet. Weiterhin erfolgt die Untersuchung von Klimavariabilität und Trends der letzten Jahrzehnte und deren Einfluss auf die Wasserbilanzen. Im zweiten Teil dieser Studie werden Auswirkungen potentieller Klimaänderungen anhand simulierter Wasserbilanzen unter veränderten Niederschlags-, Temperatur-, und Luftfeuchtebedingungen ermittelt und hinsichtlich deren Einfluss auf die erneuerbaren Wasserressourcen beurteilt. Abschließend folgt eine erste prinzipielle Simulation der hydrologischen Veränderungen, die für Zypern bis zum Ende des 21. Jahrhunderts zu erwarten sind. Diese Simulation basiert auf aktuellen Klimawandelabschätzungen für diese Teilregion des Mittelmeerraumes unter Verwendung eines Szenarios fortschreitender Zunahme von Treibhausgasen in der Atmosphäre.

Schlagwörter: Wasserhaushaltsmodell, Grundwasserneubildung, erneuerbare Wasserressourcen, Klimavariabilität, Klimawandel, Szenarien, tragfähiges Wassermanagement, Zypern

Acknowledgements

My deepest gratitude goes to my supervisor, Prof. Dr. Peter Udluft, whose expertise, understanding and encouragement added considerably to my graduate experience. I have been extremely fortunate to have had a supervisor who has cared so much about my work.

I also owe much gratitude to Prof. Dr. Baumhauer for his invaluable time and interdisciplinary expertise as a co-reviewer.

I am deeply grateful to my friend and colleague Dr. Joachim Mederer for many years of joint research activities and companionship during the whole GRC project, for the numerous scientific discussions and proof reading. I am also grateful to my colleagues, especially to Bernhard Schäfers, Dr. Holger Mainardy, Dr. Heike Wanke, Jens Widmann, Sven-Oliver Lorenz, Andreas Eizenhammer, Dr. Eleni Zagana, Dr. Ronald Pasig, Dr. Ernst E. Walter, Dr. Mohammad Al Farajat, Dr. Nedal Al Ouran, Parviz Mansourie and Adolf Heilos of the Hydrogeological section at the University of Würzburg, for manifold assistance, scientific discussion, advice, good atmosphere and enjoyable coffee breaks.

I would like to acknowledge the scientific personnel of the Geological Survey Department of Cyprus, for supporting my work and supplying data. Special thanks go to the head of the Hydrogeological Section Dr. Maria Charalambous, Dr. Costas Constantinou and Christos Christophi for the distinguished cooperation and splendid team spirit, to Mr George Petridis, former Director of the GSD, for his concern and special interest in the GRC-Project.

I would like to express many thanks to further cooperation partners of the GRC-project, especially Dr. Christoph Külls for sharing his experience and for lots of technical advice, Prof. Dr. J. Jacobeit, Dr. Elke Hertig and the staff of the Climate

Research Group Augsburg/Würzburg for cooperation, data supply and discussion with regards to the climate change assessments; Dr. Stelios Pashiardis of the Meteorological Service (Cyprus) for the valuable help with regard to the update of meteorological data in the ENVIS database, Prof. Dr. Jörg Schaller and staff for the great work of compiling and organising the GIS database and the Water Development Department for providing detailed project results of the WDD-FAO project, dealing with the re-evaluation of surface water resources.

Grateful acknowledgements for proofreading of the final version of the English manuscript goes to Alexander Hietel, Michael Malzer and Luke Sheppard.

Furthermore, I would like to mention Thomas Kopp and Kai Nagel from Qumon GmbH who financially supported the completion of the PhD thesis over the last years, by devolving the management of several geophysical terrain investigations unto my responsibility.

Very special thanks go to Biggi Rothe, Josef Kopp, Jan Bergmann, Till Sachau, Michael Latsch, Felix Kühner, Klaus Wolf and all my close friends for help, patience, constant presence and moral support. I greatly value your friendship and I deeply appreciate your belief in me.

My final acknowledgement is to my family who has been a constant source of love, concern, encouragement and strength through all these years.

Contents

List of Abbreviations

α	albedo [-]
α_c	incidence angle (angle between the perpendicular to the cell surface and the actual direction of direct solar radiation) [deg]
α_p	angle between terrain surface and flux-vector [rad]
β_c	terrain slope (slope of the cell surface) [deg] [rad]
δ	solar declination (at equator) [deg] [rad]
ϵ	ratio molecular weight of water vapour/dry air; 0.622 [-]
γ	psychrometric constant [kPa K^{-1}]
λ	latent heat of vaporisation [MJ kg^{-1}]
μ_c	unit conversion to get ET_0 in mm d^{-1}; 86400 [s d^{-1}]
ω_c	exposition of the cell surface [deg]
ω_s	solar time angle at midpoint of hourly (or shorter) time period [deg]
ω_{ss}	sunset hour angle [rad]
ϕ	angle between horizon and the actual direction of direct solar radiation [deg]
ψ_f	suction at wetting front [mm]
ρ_a	mean air density at constant pressure [kg m^{-3}]
$\rho_\infty(\lambda_{NIR})$	limiting value of the *WDVI* at very high *LAI* values (Eq. 3.75)
σ	Stefan-Bolzmann constant; $4.903 \cdot 10^{-9}$ [MJ K^{-4} m^{-2} d^{-1}]

θ_i	actual or initial soil moisture content [m^3 m^{-3}]
θ_m	minimum soil moisture content where macropore flow is assumed [m^3 m^{-3}]
θ_r	residual soil moisture content when hydraulic conductivity $k = 0$ [m^3 m^{-3}]
θ_s	soil moisture content at saturation [m^3 m^{-3}]
θ_t	threshold soil moisture content where plant water stresses start [m^3 m^{-3}]
θ_{FC}	soil moisture content at field capacity [m^3 m^{-3}]
θ_{WP}	soil moisture content at wilting point [m^3 m^{-3}]
$\theta_{k,l}$	angle between data points Z_k and Z_l (vertex is the point of interpolation) [deg]
φ	latitude [deg] [rad]
ζ	zenith angle (angle between the zenith and the actual direction of direct solar radiation) [deg]
$a.m.s.l.$	above mean sea level
a_s	fraction of extraterrestrial radiation reaching earth's surface as diffuse solar radiation [-]
A_{LAI}	effective vegetation coverage [-]
AH	absolute humidity [g m^{-3}]
AP	atmospheric pressure [kPa]
b_s	fraction of extraterrestrial radiation reaching earth's surface as direct solar radiation [-]
BY	bypass flow [mm]
c^*_{pc}	adjustment factor for precipitation [-]
c_f	complex combination of extinction and scattering coefficients (Eq. 3.75)
c_m	melting rate coefficient [mm K^{-1} d^{-1}]

c_p	specific heat of the air at constant pressure; $1.013 \cdot 10^{-3}$ [MJ kg^{-1} K^{-1}]
c_s	influence of soil reflectance (soil background)
c_{pg}	precipitation gradient [mm m^{-1} a^{-1}]
c_{te}	adjustment factor for temperature [K] (Eq. 3.28)
c_{tg}	air temperature gradient [K m−1] (Eq. 3.26)
CR	capillary rise [mm]
d_k	distance between interpolation point and data point k [m]
d_l	distance between interpolation point and data point l [m]
d_r	inverse of the square of the relative distance earth-sun (correction for eccentricity of earth's orbit around the sun)
DP	deep percolation [mm]
E_0	evaporation from a water surface (original Penman equation) [mm]
e_a	actual vapour pressure [kPa]
e_s	saturation vapour pressure [kPa]
e_{14}	actual vapour pressure at 14:30 h for Haude equation [hPa]
$e_{s,adj}$	saturation vapour pressure under adjusted temperature conditions [kPa]
$e_{s,T_{max}}$	saturation vapour pressure at daily maximum air temperature [kPa]
$e_{s,T_{min}}$	saturation vapour pressure at daily minimum air temperature [kPa]
e_{s14}	saturation vapour pressure at 14:30 for Haude equation [hPa]
EA	evaporative demand (original Penman equation) [mm]
EP	evaporation from wet surfaces [mm]
ET	evapotranspiration [mm]
ET_0	reference potential evapotranspiration [mm]
ET_{act}	actual evapotranspiration [mm]
ET_{Haude}	potential evapotranspiration rate according to Haude [mm]

ET_{pot}	potential evapotranspiration [mm]
$ET_{pot}(wet)$	adjusted potential evapotranspiration under wet surface conditions [mm]
ET_{sec}	secondary evapotranspiration [mm]
f_i	Green and Ampt infiltration rate at time step i [mm h^{-1}]
f_{Haude}	plant specific Haude factor for a month [mm hPa^{-1}]
G_{sc}	solar constant; 0.082 [MJ m^{-2} min^{-1}]
G_{sh}	soil heat flux density [MJ m^{-2} d^{-1}]
h	elevation (a.m.s.l) [m]
h_0	elevation of interpolation point [m]
h_k	elevation of data point k [m]
h_{cell}	elevation (a.m.s.l.) of the cell [m]
h_{plant}	effective vegetation height (thickness of plant canopy) [m]
h_{ref}	reference elevation (a.m.s.l.) of the interpolated value given by the weighted mean of the elevation of the meteorological stations used for interpolation [m]
h_{SI}	layer thickness of water body on a surface [mm]
h_{w0}	height at which wind speed becomes essentially zero in the plant canopy (zero-plane displacement height) [m]
h_{ws}	height of wind speed measurement [m]
h_{zo}	aerodynamic roughness length [m]
I	net irrigation infiltrating to the soil [mm]
INF	infiltration to the soil [mm]
Inf_i	cumulative infiltration at time step i [mm]
INF_s	infiltration under saturated soil surface conditions [mm]
INF_u	infiltration under unsaturated soil surface conditions [mm]
INF_{seal}	infiltration to the soil on partially sealed surface [mm]

INT	interflow [mm]
IZ	water in the interception storage [mm]
IZ_{max}	interception storage capacity [mm]
IZR	recharge of the interception storage [mm]
j	number of days of the year [-]
j_J	number of a day in the Julian calendar [-]
K	amount of data points in the neighbourhood of interpolation point (within the search radius) [-]
k_c	single crop coefficient [-]
k_e	surface evaporation coefficient [-]
k_m	retention constant that represents storage lag-time
k_p	regional calibration coefficient for adjustment of the relation between interflow and deep percolation [-]
k_s	hydraulic conductivity of the soil under saturated conditions [m s^{-1}] [mm h^{-1}]
k_{cb}	basal crop coefficient [-]
k_{R_s}	adjustment coefficient [$°C^{-0.5}$] (Eq. 3.16)
$k_{s,adj}$	adjusted hydraulic conductivity of the soil under saturated conditions considering macropore effects [m s^{-1}] [mm s^{-1}]
$k_{sub,s}$	hydraulic conductivity of the bedrock under saturated conditions [mm s^{-1}] [m s^{-1}]
LAI	Leaf Area Index [-]
LAI_{max}	maximum LAI within the annual cycle [-]
M	snow melting [mm]
M_r	ratio molecular weight of water vapour/dry air; 0.622 [-]
M_w	molecular weight of water vapour; 18.016 [kg]

MP_f	factor of macroporosity depending on root depth and season [-]
MP_t	threshold for the beginning of macropore flow [mm]
MP_{by}	effective macroporosity for bypass flow [Vol.%]
n	number of valid time steps [-]
$NDVI$	Normalised Difference Vegetation Index [-]
$NDVI_{max}$	maximum *NDVI* within the annual cycle [-]
$NDVI_{min}$	minimum *NDVI* within the annual cycle [-]
NIR	Near Infrared
OF	overland flow [mm]
OF_{seal}	overland flow on partially seal surface [mm]
P	precipitation [mm]
p_r	portion of total extractable water that plants can extract from the root zone without water stress [-]
p_w	weighting power of the inverse distance [-]
P_0	mean annual precipitation at mean sea level [mm a^{-1}]
P_{adj}	adjusted precipitation for a cell [mm]
P_{ipol}	interpolated precipitation (not adjusted) [mm]
PC	percolation [mm]
PE	effective precipitation [mm]
PI	rainfall intensity [mm h^{-1}]
PTF	pedotransfer function
Q_0	initial discharge [mm]
Q_t	discharge from the storage at time period t [mm]
Q_{base}	base flow [mm]
Q_{dir}	direct runoff [mm]

Q_{tot}	total runoff/discharge [mm]
R^*	universal gas constant; 8314.3 [J K^{-1} $kmol^{-1}$]
R^*_{spec}	specific gas constant; 0.287 [kJ kg^{-1} K^{-1}]
R_a	extraterrestrial radiation [MJ m^{-2} d^{-1}]
r_a	aerodynamic resistance [s m^{-1}]
R_n	net radiation [MJ m^{-2} d^{-1}]
R_s	solar or short wave radiation [MJ m^{-2} d^{-1}]
r_s	bulk surface resistance or canopy resistance [s m^{-1}]
R_{na}	net absorbed radiation (original Penman equation) [mm]
R_{nl}	outgoing net longwave radiation [MJ m^{-2} d^{-1}]
R_{ns}	incoming net short wave radiation [MJ m^{-2} d^{-1}]
r_{NIR}	total measured Near Infrared reflectance
r_{Red}	total measured Red reflectance
$R_{s,adj}$	adjusted solar or short wave radiation [MJ m^{-2} d^{-1}]
$r_{s,NIR}$	NIR reflectance of the bare soil
$r_{s,Red}$	Red reflectance of the bare soil
r_{sc}	minimum stomatal resistance [s m^{-1}]
r_{sd}	surface resistance for the bright day [s m^{-1}]
r_{sn}	surface resistance for the night [s m^{-1}]
r_{ss}	surface resistance of bare soil [s m^{-1}]
RH	relative humidity [%]
RH_{14}	relative humidity at 14:30 h [%]
RH_{adj}	adjusted relative humidity for a cell considering exposition [%]
RH_{max}	maximum daily relative humidity [%]
RH_{mean}	mean daily relative humidity [%]

RH_{min}	minimum daily relative humidity [%]
S	maximum possible sunshine duration [h]
s	actual sunshine duration [h]
s_s	slope of the saturation vapour pressure curve [kPa K^{-1}]
S_t	storage content at time period t [mm]
SS	snow storage [mm]
T	air temperature [°C]
t	elapsed time [d]
T_K	air temperature in Kelvin [°K]
t_l	length of time interval [s]
t_r	rainfall duration after macropore flow started [s]
t_s	solar time at the midpoint of the period [h]
t_u	time until saturation of the soil surface [h]
T_{14}	temperature at 14:30 h [°C]
$T_{adj,K}$	adjusted air temperature for a cell in Kelvin [°K]
T_{adj}	adjusted air temperature considering elevation and exposition [°C]
T_{bm}	base temperature for snow melting [°C]
T_{bs}	base temperature for snow fall [°C]
T_{cell}	interpolated and elevation corrected air temperature for a cell [°C]
T_{dif}	air temperature difference for adjustment [K]
T_{ipol}	interpolated air temperature (not adjusted) [°C]
$T_{max,K}$	maximum daily air temperature in Kelvin [K]
T_{max}	maximum daily air temperature [°C]
T_{mean}	minimum daily air temperature [°C]
$T_{min,K}$	minimum daily air temperature in Kelvin [K]

T_{min}	minimum daily air temperature [°C]
U	wind speed at 2 m height [m s^{-1}]
vc	fraction of vegetation coverage [-]
vs	areal fraction of sealed surface [-]
w_h	weighting factor (depending on elevation difference) [-]
w_k	weighting factor (depending on lateral distance) [-]
ws_c	water stress coefficient [-]
WC	plant-extractable soil water content in the root zone [mm]
WC_{FC}	plant-extractable soil water content in the root zone at field capacity [mm]
wf	weighting factor for the adjustment of solar radiation [-]
$WDVI$	Weighted Difference Vegetation Index
x_0, y_0	coordinates of interpolation point in a Cartesian surface [m,m]
x_k, y_k	coordinates of data point k in a Cartesian surface [m,m]
Z_0	data value Z (e.g. precipitation, temperature, ...) at interpolation point
Z_k	data value Z (e.g. precipitation, temperature, ...) at data point k
Z_r	effective rooting depth [m]

List of Figures

List of Tables

Chapter 1

Introduction

1.1 Background

The scarce natural water resources of the Mediterranean are controlled by a semi-arid climate with a high variability on an interseasonal, interannual and interdecadal scale. Episodically recurring droughts and a continuously increasing water demand, lead towards overexploitation of natural water resources in Cyprus and other Mediterranean regions. Water management has become important for securing the water supply and for the preservation of the regional hydrogeological system, in order to protect the existing and renewable water resources for the future. Today, sustainable water management requires advanced monitoring and hydrological techniques for the continuous observation and understanding of the regional hydrogeological resources and processes.

The extensive depletion of natural water resources in many areas began with a substantial water consumption on the island caused by the introduction of diesel pumps at the beginning of the 20th century. On Cyprus especially, the first class aquifers in the lowlands were depleted by groundwater abstractions. Major salt water intrusions appeared and large parts of the aquifers in the coastal regions became unusable for further water supply. It was not until the 1950s that beginning with a hydrological description of rocks (Burdon 1952, 1953), the first systematic hydrological studies were undertaken. In the 1960s, extensive research began in the frame of a United Nations project during which all formations were hydrologically studied

and a first hydrological map was subsequently published (UNDP 1970, Tullström 1970). Furthermore, a first monitoring network for rivers and wells was constructed. Detailed investigations of important aquifers followed in the 1970s with a focus on quantity issues and the first applications of mathematical and numerical models. Not before the end of the 1970s, when successful drillings were first performed in the fractured igneous rocks, the focus of water supply shifted towards the Troodos Mountains (Afrodisis et al. 1986, Afrodisis and Fischbach 1988). In the 1980s, the focus lay on quality issues and isotope studies before shifting towards discussions about water scarcity, artificial recharge, waste water re-use, desalinisation and new water resources in the 1990s.

Over the last decade Cyprus' upcoming integration into the European Union led to initiatives and projects to re-evaluate groundwater resources and modernise administration, data management and techniques. The current study was revealed as part of the GRC-Project (Udluft et al. 2004b), focusing on the introduction of physical water balance models for the evaluation of the renewability of the natural water resources of Cyprus. It furthermore simulates first potential climate change impacts on Cyprus' water balances and water resources, taking into account the predicted unfavourable changes in the Mediterranean for the 21st century which have been part of a widespread international discussion about climate change and the regional impact in recent years.

1.2 Objectives and Project Framework

The present study is performed within the frame of the GRC-Project (Re-evaluation of the Groundwater Resources of Cyprus) and focuses on the part of physical water balance models. The main objectives of the study are:

- Development of a completely revised and enhanced version of the physical water balance model MODBIL
- Model adaptation to the regional conditions (inventory of climatological, hydrological and hydrogeological factors for different landscape units and formations)
- Calculation and visualisation of actual water balances for a detailed under-

standing of the dynamics and sensitivity of the regional hydrological system

- Quantification of the renewability of the regional water resources (groundwater recharge and direct runoff)
- Analysis of climate variability and climate changes of the past decades and study of its influences on water balances
- Simulation of potential climate change impacts on regional water balances
- A first assessment of future water balances for the end of the 21st century
- Establishing MODBIL as modern water management tool for regional authorities (Geological Survey of Cyprus) for the calculation of actual water balances and the evaluation of the 'sustainability' of the regional water management.

The GRC-project is a scientific and technical cooperation project, financed by the Ministry of Agriculture, Natural Resources and Environment of the Republic of Cyprus (Contract No. GSD/7), performed by the Department of Hydrogeology and Environment (Prof. Dr. P. Udluft, University of Würzburg, Germany), Hydroisotop (Dr. C. Külls, Germany), Planning Bureau Prof. Dr. J. Schaller (Germany) and supervised by the Geological Survey Department (Cyprus). Further cooperating partners were the Water Development Department (Cyprus), the Department of Agriculture (Cyprus), Meteorological Service (Cyprus) and the Climate Research Group (Prof. Dr. J. Jacobeit) at the Institute of Geography of the University of Augsburg/Würzburg (Germany). The ENVIS and the GIS database used in the GRC-project were the main sources for mapping, meteorological and hydrogeological data used in this study.

Chapter 2

Study Area

2.1 General Setting

The study area comprises the whole island of Cyprus which is the Mediterranean's third largest island, situated in the East: centred on latitude 35° N and longitude 33°15' E. The distance to the continent is 75 km to the North (Turkey), 105 km to the East (Syria) and 380 km to the South (Egypt). The maximum extension of the island is about 100 km from North to South and 225 km from Northeast to Southwest, covering an area of approx. 9250 km^2.

Cyprus, a former British colony, became an independent republic in 1960 and was subdivided into two parts after the Turkish invasion in 1974. Since this time the Republic of Cyprus and the Turkish Republic of Northern Cyprus, which is not recognised by the United Nations (UN), have been separated by the UN buffer zone. The total population of the island is about 800,000.

Physically, four major natural landscape units can be distinguished, (see Fig. 2.1) which show significant differences regarding topography, climate, geology, soils and land cover (vegetation). The most prominent unit is formed by the Troodos massif which covers a large area in the southern centre of the island and reaches 1951 m (a.m.s.l.) at Mount Olympos, its highest elevation. The Troodos is surrounded by a hilly landscape, which is most distinctive on its southwestern and southeastern slopes. This unit is known as the Troodos foothills zone and does usually not rise over 800 m (a.m.s.l.). A second range, which extends along the northern coastline

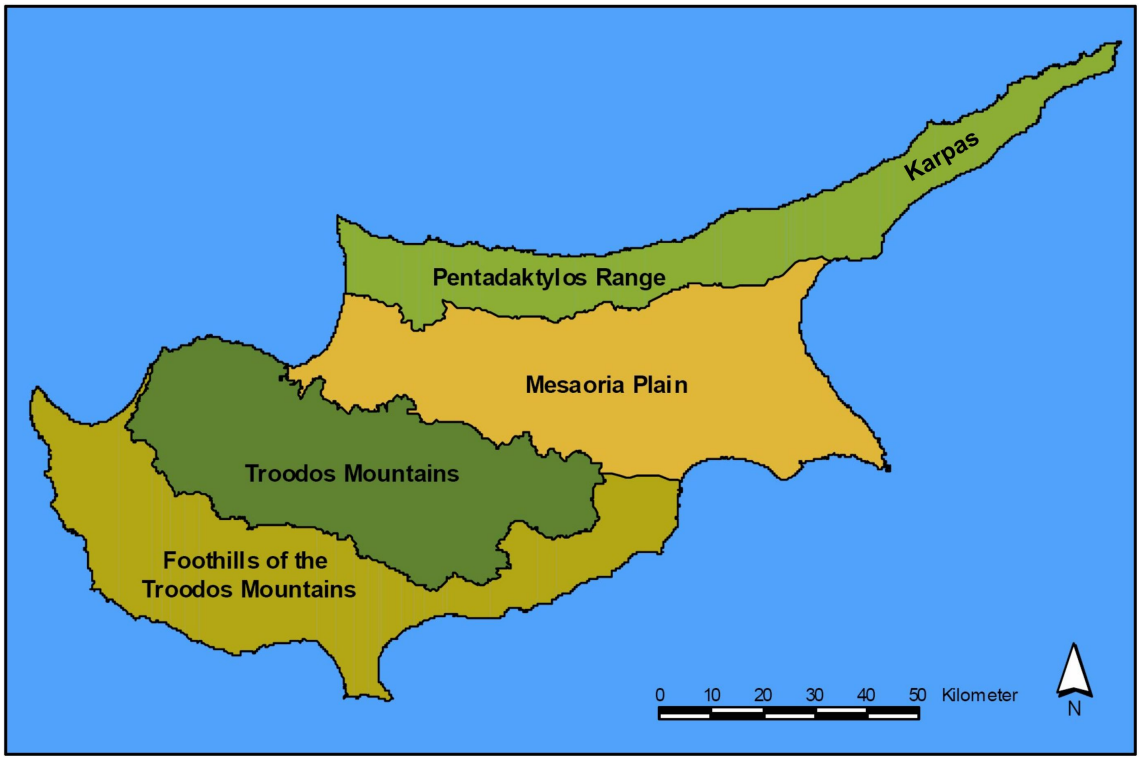

Figure 2.1: Natural landscape units of Cyprus.

is called Kyrenia or Pentadaktylos range. In large parts, the crest varies in altitude between 800 and 1024 m (a.m.s.l). At the eastern part of the Karpas peninsula the topography becomes smoother and it appears more like a hilly landscape. In-between the Troodos and the Kyrenia range, a large plain called Mesaoria opens. It extends from the West coast to the East coast and has no significant elevations above 300 m (a.m.s.l.).

2.2 Climate

A detailed description of the climate of Cyprus can be found in the publications of the Meteorological Service of Cyprus (1984, 1985a, 1985b, 1985c, 1987, 1989). An overview of the most important climate characteristics is given in this chapter. Further analyses of climatic parameters are also presented in the context of the calculated water balances (Chap. 5).

Cyprus is a semi-arid island with a typical Mediterranean climate. Hot, dry sum-

mers from mid-May to mid-September and cool, rainy winters from November to mid-March are separated by short autumn and spring seasons with rapid changes in weather conditions. The regional climate is a result of the typical alternating circulation regimes in the Mediterranean. In summer, the subtropical high leads to stable atmospheric conditions. In winter, rainfall is caused by unstable weather systems which are often connected to trough induced cyclogenesis and its frontal regimes. In the winter months, the comparatively high sea surface temperatures in relation to the lower air temperatures, enforce the unstable conditions of the atmosphere. In the summer months, the reverse situation stabilises the atmospheric conditions.

The complex topography of Cyprus provokes significant regional modifications of the climate, which mainly depend on elevation, exposition and coast distance. The most prominent influence is the terrain elevation, which shows clear correlation to temperature and precipitation. From regression analysis, a temperature gradient of about 0.5 °C/100 m was determined for Troodos and the surrounding area (see Fig. 2.2). The mean annual temperatures vary from 18 to 20 °C in the plains and coastal areas. Near the sea, the mean monthly temperatures never fall below 10 °C. In the mountains the mean annual temperatures used to range between 12 and 15 °C, and frosts, although rarely severe, are frequent in winter and spring. With increasing distance to the sea a more continental climate can be detected, consisting of hot summers and cool winters. Usually the highest absolute temperature is detected in the Mesaoria plain during the summer months. The long-term monthly means of July and August reach nearly 30 °C.

Precipitation amounts in the plains and coastal areas range between 250 to 400 mm/a and rise up to more than 1100 mm/a in the highest areas of the Troodos mountains. The regression analysis of precipitation data yield towards different results for the northeastern and southwestern slopes of the Troodos range (see Fig. 2.3). These expositional effects are a result of prevailing southwesterly or westerly winds in connection to circulation patterns favouring precipitation on Cyprus. The consequence is a difference of approx. 150 mm/a between the Paphos area (400 mm/a) and the southwestern Mesaoria plain (250 mm/a), which is located on a similar elevation level (Fig. 2.3). With increasing elevation, the effect disappears gradually. In the highest crests of the Troodos, snowfall can occur in the winter months due to the periodically low temperatures.

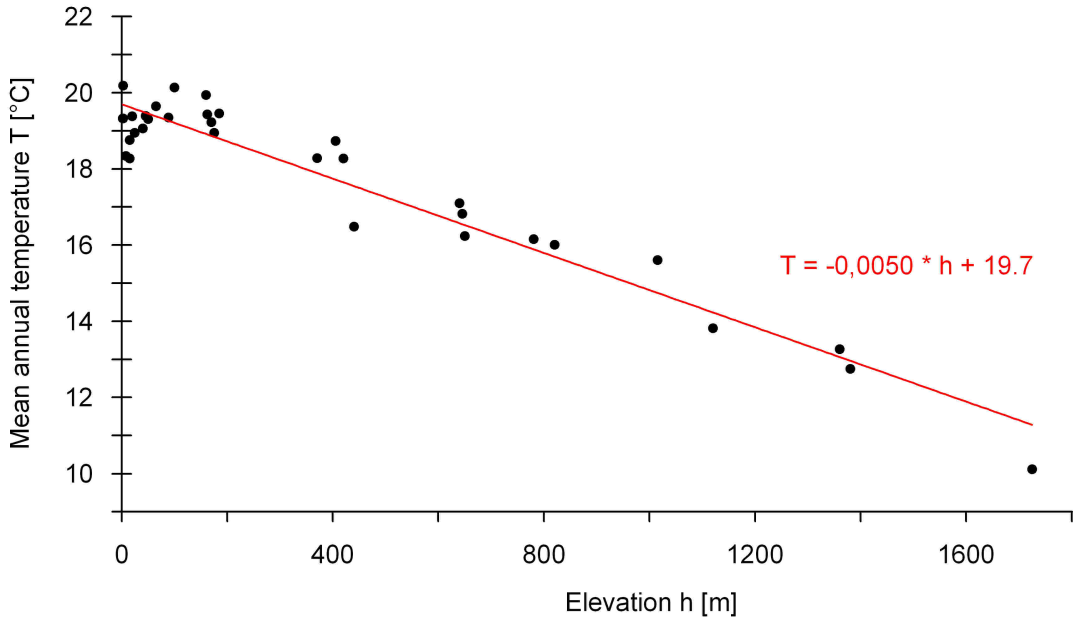

Figure 2.2: Regression of elevation and mean annual temperature (1986-1996) for stations situated in the Troodos range and surroundings.

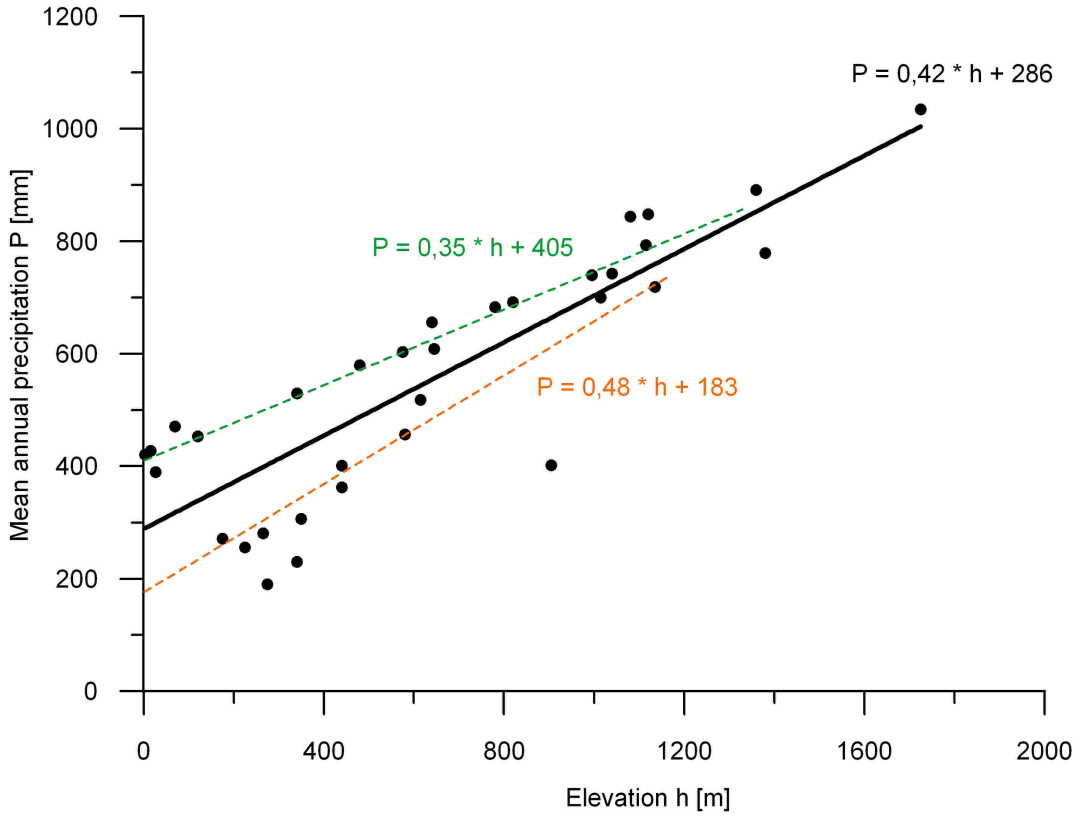

Figure 2.3: Regression of elevation and mean annual precipitation (1986-1996) for stations situated in the Troodos range and surroundings.

The relative humidity also shows dependencies to the distance and exposition from the coast and terrain elevation. The meteorological stations close to the sea are characterised by very stable conditions. The long-term monthly means usually remain between 50% and 60% throughout the whole year. The coastal stations on the west side show slightly higher relative humidity because of the more dominant westerly, landward winds. The inland stations in the central plains monitor a notable seasonal cycle with lower relative humidities in summer (less than 30%) and values similar to the coastal stations in the winter months. The mountainous areas show the same seasonal cylce but on a higher absolute level. The highest values occur in the winter months in the uppermost areas of the Troodos mountains with mean monthly relative humidities beween 70% and 80%.

Wind conditions on the island are complex. Coastal zones and exposed mountain areas are usually affected by stronger winds. The southwestern slopes of the Troodos show relatively calm conditions. With respect to the seasonal variability, the calmest months are typically those in the late summer season and the early autumn season, due to less atmospheric pressure and temperature difference. Compared to other areas of the Mediterranean, the relative sunshine duration is very high in Cyprus. The yearly mean values for the more elevated areas range at about 60% of the atronomically possible sunshine duration, and at about 75% for the coastal areas and central plains. In the summer months, the mean monthly relative sunshine duration reaches 80% to 90% in most parts of the island.

The circulation dynamics of this alternating climate environment includes a high variability of precipitation and temperature on monthly, interannual and interdecadal time scales. Furthermore, the region is a highly sensitive area for climate change impacts. The visualised yearly dataset of mean area rainfall for the whole 20th century (ENVIS Database of the Meteorological Office of Cyprus) shows a strong interannual variability, and a long-term precipitation decrease of more than 100 mm (Fig. 2.4). The non-parametric Mann-Kendall test qualifies this trend as highly significant.

Digital temperature data for the whole 20th century was not available for the analysis of the temperature variability. A study of Price et al. (1999) shows that there are also long-term changes with an unfavourable temperature trend in Cyprus (Fig. 2.5). The study is based on two stations where a temperature rise of more than 1

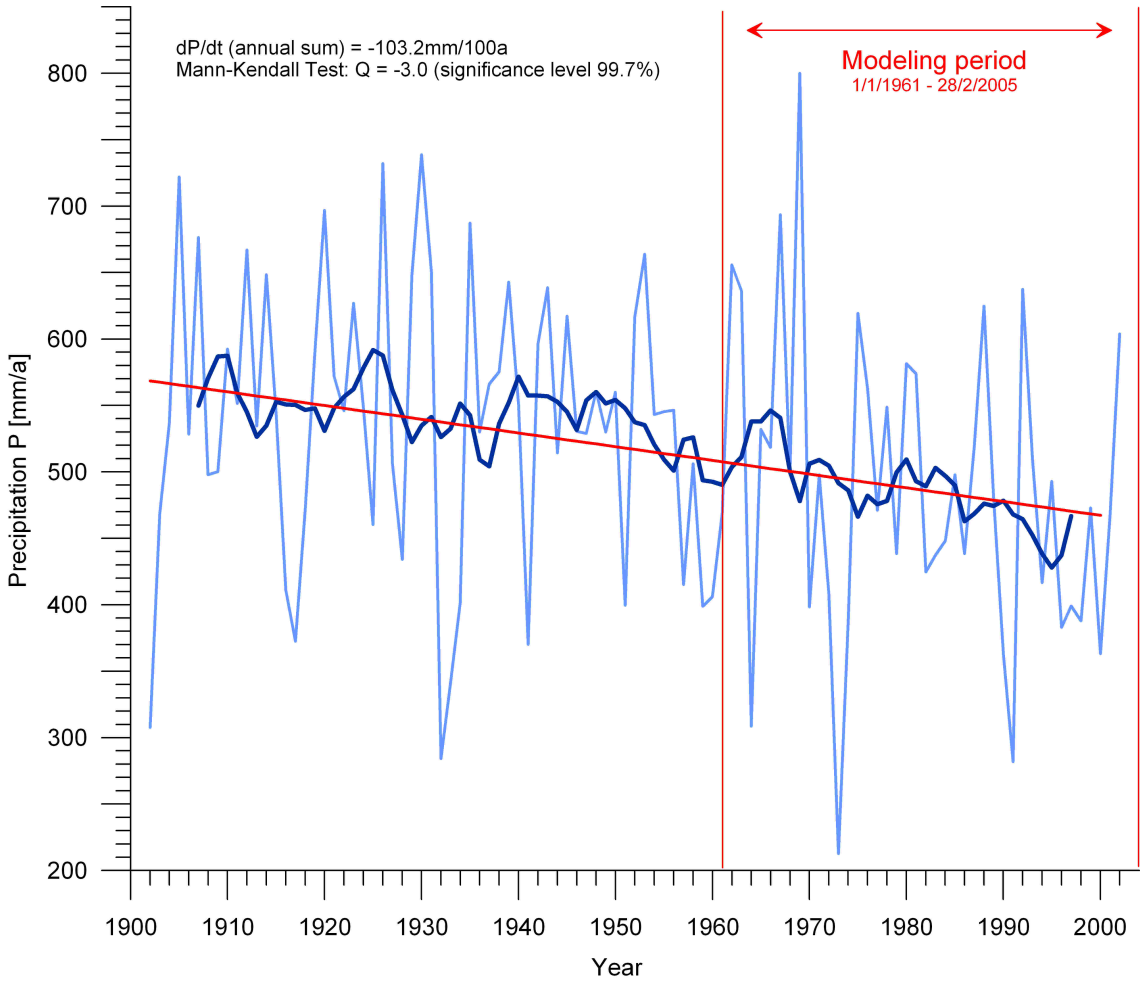

Figure 2.4: Annual variation and trend of the mean areal precipitation of Cyprus in the 20th century. The annual precipitation is represented by the light blue line, the decadal moving averages by the dark blue line, and the significant linear trend by the red line. The limits of the water balance modelling period are indicated by red lines. Data source: monthly datasets from ENVIS Database of the Meteorological Service of Cyprus (Ministry of Agriculture, Natural Resources and Environment).

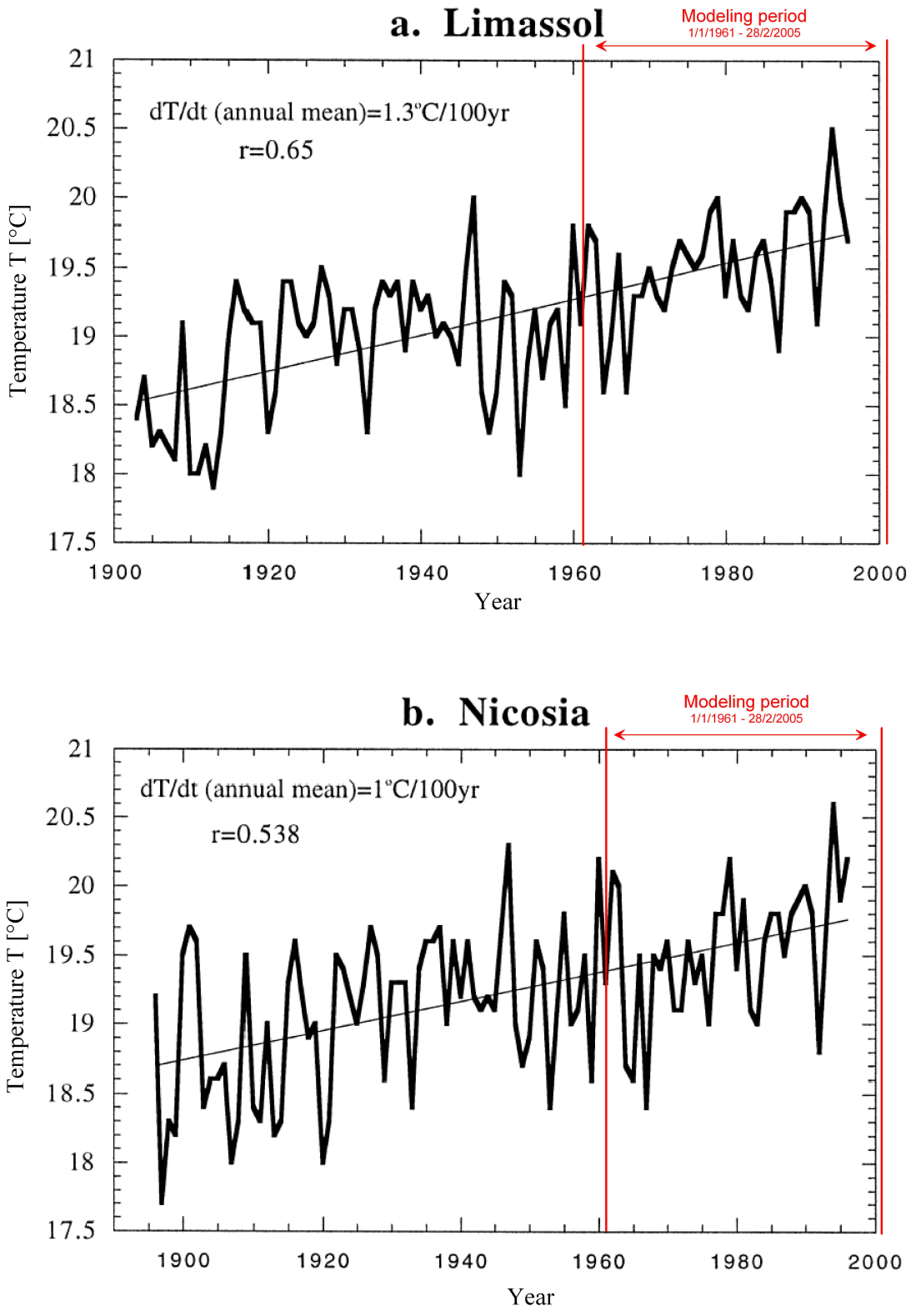

Figure 2.5: Annual temperature variation and trends for the 20th century of the stations Limassol and Nicosia according to Price et al. (1999).

K was detected during the 20th century.

Variability and trends of precipitation and temperature in the eastern Mediterranean are closely connected to atmospheric circulation and further discussed in Dünkeloh and Jacobeit (2003) and Dünkeloh et al. (2003). The unfavourable precipitation and temperature changes on Cyprus can be related to changing circulation patterns in the central and eastern Mediterranean. For instance, the change in the Mediterranean Meridional Circulation pattern (MMC) yields towards a weakening of troughs and consequently to less precipitation events in the central and eastern-central Mediterranean. Weakening of anticyclones over continental eastern Europe is connected to a decreasing amount of troughs moving to the eastern Mediterranean.

2.3 Land Cover (Vegetation)

A detailed description of typical vegetation and land cover types is given in Reger (2004). A general overview of the island is given below. The distribution and specific characteristics of the applied land cover classes are further investigated in the chapter of the remote sensing analysis of Cyprus (Chap. 4.3).

The intense use of the primary and secondary forests throughout thousands of years let most of the island be deforested. Since the 1940s, reforestation of pine forest started and was intensified in the 1980s. Today, large parts of the state forest areas in western and central Troodos are reforested. The most common tree used for reforestation is the calabrian pine (*Pinus brutia*). In some smaller protected domains, other trees, like the endemic Cyprus cedar (*Cedrus brevifolia*) and Aleppo pine (*Pinus halepensis*), can be found. In the highest areas around Mount Olympos the black pine (*Pinus nigra*) is common. High deciduous forests (*e.g. Platanus orientalis*) are rare and usually restricted to moist areas on valley floors, which benefit from shallow groundwater and the water of perennial or intermittent river streams.

The pine forest often appears in a very open form with transitions to the typical Mediterranean Maquis or Garrigue formation. Those scrublands consist of densely growing evergreen shrubs such as sage, juniper and myrtle, and become partly the aspect of a small deciduous forest with low trees. Endemic golden oak (*Quercus al-*

nifolia), strawberry tree (*Arbutus andrachne*), terebinth (*Pistacia terebinthus*), kermes oak (*Quercus coccifera*) and styrax (*Styrax officinalis*) are common in Cyprus. The Maquis formation covers wide areas, especially concerning eastern Troodos, the Kyrenia range and the foothills.

The very sparse vegetation on very poor and degraded soil consist of low scrublands, herbs, forbs and grass. This association of plants is known as Garrigue formation and is most common in the surrounding foothills of the Troodos and Kyrenia range, as well as in the dry and degraded coastal areas. Agriculture in the mountainous and hilly areas occurs only on small fields and terraces, which are mostly located in the peripherals of settlements. The areas with the most vineyards are situated in the southern foothills of the Troodos massif.

The land cover in the plains is mainly formed by agriculture and settlements. Large parts of the Mesaoria plain are cultivated with cereal fields and scattered trees (almond, olive, carob trees). In western Mesaoria, southeastern Mesaoria and the coastal plains, irrigation areas with citrus, bananas, vegetables and potatoes are typical. The coastal zone and parts of the Mesaoria plain are the most urbanised areas. Nearly all major cities and tourist areas are located in the coastal areas of the island.

2.4 Soil

Soil studies for specific areas of Cyprus were performed by Soteriades and Koudounas (1968), Grivas (1969), Koumis (1970) and Markides (1973). Calcareous soils were described by Lüken (1988). A systematic overview of soils is summarised by Boje-Klein (1982) who also discussed the FAO Soil Map of Cyprus (Soteriades and Grivas 1970) based on the FAO/UNESCO Soil Map of the World 1970 classification system. A new soil map was published by Markides (1999), which shows more connections to the geological underground than the former edition, and which is based on the new classification system (FAO 1998).

Cyprus belongs to the zone of Cambisols. These soils are widely distributed in the Mediterranean and are characteristic for those semi-arid climatic regions. Former nomenclatures referred to these as brown Mediterranean soils. Compared to cen-

tral European soils, they are retarded in weathering because the high temperature season is equivalent to the dry season and the wet season is accompanied by cool temperatures. Cambisols with moderate to deep soil profiles count as the most productive soils in southern Europe. However, in Cyprus, most Cambisols show only a 'little to medium' development stage. They have a cambic B-horizon and a not always distinctive ochric or umbric A-horizon.

On the island, the shallow Cambisols show mostly a transition to Regosols and Leptosols. The soils are kept in an initial development stage as a consequence of their young age and the disturbance of soil formation by erosion. They have no diagnostic horizons other than an ochric A-horizon and are stony and coarse grained. According to the actual FAO nomenclature, the Leptosols are related to shallow soils over hard rock or highly calcareous material, and the Regosols are related to shallow soils over unconsolidated materials. The Leptosols, Regosols and shallow Cambisols dominate most areas of Cyprus, like the Troodos mountains, the Troodos foothills, the Kyrenia range and great parts of the Mesaoria plain.

In some smaller areas, Luvisols are developed, which partly coincide with the so-called red Mediterranean soils. They are well-developed soils which main pedological characteristic is the formation of the argic subsurface horizon which has a distinctly higher clay content than the overlying horizon. This horizon is a result of eluviation and translocation processes of clayey material from the surface topsoil layer. In Cyprus this soil type occurs mainly in the area of Pleistocene fanglomerates. The Luvisols on Cyprus are typically accompanied by Calcisols that show a substantial accumulation of secondary carbonates (Petrocalcic horizon), which reduce effective soil depth.

Further soils appear in limited areas under special geological and topographical conditions. Fluvisols are soils on recent alluvial deposits showing stratification or other evidence of recent sedimentation processes. They are characterised by an irregular organic matter and the profile development is minimal as a consequence of young age and slow soil formation. Vertisols with a high clay content exist in the area of the Mamonia formation as a result of the high clay content of the weathered bedrock. Gypsisols are common in the gypsum rich formations (e.g Kalavassos formation). Solonchaks are strongly saline soils, which appear in pans nearby the coast.

2.5 Geology

First comprehensive descriptions and studies of the geology and mineral deposits of Cyprus were already published in the 19th century e.g. from Gaudry (1862), who described the 'Géologie de l'ile de Chypre' with the help of a geological map. Many publications followed, among them the extensive work of Unger and Kotschy (1865) and the geological maps and publications of Bellamy and Jukes-Browne (1905), Brown and McGinty (1946), Henson et al. (1949). In the 1950s and 1960s a more systematic geological investigation and mapping began and resulted in a series of memoirs, bulletins and detailed geological maps published by the Geological Survey of Cyprus. At that time, a first very detailed geological map of Cyprus was edited by Bear (1963). Later, after the identification of the Troodos as an ophiolite (Moores and Vine 1971), the island moved into the focus of intense international research activities. Important findings of the following years were discussed and summarised on the International Ophiolite Symposium 1979 (Panayiotou 1980). Many outstanding issues and problems were investigated in subsequent years by the Cyprus Crustal Project, based on deep drillings through the ophiolite, performed by the International Crustal Research Drilling Group (ICRDG) and the Cyprus Geological Survey Department. A summary and discussion of important results can be found in the proceedings of the 'Troodos 87' Symposium (Malpas et al. 1990) and the proceedings of the Third International Conference on the Geology of the eastern Mediterranean (Panayides et al. 2000). The subsequent research activities on the Southern Troodos Transform Fault Zone (STTFZ) are presented in Gass et al. (1994). Recent and extensive overviews of the Geology of Cyprus can be found e.g. in Panayiotou (1987), Gass et al. (1994), Robertson (1990, 2000), Robertson and Xenophontos (1997), Robertson et al. (2003) and Dünkeloh (2005a). The latest geological map of Cyprus was published by Constantinou (1995) on a scale of 1:250,000.

The geological evolution of Cyprus is closely related to the formation of the Troodos ophiolite within the complex geological environment of the Mediterranean bordered by the Anatolian, the African and the Arabian plate. In Upper Cretaceous (about 91.6 Ma) the development started with a short intercalated period of seafloor spreading in the closing Neo Tethys upon a subduction zone (see Gass et al. 1994, Lippard et al. 1986). After this short period, the closing of the Neo Tethys continued and the new developed oceanic crust became detached and ro-

tated anticlockwise towards older rocks on its southern and western part (Mamonia zone). Further ophiolites developed in a similar tectonic setting along the closing Neo Tethys, which can be found today as a sequence along Bosnia, Croatia, Greece, Turkey, Syria and Oman. The following period of less tectonic inactivity (75 to 10 Ma) is characterised by carbonate sedimentation and gradual shallowing of the sedimentary basin (Lefkara and Pakhna formation). Evaporites (Kalavasos formation) were deposited in the Upper Miocene as a result of several drying events in the Mediterranean basin by cut-offs from the Atlantic Ocean. Noticeable uplifts followed and the Kyrenia range was formed on the northern flank of the Troodos terrane at the end of Miocene (6 Ma). Allochthonous Permian and Cretaceous series were placed there, folded and uplifted over autochthonous flysch sediments. Later, the re-connection of the Mediterranean sea with the Atlantic Ocean in the Plio- and Pleistocene epoch led towards a further deposition of marls and calcarenites (Nicosia and Athalassa formation) on the Cypriot terranes. In the last tectonic episode (2 Ma), an abrupt uplift accompanied by extensive erosion formed the actual high mountain relief of the Troodos, the Kyrenia range, and led to the deposition of fanglomerates (erosion material) on the northern flanks of the Troodos. Great parts of the Troodos ophiolite became excavated, showing a stratigraphically complete, nearly undeformed fragment of a fully developed oceanic crust, consisting of plutonic, intrusive, volcanic rocks and chemical sediments. The less uplifted and eroded surroundings are covered by formations of the sedimentary cover (Lefkara, Pakhna, Kalavassos, Nicosia or Athalassa formation).

The geological evolution of Cyprus resulted in the formation of four major geological zones (see Fig. 2.6): the Troodos terrane, the Kyrenia terrane, the Mamonia terrane and the sedimentary cover (Circum Troodos Sedimentary Succession). The Troodos ophiolite forms the main structural feature in the centre of the island and also is comprised of some smaller units like the Anti-Troodos ophiolite, the Southern Troodos Transform Fault Zone and the Akamas ophiolite. Today, the original upward succession of the oceanic crust is arranged in an outward succession starting from the centrally exposed mantle sequence which forms a diapirically uplifted core with tectonised and pervasively serpentinised harzburgite. The following crustal sequence starts with plutonic rocks of peridotitic and gabbroic type, and continues with unlayered gabbros with little olivine content and plagiogranites at its top. The intrusive 'Sheeted Dyke Complex' is widely exposed in the Troodos area and consists

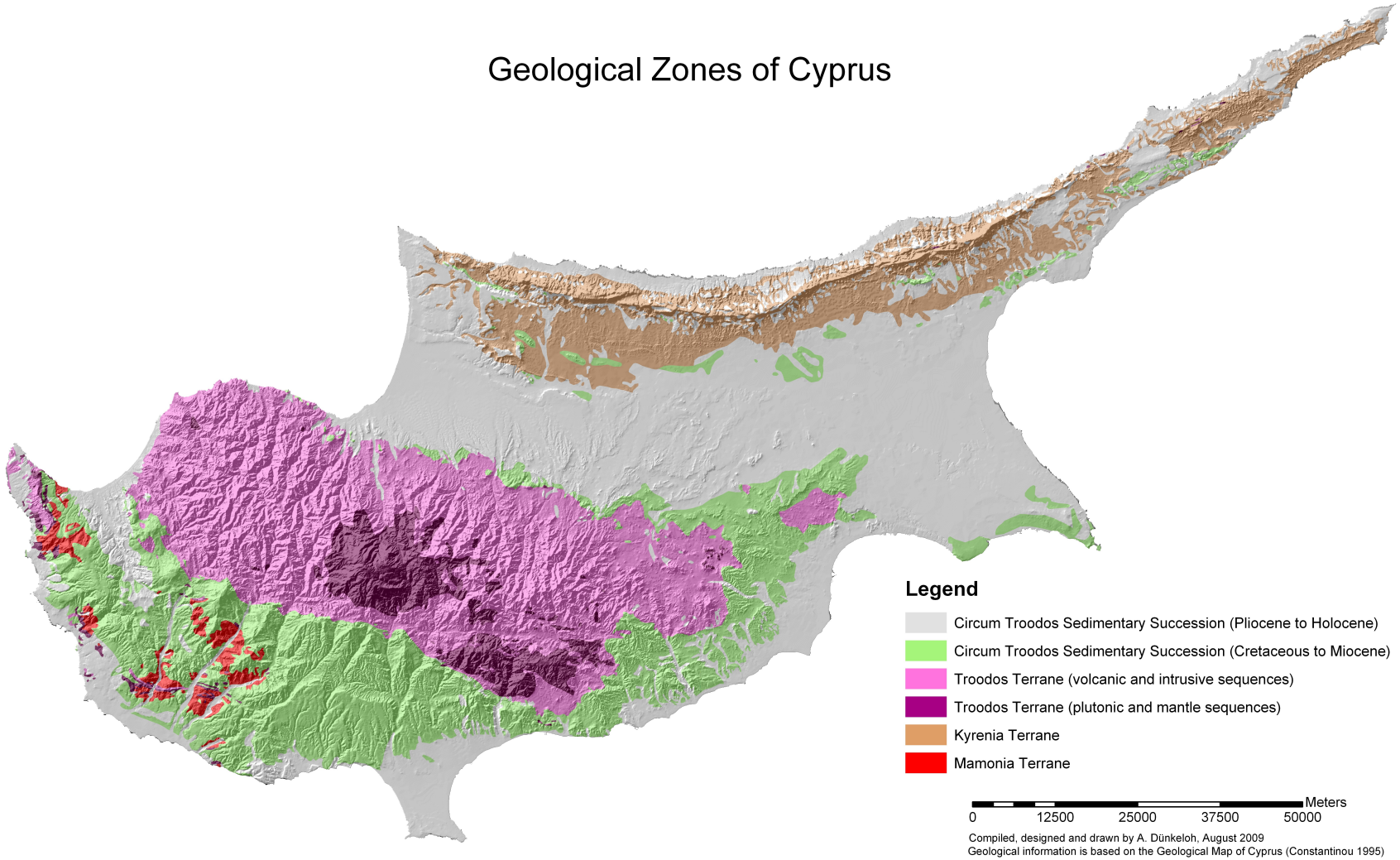

Figure 2.6: Geological zones of Cyprus.

of dykes of doleritic to basaltic composition. The top of the ophiolite sequences is formed by two series of pillow lavas and lava flows, mostly of basaltic composition as a result of submarine volcanic activity. The transitional zone, where the sheeted dykes alternate with pillow lavas is usually termed Basal Group in Cyprus. On top of the pillow lavas, ferromanganoan sediments can be found as a result of hydrothermal activity on the sea floor. The Arakapas fault zone in southern Troodos is interpreted as a preserved, fossil oceanic transform fault zone, separating Troodos from the Anti-Troodos plate (Gass et al. 1994).

The Mamonia terrane forms the basement of the southwestern part of the island and is mostly covered by autochthonous carbonate successions of Pakhna, Lefkara and other formations. Outcrops exist only in smaller areas of the Pafos region. The zone is characterised by a diverse and structurally complex assemblage of sandstones, shales/limestones and an associated volcanic suite of the Middle Triassic to Upper Cretaceous period.

The Kyrenia range on the northern coast of Cyprus consists of a complex assemblage of Permian to recent formations. Most prominent are the steeply dipping allochthonous Permian and Cretaceous limestones (Dhikomo, Sykhari and Hilarion formations), flanked by autochthonous marine sediments (flysch deposits) of the Middle Eocene to Middle Miocene epoch (Lapithos, Kalogrea-Ardana/Belapais and Kythrea formations; see Ducloz 1972, Robertson and Xenophontos 1997).

The autochthonous sedimentary cover consists of sediments and rocks of the Upper Cretaceous to Holocene epoch and is typically termed Circum Troodos sedimentary succession (see Fig. 2.6). The older series comprise gently folded marine sediments, where the carbonate successions of the Lefkara formation (pelagic marls and white chalks) and the Pakhna formation (yellowish marls and chalks) are most prominent in the southwestern and eastern foothill belt. The following upper Miocene evaporites (gypsum) of the Kalavassos formation can be found in different places on the island. The younger and less uplifted series of the sedimentary consists of sediments of the Pliocene to Holocene epoch with marls and calcarenites of the Nicosia and the Athalassa formation, fanglomerates, terraces and alluvium deposits. These series cover great parts of the Measoria plain and the coastal plains.

2.6 Hydrogeology and Hydrology

As mentioned in the introduction, the first systematic hydrogeological studies began in the 1950s and 1960s. An early hydrogeological description of rocks was published by Burdon (1952, 1953) and refers partly to the report of Raeburn (1945). Extensive studies followed in the 1960s in the frame of an international development programme financed by the United Nations. Geological formations were systematically evaluated from a hydrogeological point of view and a first hydrogeological map was developed (Tullström 1970). Results were published in a comprehensive volume of the UNDP (1970). Later studies concentrated on a detailed research of specific aquifers or regions like Hadjistavrinou (1972), Zomenis (1972), Hadjistavrinou and Afrodisis (1977), Hadjistavrinou and Constantinou (1977), Zomenis (1977), Dijon (1977), Afrodisis et al. (1986), Afrodisis and Fischbach (1988), Konteatis (1987), Kramvis (1987), Schmidt et al. (1988), Zomenis et al. (1988) and Wagner et al. (1990). The studies of the 1970s focus mainly on quantity issues and the application of mathematical and numerical models. At the end of the 1970s and in the 1980s, water quality and isotope studies grew in importance. In the 1990s the issues were extended by discussions about water scarcity, artificial recharge, wastewater re-use, water re-distribution and optimisation, desalination, or new water sources (e.g Iacovides 1997, Kambanellas 1998, Ergil 2000). In the 2000s the upcoming integration into the European Union led to initiatives and projects to re-evaluate groundwater resources and to supply technical support for the modernisation of data management and techniques (GRC Project: Udluft et al. 2004b). In this context a new hydrogeological map (Dünkeloh 2004) was published which has been revised within the present study (Fig. 2.7).

The hydrogeological map reveals that the most important aquifers in unconsolidated and semiconsolidated rocks (sand and gravels associated with partly cemented sandstone and calcarenite), which provide excellent storage and water-transmitting characteristics, are mostly located in western Mesaoria, southeastern Mesaoria and the Akrotiri peninsula. Some regions also have aquifers in several stratigraphic levels (e.g. upper and lower aquifer in western Mesaoria). Other aquifers in unconsolidated and semiconsolidated rocks are of minor thickness and limited extent. The latter can be found in many areas of the island, e.g. as coastal plains or river bed deposits. Most of those aquifers are located in comparatively dry areas with little annual pre-

cipitation. Therefore, the main source of replenishment is surface and groundwater from the adjacent mountain areas. The aquifers in the plains and coastal areas are mostly overpumped; groundwater levels are low and seawater intrusion occurs up to several kilometers inland.

Fractured and karstic rocks form fairly adequate aquifers in the area circumventing Troodos (Gypsum aquifer, the Pakhna sandstone, the Pakhna chalk aquifer, the Lefkara chalk aquifer, Terra and Koronia reef limestone aquifer) and in the Kyrenia range (Pentadaktylos limestone aquifer). Moderate precipitation amounts and their neighbouring the mountains make those areas relevant for water supply and replenishment.

The great importance of the fractured igneous rocks of the Troodos for water supply was not fully recognised until the end of the 1970s, when first drilling experiments started (see Afrodisis et al. 1986, Afrodisis and Fischbach 1988). In earlier studies the Troodos was considered more or less impervious (see e.g. hydrogeological map from Tullström, 1970) and was not recognised explicitly as a contributor to the aquifers in the surroundings of the Troodos. Today it is known that the Troodos ophiolite plays a crucial role for the water resources of the island due to its high precipitation rates and the relatively good aquiferous characteristics of many rocks. Especially the Gabbros and also the Basal Group and the Sheeted Dykes show fairly good aquifer characteristics, depending on the local fracturing state. Direct runoff and base flow from the Troodos rivers also feed the aquifers with greater storage capacity in the periphery such as the coastal plains or the Mesaoria plain.

The existing hydrological studies consist mainly of statistical analysis of river runoff and groundwater level data. The Water Development Department of Cyprus (WDD) maintains a monitoring network and has published the data in a series of hydrological year-books. The most comprehensive study in recent years was performed within the framework of the WDD/FAO project (Re-Assessment of the Water Resources and Demand of the Island of Cyprus) where a revision of groundwater levels, surface water (precipitation-runoff) and water demand was performed for the island (see WDD/FAO 2002).

So far, the existing groundwater recharge studies mostly depend on expert estimates and are limited to specific aquifers. The methodology of the water balance calculations in those studies is not always transparent. Early studies were performed and

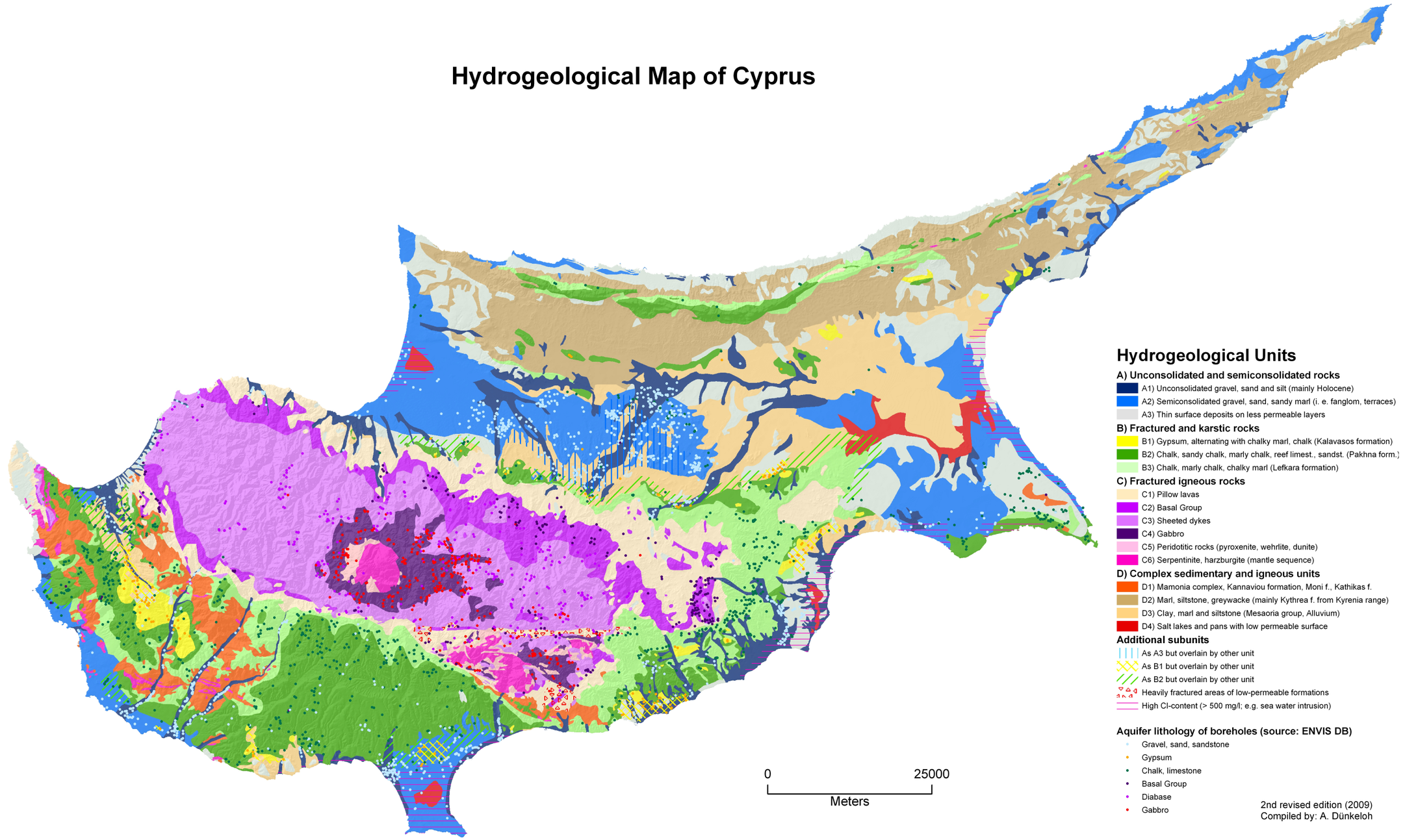

Figure 2.7: Hydrogeological map of Cyprus.

published within the UNDP project (1970). Further studies followed for important aquifers or catchments e.g. from Kitching (1975), Kitching et al. (1980) for Akrotiri aquifer, Zomenis (1977) for Mesaoria plain, Konteatis (1987), Kuells et al. (2000a) and Udluft (2002) for Kouris catchment, Boronina et al. (2003) and Boronina (2004) also for Kouris catchment.

For Cyprus, first recharge and water balance studies on the base of a distributed physical modelling concept, began with the application of former MODBIL versions for the Kouris catchment (Kuells et al. 2000a, Udluft 2002, Zagana et al. 2007). The studies were part of the INCO-DC Project GREM (Groundwater Recharge in the Eastern Mediterranean), which was a comparative study on integrated evaluation techniques for groundwater resources along a hydro-climatic gradient. Subsequently, further catchments in Cyprus were also analysed on the base of MODBIL by Mederer (2003; Limnatis catchment) and Dünkeloh (2005a, 2005b; Diarizos catchment).

In the present study, the modelling area is extended to the whole island and performed on the base of a modern, redesigned, substantially enhanced version of the water balance model MODBIL. Groundwater recharge dynamics and water balance dynamics are simulated for isolated calibration catchments and subsequently for the whole island. It is the first time that such a model has been applied for Cyprus, considering a long period of nearly five decades, revealing the sensitivity of the natural water resources in the context of climate variability and trends, as well as possible impacts of climate change.

Chapter 3

Water Balance Model

3.1 Introduction

Within the current study, a completely redesigned and substantially enhanced version of the water balance model MODBIL was developed. Early versions of the model have been developed since 1988 at the Hydrogeological Section of the University of Würzburg (Germany) by Prof. Dr. Udluft. The model has been enhanced in the framework of various projects, mostly in semiarid areas e.g. in Brazil, Greece, Israel, Jordan, Namibia, Botswana, Central African Republic, Lower Franconia/Germany and Cyprus (Rosa Filho 1991, König 1993, Albert 1994, Udluft and Zagana 1994, Kuells et al. 1998, Al-Alami 1999, Mainardy 1999, Zagana and Udluft 1999, Zagana et al. 1999, Kuells et al. 2000a, Kuells et al. 2000b, Udluft and Kuells 2000, Obeidat 2001, Weigand 2001, Zagana 2001, Klock 2002, Udluft 2002, Wijnen 2002, Al-Farajat 2003, Dünkeloh et al. 2003, Mederer 2003, Kuells 2003, Borgstedt 2004, Dünkeloh and Udluft 2004a, Dünkeloh and Udluft 2004b, Dünkeloh et al. 2004, Udluft and Dünkeloh 2004a, Udluft and Dünkeloh 2004b, Udluft et al. 2004a, Udluft et al. 2004b, Dünkeloh 2005a, Dünkeloh 2005b, Mederer 2005, Pasig 2005, Zagana et al. 2007, Wanke et al. 2007, Wanke et al. 2008, Mederer 2009, Walter 2010). The model description and modelling results of the present study are based on the latest stable version MODBIL V49/2009.

MODBIL is designed as a physical, spatially distributed and process-orientated model, which simulates all important water balance components for each cell on

a daily basis. Based upon meteorological, topographical, soil, land cover and geological data, the model generates spatially distributed maps for all important water balance parameters such as actual evapotranspiration, direct runoff and groundwater recharge. Furthermore, daily discharge time series can be calculated for closed catchment areas.

The model represents a suitable approach for a detailed understanding of regional and local water balances and their dynamics. It can serve as an important tool within sustainable management of natural water resources. Furthermore, the physical concept allows the model to be applied within the framework of coupled deterministic or deterministic-stochastic models, for instance, to reveal scenario simulations.

A model run requires the collection and pre-processing of a considerable amount of data which has become easier with the recently available remote sensing and GIS techniques. Daily meteorological data (precipitation, air temperature, relative humidity, wind speed, radiation), hydrological parameters (discharge recordings), topographical parameters (elevation, slope, exposition), vegetation parameters (vegetation coverage and interception), soil parameters (permeability, field capacity) and geological parameters (bedrock permeability) are needed particularly.

3.2 Model Structure and Work Flow

The complete water balance model consists of several concatenated models, which simulate the relevant processes on different levels. The principal concept is shown in Fig. 3.1, a detailed work flow in Fig. 3.2. In the first part of the model, the simulation of the atmospheric level starts with the interpolation of meteorological parameters. Precipitation, maximum and minimum temperature, relative humidity, wind speed and radiation data are interpolated to each cell of the study area. Subsequently, the interpolated values are corrected on the base of topographic variables (see Chap. 3.3).

In a further modelling step, effective precipitation is simulated for each cell on the base of total precipitation, snow storage and interception losses. The snow storage model controls the daily snow accumulation, snow storage state and snow melting based on daily precipitation and temperature (Chap. 3.3). The interception model

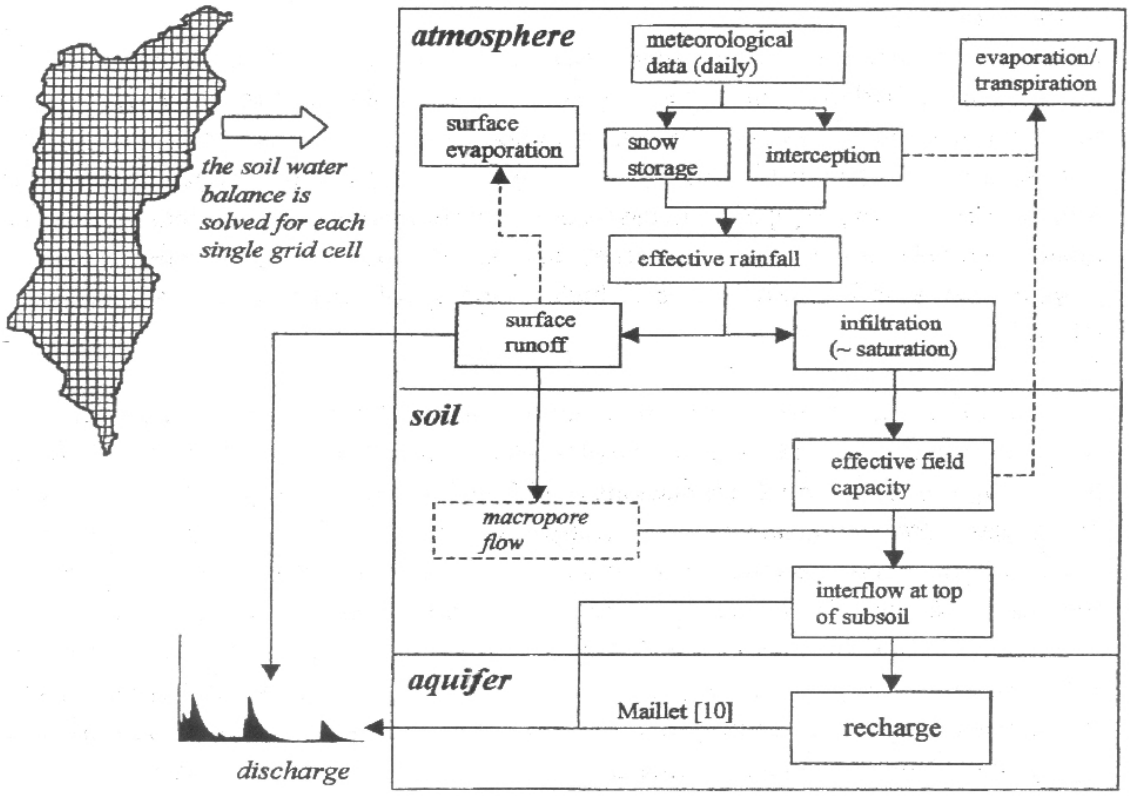

Figure 3.1: Principal model concept of the water balance model MODBIL (Udluft and Kuells 2000).

simulates water storage and evaporation on intercepting surfaces on the base of precipitation, potential evaporation and land cover specific data (Chap. 3.4).

A major part of the model comprises all processes related to the soil layer. Surface runoff, infiltration, soil water state, interflow and percolation are simulated on the base of effective precipitation, topography, land cover and physical soil parameters (see Chap. 3.5, 3.6, 3.7).

In the initial step, effective precipitation reaches the top of the soil layer and generates surface runoff, infiltration and bypass flow depending on soil physical parameters, land cover and topography (Chap. 3.5, 3.7). The infiltrating water is driven to a one-layer-soil model, which simulates the daily soil water balance based on the actual soil water storage and the depletion by actual evapotranspiration, interflow and percolation (Chap. 3.6). Actual evapotranspiration is assessed on the basis of potential evapotranspiration, soil water state and land cover (vegetation) type. Several alternative approaches are implemented and can be selected for the

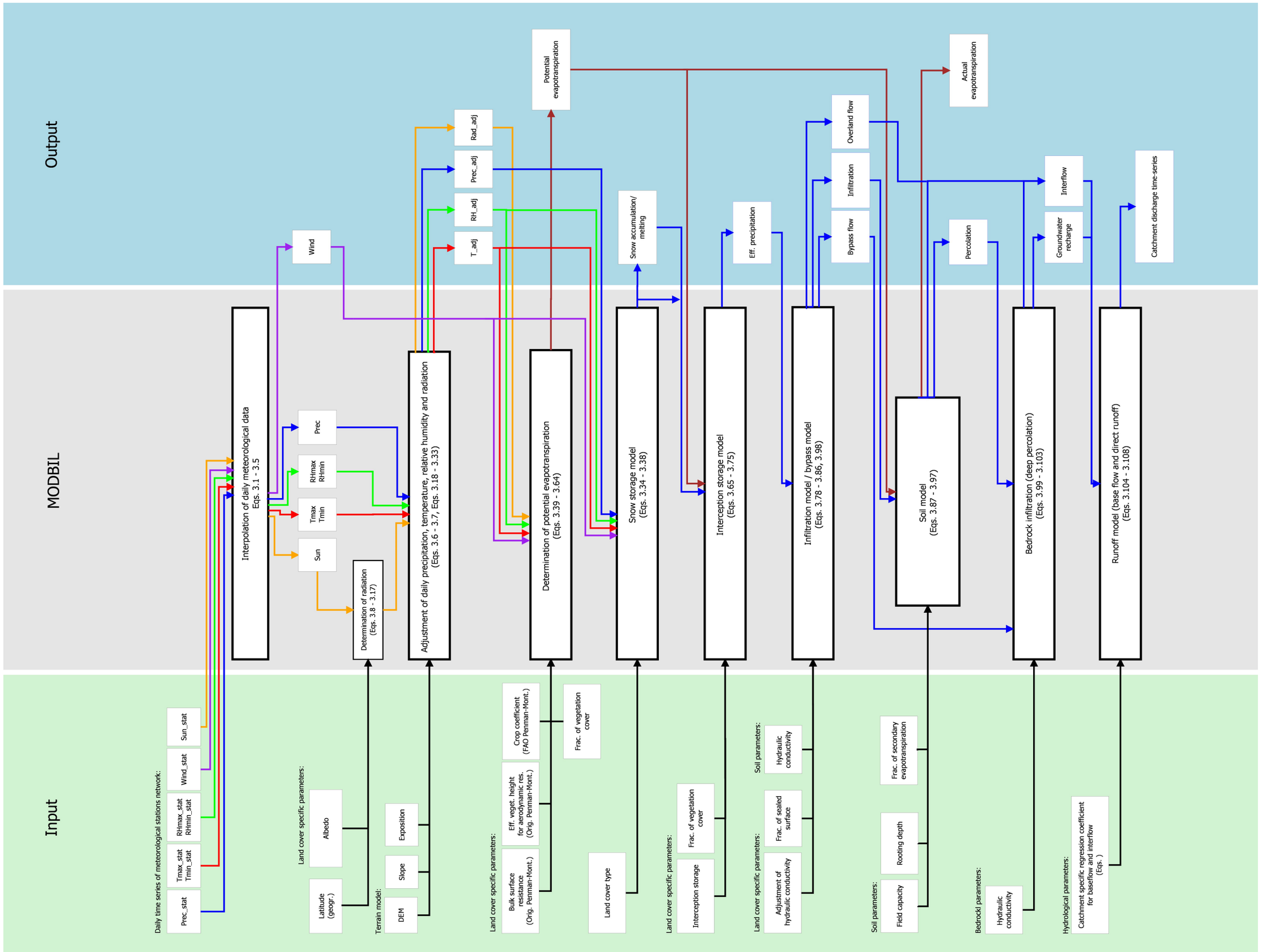

Figure 3.2: Detailed structure and work flow of the water balance model MODBIL V49/2009.

determination of the actual and potential evapotranspiration (Chap. 3.4).

The second modelling part consists of the soil water simulation. Depletion of soil water starts when soil water content exceeds field capacity. The water is drained in form of interflow and deep percolation. The fraction depends on the bedrock layer and the topographic conditions (Chap. 3.8). Additional interflow and deep percolation can be generated on the base bypass flow (Chap. 3.7).

The third part of the model consists of the calculation of daily catchment discharge. All values from direct runoff and groundwater recharge of all associated cells are integrated and discharge time series are simulated based on a combined linear reservoir equation of Maillet (1905). Calibration is best performed by the comparison of modelled and recorded catchment discharge time series (Chap. 3.9).

3.3 Meteorology

3.3.1 Meteorological Parameters

MODBIL requires daily time series for several meteorological parameters. Mandatory parameters are daily precipitation (in mm), maximum and minimum daily temperature (in °C), and maximum and minimum relative humidity (in %).

The water balance model can be improved when time series of further meteorological parameters like rainfall intensity (mm/h), wind speed at 2 m height over surface (m/s), sunshine duration (h) and global radiation ($MJ/m^2/d$) are available. Rainfall intensity and wind speed can also be defined as a (seasonal) mean value. If no values are defined by the user, then a mean wind speed of 2 m/s and a mean rainfall intensity of 5 mm/h are assumed. The mean wind speed corresponds to a value proposed by the FAO (Allen et al. 1998).

3.3.2 Interpolation of Meteorological Data

For most countries, climate datasets are only available in form of point data from meteorological stations, therefore the extension of the data to the intermediate spaces is required. In MODBIL, interpolation is done separately for each meteorological

variable and for each time step. The spatial and temporal variability of the meteorological variables is modified by topographical features of the earth surface. The further correction of the interpolation results is discussed in the following chapters.

MODBIL includes several standard methods which are designed for the interpolation of values from irregularly spaced data points (stations) to the nodes of a rectangular grid (Cartesian surface). Basic algorithms are used for this procedure to reduce computing time, because extremely large amounts of interpolation operations are needed for the water balance simulations. Nevertheless, more complex interpolation methods like thin plate splines can be used in a pre-processing step to calculate grid-based data, which can be subsequently used instead of meteorological station data.

One of the interpolation methods incorporated in MODBIL is the Thiessen Polygons method, which is a widely used standard approach in meteorology and hydrology that was originally proposed by Thiessen (1911). The concept is based on the building of polygons, the boundaries of which enclose the areas that are closest to a point relative to all other points. The polygons are respectively constructed as lines of equal distance between two adjacent points. In the case of application to a rectangular grid, this means that the value of the nearest recording station is assigned to a cell. Apart from the small amount of computing time, the maintenance of consistency is another advantage over lots of other interpolation methods. This may be of particular interest, especially in the case of the resulting time series on interpolated cells which could have a higher number of annual precipitation days than the recording stations. This arises from the effect that a cell always registers any precipitation, even if only one neighbouring record station shows precipitation. Thus, the Thiessen Polygons method keeps the consistency of interpolated time series but lacks accuracy of interpolation, especially near the polygon boundaries.

Furthermore, the Inverse Distance Weighting (IDW) method is available in MODBIL, which is one of the most commonly used methods for multivariate interpolation. It is based on a modified approach from Shepard (1968) and estimates a value for a certain cell, by averaging the values of sample data points in the cell's neighbourhood. The closer a point is to the cell being estimated, the more weight it has in the averaging process. The respective weights are inversely proportional to the distances:

$$Z_0 = \frac{\sum_{k=1}^{K} (w_k \cdot Z_k)}{\sum_{k=1}^{K} (w_k)} \tag{3.1}$$

$$w_k = \frac{1}{d_k^{p_w}} \tag{3.2}$$

$$d_k = \begin{cases} [(x_k - x_0)^2 + (y_k - y_0)^2]^{0.5} & \text{(a)} \\ [(x_k - x_0)^2 + (y_k - y_0)^2]^{0.5} + (h_k - h_0)\, w_h & \text{(b)} \end{cases} \tag{3.3}$$

(a) without weighting of elevation

(b) incl. weighting of elevation

with

Z_0	data value Z (e.g. precipitation, temperature, ...) at interpolation point
Z_k	data value Z (e.g. precipitation, temperature, ...) at data point k; $k = 1, K$
K	amount of data points in the neighbourhood of interpolation point (within the search radius) [-]
w_k	weighting factor (depending on lateral distance) [-]
w_h	weighting factor (depending on elevation difference; 0 = no weighting) [-]
d_k	distance between interpolation point and data point k; $k = 1, K$ [m]
p_w	weighting power of inverse distance; typically $p_w = 1$ or $p_w = 2$ [-]
x_k, y_k	coordinates of data point k in a Cartesian surface; $k = 1, K$ [m,m]
x_0, y_0	coordinates of interpolation point in a Cartesian surface [m,m]
h_k	elevation of data point k; $k = 1, K$ [m]
h_0	elevation of interpolation point [m]

For reasons of consistency (see discussion in relation with Thiessen Polygons method) and improving processing speeds, MODBIL uses only the closest points for interpolation. For IDW the number is limited to 1 to 4 input points for each cell's

calculation. Under specific conditions in coastal and very mountainous areas, as in the case of Cyprus, it can be helpful to use an enhanced term (see Eq. 3.3b) that allows an additional weighting of strong elevation differences between point k and the interpolated value. Consequently, the points in the same elevation level get more influence to the interpolation result.

Furthermore, MODBIL supports the application of a modified weighting algorithm described by Shepard (1984) and Willmot et al. (1985), which takes into account the directional isolation of the station data. It is intended that all points having a small angular separation in between contribute less than other points. This reduces the influence of stations that are located in a similar direction and limits the maximum of the directional isolation to twice the weight based on distance:

$$w_k = \left(\frac{1}{d_k}\right) \left(\frac{\sum_{l=1}^{K} (d_l \, [1 - cos(\theta_{k,l})])}{\sum_{l=1}^{K} d_l} \right), \; l \neq k \tag{3.4}$$

$$cos(\theta_{k,l}) = \frac{(x_k - x_0)(x_l - x_0) + (y_k - y_0)(y_l - y_0)}{d_k d_l}, \; l \neq k \tag{3.5}$$

with

	w_k	weighting factor [-]
	$\theta_{k,l}$	angle between data points Z_k and Z_l (vertex is the point of interpolation) [deg]
	d_k	distance between interpolation point and data point k [m] (Eq. 3.3)
	d_l	distance between interpolation point and data point l [m] (Eq. 3.3)
	K	amount of data points in the neighbourhood of the interpolation point (within the search radius); in MODBIL $K_{max} \leq 4$ [-]
	x_k, y_k	coordinates of data point k in a Cartesian surface; $k = 1, K$ [m,m]
	x_0, y_0	coordinates of interpolation point in a Cartesian surface [m,m]

Some of the interpolated meteorological parameters are adjusted in a further modelling step taking into account influences of topography, particularly the effects of elevation, slope and exposition. Missing meteorological parameters are assessed based

on existing data. The individual assessments and adjustments are documented in the following sections.

3.3.3 Adjustment of Precipitation

Spatial precipitation patterns show a strong correlation to topographical features, most prominent with respect to elevation, hence a further adjustment of the interpolated data is realised within an additional MODBIL procedure:

$$P_{adj} = \begin{cases} P_{ipol} \cdot c^*_{pc} \; ; & P_{ipol} > 0 \\ 0 \; ; & P_{ipol} = 0 \end{cases} \tag{3.6}$$

$$c^*_{pc} = \frac{h_{cell} \cdot c_{pg} + P_0}{h_{ref} \cdot c_{pg} + P_0} \tag{3.7}$$

with

P_{adj}	adjusted daily precipitation for the cell [mm]
P_{ipol}	interpolated daily precipitation (not adjusted) [mm]
P_0	mean annual precipitation at mean sea level; values for Cyprus see Fig. 2.3 [mm a^{-1}]
c^*_{pc}	adjustment factor for precipitation [-]
c_{pg}	precipitation gradient; values for Cyprus see Fig. 2.3 [mm m^{-1} a^{-1}]
h_{cell}	elevation (a.m.s.l.) of the cell [m]
h_{ref}	reference elevation (a.m.s.l.) of the interpolated precipitation value given by the weighted mean of the elevation of the meteorological stations used for interpolation [m]

The interpolation is performed on the base of the reference elevation of the interpolated value and the real elevation of the cell. A mean regional precipitation gradient is used for the adaptation, which has to be assessed in a preliminary step.

3.3.4 Determination and Adjustment of Radiation

The net radiation R_n is a crucial factor for the water balance modelling with respect to the Penman approach. In most cases, required radiation data time series are not available for the research area. Several approaches exist for the assessment of net

radiation on the base of other recorded parameters such as recorded global radiation, sunshine duration or daily temperature variations.

Net radiation is the balance between the energy being absorbed, reflected and emitted. This can be described as the difference between incoming net short wave radiation and outgoing net long wave radiation:

$$R_n = R_{ns} - R_{nl} \tag{3.8}$$

with	R_n	net radiation [MJ m^{-2} d^{-1}]
	R_{ns}	incoming net short wave radiation [MJ m^{-2} d^{-1}] (Eq. 3.9)
	R_{nl}	outgoing net longwave radiation [MJ m^{-2} d^{-1}] (Eq. 3.17)

The difference between incoming and outgoing longwave radiation is called net longwave radiation R_{nl} (see Eq. 3.17). Analogously, the incoming net shortwave radiation R_{ns}, also known as net solar or shortwave radiation, is defined as the part of the shortwave radiation R_s that is not reflected by the earth's surface (Eq. 3.9). It is absorbed and then converted to heat energy. The fraction defines the albedo and depends on the earth's surface conditions. The albedo typically ranges between $\alpha = 0.10-0.25$ but can differ considerably under special circumstances. For instance a snow cover can have an albedo of $\alpha = 0.95$.

$$R_{ns} = (1 - \alpha)R_s \tag{3.9}$$

with	R_{ns}	incoming net short wave radiation [MJ m^{-2} d^{-1}]
	R_s	solar or short wave radiation [MJ m^{-2} d^{-1}] (Eq. 3.14)
	α	albedo [-]

Solar radiation is also called global radiation as it comprises direct short wave radiation and diffusive sky radiation. Its magnitude is primarily controlled by the extraterrestrial radiation R_a, which may be calculated with the solar constant and the angle of incidence of the sun's rays on the top of the earth's atmosphere. In case of daily modelling steps the angle depends on the location (latitude) and the date (see Allen et al. 1998):

$$R_a = \frac{24(60)}{\pi} G_{sc}\, d_r \left[\omega_{ss}\, sin(\varphi)\, sin(\delta) + cos(\varphi)\, cos(\delta)\, sin(\omega_{ss})\right] \tag{3.10}$$

$$d_r = 1 + 0.033 \cdot cos\left(\frac{2\pi}{365} j\right) \tag{3.11}$$

$$\omega_{ss} = arccos[-tan(\varphi)tan(\delta)] \tag{3.12}$$

$$\delta = 0.409 \cdot sin\left(\frac{2\pi}{365}j - 1.39\right) \tag{3.13}$$

with

R_a	extraterrestrial radiation [MJ m^{-2} d^{-1}]
d_r	inverse of the square of the relative distance earth-sun (correction for eccentricity of earth's orbit around the sun)
ω_{ss}	sunset hour angle [rad]
δ	solar declination (at equator) [rad]
φ	latitude (positive for northern hemisphere, negative for southern hemisphere) [rad]
G_{sc}	solar constant; 0.082 [MJ m^{-2} min^{-1}]
j	number of days of the year [-]

Furthermore, the amount of solar (or global) radiation is influenced by atmospheric conditions. When penetrating the atmosphere a part of the radiation is either scattered, absorbed or reflected by atmospheric gasses, clouds and dust. While on clear days solar radiation can reach about 75% of the extraterrestrial radiation, on very cloudy days it reaches the earth's surface only as diffuse sky radiation and can be reduced to 25% of the extraterrestrial radiation. In case global radiation is not directly recorded, the Angström formula (Angström 1924, Paltineanu et al. 2002) continues to be a suitable and widely used approach to assess solar radiation from extraterrestrial radiation and local sunshine duration:

$$R_s = (a_s + b_s\frac{s}{S})\ R_a \tag{3.14}$$

$$S = \frac{24}{\pi}\ \omega_{ss} \tag{3.15}$$

with

R_s	solar or short wave radiation [MJ m^{-2} d^{-1}]
R_a	extraterrestrial radiation [MJ m^{-2} d^{-1}] (Eq. 3.10)
a_s	fraction of extraterrestrial radiation reaching earth's surface as diffuse solar radiation; recommended value according to Paltineanu et al. (2002): $a_s = 0.25$ [-]

	b_s	fraction of extraterrestrial radiation reaching earth's surface as direct solar radiation; recommended values according to Paltineanu et al. (2002): $b_s = 0$ (overcast days), $b_s = 0.5$ (clear days) [-]
	s	actual sunshine duration [h]
	S	maximum possible sunshine duration [h]
	ω_{ss}	sunset hour angle [rad] (Eq. 3.12)

In case no sunshine duration or solar radiation recordsets are available, R_s can be assessed on the base of daily temperature differences. High amplitudes of daily temperature usually correlate with clear sky conditions and low amplitudes with more cloudy or covered weather conditions. In MODBIL, the assessment is performed according to an approach proposed by the FAO guidelines (Allen et al. 1998):

$$R_s = k_{R_s} \sqrt{T_{max} - T_{min}}\, R_a \tag{3.16}$$

with	T_{max}	maximum daily air temperature [°C]
	T_{min}	minimum daily air temperature [°C]
	k_{R_s}	adjustment coefficient (coastal regions 0.16, interior regions 0.19) [$°K^{-0.5}$]

Net outgoing longwave radiation R_{nl} is the second important parameter needed for the determination of net radiation R_n. It describes the difference between incoming and outgoing longwave radiation. The latter is responsible for longwave energy emission from the earth's heated surface by the absorption of short wave radiation. The phenomenon is physically described by the Stefan-Boltzmann law, to which a correction is necessary, because the atmosphere contains several absorbers, which reduce the net outgoing flux. For this correction, humidity and cloudiness data are used (Allen et al. 1998):

$$R_{nl} = \sigma \left(\frac{T_{max,K}^4 + T_{min,K}^4}{2} \right) (0.34 - 0.14\sqrt{e_a}) \left(1.35 \frac{R_s}{(a_s + b_s) R_a} - 0.35 \right) \tag{3.17}$$

with	R_{nl}	outgoing net longwave radiation [MJ m^{-2} d^{-1}]
	R_s	solar or short wave radiation [MJ m^{-2} d^{-1}] (Eq. 3.14)
	R_a	extraterrestrial radiation [MJ m^{-2} d^{-1}] (Eq. 3.10)
	$T_{max,K}$	maximum daily air temperature in Kelvin [K]
	$T_{min,K}$	minimum daily air temperature in Kelvin [K]

e_a	actual vapour pressure [kPa] (Eq. 3.51)
a_s	fraction of extraterrestrial radiation reaching earth's surface as diffuse solar radiation [-] (see Eq. 3.14)
b_s	fraction of extraterrestrial radiation reaching earth's surface as direct solar radiation [-] (see Eq. 3.14)
σ	Stefan-Bolzmann constant; $4.903 \cdot 10^{-9}$ [MJ K^{-4} m^{-2} d^{-1}]

The term $R_s/(a_s + b_s)R_a$ describes relative short wave radiation and is limited to ≤ 1; the term $(0.34 - 0.14\sqrt{e_a})$ contains the correction of air humidity and the term $(1.35R_s/(a_s + b_s)R_a - 0.35)$ represents the influence of cloudiness (Allen et al. 1998).

3.3.5 Adjustment of Radiation by Topographic Effects

The amount of global radiation on a cell may be modified by topographic influences, especially due to slope and exposition. An adjustment is possible on the base of daily sunshine duration and topographical information. The applied concept in MODBIL is a modified variation of the methods proposed by Oke (1987) and Schulla and Jasper (1999). It is based on the angle of incidence between the direct solar radiation and the cell surface. The difference between the respective angles of a hypothetical horizontal cell and an inclined cell surface at a certain point, allows the derivation of a weighting factor for the adjustment of the global radiation over a certain point of time:

$$wf = \frac{cos(\alpha_c)}{cos(\zeta)} \tag{3.18}$$

with	wf	weighting factor for the adjustment of solar radiation [-]
	α_c	incidence angle (angle between the perpendicular to the cell surface and the actual direction of direct solar radiation) [deg]
	ζ	zenith angle (angle between the zenith and the actual direction of direct solar radiation) [deg]

Due to the continuously changing incidence angle throughout the day the calculation of the weighting factor for each hour or even smaller time steps are required. Subsequently, the mean of all valid weighting factors is calculated to get a daily

weighting factor for the adjustment of solar radiation:

$$wf_i = \frac{\sum_{i=1}^{n} \frac{cos(\alpha_{ci})}{cos(\zeta_i)}}{n} \tag{3.19}$$

with
- wf_i weighting factor for the adjustment of solar radiation at (daily) time step i [-]
- α_{ci} incidence angle at time step i (angle between the perpendicular to the cell surface and the direction of direct solar radiation) [deg]
- ζ_i zenith angle at timestep i (angle between the zenith and the actual direction of direct solar radiation) [deg]
- n number of valid time steps [-]

A calculated weighting factor only contributes to the mean of a daily weighting factor when a minimum of twelve degrees is given between the angle of sun and the earth's horizon (see Eq. 3.20). If the angle is too small, the value is discounted because short wave radiation is scattered due to the greater thickness of the atmosphere that has to be penetrated (see Schulla and Jasper 1999).

Furthermore, the zenith angle ζ and the incidence angle α_c are needed. The zenith angle ζ can be calculated according to Garnier and Ohmura (1968), Schulla and Jasper (1999), Allen et al. (1998):

$$cos(\zeta) = sin(\phi) = sin(\varphi)\ sin(\delta) + cos(\varphi)\ cos(\delta)\ cos(\omega_s) \tag{3.20}$$

$$\delta = -23.4 \cdot cos\left(\frac{360°(j_J + 10)}{365}\right) \tag{3.21}$$

$$\omega_s = 15\ (t_s - 12) \tag{3.22}$$

$$cos(\alpha_c) = cos(\beta_c)\ cos(\zeta) + sin(\beta_c)\ sin(\zeta)\ cos(\omega_s - \omega_c) \tag{3.23}$$

with
- ζ zenith angle (angle between zenith and direction of direct solar radiation) [deg]
- ϕ angle between horizon and the actual direction of direct solar radiation [deg]

δ	solar declination (at equator) [deg]
φ	latitude (positive for northern hemisphere, negative value for southern hemisphere) [deg]
ω_s	solar time angle at midpoint of hourly (or shorter) time period; E=-90°, S=0°, W=90°, N=180° [deg]
ω_c	exposition of cell surface; E=-90°, S=0°, W=90°, N=180° [deg]
α_c	incidence angle (angle between the perpendicular to the cell surface and the actual direction of direct solar radiation) [deg]
β_c	slope of cell surface; $\beta_c \leq 45°$ [deg]
j_J	number of a day in the Julian calendar (1st January = 1, 31st of December = 365) [-]
t_s	solar time at the midpoint of the period (e.g. 13:30 = 13.5) [h]. (Note that in some cases the solar time differs from standard clock time. A correction may be required considering the actual position, longitude of the centre of the local time zone, and seasonal correction of solar time; consider Eq. 31 from Allen et al. (1998))

The final adjustment of global radiation requires its separation into direct solar radiation and diffuse radiation, because the weighting factor only describes the influence on the clear-sky radiation. Hence the adjustment of global radiation is applied as follows:

$$R_{s,adj} = R_s \left[1 + (1 - a_s) \left(\frac{s}{S}\right) wf_i\right] \tag{3.24}$$

with	$R_{s,adj}$	adjusted solar or short wave radiation [MJ m^{-2} d^{-1}]
	R_s	solar or short wave radiation [MJ m^{-2} d^{-1}] (Eq. 3.14)
	a_s	fraction of extraterrestrial radiation reaching earth's surface as diffuse solar radiation [-] (see Eq. 3.14)
	s	actual sunshine duration [h]
	S	maximum possible sunshine duration [h] (Eq. 3.15)
	wf_i	weighting factor for the adjustment of solar radiation at (daily) time step i [-] (Eq. 3.19)

3.3.6 Adjustment of Air Temperature

In MODBIL, temperature information is required in form of maximum and minimum daily air temperature (°C). Depending on the meteorological datasets available, mean daily air temperature can also be used instead of minimum daily air temperature (not recommended). In this case the required data are internally assessed based on the following equations according to the FAO-Guidelines (see Allen et al. 1998):

$$T_{min} = 2 \cdot T_{mean} - T_{max} \tag{3.25}$$

with
- T_{min} minimum daily air temperature [°C]
- T_{mean} mean daily air temperature [°C]
- T_{max} maximum daily aor temperature [°C]

Topography has a notable influence on local temperature variation. The most important influence is given by elevation differences. The typical gradient is about -0.5 K to -0.6 K/100 m. During the modelling process, the interpolated temperature values for each cell are corrected by taking into account the difference between the real elevation and the weighted mean elevation of the meteorological stations used for interpolation:

$$T_{cell} = T_{ipol} + (h_{cell} - h_{ref})\, c_{tg} \tag{3.26}$$

with
- T_{cell} interpolated and elevation corrected air temperature for the cell [°C]
- T_{ipol} interpolated air temperature (not adjusted) [°C]
- h_{cell} elevation (a.m.s.l.) of the cell [m]
- h_{ref} reference elevation (a.m.s.l.) of the interpolated temperature value given by the weighted mean of the elevation of the meteorological stations used for interpolation [m]
- c_{tg} air temperature gradient (typically -0.5 to -0.6 K/100 m; for Cyprus: -0.5 K/100 m; see Fig. 2.2)

On sunny days cell slope and exposition can also have an influence on local temperature variations owing to differences between emitted long wave radiation. The latter is related to the absorbed short wave radiation. The topographic effects on radiation are described in the previous chapter. For the adjustment of temperature data a modified approach based on Schulla and Jasper (1999) was incorporated into

MODBIL. The zenith angle, incidence angle, daily sunshine data and interpolated temperature data are required for the adjustment:

$$T_{adj} = T_{cell} + T_{dif} \tag{3.27}$$

$$T_{dif} = ln\left[\frac{cos(\alpha_c)}{cos(\zeta)}\right]\frac{s}{S}\,c_{te}; \qquad -5\ K \leq T_{dif} \leq 5\ K \tag{3.28}$$

with

T_{adj}	adjusted air temperature for the cell considering local exposition [°C]
T_{dif}	air temperature difference for adjustment [K]
T_{cell}	interpolated and elevation corrected air temperature for the cell [°C] (Eq. 3.26)
s	actual sunshine duration [h]
S	maximum possible sunshine duration [h] (Eq. 3.15)
α_c	incidence angle [deg] (Eq. 3.23)
ζ	zenith angle [deg] (Eq. 3.20)
c_{te}	adjustment factor (should be validated or adjusted for each climate or region); $c_{te}\approx 5$ [K] (Schulla and Jasper 1999)

When the correction is applied to mean daily temperature data, then the weighting factor has to be derived as the mean factor from the hourly or smaller time periods (same procedure as in Eq. 3.28).

3.3.7 Adjustment of Relative Humidity

MODBIL requires humidity time series in form of daily maximum and minimum relative humidity (in %). If necessary, daily maximum and minimum relative humidity can be assessed with the help of mean daily relative humidity and the following equation proposed by the FAO-Guidelines (see Allen et al. 1998):

$$RH_{min} = 2 \cdot RH_{mean} - RH_{max} \tag{3.29}$$

with

RH_{min}	minimum daily relative humidity [%]
RH_{mean}	mean daily relative humidity [%]
RH_{max}	maximum daily relative humidity [%]

The influence of topography on local relative humidity is mainly controlled by temperature variations. Therefore, interpolation and adjustment can be performed on the basis of absolute humidity revealing better results than a direct interpolation and adaptation of relative humidity. For the calculation of absolute humidity, temperature data is mandatory for each monitoring station of relative humidity:

$$AH = 10^5 \cdot \frac{M_w}{R^*} \frac{e_a}{T_K} \tag{3.30}$$

$$e_a = e_s \frac{RH}{100} \tag{3.31}$$

$$e_s = 6.1078 \cdot 10^{\left(\frac{7.5T}{T+237.3}\right)} \tag{3.32}$$

with

	AH	absolute humidity [g m^{-3}]
	RH	relative humidity [%]
	e_a	actual vapour pressure [kPa]
	e_s	saturated vapour pressure [kPa]
	T_K	air temperature in Kelvin [°K]
	T	air temperature [°C]
	M_w	molecular weight of water vapour; 18.016 [kg]
	R^*	universal gas constant; 8314.3 [J K^{-1} kmol^{-1}]

The reconversion to adjusted local relative humidity is calculated with the transformed Eqs. 3.30 and 3.31. This requires a previous calculation of adjusted saturated vapour pressure on the base of the adjusted temperature (see Eq. 3.28):

$$RH_{adj} = \frac{AH}{10^5 \frac{M_w}{R^*} \frac{e_{s,adj}}{T_{adj,K}}} 100 \tag{3.33}$$

with

	RH_{adj}	adjusted relative humidity for the cell considering exposition [%]
	$T_{adj,K}$	adjusted air temperature for the cell in Kelvin [°K]
	$e_{s,adj}$	saturation vapour pressure under adjusted temperature conditions [kPa]

3.3.8 Snow Model

Snow accumulation and snow melting play an important role within the modelling of hydrological processes. The snow module in MODBIL is implemented as an additional storage layer above the soil layer. A general problem of snow modules is that most energy budget variables necessary for the calculation of snow melting are usually unavailable. Therefore, most hydrological approaches are based on air temperature, which is a frequently available and important variable (Anderson 1973, USACE 1994, Hock 2003). A widely used approach in modelling is known as 'temperature-index-solution' or degree-day method (see Linsley 1943). An enhancement of the method incorporates wind data into the equation and is known as 'temperature-wind-index-solution' (Braun 1985). However, Kane et al. (1997) pointed out that no significant improvement of the results could be detected on the basis of this equation, therefore, in MODBIL wind effects are considered within the melting rate coefficient.

In the present model, the snow storage content is measured as an equivalent of liquid water in mm. Snow accumulation (filling of snow storage) is modelled on rainfall days with air temperature below zero:

$$SS_i = \begin{cases} SS_{i-1} + P_i; & T_i < T_{bs} \\ SS_{i-1}; & T_i \geq T_{bs} \end{cases} \tag{3.34}$$

with	SS_i	snow storage at time interval i [mm]
	SS_{i-1}	snow storage at previous time interval [mm]
	P_i	precipitation at time interval i [mm]
	T_i	mean air temperature at time interval i [°C]
	T_{bs}	base temperature for snow fall ($T_{bs} \approx 0$) [°C]

For the simulation of snow melting, an approach based on a melting rate coefficient is sufficient for study areas with limited importance concerning snow melting processes. In the basic equation, the amount of available water from melting depends on air temperature, melting rate coefficient and state of the snow storage:

$$M_i = \begin{cases} c_m(T_i - T_{bm})\frac{\Delta t}{24}; & T_i > T_{bm} \\ 0; & T_i \leq T_{bm} \end{cases} \tag{3.35}$$

with	M_i	snow melting at time interval i with the length $\frac{\Delta t}{24}$; [mm]
	c_m	daily melting rate coefficient [mm K^{-1} d^{-1}] (Eqs. 3.36-3.38)
	T_i	mean air temperature at time interval i [°C]
	T_{bm}	base temperature for snow melting ($T_{bm} \approx 0$) [°C]
	Δt	length of time interval i [h]

The coefficient depends on land cover and meteorological conditions. In forested areas the coefficient varies less than in open areas where shortwave radiation or wind velocity plays a more important role within melting processes. Furthermore, rainfall events could have an influence on the melting rate. The factor can differ significantly between different study areas.

The melting rate coefficient can be adjusted individually in MODBIL. The applied coefficients for Cyprus are derived from several empirical studies of USACE (1994), ASCE (1996), WMO (1986, 1994), Anderson (1973) and Kuusisto (1984, 1986). They are rough estimates due to the limited importance of snow processes on Cyprus and should not be applied for other regions without validation:

$$c_m = \begin{cases} 1.0; & \text{forests (100\% covergage)} \\ 2.5; & \text{forests (20\% coverage)} \\ 4; & \text{open land} \end{cases} \tag{3.36}$$

$$c_m = c_m + 0.2 \cdot U \tag{3.37}$$

$$c_m = c_m + 0.0125 \cdot P \tag{3.38}$$

with	c_m	daily melting rate coefficient [mm K^{-1} d^{-1}]
	U	mean daily wind speed at 2 m height [m s^{-1}]
	P	daily precipitation [mm]

Land cover, mean daily wind speed and daily precipitation are used for the adjustment of the melting rate factor to the local conditions (see Eqs. 3.36 - 3.38). The influence of favourable or unfavourable radiation conditions due to topographical effects is respected by the adjustment of daily temperature (see p. 37 ff.).

3.4 Evapotranspiration

Evapotranspiration ET is a crucial factor within water cycle processes. The term defines the sum of two processes in which water is moving from the earth's land surface to the atmosphere. One is the evaporation, which is defined by the conversion of liquid water to water vapour on wet surfaces (soil, plant canopy and water bodies). The second one is called transpiration and refers to the transmission of vapour to the atmosphere by the stomata of plant leaves.

The term potential evapotranspiration (ET_{pot}) describes the maximum possible rate of evapotranspiration assuming optimal water supply. Reference evapotranspiration (ET_0) is defined as potential evapotranspiration of a reference crop. Clipped grass ($\approx$ 0.12 m tall) and alfalfa ($\approx$ 0.5 m tall) are the most common reference crops (Jensen et al. 1990). The actual evapotranspiration (ET_{act}) refers to the amount of evapotranspiration of a specific crop, vegetation formation, or earth surface under the actual conditions of water supply.

Many simple methods for the determination of evapotranspiration were proposed in the last decades, e.g. by Thornthwaite (1948), Blaney and Criddle (1950), Haude (1955, 1959), Turc (1961), Jensen and Haise (1963), Hargreaves and Samani (1982, 1985). Most of these methods are based on simple, usually empirical terms requiring only few meteorological parameters. The equations allow a relatively good assessment of evapotranspiration considering the little calculation effort. However, complex physical processes can not be represented on the base of these methods. Furthermore, the equations were developed under specific regional and climatological conditions, so that their application under other climatic conditions is of limited reliability. Detailed reviews are published in Allen et al. (1986), Roth (1992), DVWK (1996), Vörösmarty et al. (1998) and Beyazgül et al. (2000). To allow comparisons with other research results, the Haude (1955) approach is incorporated into MODBIL as an optional calculation procedure for potential evapotranspiration, owed to its common use in applied geosciences in Germany.

3.4.1 Haude Equation

The approach of Haude (1955, 1959) is designed for German longitude-latitude conditions and should not be transferred to other climatological conditions without validation. While individual results within daily time steps are not very precise, the values are proven for monthly sums and long-time mean values for regional water balances (Dommermuth and Trampf 1990/91). Required input variables for the base function are the Haude factor and the saturation vapour deficit:

$$ET_{Haude} = f_{Haude}(e_{s14} - e_{14}) \tag{3.39}$$

with	ET_{Haude}	potential evapotranspiration rate according to Haude [mm d^{-1}]
	f_{Haude}	plant specific Haude factor for a month [mm hPa^{-1}]
	e_{s14}	saturation vapour pressure at 14:30 h [hPa]
	e_{14}	actual vapour pressure at 14:30 h [hPa]
	$e_{s14}-e_{14}$	saturation pressure deficit at 14:30 h [hPa]

The equation for the calculation of saturation deficit (Eq. 3.41) is derived with the help from the MAGNUS-equation, new coefficients of Sonntag (1994) (see Eq. 3.43) and the relationship of saturation pressure deficit and relative humidity RH (see Eqs. 3.42, 3.41), resulting in an adapted Haude-equation according to DVWK (1996; Eq. 3.40).

$$ET_{Haude} = f_{Haude} \cdot 6.11 \cdot e^{\left(\frac{17.62\, T_{14}}{243.12+T_{14}}\right)} \cdot (1 - RH_{14}) \tag{3.40}$$

$$(e_{s14} - e_{14}) = e_{s14}\left(1 - \frac{e_{14}}{e_{s14}}\right) \tag{3.41}$$

$$\frac{e_{14}}{e_{s14}} = RH_{14} \tag{3.42}$$

$$e_{s14} = 6.11 \cdot e^{\left(\frac{17.62\, T_{14}}{243.12+T_{14}}\right)} \tag{3.43}$$

with	RH_{14}	relative humidity at 14:30 h [%/100]
	T_{14}	temperature at 14:30 h [°C]

Typical Haude factors f_{Haude} for different land cover (vegetation) types can be looked up in tables (e.g. DVWK 1996) or have to be revealed empirically. The Haude factors for the assessment of potential grass reference evapotranspiration with high groundwater level has been listed in Table 3.1.

3.4.2 Original Penman Equation

Modern water balance models require evapotranspiration approaches based on physical relationships (e.g. Hartmann 2007). Such concepts allow the calculation of ET for short periods (<1 day), which are of significant importance for the modelling of complex processes. One concept is to derive ET from the energy needed to change the phase of water from liquid to gaseous. In this case net radiation, soil heat flux and the sensible heat flux are required for solving the energy balance (DVWK 1996). Further concepts are given by aerodynamic methods (mass transfer equations). These methods focus on the processes which control the removal of vapour from the evaporating surface. The evapotranspiration is derived from the vertical gradient of humidity and the turbulence of the air flow which can be linked to vapour pressure deficit and wind speed.

Several equations combine the concepts of energy balance and aerodynamic approaches. The so-called combination methods are widely used and are often regarded as the most sophisticated methods. Typically, the vapour pressure deficit is calculated as a function of temperature, actual vapour pressure and empirical wind speed function. Enhanced equations include a bulk surface resistance term. For instance, the widely used Penman-Monteith equation incorporates both, climatic and vegetation characteristics, for quantifying mass transfer effects. It requires a considerable amount of daily meteorological data like temperature, radiation, humidity and wind speed, as well as various characteristics of the land cover (see below).

Table 3.1: Haude factors f_{Haude} for the calculation of potential evapotranspiration on short grass with high groundwater level (DVWK 1996).

Month	Jan	Feb	Mar	Apr	May	Jun	Jul	Aug	Sep	Oct	Nov	Dec
f_{Haude}	0.22	0.22	0.29	0.29	0.28	0.26	0.25	0.23	0.22	0.22	0.22	0.22

The original evapotranspiration equation of Penman (1948, 1956) is based on a combination of an energy balance and a mass-transfer method. Initially, it was designed for the assessment of evaporation E_0 on open water surfaces and later extended for dealing with land surfaces. The central term in many established approaches is the original and condensed Penman equation:

$$E_0 = \frac{s_s \, R_{na} + \gamma \, EA}{s_s + \gamma} \tag{3.44}$$

with	E_0	evaporation from a water surface [mm]
	R_{na}	net absorbed radiation [mm]
	EA	evaporative demand [mm]
	s_s	slope of saturation vapour pressure curve [kPa K^{-1}]
	γ	psychrometric constant [kPa K^{-1}]

For this equation, the required input is usually not available, which is why lots of modifications were performed on the original equation by Penman and other researchers. Several simplifications were applied to reduce the input variables to standard climatological records like sunshine, air temperature, air humidity and wind speed. For instance, net absorbed radiation is determined on the base of incoming global radiation, net outgoing long-wave radiation, latent heat and the reflection coefficient of the surface (albedo). The evaporative demand depends on humidity, wind speed and surface roughness. Such enhanced equations were proposed by Penman (1953), Rijtema (1965), Monteith (1965) and others. For a more detailed description of the original Penman equation and its modifications the publications of Penman (1948), DVWK (1996) and Allen et al. (1998) can be considered.

3.4.3 Penman-Monteith Equation

Modified equations, like the Penman-Monteith approach (Monteith 1965), seem to be the most commonly used and sophisticated methods. Many comparative model studies confirm the equation to be reliable approach. For validation purposes the calculated evapotranspiration was also compared with values from monitoring data of weighting lysimeters or the Bowen ratio-energy balance technique (BREB). The BREB is a micrometeorological, indirect method for estimating latent heat flux under known boundary conditions.

In the original Penman approach the bulk surface resistance from soil and vegetation was not explicitly defined and incorporated into the wind function. In later models, resistance factors of water vapour flow were introduced to enhance the model for the calculation of evapotranspiration of vegetated surfaces. In the Penman-Monteith equation (Eq. 3.45) the evaporating surface is abstracted as a single 'big leaf' with two resistance parameters, derived from surface resistance and aerodynamic resistant factors. Surface resistance factors are combined within the bulk surface resistance r_s, which includes the resistance of vapour flow through stomata openings, total leaf area and soil surface. The aerodynamic resistance r_a involves friction from airflow depending on vegetation canopy architecture.

$$ET_{pot} = \frac{1}{\lambda} \frac{s_s \, (R_n - G_{sh}) + \mu_c \, \frac{\rho_a \, c_p \, (e_s - e_a)}{r_a}}{s_s + \gamma \left(1 + \frac{r_s}{r_a}\right)} \tag{3.45}$$

The applied equation in MODBIL (Eq. 3.46) is rearranged similar to the transformations by Allen et al. (1998) with substituting c_p (Eq. 3.47) and considering the ideal gas law for ρ_a (Eq. 3.48).

$$ET_{pot} = \frac{\frac{1}{\lambda} \, s_s \, (R_n - G_{sh}) + \frac{185400 \, \gamma \, (e_s - e_a)}{(T + 273) \, r_a}}{s_s + \gamma \left(1 + \frac{r_s}{r_a}\right)} \tag{3.46}$$

$$c_p = \frac{\gamma \, M_r \, \lambda}{AP} \tag{3.47}$$

$$\rho_a = \frac{AP}{1.01(T + 273) \, R^*_{spec}} \tag{3.48}$$

with

ET_{pot}	potential evapotranspiration rate per day [mm]
c_p	specific heat of air at constant pressure; $1.013 \cdot 10^{-3}$ [MJ kg^{-1} K^{-1}]
ρ_a	mean air density at constant pressure [kg m^{-3}]
R_n	net radiation at plant surface [MJ m^{-2} d^{-1}] (Eq. 3.8)
G_{sh}	soil heat flux density [MJ m^{-2} d^{-1}] (see p. 49)
R^*_{spec}	specific gas constant; 0.287 [kJ kg^{-1} K^{-1}]
e_s	saturation vapour pressure [kPa] (Eq. 3.50)
e_a	actual vapour pressure [kPa] (Eq. 3.51)
$e_s - e_a$	vapour pressure deficit [kPa]

s_s	slope of saturation vapour pressure curve [kPa K^{-1}] (Eq. 3.52)
r_s	bulk surface resistance or canopy resistance [s m^{-1}] (Eq. 3.59)
r_a	aerodynamic resistance [s m^{-1}] (Eq. 3.55)
γ	psychrometric constant [kPa K^{-1}] (Eq. 3.53)
AP	atmospheric pressure [kPa]
λ	latent heat of vaporisation [MJ kg^{-1}]
M_r	ratio of molecular weight of water vapour/dry air; 0.622 [-]
μ_c	unit conversion to get ET_0 in mm d^{-1}; 86400 [s d^{-1}]

The data required for solving the Penman-Monteith equation is daily maximum and minimum air temperature, mean daily dew point temperature (or daily maximum and minimum RH), daily solar irradiance, mean daily wind speed, latitude, longitude and site elevation. In MODBIL, the original Penman-Monteith equation is used by default, but many of the accompanying equations are corresponding to the FAO guidelines (Allen et al. 1998), and therefore described in the following chapter describing the FAO-56-Penman-Monteith approach. For the original Penman-Monteith approach further required parameters, in particular land cover specific parameters as bulk surface resistance and aerodynamic resistance, are discussed in a separate chapter (Chap. 3.4.6).

3.4.4 FAO-56-Penman-Monteith Equation

The inconsistent definitions for the terms evaporation and evapotranspiration were the reason that Allen et al. (1998) proposed the term 'grass reference evapotranspiration', based on a clear definition. He points out that the defined method establishes a standardised technique to calculate a reference potential evapotranspiration for a standardised vegetation based on common meteorological datasets.

The FAO-56-Penman-Monteith approach, drafted in the FAO Expert Consultation Panel (Allen et al. 1989, 1994, 1998) reduces the original Penman-Monteith equation by assuming several constant parameters for a well-watered hypothetical grass reference surface (see Table 3.2). Furthermore, a constant for λ is set, and the air density term ρ_a and the vapour aerodynamic resistance are simplified. Besides the

Table 3.2: Constant parameters for the calculation of FAO hypothetical reference crop.

Parameter	Value
albedo [-]	0.23
reference vegetation height [m]	0.12
height of air temperature, humidity and wind measurements [m]	2
zero plane displacement height [m]	0.08
surface resistance, whole day [s m^{-1}]	70
surface resistance, daytime [s m^{-1}]	50
surface resistance, nighttime [s m^{-1}]	200
aerodynamic resistance [s m^{-1}]	208 U^{-1}
latent heat of vaporisation [MJ kg^{-1}]	2.45

U = wind speed at 2 m height over surface [m s^{-1}]

original Penman-Monteith equation, MODBIL also supports the FAO-56-Penman-Monteith approach. The greatest differences are given by the parameters describing the land cover (vegetation) specific characteristics.

The FAO-56-Penman-Monteith equation for the determination of daily ET_0 of a hypothetical grass reference surface is defined as follows (Allen et al. 1998):

$$ET_0 = \frac{0.408 \cdot s_s \, (R_n - G_{sh}) + \gamma \, \frac{900 \, U \, (e_s - e_a)}{T + 273}}{s_s + \gamma \, (1 + 0.34 \, U)} \tag{3.49}$$

with

ET_0	reference potential evapotranspiration [mm d^{-1}]
R_n	net radiation at the plant surface [MJ m^{-2} d^{-1}] (Eq. 3.8)
G_{sh}	soil heat flux density [MJ m^{-2} d^{-1}]
U	wind speed at 2 m height [m s^{-1}]
T	air temperature at 2 m height [°C]
e_s	saturation vapour pressure [kPa] (Eq. 3.50)
e_a	actual vapour pressure [kPa] (Eq. 3.51)
s_s	slope of saturation vapour pressure curve [kPa K^{-1}] (Eq. 3.52)
γ	psychrometric constant [kPa K^{-1}] (Eq. 3.53)

The meteorological data required for the model application is daily maximum and minimum air temperature, daily maximum and minimum relative humidity, daily so-

lar irradiance, mean daily wind speed, latitude, longitude and site elevation. Further accompanying equations are required for solving the equation with meteorological data. For a detailed documentation also see the extensive publication of the FAO Expert Consultation Panel (Allen et al. 1998).

Net radiation is one of the crucial variables needed within the Penman-Monteith equation. The derivation of daily values for net radiation is described in the radiation chapter of the meteorology section (see p. 30 ff.). The adjustment of radiation as a result of topographic influences is described in the same chapter.

The soil heat flux G_{sh} usually has to be added to the net radiation. In the case of daily modelling steps it can be set to zero, owed to its very small magnitude compared to net radiation.

Saturation vapour pressure and actual vapour pressure are calculated according to recommendations of the FAO guidelines. The former is derived based only on air temperature (Eq. 3.50) using a slightly modified version of Eq. 3.32. The latter is derived using air temperature and relative humidity data (Eq. 3.51). The slope of saturation vapour pressure curve can be described as the slope of saturation vapour pressure - temperature relationship (Eq. 3.52).

$$e_s = 0.6108 \cdot e^{\left(\frac{17.27\,T}{T+237.3}\right)} \tag{3.50}$$

$$e_a = \frac{e_{s,T_{min}}\, RH_{max} + e_{s,T_{max}}\, RH_{min}}{2} \tag{3.51}$$

$$s_s = \frac{4098\left[0.6108 \cdot e^{\left(\frac{17.27\,T}{T+237.3}\right)}\right]}{(T+237.3)^2} \tag{3.52}$$

with

e_s	saturation vapour pressure [kPa]
e_a	actual vapour pressure [kPa]
s_s	slope of saturation vapour pressure curve [kPa K^{-1}]
T	air temperature [°C]
RH_{max}	maximum daily relative humidity [%/100]
RH_{min}	minimum daily relative humidity [%/100]

$e_{s,T_{max}}$ saturation vapour pressure at daily maximum air temperature [kPa]

$e_{s,T_{min}}$ saturation vapour pressure at daily minimum air temperature [kPa]

The required psychrometric constant depends mainly on atmospheric pressure (Eq. 3.53) which may be influenced by a lower atmospheric pressure in higher areas. However, the use of a mean annual pressure for most areas (Eq. 3.54) is usually sufficient due to the little influence on the psychrometric constant and further calculation results.

$$\gamma = \frac{R^*_{spec}\, AP}{\epsilon\, \lambda} = 0.665 \cdot 10^{-3}\, AP \tag{3.53}$$

$$AP = 101.3 \left(\frac{293 - 0.0065 \cdot h}{293} \right)^{5.26} \tag{3.54}$$

with

γ psychrometric constant [kPa K^{-1}]

AP atmospheric pressure [kPa]

λ latent heat of vaporisation; 2.45 [MJ kg^{-1}]

ϵ ratio molecular weight of water vapour/dry air; 0.622 [-]

R^*_{spec} specific gas constant; 0.287 [kJ kg^{-1} K^{-1}]

h elevation (a.m.s.l) [m]

3.4.5 Land Cover Coefficients for Haude Equation

The evapotranspiration of different vegetation types under disease-free, well fertilised plants and optimum soil water condition can be termed as 'land cover specific potential evapotranspiration' or simply 'potential crop evapotranspiration' (Allen et al. 1998). Specific land cover or vegetation factors are required for the calculation depending on the selected potential evapotranspiration equation.

The Haude equation can be customised on the base of the empirical Haude factor (Table 3.1). After rearrangement, the factor is similar to the k_c factor of the FAO-56-Penman-Monteith equation, which gives the ratio of a specific land cover (vegetation) and the grass reference evapotranspiration. Compilations of Haude factors for different land cover (vegetation) types can be found in DVWK (1996) or Löpmeier (1994).

3.4.6 Land Cover Coefficients for Penman-Monteith Equation

Solving the original Penman-Monteith approach requires the determination of albedo, aerodynamic resistance and surface resistance for the calculation of land cover specific evapotranspiration. The albedo determines the ratio of solar radiation of all wavelengths reflected by the earth's surface. Values for the albedo of different land cover types can be found in many publications like DVWK (1996), Schulla and Jasper (1999), Hörmann (2005), Fritsch and Katzenmaier (2001). The applied values in MODBIL for the current project are listed in Table A.1-A.7 (Appendix).

Aerodynamic resistance quantifies the transfer of heat and water vapour from the evaporating surface into the air. Based on the Monin-Obukhov similarity theory many authors have proposed parametrisations to estimate aerodynamic resistances to heat transfer (e.g. Monteith 1973, Thom 1975, Verma et al. 1976, Choudhury et al. 1986). A discussion is given by Liu et al. (2006). The variant used in MODBIL is based on Thom and Oliver (1977) and is widely used in meteorology and hydrology practices:

$$r_a = \frac{4.72 \left(ln \frac{h_{ws}}{h_{zo}} \right)^2}{1 + 0.54U} \tag{3.55}$$

$$h_{zo} = 0.123 \cdot (h_{plant} - h_{w0}) \tag{3.56}$$

$$h_{w0} = \frac{2}{3} h_{plant} \tag{3.57}$$

For high plants the minimum of ra is defined as:

$$r_a = \frac{64}{1 + 0.54U} \tag{3.58}$$

with

r_a	aerodynamic resistance (for daily time steps) [s m^{-1}]
h_{ws}	height of wind speed measurement [m]
h_{zo}	aerodynamic roughness length [m]
h_{w0}	height at which wind speed becomes essentially zero in the plant canopy (zero-plane displacement height) [m]

	h_{plant}	effective plant height (thickness of plant canopy) [m]
	U	wind speed, U $\geq$ 0.5 [m s^{-1}]

The equation approaches infinity (a turbulent transfer process no longer occurs) when wind speeds approach zero. Thus, wind speed values less than 0.5 are set to U = 0.5 m/s. It should be mentioned that the equation is restricted to neutral stability conditions, but a stability correction is normally not required in case of daily time steps (see Allen et al. 1998).

The surface resistance describes the resistance of vapour flow through transpiring plants and evaporating surface. The approximation according to Ben-Mehrez et al. (1992), Schulla (1997) and Allen et al. (1998) for densely growing vegetation is based on the minimum stomatal resistance of plant under well-watered conditions, the effective coverage and the day length:

$$r_s = \left(\frac{S}{24 \cdot r_{sd}} + \left(1 - \frac{S}{24}\right) \cdot \frac{1}{r_{sn}} \right)^{-1} \tag{3.59}$$

$$r_{sd} = \left(\frac{A_{LAI}}{r_{sc}} + \frac{1 - A_{LAI}}{r_{ss}} \right)^{-1} \tag{3.60}$$

$$r_{sn} = \left(\frac{LAI}{2500} + \frac{1}{r_{ss}} \right)^{-1} \tag{3.61}$$

$$A_{LAI} = 1 - f^{LAI}; \qquad f \approx 0.7 \tag{3.62}$$

with	r_s	(bulk) surface resistance [s m^{-1}]
	r_{sd}	surface resistance for the bright day [s m^{-1}]
	r_{sn}	surface resistance for the night [s m^{-1}]
	r_{sc}	minimum stomatal resistance [s m^{-1}]
	r_{ss}	surface resistance of bare soil, $r_{ss} \approx 150$ [s m^{-1}]
	S	day length (maximum possible sunshine duration) [h]
	LAI	leaf area index (one sided leaf area per unit ground surface area) [-]
	A_{LAI}	effective vegetation coverage [-]

The effective vegetation coverage defines the part of the leaves that actively contribute to surface heat and vapour transfer (by transpiration processes), which are

usually part of the upper, sunlit areas of a dense canopy. *LAI* values from 2-6 are common for many vegetation and crop types. The minimum stomatal resistance r_{sc} refers to the average resistance of the plant (or individual leaf) under well-watered conditions. It depends mainly on the vegetation type and season. For many plants, a mean daily value of 100 s/m can be estimated when calculations are based on a 24-hr basis (ASCE 1996). Tables for r_{sc} are published in Schulla and Jasper (1999), Krause (2001), Fritsch and Katzenmaier (2001), ASCE (1996). The applied values in MODBIL are listed in Table A.1-A.7 (Appendix).

3.4.7 Land Cover Coefficients for FAO-56-Penman-Monteith Equation

A principal idea of FAO-56-Penman-Monteith approach is the simplification of the vegetation specific physical factors for the calculation of ET_{pot}, because physical factors like the surface resistance factor, albedo or aerial resistance, are difficult to determine. Doorenboos and Pruitt (1977) established empirical coefficients based on world-wide studies, which are documented in the FAO report 'Food and Agriculture Organisation of the United Nations, Irrigation and Drainage Paper 24'. This approach was revised in the later FAO-56 report by Allen et al. (1998).

The principal idea is to estimate the potential evapotranspiration ET_{pot} of a certain crop or vegetation by multiplying the empirical crop coefficient k_c by the reference evapotranspiration ET_0. The crop coefficient k_c merges two different processes: plant transpiration and soil evaporation and can therefore also be expressed by two separate coefficients, the basal crop coefficient k_{cb} and the soil water evaporation coefficient k_e. This is known as the dual crop coefficient approach:

$$ET_{pot} = (k_{cb} + k_e) \cdot ET_0 = k_c \cdot ET_0 \tag{3.63}$$

with	ET_{pot}	potential (crop) evapotranspiration [mm]
	ET_0	reference potential evapotranspiration [mm] (Eq. 3.49)
	k_c	single crop coefficient [-]
	k_{cb}	basal crop coefficient [-]
	k_e	surface evaporation coefficient [-]

According to Burman et al. (1980), Wright (1982), Allen et al. (1989), Allen et al. (1998) the basal crop coefficient k_{cb} defines the ratio of ET_{pot} and ET_0 under conditions in which the soil surface layer is dry and the average water content of the root zone is adequate to sustain full plant transpiration. Thus, k_{cb} marks the baseline potential k_c in the absence of additional effects. The soil water evaporation coefficient k_e describes the surface evaporation component of ET_{pot}. When the earth's surface is wet then k_e is maximal, when it gets drier k_e becomes small and falls near zero once no water is left on the surface. Thus, the difference between k_{cb} and k_c is usually very small for plants that are fully grown. Generally, it can be assumed $k_c \geq k_{cb} + 0.05$ (Allen et al. 1998).

When the FAO-56-Penman-Monteith equation is selected for modelling, then MODBIL requires k_c or k_{cb} coefficients for each land cover type. k_e is not required because MODBIL uses another approach for assessing evaporation and interception effects (see p. 55). Several ways exist for assessing the land cover specific k_c or k_{cb} coefficient. One possibility is to derive the differences between the reference evapotranspiration and the measured ET_{pot} of a vegetated surface, e.g. with the help of lysimeters. Such methods are mostly too expensive and time-consuming, which is why often established values are used from extensive studies like, e.g. Doorenbos and Pruitt (1977), Doorenbos and Kassam (1979), Wright (1982), Allen et al. (1989, 1998). In those studies k-factors were revealed for different land cover types under different climate characteristics. The initial k_c and k_{cb} values used in MODBIL area are derived from those studies and adapted to local conditions. For calibration purposes, the values can be adjusted individually. For better modelling results, it is always recommended to use the dual crop coefficient approach based on k_{cb}, because the evaporation processes, which depend strongly on regional climatic characteristics, can be modelled separately and the crop coefficient k_{cb} is reduced to a plant (transpiration) specific factor.

Both k_c and k_{cb} have to be adjusted if the vegetation and ground cover in different phenological stages differ significantly from normal (mid-season) conditions. For agricultural plants, the determination of three values (initial stage, mid-season stage, late season stage) is sufficient for a good representation of the varying crop. Extensive tables and instructions are given in Allen et al. (1998). The published standard crop coefficients k_c or k_{cb} are valid for a common sub-humid climate with

an average relative daily minimum humidity of 45% and wind speeds averaging 2 m/s. An adjustment for the factors larger than 0.45 is proposed when there are notable differences to the reference climate (see Allen et al. 1998):

$$k_{c,cb} = k_{c,cb(Tab)} + [0.04(U-2) - 0.004(RH_{min} - 45)] \left(\frac{h_{plant}}{3}\right)^{0.3} \tag{3.64}$$

with

$k_{c,cb}$	single or basal crop coefficient [-]
$k_{c,cb(Tab)}$	single or basal crop coefficient for reference climate (see Tables in Allen et al. 1998) [-]
RH_{min}	mean minimum relative humidity ($20\% \leq RH_{min} \leq 80\%$)
U	mean wind speed at 2 m height [m s^{-1}]
h_{plant}	effective plant height [m]

Often, vegetation is not in the state of full cover conditions (for crops defined as $LAI \geq 3$) like natural, non-pristine vegetation, which is usually formed and distributed relatively heterogeneously in space, especially in areas where topography and soil properties are more complex. Several approaches allow an adjustment on the basis of relations between LAI measurements and crop coefficient. Instead of e.g. LAI the adjustments can also be performed using ground cover data describing the fraction of soil surface that is shaded by vegetation. For further details consider Allen et al. (1998).

3.4.8 Surface Evaporation (Interception Losses)

Interception describes the phenomenon of rainfall water collected and temporarily stored on leaves, stems of plants, organic materials or other natural or artificial surfaces. The water is held until it evaporates (surface evaporation), drips off (drip precipitation), or trickles down to the ground (stem flow). The amount of intercepted water depends largely on the type and density of plants, thickness of layer of organic material above the soil, and the properties of artificial surfaces. The highest amounts of interception can be found in forests. Coniferous trees usually intercept more water than deciduous trees because of the higher total surface of the needles holding back the water.

The interception module of MODBIL is designed as a simplified variant of the models from Rutter and Morton (1977), Gash and Morton (1978) and Schulla (1997). More detailed approaches for interception modelling were presented by several authors (e.g. Menzel 1997). They are often not suitable for mesoscale models due to the lack of data required. The incorporated model consists of a simple linear storage that integrates canopy interception storage and other intercepting surfaces, like the layers of organic material, stems of trees, or artificial surfaces (roofs, asphalt, etc.). The storage is modelled on the basis of the cells' specific interception storage capacity IZ_{max}, which represents the amount of water (under zero evaporation conditions) that is left on the saturated, intercepting surfaces after drainage from intercepting surfaces have ceased. MODBIL can handle the IZ_{max} input data as land cover specific information or as spatially distributed information derived from remote sensing products.

MODBIL simulates the dynamics of the interception processes for each time interval in two consecutive modelling steps. In the first step, the filling of the interception storage is simulated. Depending on the storage capacity of the intercepting surface, all or part of the precipitated water is transferred to the interception storage (Eqs. 3.65, 3.66). The other part of the water reaches the soil surface and is considered as throughfall. If the canopy interception storage reaches the maximum storage capacity, then all further (overrunning) water is transferred directly to the the soil surface by drip precipitation and stemflow. The sum of throughfall, drip precipitation and stemflow defines the effective precipitation (Eq. 3.67).

$$IZ_i = IZ_{i-1(end)} + P_i; \qquad IZ_i \leq IZ_{max} \tag{3.65}$$

$$IZR_i = IZ_i - IZ_{i-1(end)} \tag{3.66}$$

$$PE_i = P_i - IZR_i \tag{3.67}$$

with

IZ_i	water in the interception storage at time interval i [mm]
$IZ_{i-1(end)}$	water in the interception storage at the end (after evaporation) of time interval i-1 [mm]
IZR_i	recharge of the interception storage at time interval i [mm]

IZ_{max}	interception storage capacity [mm]
PE_i	effective precipitation at time interval i [mm]
P_i	precipitation at time interval i [mm]

The interception storage capacity is determined as the weighted average of the respective interception storages of vegetated areas (canopy) and non-vegetated areas, depending on the ratio of the covered area. For non-vegetated surfaces a storage capacity of 1 mm is assumed, to take into account evaporation from all types of wet surfaces (rocks, humus, soil, or sealed areas).

The second modelling step refers to the depletion of water from interception storage. Some approaches like Rutter and Morton (1977) mark out a correlation of interception evaporation and potential evapotranspiration considering the ratio of actual stored water and maximum interception storage capacity. In MODBIL an alternative equation is used, which is similar to approaches incorporated in modern water balance models like WaSiM-ETH (Schulla 1997). There, the maximum surface evaporation is related only to potential evapotranspiration and the amount of water in the interception storage:

$$EP_i = \begin{cases} ET_0; & 1.3 \cdot ET_0 \leq IZ_i \\ IZ_i; & 1.3 \cdot ET_0 > IZ_i \end{cases} \tag{3.68}$$

The maximum evapotranspiration under wet surface conditions is known to be higher than the potential evapotranspiration under dry conditions. Hence for days with evaporation from wet surfaces, the potential evapotranspiration is adjusted as follows:

$$ET_{pot}(wet) = ET_{pot} + EP_i; \qquad ET_{pot}(wet) \leq 1.3 \cdot ET_0 \tag{3.69}$$

with	$ET_{pot}(wet)$	adjusted potential evapotranspiration under wet surface conditions at time interval i [mm]
	ET_{pot}	potential (crop) evapotranspiration at time interval i [mm]
	EP_i	evaporation from wet surfaces at time interval i [mm]
	ET_0	reference potential evapotranspiration at time interval i [mm]
	IZ_i	water in the interception storage at time interval i [mm]

Surface evaporation processes provoke a reduced transpiration within the subsequent modelling steps of the time interval as the total sum of evaporation and transpiration processes is limited (see Eq. 3.69).

Interception storage capacity is calculated as the weighted average from the vegetated and non-vegetated parts, depending on the respective vegetation coverage ratio (canopy cover). For non-vegetated surfaces a storage capacity of 1 mm is assumed. The IZ_{max} data for the vegetated area can be retrieved from different publications containing extensive tables or datasets for many land cover classes and vegetation types (e.g. DVWK 1986, Breuer et al. 2003, Schulla 1997, Scurlock et al. 2001). The set of values for the land cover classes used in MODBIL are compiled in Table A.6.

For the individual adjustment of the interception storage data of the study area, the application of further methods is recommended. Several promising approaches are based on the Leaf Area Index LAI, which describes the one-sided leaf area per unit ground surface area. In the present model context it is convenient to consider the LAI as a more general index describing the amount of all intercepting surfaces (natural and artificial) per area. A universally applicable model from Schulla (1997) can be applied for the calculation of the interception storage capacity:

$$IZ_{max} = vc\, h_{SI}\, LAI + (1 - vc)\;\; h_{SI} \tag{3.70}$$

with	IZ_{max}	interception storage capacity [mm]
	LAI	leaf area index (one sided leaf area per unit ground surface area) [-]
	h_{SI}	layer thickness of water body on a surface, 0.1-0.4 (Schulla 1997) [mm]
	vc	fraction of vegetation coverage [-]

This approach has the advantage that it allows the assessment of interception values for areas with or without active vegetation. In the current project, the equation was combined with vegetation specific ratios derived from Breuer et al. (2003). Other approaches, like the empirical equation proposed by Hoyningen-Huene (1983), are used to check the range and plausibility for the values derived:

$$IZ_{max} = 0.935 + 0.498 \cdot LAI - 0.00575 \cdot LAI^2 \tag{3.71}$$

An improvement of the spatial and temporal representation of *LAI*, especially in areas with dense vegetation, may be obtained by the application of remote sensing techniques. Many established approaches are based on the Normalised Difference Vegetation Index *NDVI*, which is highly correlated to the *LAI*, and a well established procedure in remote sensing. The *NDVI* is defined as the ratio between the difference and the sum of near infrared and red spectral data. This works like a measure for green vegetation (amount of chlorophyll), since the active vegetation performing photosynthesis reflects little in the visible spectral range (400 to 700 nm) but strongly in the spectral range of near infrared (700 to 1300 nm). Better results can be obtained if a composite image from different days is calculated allowing to exclude atmospherically contaminated and cloudy areas. For the subsequent conversion from *NDVI* to *LAI* various methods exist (e.g. Myneni and Williams 1994, Sellers et al. 1994). If LAI_{max} for each vegetation unit is known, then the annual cycle of *LAI* can be derived from the monthly or seasonal changes of *NDVI* (Zhangshi and Williams 1997):

$$LAI_i = LAI_{max} \frac{NDVI_i - NDVI_{min}}{NDVI_{max} - NDVI_{min}} \tag{3.72}$$

with
- LAI_i Leaf Area Index at time interval i [-]
- LAI_{max} maximum *LAI* within the annual cycle [-]
- $NDVI_i$ Normalised Difference Vegetation Index at time interval i [-]
- $NDVI_{max}$ maximum *NDVI* within the annual cycle [-]
- $NDVI_{min}$ minimum *NDVI* within the annual cycle [-]

A further possibility is the commonly used approach from Clevers (1989), who described a simplified, semi-empirical model for estimating *LAI* of a green canopy. It is based on the Weighted Difference Vegetation Index *WDVI*, which has the advantage that effects of soil reflectances on *NDVI* are considered. *WDVI* is ascertained as a weighted difference between the measured Near Infrared and Red reflectance, assuming that the ratio between these reflectances for bare soil is constant, which is an assumption that is valid for most soil types (see Eckert and Kneubühler 2004). *WDVI* is ascertained as a weighted difference between measured NIR and red reflectances:

$$WDVI = r_{NIR} - c_s \cdot r_{Red} \tag{3.73}$$

$$c_s = \frac{r_{s,NIR}}{r_{s,Red}} \tag{3.74}$$

Secondly, the *WDVI* is used for the estimation of *LAI* based on an inverse exponential relation (Clevers 1989):

$$LAI = -\frac{1}{c_f}\, ln\left(1 - \frac{WDVI}{\rho_\infty(\lambda_{NIR})}\right) \tag{3.75}$$

with	$WDVI$	Weighted Difference Vegetation Index [-]
	LAI	Leaf Area Index [-]
	c_s	influence of soil reflectance (soil background)
	r_{NIR}	total measured Near Infrared reflectance
	r_{Red}	total measured Red reflectance
	$r_{s,NIR}$	NIR reflectance of the bare soil
	$r_{s,Red}$	Red reflectance of the bare soil
	c_f	complex combination of extinction and scattering coefficients
	$\rho_\infty(\lambda_{NIR})$	limiting value of the *WDVI* at very high *LAI* values

The parameters c_f and $\rho_\infty(\lambda_{NIR})$ have a physical interpretation but have to be estimated empirically (Clevers 1989). Typical values for various plants, seasons and locations can be taken from literature (Bouman et al. 1992, Uenk et al. 1992, Clevers et al. 1994).

3.4.9 Evaporation on Frozen and Snow-Covered Surfaces

Vegetation is largely non-responsive and non-contributing to evapotranspiration when ground surface is frozen or snow-covered. In that case ET_{pot} is reduced and evapotranspiration will be closely related to the albedo and the availability of free water on the surface. Many different studies show that a large amount of factors which control the snow evaporation processes. The values range between -1 and 2 mm/d (see e.g. DVWK 1996, Allen et al. 1998). Snow evaporation is of limited importance compared to snow melting and other processes within the whole water balance. Therefore, a simple approach according to Allen (1996), Allen et al. (1998) was incorporated into MODBIL. On days with snow cover the crop coefficients are

adjusted to $k_c = 0.5$. If the original Penman-Monteith equation is selected then surface resistance and albedo are modified for the respective days. The albedo is set to 0.8 for fresh snow and is reduced gradually to 0.5 for older, possibly discontinuous snow covers.

3.4.10 Evapotranspiration under Water Stress Conditions

The equations discussed for the calculation of potential (crop) evapotranspiration ET_{pot} refer to optimum, disease-free and well fertilised soil water conditions, however environmental stresses have a strong influence on evapotranspiration. In most cases the strongest environmental stress is caused by water limitations. If the plant-extractable soil water drops below a certain threshold, then the plants suffer water stresses and transpiration is reduced. In the model water stress is expressed by the water stress coefficient ws_c and describes the relation between plant-extractable soil water and transpiration (see Chap. 3.6).

The water stress coefficient is primarily related to the plant-extractable soil water content WC and can be influenced by soil and plant properties. If there are no limiting soil water conditions then $ws_c = 1$, else ws_c ranges between 1 and 0 depending on the strength of the water stresses. ws_c becomes 0 when no plant-extractable soil water is left. Several equations were developed for the assessment of the current water stress coefficient at a certain point in time, e.g. by Albrecht (1962), Renger et al. (1974), Sponagel (1980), DVWK (1996), Allen et al. (1998). MODBIL allows the use of three different equations, which are discussed within the soil water balance model description (see Chap. 3.6).

3.5 Infiltration of the Soil

Infiltration refers to the access of water through the upper soil surface into the soil layer. The infiltration rate is primarily controlled by the physical soil properties depending mainly on particle size distribution. Furthermore, land cover characteristics may have some influences, especially regarding sealing, soil compactness and the amount of macropores. Another influence is given by topography through retarded or benefited drainage on the soil surface. During any infiltration event overland flow

is generated on the soil surface in case the top of the soil layer is becoming saturated. This process is also known as 'ponding'.

The simulation of infiltration in MODBIL is based on a modified concept of the infiltration rate equation of Green and Ampt (1911) and enhancements similar to Peschke (1977), Peschke and Gurtz (1987). The approach is used to quantify the infiltrated water and to separate the overrunning water drained by overland flow. The infiltration model is designed as a two-stage model, which respects the consecutive wetting stages. The initial wetting stage, characterised by high infiltration rates, is driven by high adsorption and capillary forces. In the second stage, the wetting and infiltration process is maintained by gravitational forces, while the influence of the capillary forces becomes reduced. The quality of the model results depends on accurate estimates of soil parameters - especially the Green-Ampt infiltration parameters - the saturated hydraulic conductivity and the wetting front suction. Furthermore, the soil water content at the beginning of a rainfall event is required.

For the infiltration model, a homogeneous, one-layer soil model concept is applied, whereby matrix flow is assumed to be dominant (macropore flow is simulated separately). The wetting front is approximated as abrupt transition and the intensity of rainfall is regarded as constant for the time interval. In the first stage of the model the time needed until soil surface saturation occurs under a given intensity of rainfall is calculated. In the second stage the maximum infiltration rate under saturated soil surface conditions for the remaining time of the rainfall event is determined. The surplus of water that can not infiltrate to second stage is diverted and categorised as overland flow.

In the original equation of Green and Ampt (1911), the infiltration rate f_i is related to the saturated hydraulic conductivity k_s and the soil water state θ_i:

$$f_i = -k_s \left(\psi_f \, \frac{\theta_s - \theta_i}{Inf_i} + 1 \right) \tag{3.76}$$

Inf_i, f_i, and ψ_f becomes positive by a rearrangement of the equation:

$$f_i = k_s \left(\psi_f \, \frac{(\theta_s - \theta_i)}{Inf_i} + 1 \right) \tag{3.77}$$

with f_i Green and Ampt infiltration rate at time step i [mm h^{-1}]

k_s hydraulic conductivity of the soil under saturated conditions [mm h^{-1}]

θ_i	initial soil moisture content [$m^3\ m^{-3}$]
θ_s	soil moisture content at saturation [$m^3\ m^{-3}$]
ψ_f	suction at wetting front [mm]
Inf_i	cumulative infiltration at time step i [mm]

When θ_i approaches θ_s then one has $(\theta_s - \theta_i) \approx 0$ and $f_i \approx k_s$. In the next step modifying Eq. 3.76 gives the cumulative infiltration Inf_i as a function of infiltration rate f_i:

$$Inf_i = -\psi_f \frac{\theta_s - \theta_i}{1 + \frac{f_i}{k}}; \qquad |f_i| < -k, \quad Inf_i < 0 \tag{3.78}$$

If rainfall intensity is constant and exceeds saturated hydraulic conductivity ($PI > k_s$), then at a defined point in time the surface will become saturated. At this moment infiltration rate equals precipitation rate. The depth INF_u infiltrated at this moment can be calculated by modifying Eq. 3.77 and then solving the equation for INF_u (Eq. 3.79). The infiltration rate f_i is given by the rainfall intensity PI:

$$INF_u = \frac{(\theta_s - \theta_i)\psi_f}{\frac{PI}{k_s} - 1}; \quad PI > k_s \tag{3.79}$$

The time t_u needed until surface saturation can be derived by transformation of this equation (Peschke 1977, Peschke and Gurtz 1987):

$$t_u = \frac{INF_u}{PI} = \frac{\left(\frac{(\theta_s - \theta_i)\ \psi_f}{PI/k_s - 1}\right)}{PI}; \quad PI > k_s \tag{3.80}$$

And the infiltrated amount of the first wetting stage under unsaturated conditions is given by:

$$INF_u = t_u \cdot PI \tag{3.81}$$

with	INF_u	infiltration under unsaturated soil surface conditions [mm]
	PI	rainfall intensity [mm h^{-1}]
	k_s	hydraulic conductivity of the soil under saturated conditions [mm h^{-1}]
	t_u	time until saturation of the soil surface [h]
	ψ_f	suction at wetting front [mm]

In the second modelling stage, the amount of infiltrated water under saturated conditions is calculated. There, the maximum infiltration rate INF_s is assumed to be equal to the hydraulic conductivity under saturated conditions ($f \approx k_s$) as a result of Eq. 3.77:

$$INF_s = PE - INF_u; \qquad PE < INF_s + INF_u \tag{3.82}$$

with	INF_s	infiltration under saturated soil surface conditions [mm]
	INF_u	infiltration under unsaturated soil surface conditions [mm]
	PE	effective precipitation [mm]

Total infiltration INF is calculated from the sum of infiltration under saturated and unsaturated conditions of the soil surface:

$$INF = INF_u + INF_s \tag{3.83}$$

The amount of water that cannot be infiltrated is diverted as overland flow OF, which is also known as direct runoff or also runoff of soil surface:

$$OF = \begin{cases} PE - INF; & INF < PE \\ 0; & INF \geq PE \end{cases} \tag{3.84}$$

with	OF	overland flow [mm]
	INF	infiltration to the soil [mm]
	PE	effective precipitation [mm]

In the case of urbanised or industrialised areas, where the land surface is partially sealed, the infiltration and the overland flow is modified as follows:

$$INF_{seal} = (1 - vs) \cdot INF \tag{3.85}$$

$$OF_{seal} = OF + vs \cdot INF \tag{3.86}$$

with	INF_{seal}	infiltration to the soil on partially sealed surface [mm]
	OF_{seal}	overland flow on partially sealed surface [mm]
	vs	areal fraction of sealed surface [-]

The saturated hydraulic conductivity k_s and the wetting front suction ψ_f are the key parameters of the infiltration module. A distributed model like MODBIL requires

the definition of a k_s value for each soil type of the study area spatially resolved for each cell. The parameters can either be estimated by laboratory or field techniques, or by the application of equations like pedotransfer functions (PTFs) or specific tables (Allen et al. 1998, AG Boden 1994). PTFs allow the assessment of soil hydraulic properties on the basis of easily measured soil physical properties, such as particle size distribution and bulk density. For the current project a PTF published by Saxton et al. (1986) was used, which is also available as a free software tool called 'Soil Water Characteristics' (Saxton 2007). For a detailed description of the respective equations please consider the publication of Saxton et al. (1986). The good performance of the Saxton PTF compared to others was confirmed by Tietje and Hennings (1996). Alternative PTF approaches used for valuation were also presented by Cosby et al. (1984), Brakensiek et al. (1984), Vereecken et al. (1990) and Schaap et al. (2001).

The value of the wetting front suction ψ_f can be determined by PTFs. Furthermore, an equation of Schulla and Jasper (1999) can be used for the determination of the wetting front suction:

$$\psi_f = \frac{1}{\alpha}\left[\left(\frac{\theta_i - \theta_r}{\theta_s - \theta_r}\right)^{-\frac{1}{m}} - 1\right]^{\frac{1}{n}} \cdot 1000 \tag{3.87}$$

However, the derivation of the required empirical soil parameters can be avoided if another, less precise and very rough estimation is applied in MODBIL, which is tested here, to be sufficient within this model scale:

$$\psi_f = 10 \cdot 10^{\left(4.2 - 2.2\frac{\theta_i}{\theta_{FC}}\right)} \tag{3.88}$$

with	ψ_f	suction at wetting front [mm]
	θ_i	actual soil moisture content on time interval i [m^3 m^{-3}]
	θ_r	residual soil moisture content when hydraulic conductivity is $k = 0$ [m^3 m^{-3}]
	θ_s	soil moisture content at saturation [m^3 m^{-3}]
	θ_{FC}	soil moisture content at field capacity [m^3 m^{-3}]
	α, m, n	empirical parameters depending on the soil physical properties (see Schulla and Jasper 1999)

3.6 Soil Water Balance

The soil-water module in MODBIL calculates the daily soil water balance for each time step and each cell. The processes are simulated based on a one-layer model, which is represented by means of a container in which water content can fluctuate. In a preliminary step, the determination of field capacity, wilting point and effective rooting depth for each cell are required in order to assess both the actual plant-extractable soil water content and the plant-extractable soil water content at field capacity.

Field capacity and wilting point can either be derived from tables (e.g. Allen et al. 1998, AG Boden 1994) or more accurately by Pedo Transfer Functions (PTFs), as well as through field and laboratory studies (see p. 65). The derived and applied values for the soils on different hydrological units of Cyprus are listed in Table 4.4.

Rooting depth can be assessed from field observations and from established values in literature. Extensive studies and tables for specific plants and land cover types can be found in various publications, such as Breuer et al. (2003), Allen et al. (1998), DVWK (1996), Schulla (1997), Fritsch and Katzenmaier (2001). For Cyprus, field observations, as well as studies from Reger (2004) and Dünkeloh (2005a) were considered and listed in Tab A.3 (Appendix).

The plant-extractable soil water content in the root zone defines the amount of water which can be held against gravity and can be extracted at the same time by plant roots. The water above field capacity is drained as it cannot be held against gravity. Residual water below wilting point cannot be extracted any more from plant roots due to the high adsorption and capillary forces. The plant-extractable soil water content WC in the root zone can be derived from the soil moisture content and the effective rooting depth through the following equations:

$$WC_i = 1000\ (\theta_i - \theta_{WP})\ Z_r \tag{3.89}$$

$$WC_{FC} = 1000\ (\theta_{FC} - \theta_{WP})\ Z_r \tag{3.90}$$

with
- WC_i actual plant-extractable soil water content in the root zone on time interval i [mm]
- WC_{FC} plant-extractable soil water content in the root zone at field capacity [mm]

	θ_i	actual soil moisture content on time interval i [m^3 m^{-3}]
	θ_{FC}	soil moisture content at field capacity [m^3 m^{-3}]
	θ_{WP}	soil moisture content at wilting point [m^3 m^{-3}]
	Z_r	effective rooting depth [m]

The plant-extractable soil water content depends on several variables like inflow, soil water state, outflow and extraction from the soil. Water is added to the soil layer by soil surface infiltration after rainfall and irrigation events or by capillary rise from the groundwater. In contrast, water is removed from soil water storage by evapotranspiration, interflow and deep percolation:

$$WC_i = WC_{i-1} + (INF_i + CR_i + I_i - ET_{act,i} - INT_i - DP_i) \tag{3.91}$$

with	WC_i	actual plant-extractable soil water content in the root zone on time interval i [mm]
	WC_{i-1}	plant-extractable soil water content in the root zone on the previous time interval [mm]
	INF_i	infiltration to the soil on time interval i [mm] (Eq. 3.83)
	CR_i	capillary rise at time interval i [mm]
	I_i	net irrigation infiltrating to the soil at interval i [mm]
	$ET_{act,i}$	actual (crop) evapotranspiration adjusted to water stress conditions at time interval i [mm] (Eq. 3.93)
	INT_i	interflow at time interval i [mm] (Eq. 3.103)
	DP_i	deep percolation at time interval i [mm] (Eq. 3.102)

The daily interflow INT and deep percolation DP are controlled by soil properties and soil water state (see Chap. 3.8). The amount of daily infiltrated water INF_i depends on soil properties and effective precipitation (see Chap. 3.5). In some areas additional water is available by irrigation I or capillary rise CR from shallow groundwater tables. The additional water prevents plants from water stresses. The respective cells must be specified in a preliminary step. Remote sensing techniques (different vegetation activity) or the application of topographic indices, facilitate identification and classification of such areas. Usually, these areas are located in flood plains of valleys, nearby lakes, coastal areas or other depressions.

In MODBIL the surplus of evapotranspiration due to additional water is called sec-

ondary evapotranspiration. It plays an important role especially for water balancing in semiarid and arid areas.

$$ET_{sec} = ET_{pot} - ET_{act} \tag{3.92}$$

with	ET_{sec}	secondary evapotranspiration [mm]
	ET_{pot}	potential evapotranspiration (without water stress) [mm]
	ET_{act}	actual evapotranspiration adjusted to water stress conditions without additional water from shallow groundwater or irrigation [mm]

If no water from shallow groundwater or irrigation is available, then the consideration of water stress is necessary for the determination of daily water extraction from soil by evapotranspiration. Water stress can be expressed by the water stress coefficient ws_c, describing the relation between actual plant-extractable soil water and transpiration:

$$ET_{act} = ws_c \cdot ET_{pot} \tag{3.93}$$

with	ET_{act}	actual (crop) evapotranspiration adjusted to water stress conditions [mm]
	ET_{pot}	potential (crop) evapotranspiration without water stresses [mm]
	ws_c	water stress coefficient [-]

ws_c depends primarily on the actual plant-extractable soil water and can be modified by specific soil and plant properties. Three different approaches describing the relationship between actual plant-extractable water content and transpiration are incorporated in MODBIL and can be individually selected for a model run.

The simplest equation is based on the original approach of Albrecht (1962), who assumes that the ratio of the actual plant-extractable water content in the root zone to the plant-extractable water content at field capacity is similar to the ratio of actual and potential evapotranspiration. Later studies show that this relationship often underestimates the actual evapotranspiration, because plants do not necessarily suffer water stress when the actual soil water content drops below field capacity.

An advanced relationship was proposed by Renger et al. (1974) respectively:

$$ws_c = 0.2 + 2\left(\frac{\theta_i - \theta_{WP}}{\theta_{FC} - \theta_{WP}}\right) - 1.2\left(\frac{\theta_i - \theta_{WP}}{\theta_{FC} - \theta_{WP}}\right)^2 \tag{3.94}$$

Later this equation was also recommended for the study of local climatological conditions by the German Institute for Standardisation published in DIN 19685 (DIN 1997/2002). The equation gives a mean relationship that cannot be adjusted easily to specific vegetation types. Therefore, the FAO approach from Allen et al. (1998) presented a different concept similar to Albrecht (1962) assuming a linear relationship of the evapotranspiration in relation to the plant-extractable soil water:

$$ws_c = \begin{cases} 1; & \theta_t \leq \theta_i \\ \left(\frac{\theta_i - \theta_{WP}}{\theta_t - \theta_{WP}}\right); & \theta_{WP} < \theta_i < \theta_t \\ 0; & \theta_i \leq \theta_{WP} \end{cases} \tag{3.95}$$

$$\theta_t = (1 - p_r)(\theta_{FC} - \theta_{WP}) \tag{3.96}$$

with

ws_c	water stress coefficient [-]
θ_i	actual soil moisture content on time interval i [m^3 m^{-3}]
θ_t	threshold soil moisture content where plant water stresses start [m^3 m^{-3}]
θ_{FC}	soil moisture content at field capacity [m^3 m^{-3}]
θ_{WP}	soil moisture content at wilting point [m^3 m^{-3}]
p_r	portion of total extractable water that plants can extract from the root zone without water stress (typical range: $p_r = 0.3...0.7$; standard value: $p_r = 0.5$) [-]

The approach is enhanced by a plant specific threshold θ_t, which marks the soil moisture state up to which all readily available water is consumed and at which plants begin to experience water stress. Then, soil water becomes more strongly bound to the soil matrix and more difficult to extract. The reduced plant evapotranspiration is expressed by the factor ws_c. When water content drops below the wilting point θ_{WP}, no further soil water is extracted by plants any more.

The threshold θ_t depends mainly on plant and also partly on soil characteristics. This is introduced in the model by the parameter p_r, which has to be determined

according to local conditions. Alternatively, values from extensive tables, e.g. in Allen et al. (1998), can be used. If no detailed data is available, then $p_r = 0.5$ is commonly assumed for typical plant conditions (see Allen et al. 1998: p. 162).

3.7 Macropore and Bypass Flow

The quick movement of water in structural soil features like root channels, wormholes, soil cracks or other large cavities or fractures in soils, is called macropore flow. The movement into and through the macropores is driven only by the force of gravity. It controls water transfer from macropores into the surrounding soil matrix, as well as the amount of infiltration, interflow and deep percolation (Germann and Beven 1981, Beven and Germann 1982, Ghodrati and Jury 1990, van Genuchten et al. 1990, Gish and Shirmohammadi 1991).

According to Dyck and Peschke (1995), the diameters of macropores are greater than 2-3 mm but there is no general convention for the definition of macropores (Uhlenbrook and Leibundgut 1997). Weiler and Naef (2003) mark that the mechanisms controlling macropore flow are not very well known. It was observed that only a few macropores contributed significantly to the total macropore flow, whereas the majority of macropores received little water. Furthermore, a large spatial variation of macropores is also typical for small areas.

Through the macropores, water can bypass the soil layer and move rapidly into deeper layers. This process is known as bypass flow, and can be relevant for the assessment of groundwater recharge and interflow within water balance studies. Bypass flow is most notably controlled by the amount and intensity of rainfall, the value of saturated hydraulic conductivity at the soil surface, absorption of water by the soil matrix and the geometry of the macropore system (Hoogmoed and Bouma 1980, Booltink and Bouma 1993, Booltink et al. 1993).

Several studies marked that the application of complex physical approaches does not often lead towards better results. Moreover, the approaches are mostly not well-founded concerning the representation of the complex and varying natural conditions, especially when modelling large areas (Braun 2002, Beisecker 1994). Therefore, conceptional approaches are preferred, which are nowadays typically based on

two principal ideas. One concept is the adjustment of saturated hydraulic property of the soil (see e.g. Bronstert 1994, Merz 1996):

$$k_{s,adj} = \left[1 + (MP_f - 1)\frac{\theta_i - \theta_m}{\theta_s - \theta_m}\right]; \quad \theta_m < \theta_i < \theta_s \tag{3.97}$$

with
- $k_{s,adj}$ adjusted hydraulic conductivity of the soil under saturated conditions considering macropore effects [m s^{-1}]
- k_s hydraulic conductivity of the soil under saturated conditions (without macropore effects) [m s^{-1}]
- θ_i actual soil moisture content on time interval i [m^3 m^{-3}]
- θ_s soil moisture content at saturation [m^3 m^{-3}]
- θ_m minimum soil moisture content where macropore flow is assumed [m^3 m^{-3}]
- MP_f factor of macroporosity depending on root depth and season (see Bronstert 1994, Braun 2002) [-]

The concept is based on the idea that the drainage through macropores becomes higher through higher soil water content. The factor MP_f depends primarily on root density, depth, and biological activities within the soil layer. In deeper zones, effective macroporosity becomes lower. On soils without relevant macroporosity, the factor is $MP_f = 1$. Under normal conditions, MP_f typically varies between 2 and 3 in depths of 0.6 to 0.8 m (see Braun 2002). Values of $MP_f > 10$ can be found, especially in areas with a very dense root network as in forests, or at the climax of the vegetation period in the upper soil zone. Therefore, hydraulic conductivities can easily become ten times higher then they would in the same soil without vegetation. For further details determining MP_f, Bronstert (1994) and Braun (2002) may be considered.

The concept serves for the adjustment of hydraulic conductivity of the soil, but macropore flow events bypassing the whole soil layer cannot be dissolved. However, modelling results for Cyprus showed that the consideration of bypass flow is of importance for a better simulation of groundwater recharge. Hence an individual concept was incorporated into MODBIL based on a dual-permeability approach, which is also known as the double porosity approach (see e.g. MACRO model by Jarvis et al. 1991 and Ludwig et al. 1999). It describes water flow in the soil layer

by separating the flow in the soil matrix domain and flow in the macropore domain. The macropore domain includes the overcapillary-sized pores as well as the larger and more continuous capillary-sized pores bigger than 30 μm (Germann 1990). The fractions of macropores vary typically between 0.2 and 5 Vol.% (Chen and Wagenet 1992) and flow speed up to 25 cm/s are possible within the macropores (Bouma et al. in Zuidema 1985). Therefore, it can occur that 40-80% of the effective precipitation infiltrates through macropores (Beisecker 1994, Liermann 1999). According to Beven and Germann (1981), macropore flow can only be generated after minimum rainfall intensities of 1-10 mm/h. Hydraulic conductivity of macropores depends on a couple of factors; normallly soil water content of the surrounding matrix, geometry of the macropores and water available within the macropores. Fast macropore flow due to hydrophobicity of very dry soils is also possible and documented, e.g. in Beven and Germann (1982). The definition of hydraulic conductivity of macropores, as it is implemented in several models (see e.g. MACRO model Jarvis et al. (1991), is often considered as not well founded (Beisecker 1994) due to complex and varying natural conditions, especially for large areas.

The individual solution designed for MODBIL considers only the part of infiltrating water that bypasses the entire soil column by fast vertical flow through macropores. The concept principally considers the theoretical ideas for the generation of macropore flow from Beven and Germann (1981). It deals with the problem that macropore flow can also occur after small rainfall events and depends strongly on the amount of macropores that effectively drain water through the soil layer. For the incorporated approach, a factor called effective macroporosity for bypass flow, was introduced. It refers only to the network of active macropores contributing to the fast vertical flow through the complete soil column.

The bypass flow module consists of two stages. The first stage simulates the beginning of a rainfall event in which only matrix flow is prevalent. A threshold MP_t up to the beginning of macropore flow is calculated. This can be defined as a specific amount of rainfall or alternatively as the time till ponding on the soil surface (see Chap. 3.5).

In the second stage, matrix and macropore flow occur at the same time. The model for this stage is based on the widely used concept of dual porosity, where the macropore flow is controlled by the fraction of effective macroporosity of the whole cell

area. A value for the hydraulic conductivity of the macropores is not applied because in this context the only relevant part of macropore flow is that, which bypasses the whole soil layer and percolates to the bedrock. All further macropore flow is assumed to be secondarily infiltrated into the soil matrix. Therefore, this bypass flow through macropores BY is especially limited by the hydraulic conductivity of the bedrock and the effective precipitation:

$$BY = (PE - MP_t)\,\frac{MP_{by}}{100}; \qquad BY \leq k_{sub,s}\,t_r\,\frac{MP_{by}}{100} \tag{3.98}$$

with

	BY	bypass flow [mm]
	MP_t	threshold for the beginning of macropore flow [mm]
	MP_{by}	effective macroporosity for bypass flow [Vol.%]
	PE	effective precipitation [mm]
	$k_{sub,s}$	hydraulic conductivity of the bedrock under saturated conditions [mm s^{-1}]
	t_r	rainfall duration after macropore flow started [s]

3.8 Direct Runoff and Groundwater Recharge

High soil water state and bypass flow processes initiate lateral drainage of soil water and percolation to deeper layers. The term interflow refers to the part of water, which drains laterally through the uppermost layers without contact to the water table until reaching a stream channel or another body of water at the land surface. The deep percolation comprises the other part of the water, which percolates to the layers below the root zone and becomes unavailable for vegetation and evapotranspiration. It is assumed that under normal geological conditions, most of the water percolates to the water table and can therefore be considered potential groundwater recharge.

The model simulates deep percolation and interflow on the base of soil water state, bypass flow, physical soil properties, physical bedrock properties and terrain slope. The drainage starts when bypass flow occurs or when soil water content exceeds field capacity caused by an infiltration event. Then soil water, which cannot be held

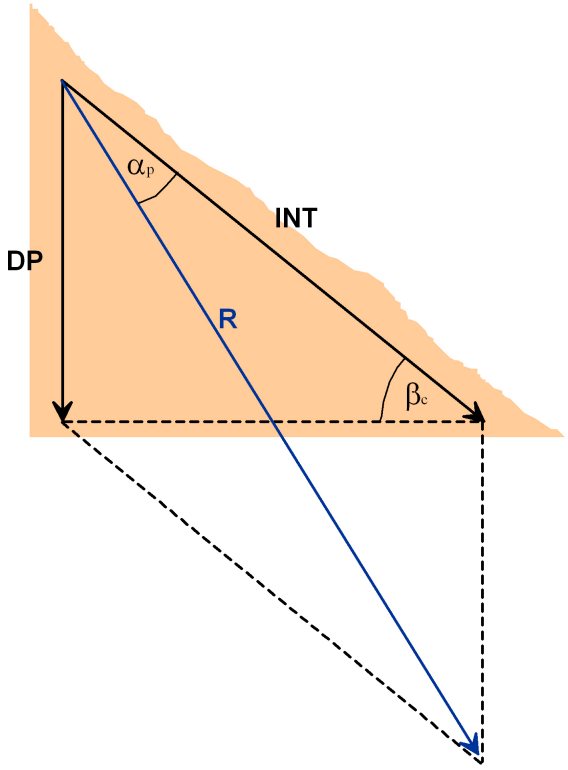

Figure 3.3: Geometrical simplification used for describing the relation between interflow *INT* and deep percolation *DP* based on Cabral et al. (1992) and Rasmussen (2005).

against gravity, percolates downwards:

$$PC_i = \begin{cases} BY_i; & \theta_i \leq \theta_{FC} \\ (\theta_i - \theta_{FC}) + BY_i; & \theta_i > \theta_{FC} \end{cases} \tag{3.99}$$

with	PC_i	percolation at time interval i [mm]
	BY_i	bypass flow at time interval i [mm]
	θ_i	actual soil moisture content at time interval i [m^3 m^{-3}]
	θ_{FC}	soil moisture content at field capacity [m^3 m^{-3}]

Depending on terrain slope and hydraulic conductivity of the bedrock, the percolating water is divided into a vertical and a lateral component. Cabral et al. (1992) point out that a geometrical simplification shown in Fig. 3.3 is suitable for most issues. Therefore, the basic relation between interflow and deep percolation can be

described as follows (see also Rasmussen 2005):

$$\frac{DP_i}{INT_i} = \frac{sin(\alpha_p)}{sin(\frac{\pi}{2} - (\beta_c + \alpha_p))} = \frac{sin(\alpha_p)}{cos(\beta_c + \alpha_p)} \tag{3.100}$$

$$\alpha_p = \frac{\pi}{2} \cdot e^{-k_p \cdot \beta_c} \tag{3.101}$$

$$DP_i = PC_i \left[\frac{sin(\alpha_p)}{\left(\frac{sin(\alpha_p)}{cos(\beta_c + \alpha_p)} + 1 \right) cos(\beta_c + \alpha_p)} \right]; \quad DP_i \leq k_{sub,s} \cdot t_l \tag{3.102}$$

$$INT_i = PC_i \left[1 - \frac{sin(\alpha_p)}{\left(\frac{sin(\alpha_p)}{cos(\beta_c + \alpha_p)} + 1 \right) cos(\beta_c + \alpha_p)} \right] \tag{3.103}$$

with

	INT_i	interflow at time interval i [mm]
	DP_i	deep percolation at time interval i [mm]
	PC_i	percolation at time interval i [mm]
	$k_{sub,s}$	hydraulic conductivity of the bedrock under saturated conditions [mm s^{-1}]
	β_c	terrain slope [rad]
	α_p	angle between terrain surface and flux-vector [rad] (see Fig. 3.3)
	k_p	regional calibration coefficient for adjustment of the relation between interflow and deep percolation; (Cyprus: $k_p = 1.35$) [-]
	t_l	length of time interval i [s]

The maximum amount of DP_i is limited by the hydraulic conductivity of the bedrock $k_{sub,s}$ (see Eq. 3.102). In case of the calculated DP_i being greater than DP_{max}, the surplus of water is added to interflow INT_i. Exceptional cases include saturated conditions, when water is drained by saturation excess in form of overland flow. Under plain terrain conditions ($\beta_c = 0$), lateral drainage does not start before soil water content reaches saturation ($\theta_i = \theta_s$).

Direct runoff is the sum of overland flow and interflow. Total runoff or discharge refers to the total amount of water flowing into a stream consisting of the sum

of direct runoff and baseflow. In a quasi-closed catchment the generated baseflow results from the re- and discharge of the aquifer reservoir (see Chap. 3.9):

$$Q_{dir} = OF + INT \tag{3.104}$$

$$Q_{tot} = Q_{dir} + Q_{base} \tag{3.105}$$

with

Q_{dir}	direct runoff [mm]
Q_{tot}	total runoff/discharge [mm]
Q_{base}	base flow [mm]
OF	overland flow [mm]
INT	interflow [mm]

3.9 Calibration by Catchment Response

Calibration of the water balance model was performed by the comparison of recorded and modelled discharge. Suitable data are river discharge time series of smaller catchments (subcatchments), which are mostly dominated by outflow from a shallow groundwater reservoir, interflow and direct runoff. The algorithm of single linear reservoirs (Maillet 1905), which may still be regarded as one of the most important approaches in hydrogeology, can be applied (Fröhlich et al. 1994, Nathan and McMahon 1990, Wood et al. 1992, Schwarze et al. 1997). Some studies point out that natural storage effects are not always linear (Prasad 1967). In this case, more complex approaches with nonlinear relationships between discharge Q and storage S_t (e.g. Wittenberg 1999) can be applied. In the current project adequate results were achieved with the linear approach.

For the calibration of MODBIL, an additional module called MODBIL-DC was developed, allowing the discharge simulation for defined catchments with a combined linear catchment response routine. The module is designed as a two reservoir concept based on the linear reservoir equation by Maillet (1905). The first reservoir simulates discharge by base flow, the second one discharge by direct runoff. Overland flow is assumed to drain directly without passing a reservoir. The total discharge is given by the sum of three single discharge processes.

As input data, daily groundwater recharge, interflow and direct runoff results from the main water balance model MODBIL are required. Furthermore, the analysis of recorded stream hydrograph recession curves is necessary for the determination of reservoir discharge characteristics. According to the function of Maillet (1905), the recession of base flow is described as follows:

$$Q_t = Q_0 \, e^{(-t/k_m)} \tag{3.106}$$

This implies that the storage is proportional to outflow:

$$S_t = k_m \cdot Q_t \tag{3.107}$$

$$Q_t = \frac{S_t}{k_m} \tag{3.108}$$

with	Q_t	discharge from the storage at time step t [mm]
	Q_0	initial discharge [mm]
	k_m	retention constant that represents storage lag-time
	t	elapsed time [d]
	S_t	storage content at time step t [mm]

The interflow reservoir depletes quickly and discharge occurs only for a short period of time (usually not more than 2-7 days after the rainfall event). It is mainly influenced by topography and soil properties. The depletion from the groundwater reservoir is slower and depends mainly on geological conditions. Both reservoirs are supposed to have quick responses after a recharge event. For many groundwater reservoirs, this can be explained by a mobilisation of old, pre-event groundwater, whenever percolating rain water raises the level and hydraulic head of the groundwater reservoir.

For the determination of the catchment specific parameter k_m MODBIL-DC analyses, the whole hydrograph time series and extracts, all segments that are not influenced by rainfall or snow melting processes. This extraction is based on precipitation and temperature information, which is retrieved from meteorological station data. A threshold of five dry days is used to separate undisturbed baseflow from the whole

discharge. Then for each separated segment, the gradient of $log(Q_t)$ against t is calculated. The parameter k_m is finally retrieved as the weighted mean gradient of all segments. The weighting depends on the total time length of each segment and aims to give more importance to longer and less disturbed segments.

The parameter k_m and the actual storage content S_t allow the simulation of the baseflow Q_{base} of each catchment or subcatchment using Eq. 3.108. For the interflow, a simple storage can also be assumed, or a simple empirical relationship can be applied for simulating the depletion.

After the determination of k_m, the parameter serves for analysing the baseflow in the recorded hydrograph time series. MODBIL-DC performs an automatic baseflow separation for long time series of daily discharge, based on a modified approach from Fröhlich et al. (1994), Wittenberg (1999). The calculation starts at the end of the time series and proceeds backwards along the time axis. Eq. 3.106 is used to calculate the baseflow value for the previous day based on the baseflow of the actual day and recession constant (see also Fig. 3.4).

At a certain point, the reverse computed recession curve reaches the transition point when the total hydrograph switches from a falling limb to a rising limb. For the rising limb, base flow values are found as computed recession for one time step forward for each given total flow value (see transition curves, Fig. 3.4). If the conditions of the total hydrograph nearby the transition point become unclear due to multiple alternations of rising and falling limbs, then both variants are calculated and the smaller of both values is selected.

The original recorded hydrograph time series may have errors due to inaccuracies of monitoring techniques. Therefore, some routines are implemented for error detection and correction. Several algorithms check for outliers or consistency within dry time periods (> 5 days and no snow melting) when total discharge is controlled exclusively by baseflow. Unreasonable high or low discharge values on subsequent days in the recorded time series are corrected.

Calibration is performed by comparing modelled and recorded base flow and total runoff/discharge of defined catchments or subcatchments. For a study area with a great diversity, the calibration of several catchments with different conditions is recommended to optimise the values for most land cover, soil and geological units.

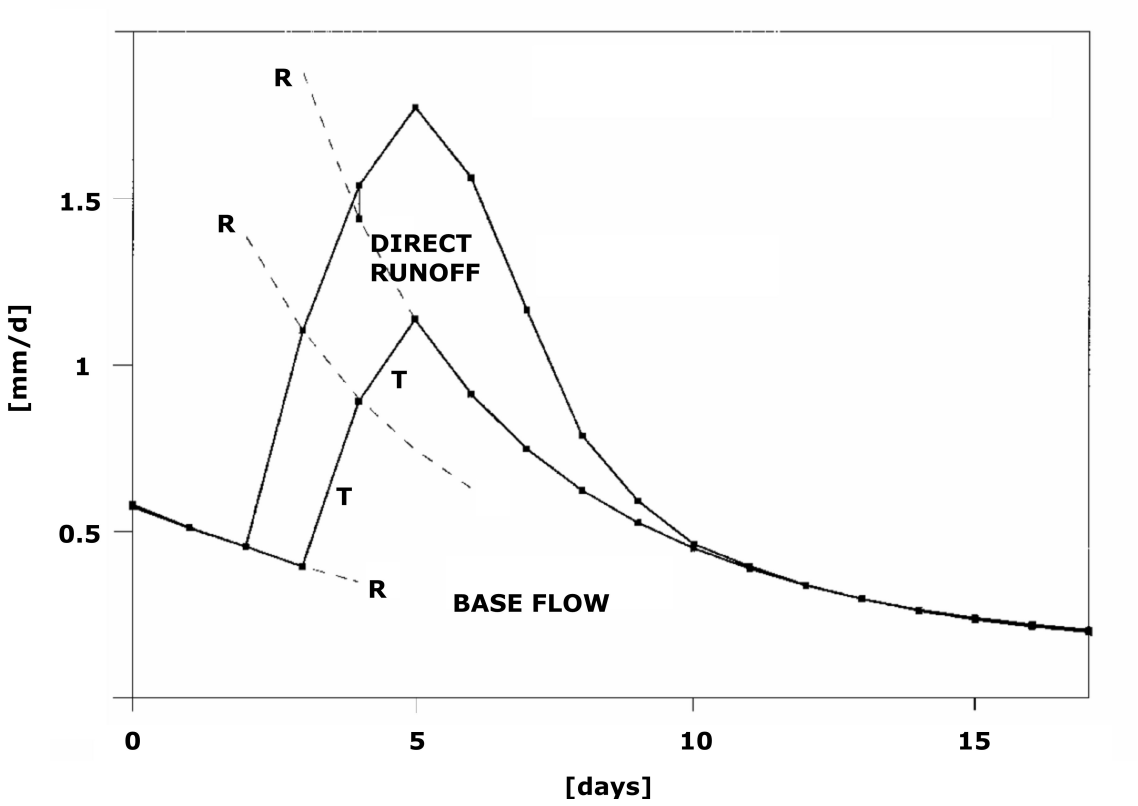

Figure 3.4: Separation of direct runoff and base flow on the base of recession curves (R) calculated by Eq. 3.106. The figure also describes the construction of transition curves (T) between two or more recession curves according to Wittenberg (1999).

Validation can be performed by application of calibrated values in further catchments. If available, groundwater recharge results can also be compared to groundwater level records or to the results of other methods, like the chloride mass balance or isotope methods. The results are influenced notably by input data quality. A dense network of meteorological stations with daily data and application of remote sensing techniques contribute substantially to better model results.

3.10 MODBIL User Interface

A new graphic user interface for MODBIL V49/2009 (Dünkeloh and Udluft, 2009) was developed in the framework of this project. It allows an easy and comfortable handling of all important files and parameters of the water balance model. Profiles

can be created for saving the configuration of each model run. The core of the water balance model was developed in Visual Basic 6 and Fortran 95 and is compatible to all common Microsoft Windows Versions (95/98/Me/NT/2000/XP/Vista/7) as well as to most Unix and Linux operating systems. The interface of the Windows version consists of eight tab controls of different categories with which the files and parameters can be specified. In the Unix Version, all files and parameters are defined directly in a pre-formatted control file.

Profiles

The first tab 'Profiles' is opened automatically when the model software is started. Existing profiles can be loaded by navigating through directories, selecting and loading a profile file (file extension '.ctrl'). The stored settings are imported and shown in different tabs of the interface. The profile can be modified and later exported to a new profile. It is recommended to save the profile in the same directory where all other associated input data files are stored.

Raster

The 'Raster' tab allows the specification of a template file, which consists of a rectangular raster map defining relevant and non-relevant cells for water balancing. It facilitates the definition of study areas and subsequent modelling of different catchments within the study area without changing any other input data.

If a template file is selected, important control parameters are displayed automatically, showing the dimension and references of the base raster. The given columns, rows, referencing (specified by x and y coordinates of the lower left corner) and the cell size are required to be identical in all raster files. The referencing must be based on a metric reference system (metric coordinates). Additionally, the mean latitude (geographical) of the study area has to be defined in this tabular.

Topography

The 'Topography' tab allows the determination of the raster files with the topographical information for the study area. Raster files for elevation, slope and exposition

are required. The raster must be congruent to the raster stored in the template file (see above). Further file format specifications and instructions can be found in Chap. 3.11.

Meteorology

In the 'Meteorology' tab, all meteorological parameters and files have to be specified for a model run. Mandatory time series are daily precipitation, minimum temperature, maximum temperature and minimum relative humidity. Optionally, the model can be enhanced by adding maximum relative humidity, wind speed, sunshine duration (or global radiation) and rainfall intensity.

Furthermore, the regional precipitation gradient (%/100 m) and the temperature gradient (°C/100 m) are required to be specified in the tab. These parameters serve for an enhanced interpolation routine considering elevation effects of the study area.

Several options serve as an automatic adaptation or transformation of improper input data types. One option allows the use of mean temperature time series instead of minimum temperature. A second option enables an analogue feature for mean and maximum relative humidity data. The internal adaptation of the time series is performed according to the FAO guidelines described in Allen et al. (1998). A further setting allows the determination of a land-sea factor if no sunshine or global radiation time series exist. The procedure estimates radiation based on the daily maximum and minimum temperature according to the FAO guidelines (Allen et al. 1998).

If no wind speed time series and rainfall intensities are available, then the used mean monthly or yearly values can be defined in an additional meteorological parameter file. The name of the parameter file can be specified in the 'Meteorology' tabular.

Land Cover

The 'Land Cover' tab helps to organise all files containing land cover (vegetation) and irrigation characteristics. The land cover raster file contains a land cover identification number (or land cover class) for each cell of the study area. The raster must be congruent (same resolution and extension) to the standard raster (template file).

In an associated land cover parameter file, all relevant parameters and characteristics for each land cover class are stored. Handled parameters are interception storage, fraction of vegetation coverage, secondary evapotranspiration (general), secondary evapotranspiration (by irrigation), fraction of sealed surfaces, adjustment factor for hydraulic conductivity, factor of macroporosity for effective bypass flow, land cover specific crop coefficient for evapotranspiration (k_c, k_{cb} or f_{Haude}), effective rooting depth, fraction of plant-extractable water without water stress (plant specific factor p), albedo, effective vegetation height, leaf area index and surface resistance. Whether a parameter is really needed, depends on the configuration of a model run, e.g. albedo, effective vegetation height, leaf area index and surface resistance are only required when the original Penman-Monteith approach is applied. In contrast, for the application of the FAO-56-Penman-Monteith or Haude equation, the land cover (vegetation) specific crop coefficient or Haude factor is required. The fraction p of plant-extractable water without water stress is required only if the actual evapotranspiration is calculated on the base of the water stress approach according to Allen et al. (1998). Furthermore, in the 'Land Cover' tab an optional irrigation raster file can be defined, which allows allocation of cells with irrigation and individual irrigation periods.

Soil and Geology

In the 'Soil and Geology' tab, the files and model options for soil and geology are specified. For both layers, the saturated hydraulic conductivity is required as spatially distributed information. As in all other raster files, the stored raster must be congruent to the standard raster in the template file. Furthermore, the field capacity is required for the soil layer, which can be specified as absolute field capacity in millimeters or as relative field capacity in mm/m. If the raster is based on relative field capacity, an additional raster with effective rooting depth in meters is required. Alternatively, the effective rooting depth from the land cover parameter file can be used, which allows the specification of monthly variable values (see above). A further option in this tab is the deactivation of the macropore/bypass flow module.

Model Options

The 'Model Options' tab contains all further options and preferences for a run of the water balance model. A start and end day can be determined when the model period should only comprise a part of the total meteorological time series. Furthermore, the relevant equations for potential and actual evapotranspiration have to be selected. For potential evapotranspiration, the current software version supports the original Penman-Monteith, FAO-56-Penman-Monteith and Haude equations. If the Haude equation is selected then temperature and relative humidity at 14 h are required, instead of maximum temperature and minimum relative humidity. For the calculation of actual evapotranspiration, a proprietary MODBIL approach or the equations from Renger et al. (1974) and Allen et al. (1998) are supported.

The 'Model Options' tab also allows the configuration of the interpolation routine. First the amount of comprised neighbouring stations for interpolation has to be determined. The Shepard (1984) routine for directional isolation can be activated for an enhanced weighting. A second option allows additional weighting of elevation differences. A further option allows performing interpolation of relative humidity on the base of absolute humidity. This option is only given if temperature data is available for all stations with records of relative humidity. Current project results showed that the last two options lead towards better interpolation results, especially in mountainous regions. A further option allows the enabling or disabling of an additional adjustment of meteorological values (radiation, temperature and humidity) on the base of cell inclination and exposition.

Output Options

In the 'Output Options' tab, an output directory and output filename prefix for all results of a model run (raster maps and time series) have to be specified. For all water balance parameters mean raster maps for the whole modelling period are automatically exported. Additionally, yearly, monthly, 5-day or daily raster maps can be created for desired water balance parameters. Daily time series with mean values for the whole study area are also saved. A further option allows the export of additional files, which are suitable for a visualisation of the water balance dynamics within the IDL (Data Visualisation Solutions) software package.

3.11 MODBIL File Formats

Raster Files

MODBIL V49/2009 handles all input and output raster files in the ArcRaster file format. This file type is also known as 'ArcInfo ASCII grid' or 'ASCII raster' file. It refers to a widely used interchange file format within geographical information systems and was originally developed for the ESRI ArcInfo software package. The typical extension of an ArcRaster file is 'asc'. The format consists of a 6-line header that specifies the geographic domain and resolution followed by the actual cell values.

The geographic header of the file contains important parameters for the raster file (see example in Fig. 3.5). 'ncols' refers to the number of columns in the grid; 'nrows' to the number of rows in the grid; 'xllcorner' to the lower left corner of the grid and gives the x-coordinate as a numerical value; 'yllcorner' to the lower left corner giving the y-coordinate as a numerical value; 'cellsize' to the dimension of a cell. 'Nodata_value' is an optional header line and refers to the value used for missing data.

MODBIL requires that the coordinates given in 'xllcorner', 'yllcorner' are based on a metric reference system (e.g. UTM, Gauss-Krüger). Furthermore, 'xllcorner', 'yll-corner' and 'cellsize' must be given as integer values (not floating point values). For a correct interpolation during the model run, all coordinates of the meteorological stations are required to be in the same reference system.

The data block follows below the header lines. Each integer or floating point value represents information for an individual cell. Each row of the grid is stored in a separate row/line of the file. The data block starts with the upper left corner of the whole grid and ends with the lower right corner. All values must be separated by one or more blanks (blank space). Special characters, like tabs, semicolons or commas are not allowed.

The import and export of the ArcRaster file type is possible to and from nearly all of the established GIS software packages, like Clark Labs IDRISI GIS, ESRI ArcView 3.x, ESRI ArcGIS, Manifold, GRASS GIS (open source), etc. In some packages the activation or installation of extensions may be necessary, as in the case of ArcGIS. A detailed description about the import and export of ArcRaster files to different

```
ncols 12                                          <- header row 1
nrows 60                                          <- header row 2
xllcorner 438700                                  <- header row 3
yllcorner 3876300                                 <- header row 4
cellsize 50                                       <- header row 5
nodata_value -99                                  <- header row 6 (optional)
22 23.5 21 -21 20.4 21.8 23 23.3 25 26 ...        <- data row 1
-59 66 73 79.6 86 92 97.4 102 106 100 ...         <- data row 2
103.1 98.7 94 89.5 83 78.1 72 67 61 56 ...        <- data row 3
...                                               <- data row x
```

Figure 3.5: Format convention for MODBIL raster files based on ArcRaster file format.

GIS systems can be found as attachment file in the MODBIL V49/2009 software package.

Meteorological Station and Data Files

The development of MODBIL V49/2009 was accompanied by the reorganisation of meteorological data file formats to take into account the individual station network architecture of the different meteorological parameters. It considers that there are, for instance, more rain gauges than thermometers or hydrometers. The network of wind and radiation recorders is often very sparse. The new file structure allows an independent interpolation for each meteorological parameter.

Each meteorological parameter has its own station and data file. The station file contains the monitoring network for the respective meteorological parameter. Each row defines a name, X-coordinate, Y-coordinate and elevation of a station (see Fig. 3.6).

A minimum of one station is required in a valid station file. The different values must be separated by one or several blanks (blank space). Special characters like tabs, semicolons or commas are not allowed. The station coordinates should be consistent with the reference system of the ArcRaster files. The file name extension 'dat' is proposed for the files.

"S2 SMIGIES" 438700 3876300 330	<- data row 1
"S15 KATHIKAS" 448238 3863948 650	<- data row 2
"S18 POLIS CHRYSOCHOUS" 448311 3876886 15	<- data row 3
"S30 ACHELEIA" 452700 3843592 45	<- data row 4
...	<- data row x

Col. 1: Number and/or name of the station. Quotation marks are required to enclose expression!

Col. 2: X-coordinate of the station's location.

Col. 3: Y-coordinate of the station's location.

Col. 4: Elevation in meters.

Figure 3.6: Format convention for MODBIL meteorological stations files.

"precip" S2 S15 S18 S30 ...	<- header row
"01.10.1987" 16 0.3 0 0.7 ...	<- data row 1
"02.10.1987" 11 2.3 3 7.1 ...	<- data row 2
"03.10.1987" 0 0 0 0 ...	<- data row 3
"04.10.1987" 2 0.6 0 0 ...	<- data row 3
...	<- data row x

Figure 3.7: Format convention for MODBIL meteorological data files.

The data file contains the time series of all stations defined in the station file (see Fig. 3.7). The header row does not have to be formatted in a specific way. It can be used to associate the station names to each column for improved clarity. The number of data rows is equivalent to the number of days in the time series. Each row stores the respective date in the first column and the values for the stations in the consecutive columns. The requested date format is: "DD.MM.YYYY". Leading zeros are not necessary (e.g. "10.9.2004" instead of "10.09.2004" is possible). The date information has to be enclosed by quotation marks.

The first data column will automatically be associated with the station in the first line of the station file, the second data column to the second station in the station file, etc. The given station name in the data file is not relevant for the association. Consequently, the number of data columns must be equivalent to the number of rows given in the station file.

In the station file all values must be separated by one or several blanks (blank

space). Special characters like tabs, semicolons or commas should not be used. Missing values are not allowed and should be eliminated in a preliminary step by the application of the additional module MODBIL EMV 2.0. Its recommended to use the file name extension 'dat' for all data files.

A large variety of software can be used to create and export the required ASCII files. Golden Software Surfer or Golden Software Grapher software package are particularly suitable for the creation and formatting of the files because the data files are directly compatible to the required format. A detailed description about the creation and export of ASCII data files can be found there attached to the MODBIL V49/2009 software package.

Chapter 4

Data

4.1 Topography

All spatial data of the study area is arranged in the Universal Transverse Mercator (UTM) coordinate system, which allows the application of a two-dimensional Cartesian coordinate system for modelling. The International Ellipsoid WGS84 is used as the underlying ellipsoidal model for the UTM coordinate system. The coordinates for Cyprus are arranged within the sector UTM zone 36 North.

For the generation of the digital elevation model (DEM) of Cyprus, digitised topographical maps (vector files of contours) were used and subsequently processed with GIS routines. The test of several routines showed that optimum results are retrieved when the raster DEM is not derived directly from the contours file, but rather on the basis of a TIN (Triangulated Irregular Network) elevation model, which has to be calculated in an earlier step from the digital contours map data. Subsequent model corrections are performed by the application of a 'pit removal' routine, which eliminates blind drainage areas and depressions in valleys, resulting from raster effects in the interpolation routine. The final DEM for Cyprus comprises an area of 9246 km^2 in a 50 m x 50 m raster box resolution (see Fig. 4.2). The small difference to the official size of Cyprus (9251 km^2) results from generalisation effects at parts of the coast line.

Raster models for slope and exposition (Fig. 4.3, 4.4) are also calculated with GIS routines based on the TIN elevation model. The retrieved models are arranged as

Figure 4.1: Regional division of Cyprus used for the description of parameters and water balance results. For delimitation criteria see Table 4.1.

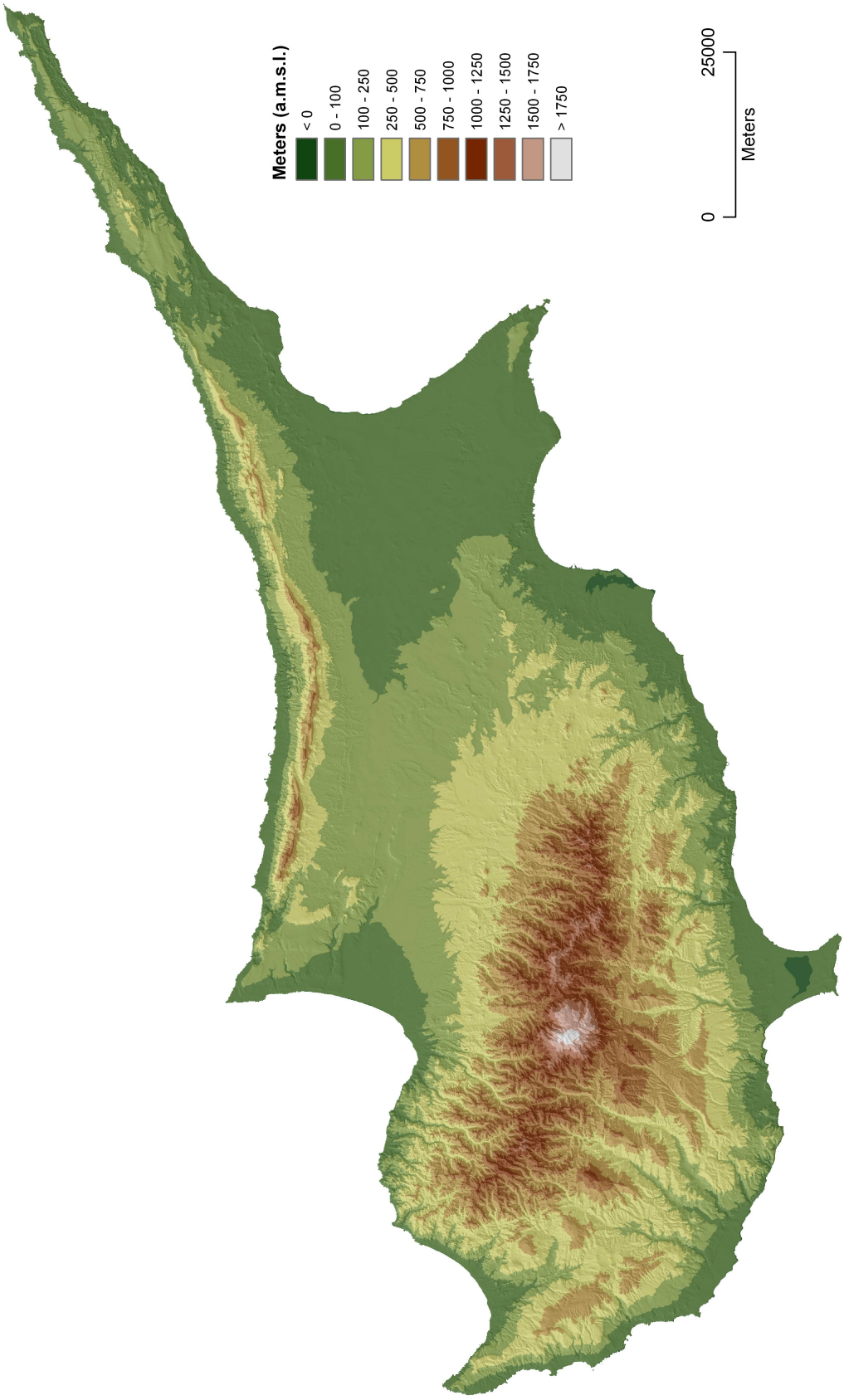

Figure 4.2: Digital elevation model of Cyprus.

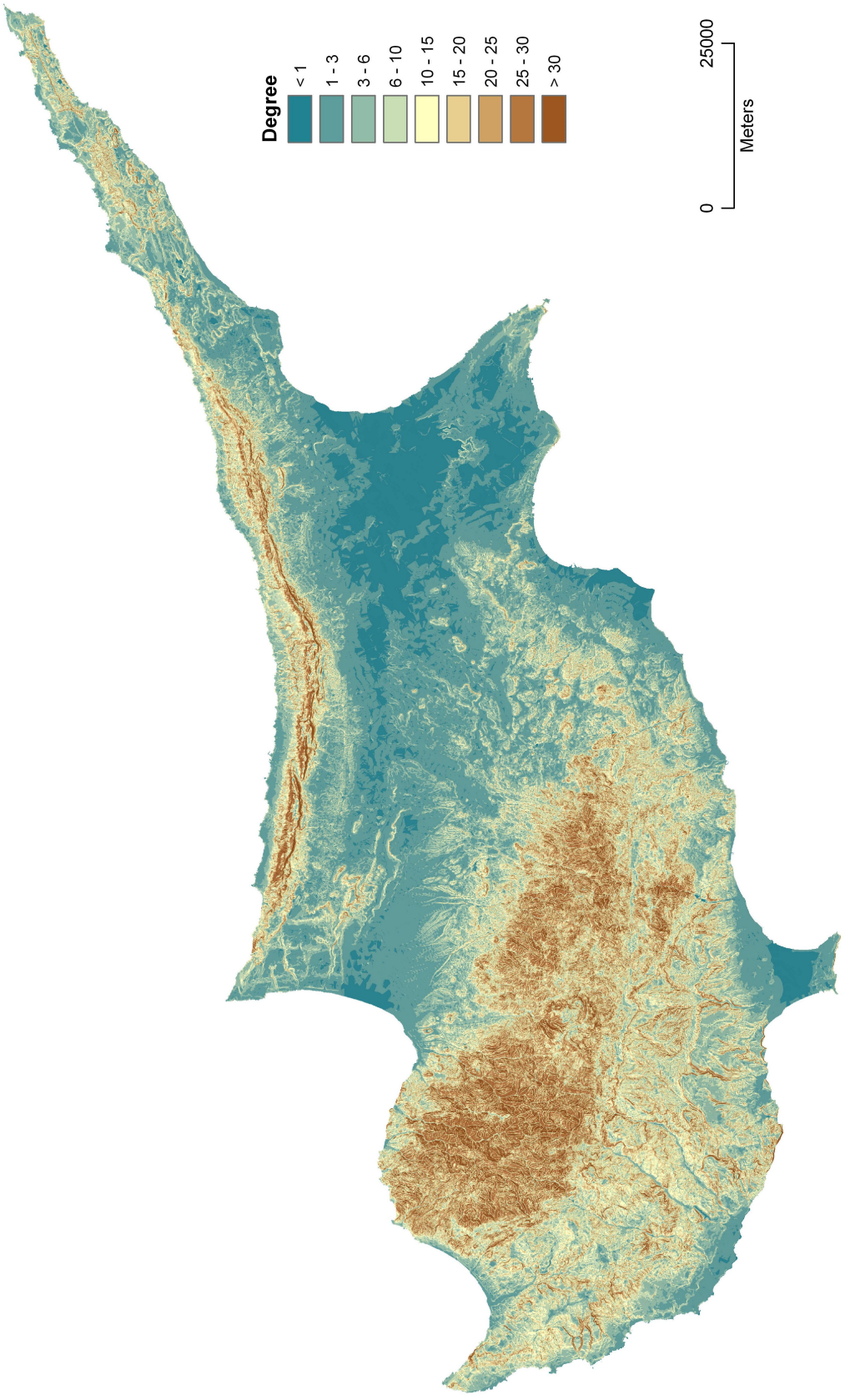

Figure 4.3: Digital slope model of Cyprus.

Figure 4.4: Digital exposition model of Cyprus (N = 0°, E = 90°, S = 180°, W = 270°).

Table 4.1: Compilation of topographical parameters for Cyprus on the base of the regionalisation shown in Fig. 4.1.

Parameter	Cyprus	Southern Cyprus[a]	Troodos[c]	Northern Cyprus
Area[b] [km^2]	9245.8	5995.4	1601.7	3250.5
Mean elevation [m]	297.1	388.2	740.4	129.1
Maximum elevation [m]	1951.0	1951.0	1951.0	1024.0
Mean slope [degree]	8.7	10.7	19.8	5.0

[a] includes the Republic of Cyprus, UK Sovereign Base Areas, United Nations Buffer Zone

[b] the difference between the DEM and the official area (9251 km^2) arises from generalisation effects at the coastline

[c] area delimitation on the base of geological formations: Basal Group, Sheeted Dyke Complex, and all plutonic rocks of the Troodos terrane (not Anti-Troodos)

congruent rasters with respect to the DEM raster. The analysis of the results allows the determination of mean topographical characteristics for bot the whole island and specific areas (see Table 4.1). The derived mean elevation of Cyprus is approx. 297 m. Single values range between -2 and 1951 m. This reflects the mountainous character of the island, which is more distinctive in the southern part where large parts are dominated by the Troodos massif.

The calculated raster models serve for the calculation of further GIS products, such as the stream network, watershed limits and watershed areas of specific gauging stations, which are needed for calibration purposes (see Fig. 4.12).

4.2 Meteorology

In contrast to other Mediterranean countries, the Meteorological Service of Cyprus maintains an excellent network of meteorological stations. It is characterised by a dense monitoring network, which registers all important meteorological parameters on daily or smaller time units. For some important parameters, like precipitation, very long time series exist, covering most of the 20th century. Common problems are missing values within the times series and network changes, which arise due to abandonment, new installations and changes of sites.

For the water balance model, daily datasets between January 1961 and February

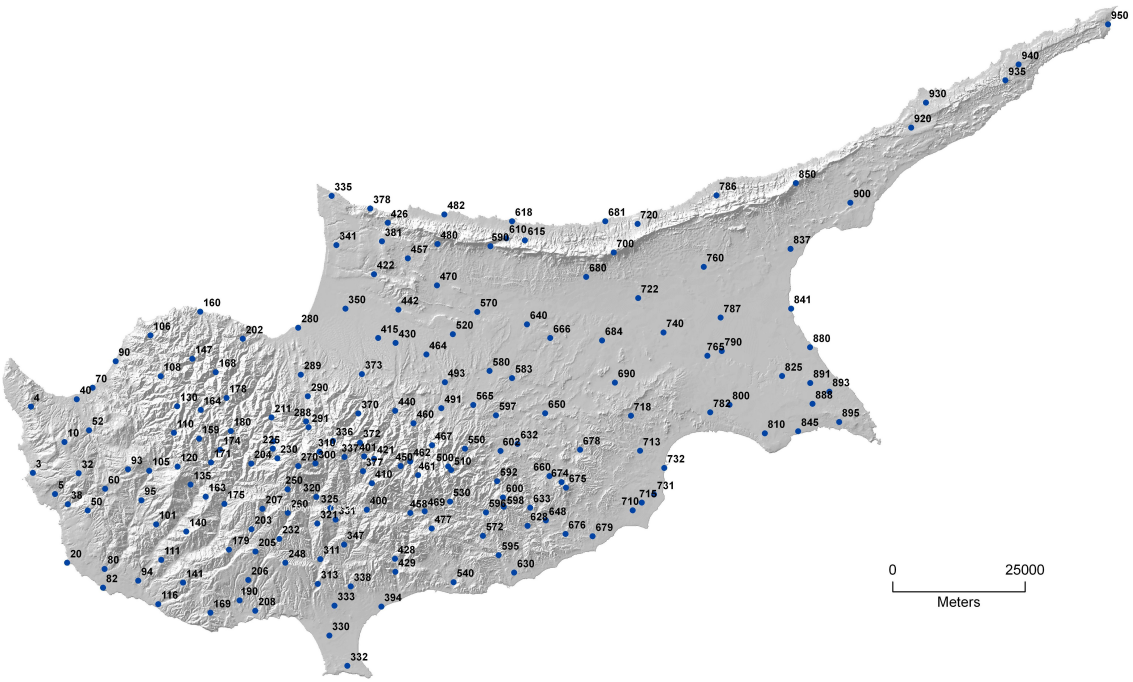

Figure 4.5: Network of 191 selected rain gauges on Cyprus.

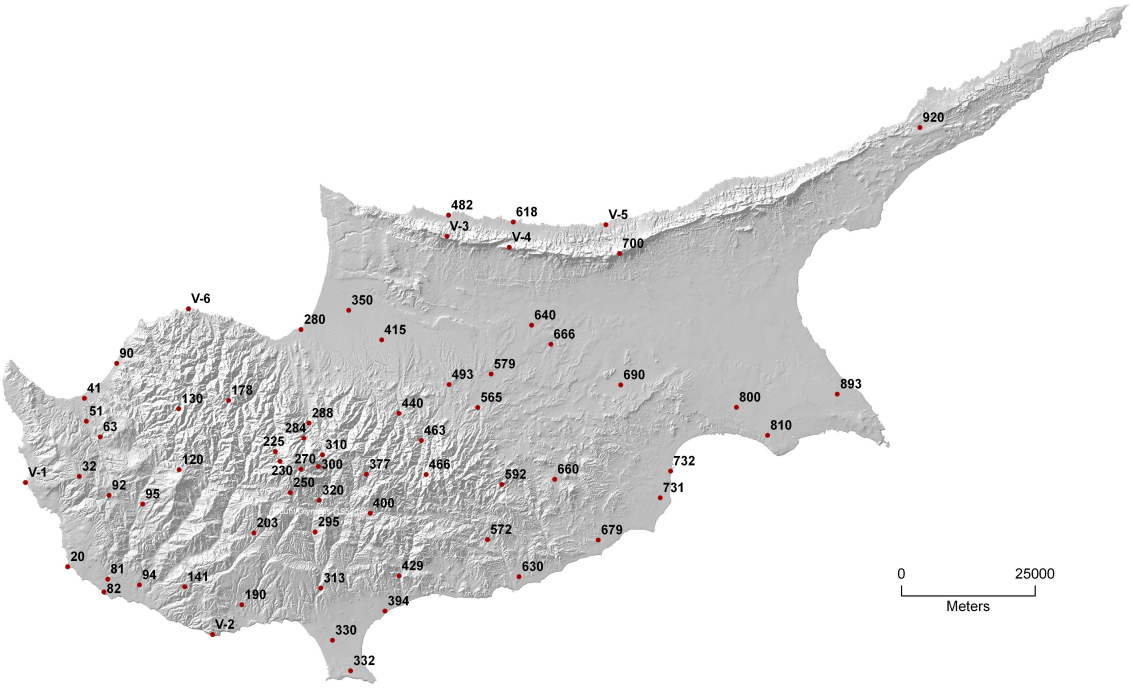

Figure 4.6: Network of 60 selected recording stations and 6 virtual stations for temperature and relative humidity.

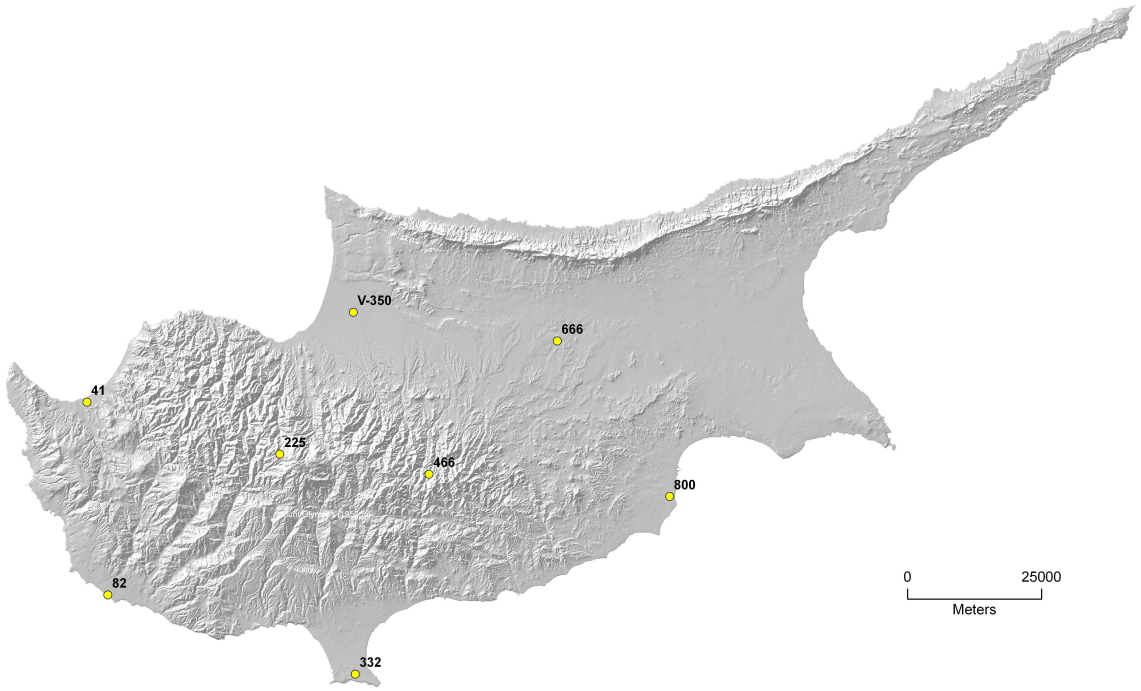

Figure 4.7: Network of seven selected recording stations and one virtual station for sunshine duration.

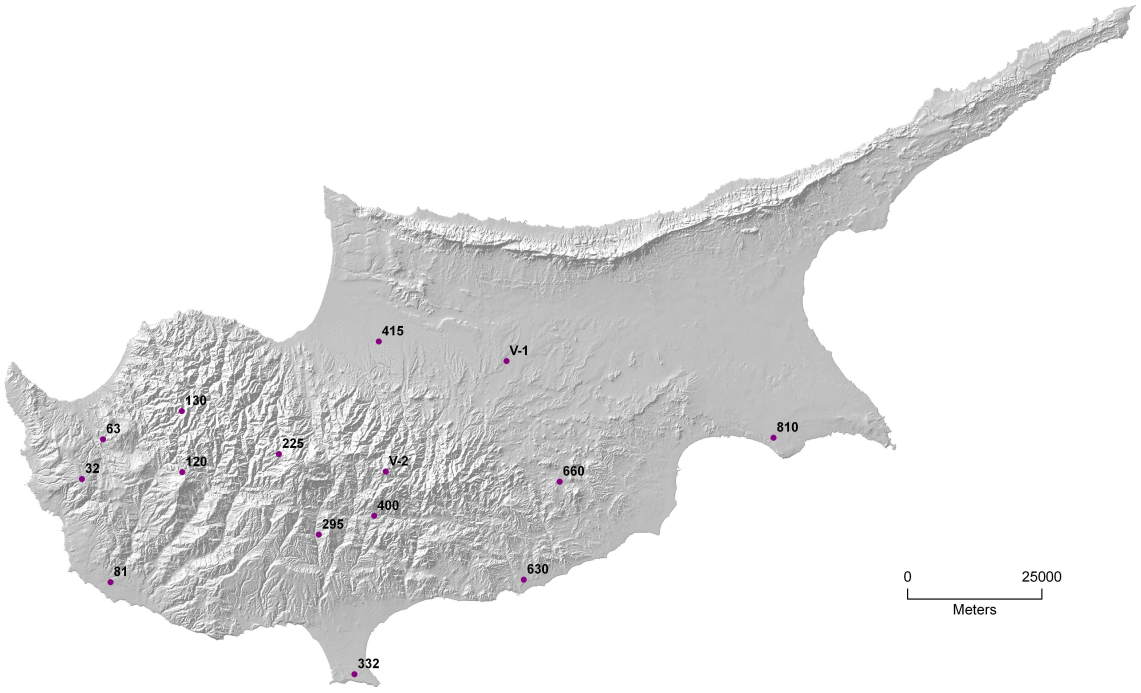

Figure 4.8: Network of 13 selected recording stations and two virtual stations for wind speed.

2005 were prepared. The selected period includes the climate normal period 1961-1990, 1971-2000 and the compete climate record period including the most recent datasets up to February 2005. In a pre-processing step, all stations, parameters and time series were checked. Stations with insufficient amount of total daily datasets were discarded. A minimum of ten years for precipitation and five years for other parameters was required. In some exceptional cases in Northern Cyprus, shorter time series were also included, due to very sparse available recordsets for that area and the lack of data since 1974.

The rain gauges network used for precipitation consists of a total of 191 stations (see Fig. 4.5). 40 stations are located in Northern Cyprus with time series ending in 1974. For temperature and humidity 60 stations (six stations in Northern Cyprus) are used and complemented by six virtual supporting stations (see Fig. 4.6). These virtual stations are constructed for the improvement of the final interpolations results of MODBIL. Such virtual supporting stations are added to coastal areas without stations. Time series are retrieved from the neighbouring coastal stations with similar characteristics. Further virtual stations were also added to places in Northern Cyprus like the Kyrenia range, which is scarcely covered by the network available.

Only a sparse network exists for sunshine duration and wind speed. The prepared network of sunshine data consists of seven stations and one supporting virtual station in the western Mesaoria (see Fig. 4.7). Missing data in some station time series is filled with data from neighbouring stations, or by interpolation based on standardised time series (see below). Sunshine duration data for Northern Cyprus is not available.

The applied final network of wind speed data consists of 13 stations and two virtual supporting stations (one coastal and one in the Troodos massif; see Fig. 4.8). Reliable wind speed datasets before January 1976 are not available. Missing values are filled with monthly averages for the period of January 1976 until December 2004. The density of the station network available seems to be insufficient for a good interpolation of wind speed in this complex topographical island environment, where wind speeds differ extremely within small areas. Furthermore, wind speed data for Northern Cyprus is not available. For those reasons, the influence of wind speed had to be reduced within the water balance modelling for Cyprus.

Erroneous values (outliers) or stations with anomalous trends are discarded in a further consistency check. Missing values are filled by interpolation from neighbouring stations based on standardised data calculated for the overlapping periods (not for precipitation). The applied interpolation routine is equivalent to that from MODBIL (see Chap. 3.3.2: p. 26). After a destandardisation of the estimated values, a consistent set of time series without missing values is obtained for water balance processing. For humidity data, better interpolation results are retrieved by converting all data from relative humidity to absolute humidity before interpolation.

Unavailable and sparse data for Northern Cyprus since 1974 are a result of the political situation. Existing stations serve as supporting points for the missing years, keeping the local climate characteristics on the basis of averages and standard deviations. The yearly, monthly and daily variability for the later years are simulated by extrapolation from stations of Southern Cyprus.

4.3 Land Cover

A first classified map of hydrological relevant land cover units was developed within the GRC-project (Udluft et al. 2004b). Remote sensing techniques were used for the classification of a LANDSAT-TM5 scene and the creation of a land cover map in a 50 x 50 m resolution (Reger 2004). This map was revised and enhanced by field studies and further analysis of LANDSAT-TM5 data. Additional land cover classes were defined, and further remote sensing techniques (unsupervised classification routines) were applied for the improvement of the distribution of land cover units. The final map describes the land cover of the island based on 13 different classes (see Fig. 4.9). Areal statistics of the different classes are compiled in Table 4.2). Generalisation effects as a result of raster resolution can cause areal underestimation of less frequent land cover types, which appear in disconnected, very small pieces, such as vineyards, smaller irrigation areas, or sealed areas.

The final map shows the detailed land cover unit distribution and reveals typical characteristics of different landscape units in Cyprus. The Troodos massif and the Kyrenia range are the most densely wooded areas on the island. The high forest areas are mainly pine forests with trees of *Pinus brutia*. The forests often are not very dense and show more resemblance to Maquis or Garrigue formations with some

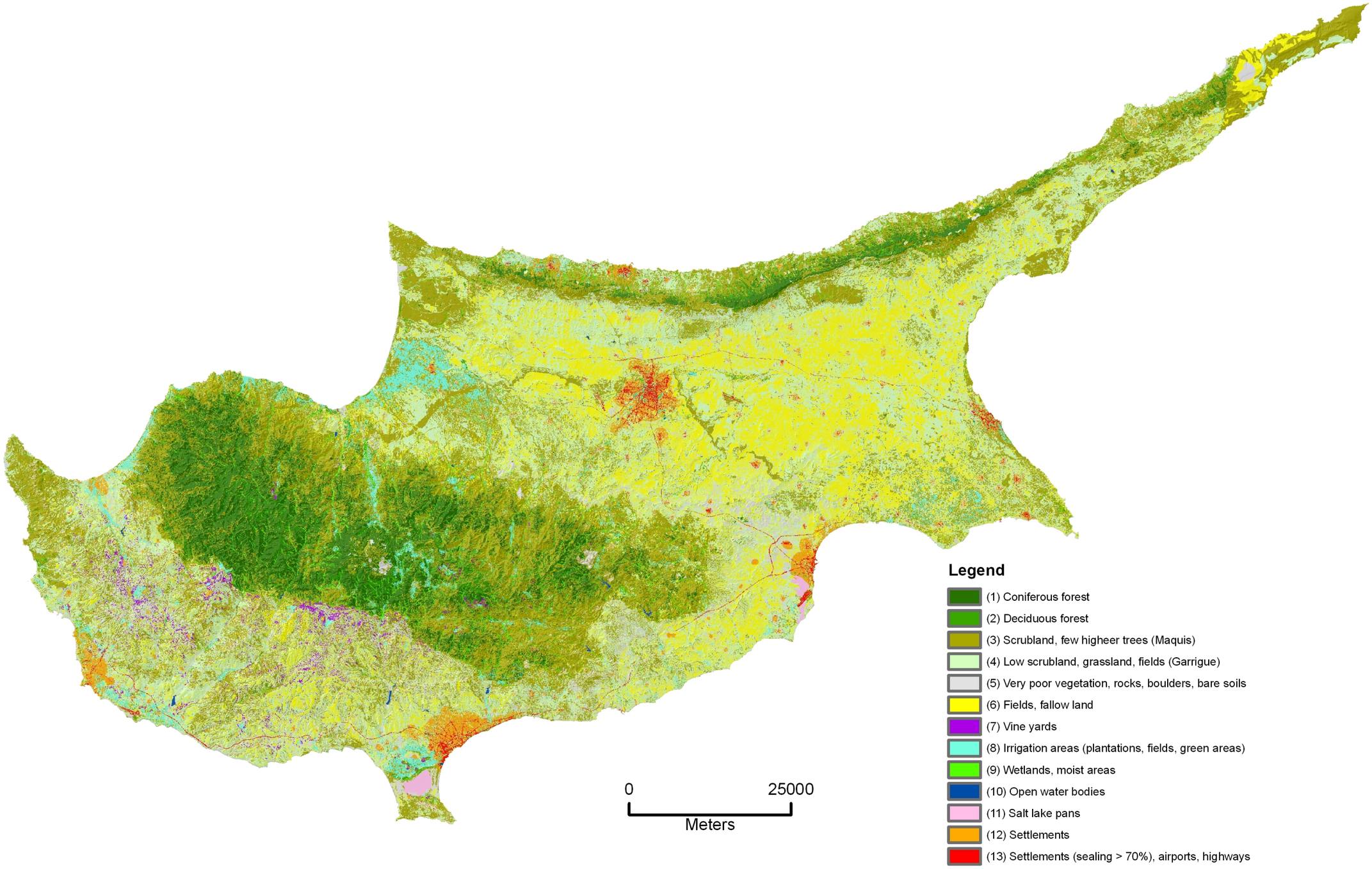

Figure 4.9: Hydrological land cover classes for Cyprus.

Table 4.2: Areal extension of land cover classes of Cyprus. The calculated areas are based on the classified land cover map of 50 x 50 m cells (Fig. 4.9). Areal underestimation can occur due to generalisation effects, especially for land cover types of limited extend, which often appear in very small isolated areas (e.g. vineyards).

Land cover class		Cyprus		Southern Cyprus		Troodos		Northern Cyprus	
		Area [km^2]	Prop. [%]	Area [km^2]	Prop. [%]	Area [km^2]	Prop. [%]	Area [km^2]	Prop. [%]
1	Coniferous forest	850.9	9.2	749.6	12.5	671.0	41.9	101.3	3.1
2	Deciduous forest	200.5	2.2	146.9	2.5	100.8	6.3	53.6	1.6
3	Scrubland, few higher trees (Maquis)	2814.4	30.4	1928.9	32.2	665.7	41.6	885.5	27.2
4	Low scrubland, grassland, fields (Garrigue)	2569.5	27.8	1427.9	23.8	10.9	0.7	1141.6	35.1
5	Sparse vegetation, rocks, boulders, bare soils	492.9	5.3	407.8	6.8	16.1	1.0	85.1	2.6
6	Fields, fallow land	1592.8	17.2	760.5	12.7	10.7	0.7	832.3	25.6
7	Vine yards	69.2	0.7	69.2	1.2	3.9	0.2	0.0	0.0
8	Irrigated areas (plantations, fields, green areas, parks)	235.1	2.5	160.9	2.7	34.1	2.1	74.2	2.3
9	Wetlands, moist areas	160.0	1.7	132.7	2.2	83.9	5.2	27.3	0.8
10	Open water bodies	6.3	0.1	5.3	0.1	1.1	0.1	1.0	0.0
11	Salt lake pans	16.5	0.2	16.5	0.3	0.0	0.0	0.0	0.0
12	Settlements	181.5	2.0	145.8	2.4	3.6	0.2	35.7	1.1
13	Settlements (sealing >70%), aiports, highways	56.2	0.6	43.3	0.7	0.0	0.0	12.9	0.4
$\sum$		9245.8	100.0	5995.4	100.0	1601.7	100.0	3250.5	100.0

high trees. Therefore, the area classified as forest appears comparably small. The biggest forest domains are located in the western Troodos as part of the state forest territory. Dense deciduous forests are rare and exist only in some higher areas (e.g. *Quercus alnifolia*), and on the valley floors (*e.g. Platanus orientalis*). In most cases, the deciduous trees on the valley floors also belong to the moist area class due to additional water supply from river runoff or shallow groundwater.

The foothills of the Troodos mountains are largely characterised by the calcareous formations of the Circum Troodos sedimentary succession (see Chap. 2.5). The formations crop out predominantly to the East and South of the Troodos massif and typically show a very sparse vegetation coverage (Garrigue type) with low scrublands, herbs, forbs and grasslands. Higher scrublands (Maquis) occur in some beneficial areas. Agriculture in this area is mostly limited to small fields, irrigated terraces and pasture. The area is also the domain of the most important vine region.

The Mesaoria plain and coastal plains are the most important agricultural areas of Cyprus. In central and eastern Mesaoria cereal fields complemented by grasslands and/or low scrublands (Garrigue) are typical. The western Mesaoria and coastal plains show extended irrigation areas with citrus trees, bananas, vegetables, etc. Smaller irrigation areas can be found in many areas of the island, predominantly in the peripherals of the settlements.

Differences between Northern and Southern Cyprus are most evident regarding forest and field areas (cereals). Nearly all large forest domains are situated in the Troodos mountains of Southern Cyprus. In contrast, extended cereal fields are most common in central and eastern Mesaoria, which comprise a large part of Northern Cyprus.

For each land cover type, several specific coefficients have to be defined and calibrated. Coefficients are respectively needed for albedo; fraction of vegetation coverage and sealing; secondary evapotranspiration/irrigation; mean effective root depth; interception storage; effective vegetation height for aerodynamic resistance; surface resistance and an adjustment factor for soil hydraulic conductivity.

A first estimate for the respective coefficients can be retrieved from a large variety of publications. Important papers and data sources are given in Chap. 3 within the respective discussion of different parameters. A compilation of applied coefficients for land cover types of Cyprus is given in Table A.1 - A.7.

4.4 Soil (Root Zone)

Water balance modelling requires information about physical soil properties. For each raster cell hydraulic conductivity of the soil, field capacity and effective rooting depth have to be determined. The model is improved by the inclusion of macropore and sealing information, which can often be related to land cover characteristics.

The soil texture controls water-holding characteristics in most soils and allows the assessment of the soil physical properties based on Pedo Transfer Functions (PTFs). The PTF equations of Saxton et al. (1986) calculate hydraulic conductivity and field capacity from grain size distribution (see Chap. 3.6). The required soil texture data in the present study is derived from soil samples and infiltration tests from field studies (Mederer 2003, Dünkeloh 2005a); from the soil samples database of the Geological Service Department; from values from soil series reports of the Department of Agriculture (Soteriades and Koudounas 1968, Grivas 1969, Koumis 1970, Markides 1973), from results of the technical cooperation between the Ministry of Agriculture and Natural Resources of Cyprus and the Federal Institute for Geosciences and Natural Resources of Germany (Lüken 1988), from further soil projects like Boje-Klein (1982), and from calibrated modelling results of isolated catchments (Dünkeloh 2005a, Dünkeloh 2005b, Mederer 2009).

The published general soil maps (see Chap. 2.4) are not optimal for a classification of the whole island with respect to soil texture and bedrock. Therefore, geological units are used because soil texture distribution can be sufficiently related to weathered material of different geological formations. Furthermore, the root zone often comprises major parts of the bedrock. For each important geological unit soil physical values are derived with the help of the above listed data sources and PTFs. The unit borders are compiled from the Geological Map of Cyprus (Constantinou 1995) and from two Hydrogeological Maps of Cyprus (Tullström 1970, Dünkeloh 2004 [see new version in Fig. 2.7]). The results for the different units are listed in Table 4.4 and discussed in the following paragraphs.

Soil formation on the geologically young and mostly flat areas (Mesaoria plain, coastal plains, terraces) is comparably well developed due to little degradation by erosion. In some favourable areas typical red clayey Mediterranean soils occur (e.g. on the fanglomerates). On terraces clayey loam is prevalent. In other areas, the

material of the soil layer corresponds strongly to the bedrock material (e.g. marls of the Mesaoria plain, Alluvium). The comparably high fine fraction of soils with clay content causes slightly higher field capacities in those areas.

Calcareous formations like Pakhna and Lefkara formations are covered by very poor soils. The soil genesis has usually not exceeded the initial stage because decomposition by biochemical processes is reduced by high carbonate content. Furthermore, degradation processes erode the fine fraction of the soil. In some morphologically protected places, thin loamy to clayey deposits are accumulated. The sparse vegetation shows deep rooting through fissures into the bedrock material with low field capacities. The soil and bedrock of the gypsum areas (Kalavassos formation) consist of more fine-grained and clayey material, resulting in somewhat higher field capacities.

Most soils on the igneous rocks of the Troodos mountains are typical stony and flat initial soils. Some more profound but hardly differentiated soils arise on colluviums. The decomposition of the bedrock is mainly a result of physical, chemical and mechanical weathering in connection with precipitation and temperature (frost), surface runoff and rock slides. The influence of biological weathering is comparably small, especially in the areas with little vegetation. The steep relief with its strong erosion processes, is the substantial factor in the mountains area for keeping the soil formation in an initial stage. In areas with denser vegetation coverage (forest and Maquis), the soil material is somewhat better protected against erosion and the soil layer can be enriched with some fine-grained material. Nevertheless, the thin soil blankets are usually not sufficient for plant roots, which continue to grow along block cutting fissures.

In several areas a 'sea of blocks' covers the landscape where resistant formations - like the serpentinites of the mantle sequence - peridotitic rocks or sheeted dykes are present, and weathering generates only bigger blocks and stones. In contrast, the gabbro and pillow Lavas are less resistant and weather into gravel, sand and some clayey material. The better rooting conditions and high precipitation amounts in the gabbro area result in a denser vegetation coverage, and slightly higher field capacities.

The Mamonia terrane covers parts of the hilly southwestern island. As in the Troodos mountains, erosion keeps soils in an initial state. Rooting conditions for plants

depend mainly on the bedrock type, which in case of the Mamonia terrane can be distinguished into rocks of the igneous unit with crushed serpentine and subordinate pillow lavas, the sedimentary domain with sandstone, clays, cherts and shales. On the igneous and shale series, very poorly developed soils consist of coarse fragments and sandy or loamy residuals of weathered lavas. The sedimentary series with clays and sandstone lead towards weathered and semi-weathered clays, which are easily eroded. In those areas landslides are very common.

The soils of the Kyrenia terrane are also poorly developed. The Kythrea formation surrounding the Kyrenia range has the largest extent and is dominated by flysch consisting of sandstones and marls. Tectonised and metamorphosed limestones and dolomites appear in the core of the range. Erosion processes keep the soil in an initial stage in all those formations. Vegetation roots through fissures of the bedrock.

It can be concluded that most of the soils on the island are initial soils. Some better developed soils exist only on younger geological units and terraces. Furthermore, in some areas of dense vegetation, blankets of medium and fine grained material can be found covering the bedrock. Nevertheless, vegetation roots usually grow into the bedrock sediments or along the bedrock block fissures. The field capacity is typically very low and only partly influenced by the existence of thin covers of fine-grained and clayey material. Silty, marly and clayey bedrocks can hold more water against gravity and could lead to higher field capacities, but the hydraulic conductivity in these formations is often very small (see Table 4.4).

The total plant-extractable water content of the root zone at field capacity (absolute field capacities) is determined (Eq. 3.90) by the field capacity (Table 4.4) and the effective rooting depth (Table A.3). The resulting map (Fig. 4.10) shows that the absolute plant-extractable field capacity is strongly related to the effective rooting depth, because in most cases the soil physical properties of the different units do not differ very much. Higher values can therefore be detected, especially in areas with forest, Maquis and agriculture. In those areas a higher fraction of fine-grained material can also be found because of better protection against erosion. The lowest values occur in zones with very sparse vegetation, bare soils, or rocks. The absence of vegetation allows erosion of the fine fraction of the soil. Therefore, in many mountainous areas, the bedrock appears directly on the surface.

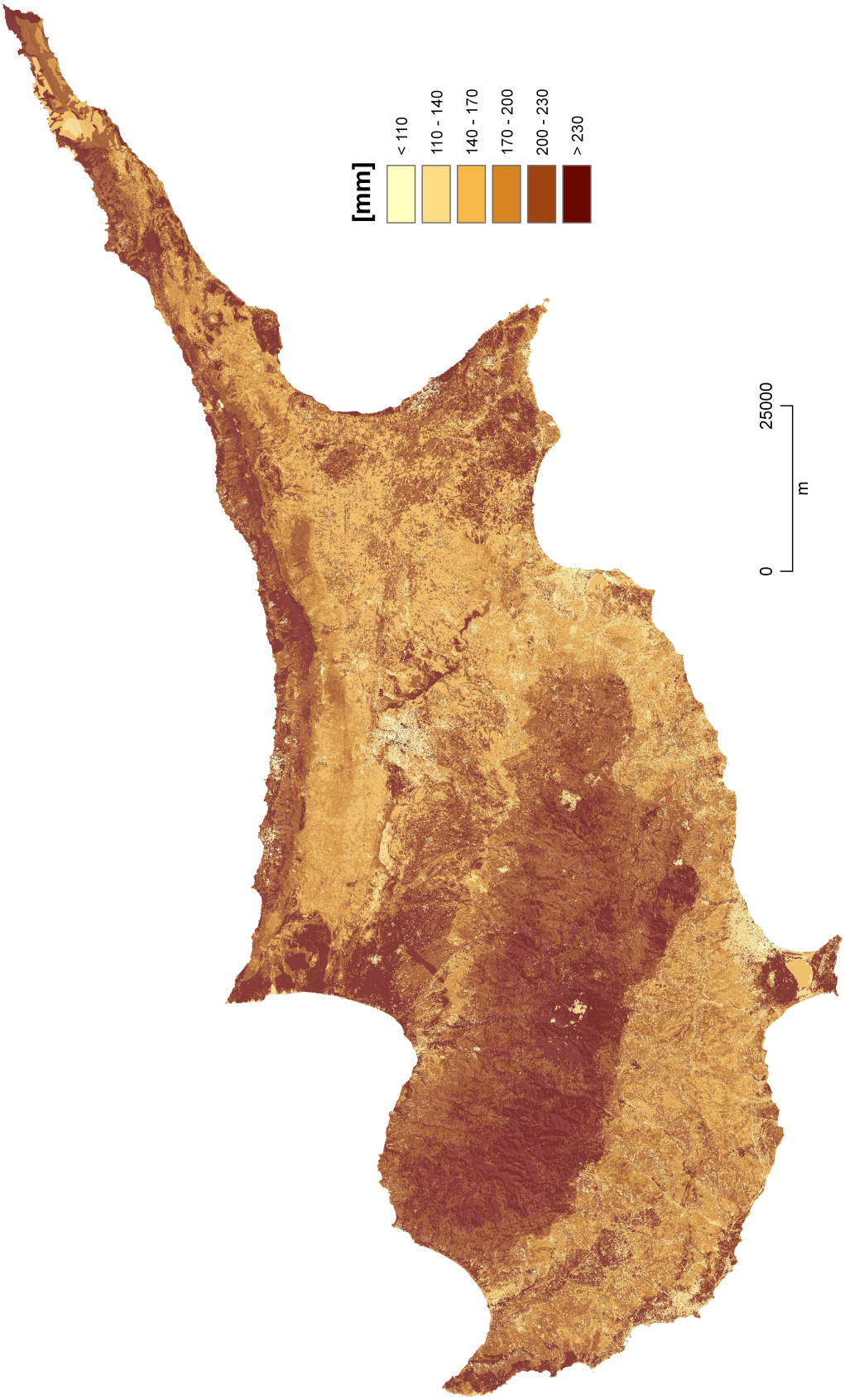

Figure 4.10: Plant-extractable field capacity of the root zone.

4.5 Bedrock

The soil water state and physical properties of the bedrock control the deep percolation processes. Physical bedrock properties depend on local geological or hydrogeological conditions. The key parameter for water balance modelling is the hydraulic conductivity, which has to be determined for all important hydrogeological units. The areal delimitation of the units is derived from geological and hydrogeological maps.

In the present study, the assessment of the hydraulic conductivity was performed on the basis of several sources. A large number of pumping test data from many drilling projects, stored in the ENVIS-Database from the Geological Survey Department of Cyprus, was analysed with the software package AquiferTest (Waterloo Hydrogeologic 2002), for determining hydraulic characteristics of different formations. Moreover, calibrated model results from smaller study areas were used (Udluft et al. 2004a, Dünkeloh 2005a, Dünkeloh 2005b, Mederer 2009) and the results from some earlier studies were checked, especially with regard to areas lacking information. Publications of general interest are from Burdon (1952, 1953) and the United Nations in the 1960s (UNDP 1970) which evaluated geological formations from a hydrogeological point of view. The first hydrogeological map (Tullström 1970), with qualitative information for different units was also developed within the UNDP project. Later studies refer to special aquifers, e.g. Zomenis (1977), Dijon (1977), Konteatis (1987), Wagner et al. (1990). Aquifers in the igneous rocks of the Troodos ophiolite were discussed by Afrodisis et al. (1986), Afrodisis and Fischbach (1988).

The hydraulic conductivities of the bedrock are shown in Fig. 4.11. The highest values can be found in young geological formations of unconsolidated and semiconsolidated, coarse and medium grained sediments (gravel, sand). Those areas are located mainly in the western, central and southeastern Mesaoria plain, and in the coastal plains (e.g. Akrotiri aquifer, terraces). Also of major importance are several alluvial aquifers on the valley floors of Ezusa, Xeros, Diarizos, Pediaios, Gialias, Kambos, Karyotis, Chrysochou and other rivers. They are characterised by high infiltration capacities and controlled by the discharge of Troodos and surroundings. Of secondary importance are thin, unconsolidated to semiconsolidated, Plio-Pleistocene

Table 4.3: Areal extension of hydrogeological units of Cyprus (see also Fig. 2.7).

Hydrogeological unit		Cyprus		Southern Cyprus[1]		Troodos		Northern Cyprus	
		Area [km^2]	Prop. [%]	Area [km^2]	Prop. [%]	Area [km^2]	Prop. [%]	Area [km^2]	Prop. [%]
Unconsolidated and semiconsolidated rocks:									
A1	Unconsolidated gravel, sand and silt (mainly Holocene)	593.8	6.4	417.4	7.0	5.9	0.4	176.4	5.4
A2	Semiconsolid. gravel, sand, sandy marl (e.g. fanglom., terraces)	1141.5	12.3	639.5	10.7	0.0	0.0	502.0	15.4
A3	Thin surface deposits on less permeable layers	914.1	9.9	294.9	4.9	0.9	0.1	619.2	19.0
Fractured and karstic rocks:									
B1	Gypsum, alternating with chalky marl, marly chalk (Kalavassos f.)	90.0	1.0	73.7	1.2	0.0	0.0	16.3	0.5
B2	Chalk, sandy chalk, marly chalk, sandstone (Pakhna formation)	746.5	8.1	617.8	10.3	0.0	0.0	128.8	4.0
B3	Chalk, marly chalk, chalky marl (Lefkara formation)	869.0	9.4	821.8	13.7	0.0	0.0	47.2	1.5
B4	Massive, dolomitic and reef limestones (Pakhna f., Hilarion f. ...)	210.6	2.3	120.5	2.0	0.0	0.0	90.1	2.8
Fractured igneous rocks:									
C1	Pillow lavas	619.0	6.7	577.4	9.6	12.9	0.8	41.5	1.3
C2	Basal Group	397.5	4.3	387.3	6.5	319.0	19.9	10.2	0.3
C3	Sheeted dykes	1069.8	11.6	1069.3	17.8	1019.5	63.7	0.4	0.0
C4	Gabbro	225.8	2.4	225.8	3.8	190.1	11.9	0.0	0.0
C5	Peridotitic rocks (pyroxenite, wehrlite, dunite)	55.0	0.6	55.0	0.9	17.7	1.1	0.0	0.0
C6	Serpentinite, harzburgite (mantle sequence)	116.0	1.3	114.3	1.9	35.7	2.2	1.8	0.1
Complex sedimentary and igneous units:									
D1	Mamonia complex, Kannaviou formation, Moni f., Kathikas f.	269.9	2.9	269.9	4.5	0.0	0.0	0.0	0.0
D2	Marl, siltstone, greywacke (mainly Kythrea f. from Kyrenia range)	1062.7	11.5	0.0	0.0	0.0	0.0	1062.7	32.7
D3	Clay, marl, siltstone (Mesaoria group, Alluvium)	771.2	8.3	290.2	4.8	0.0	0.0	481.0	14.8
D4	Salt lakes and pans with low permeable surface	93.4	1.0	20.6	0.3	0.0	0.0	72.8	2.2
$\sum$		9245.8	100.0	5995.4	100.0	1601.7	100.0	3250.5	100.0

Table 4.4: Physical soil (root zone) and bedrock properties for the hydrogeological units of Cyprus.

Hydrogeological unit		Soil (root zone)			Bedrock
		Eff. macroporosity for bypass flow [%]	Plant-extractable field capacity [mm/m]	Hydraulic conductivity [m/s]	Hydraulic conductivity [m/s]
Unconsolidated and semiconsolidated rocks:					
A1	Unconsolidated gravel, sand and silt (mainly Holocene)	4	140	$4.0 \cdot 10^{-6}$	$4.0 \cdot 10^{-6}$
A2	Semiconsolidated gravel, sand, sandy marl (e.g. fanglom., terraces)	2	155	$3.0 \cdot 10^{-6}$	$2.0 \cdot 10^{-6}$
A3	Thin surface deposits on less permeable layers	2	155	$2.0 \cdot 10^{-6}$	$2.0 \cdot 10^{-7}$
Fractured and karstic rocks:					
B1	Gypsum alternating with chalky marl, marly chalk (Kalavassos f.)	6	155	$2.0 \cdot 10^{-6}$	$4.0 \cdot 10^{-7}$
B2	Chalk, sandy chalk, marly chalk, sandstone (Pakhna formation)	8	145	$2.0 \cdot 10^{-6}$	$1.5 \cdot 10^{-7}$
B3	Chalk, marly chalk, chalky marl (Lefkara formation)	8	145	$2.0 \cdot 10^{-6}$	$1.5 \cdot 10^{-7}$
B4	Massive, dolomitic and reef limestone (Pakhna f., Hilarion f., ...)	12	135	$3.0 \cdot 10^{-6}$	$4.0 \cdot 10^{-7}$
Fractured igneous rocks:					
C1	Pillow lavas	6	150	$1.0 \cdot 10^{-6}$	$8.0 \cdot 10^{-8}$
C2	Basal Group	8	140	$2.0 \cdot 10^{-6}$	$3.0 \cdot 10^{-7}$
C3	Sheeted dykes	15	135	$3.0 \cdot 10^{-6}$	$2.0 \cdot 10^{-7}$
C4	Gabbro	10	150	$2.0 \cdot 10^{-6}$	$4.5 \cdot 10^{-7}$
C5	Peridotitic rocks (pyroxenite, wehrlite, dunite)	15	140	$3.0 \cdot 10^{-6}$	$1.5 \cdot 10^{-7}$
C6	Serpentinite, harzburgite (mantle sequence)	15	160	$2.0 \cdot 10^{-6}$	$1.5 \cdot 10^{-7}$
Complex sedimentary and igneous units:					
D1	Mamonia complex, Kannaviou formation, Moni f., Kathikas f.	5	140	$2.0 \cdot 10^{-6}$	$6.0 \cdot 10^{-8}$
D2	Marl, siltstone, greywacke (mainly Kythrea f. from Kyrenia range)	5	150	$1.0 \cdot 10^{-6}$	$8.0 \cdot 10^{-8}$
D3	Clay, marl, siltstone (Mesaoria group, Alluvium)	2	170	$6.0 \cdot 10^{-7}$	$1.0 \cdot 10^{-7}$
D4	Salt lakes and pans with low permeable surface	0	170	$1.0 \cdot 10^{-7}$	$4.0 \cdot 10^{-8}$

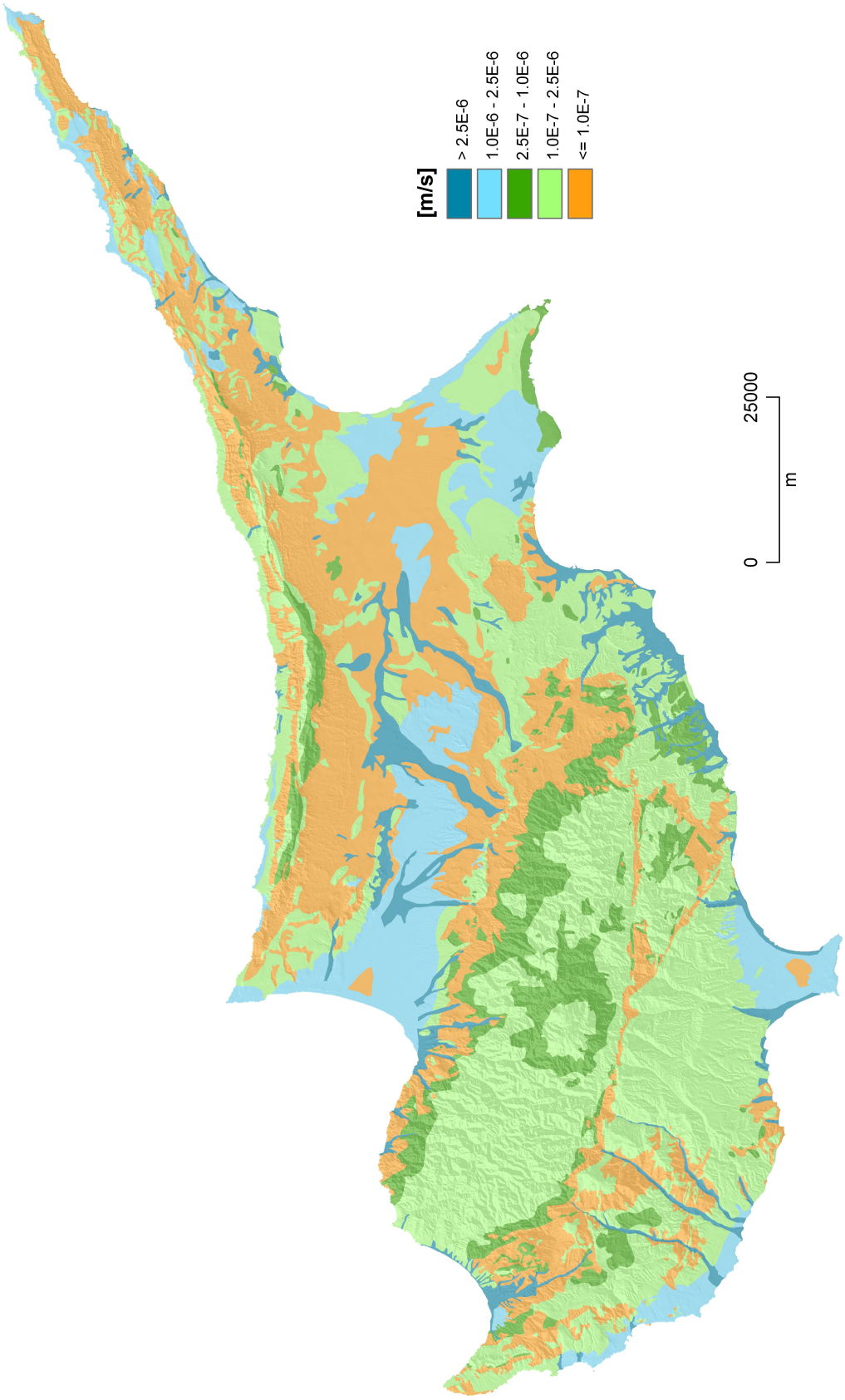

Figure 4.11: Hydraulic conductivity of the bedrock based on the hydrogeological units (Fig. 2.7) and values of Table 4.4.

sediments on the northern side of the Kyrenia range and on the Karpas peninsula, which are partly suitable for water supply. Those sediments of limited extension are situated over less permeable Kythrea formation.

The zones of fractured and karstic rocks are dominant in great parts of the Circum Troodos sedimentary successions and in smaller parts of the Kyrenia range (see Fig. 4.11). The formations consist of more or less porous parts. Some intercalated layers show aquifer characteristics, which are suitable for water supply. Most important are the Gypsum aquifer of the Kalavassos formation, Pakhna sandstone and chalk aquifer, Terra and Koronia reef limestone aquifers, Lefkara chalk aquifer and the karstic limestone and dolomitic formations of the Kyrenia range. Together, all areas together can be subsumed to a medium permeable zone with second class aquifers.

The Troodos ophiolite shows aquiferous characteristics because of the intense fracturing and fault network of igneous rocks. Therefore, infiltration, movement and retention of rainwater in the subsurface are also favoured. The igneous rocks of the Troodos can be separated in several units with different characteristics. The analysis of the drilling projects show that the Gabbros are the best aquifers with highest permeabilities. Basal Group, Sheeted Dykes and part of the peridotitic rocks are of intermediate quality. Pillow lavas and the serpentinised rocks show the poorest permeabilities, because faults and fractures are often filled and cemented with secondary minerals. High precipitation rates and aquiferous characteristics of several units make the Troodos massif the most important area for the renewal of natural water resources.

Outside the Troodos ophiolite, further zones of less permeable rocks exist. Most important are the rocks of the Mamonia terrane in the southwestern segment of the island and the flysch of the Kythrea formation covering great parts of the Kyrenia range and the Karpas peninsula (see Fig. 4.11). Those formations are usually not suitable for water supply and show relatively poor infiltration characteristics. Furthermore, the eastern Mesaoria plain is widely covered by less permeable unconsolidated and semiconsolidated sediments (Mesaoria group and Alluvium), consisting of fine-grained marls, clays and siltstones.

4.6 Hydrology

Daily records of gauging stations of many larger catchments of Cyprus are available and organised in the ENVIS-Database of the Ministry of Agriculture and Natural Resources. Most of the catchments belong to river systems rising from the Troodos massif. Apart from those, only few other large catchments exist outside the Troodos area. Although many of the recorded gauging station time series cover only a few years, they are still sufficient for calibration and verification purposes due to the long modelling period of the water balance model from 1961-2004. The stored data is given in m^3/s and transformed to mm/d during further data processing.

The selection of calibration catchments was performed based on miscellaneous criteria. In the first step, all catchments with too short, fragmentary, obviously inconsistent or unsuitable discharge time series are discarded. Unsuitable time series exist, e.g. due to a large dam in the upstream area. The remaining catchments are analysed with regards to their relation to different hydrological units. Catchments only extending to single hydrological units are selected as far as possible, allowing an individual calibration of the respective unit characteristics. This is done to find a calibration catchment for all larger hydrological units. Model verification is done with larger catchment areas controlled by several hydrological units.

A set of twelve calibration catchments, which location is shown in Fig. 4.12, was finally selected. In Table 4.5, the relevant data for the gauging stations and all relevant hydrological units of the respective catchments are given. Nine of the twelve catchments were selected for calibration of single hydrological units. The remaining catchments Diarizos, Limnatis and Elia serve for validation in a complex hydrological and hydrogeological environment, and are furthermore located in key areas with respect to the natural water resources of Cyprus.

In the plains, suitable calibration catchments could not be found, because baseflow is usually not generated due to the predominantly unconsolidated, permeable rocks and the deep groundwater levels in those areas. The possible inaccuracy in the water balances of those areas becomes comparably small due to low precipitation amounts.

In the calcareous series of fractured and karstic rocks, the discharge data of the gauging stations Avdimou and Aradippou are of limited suitability, because of the

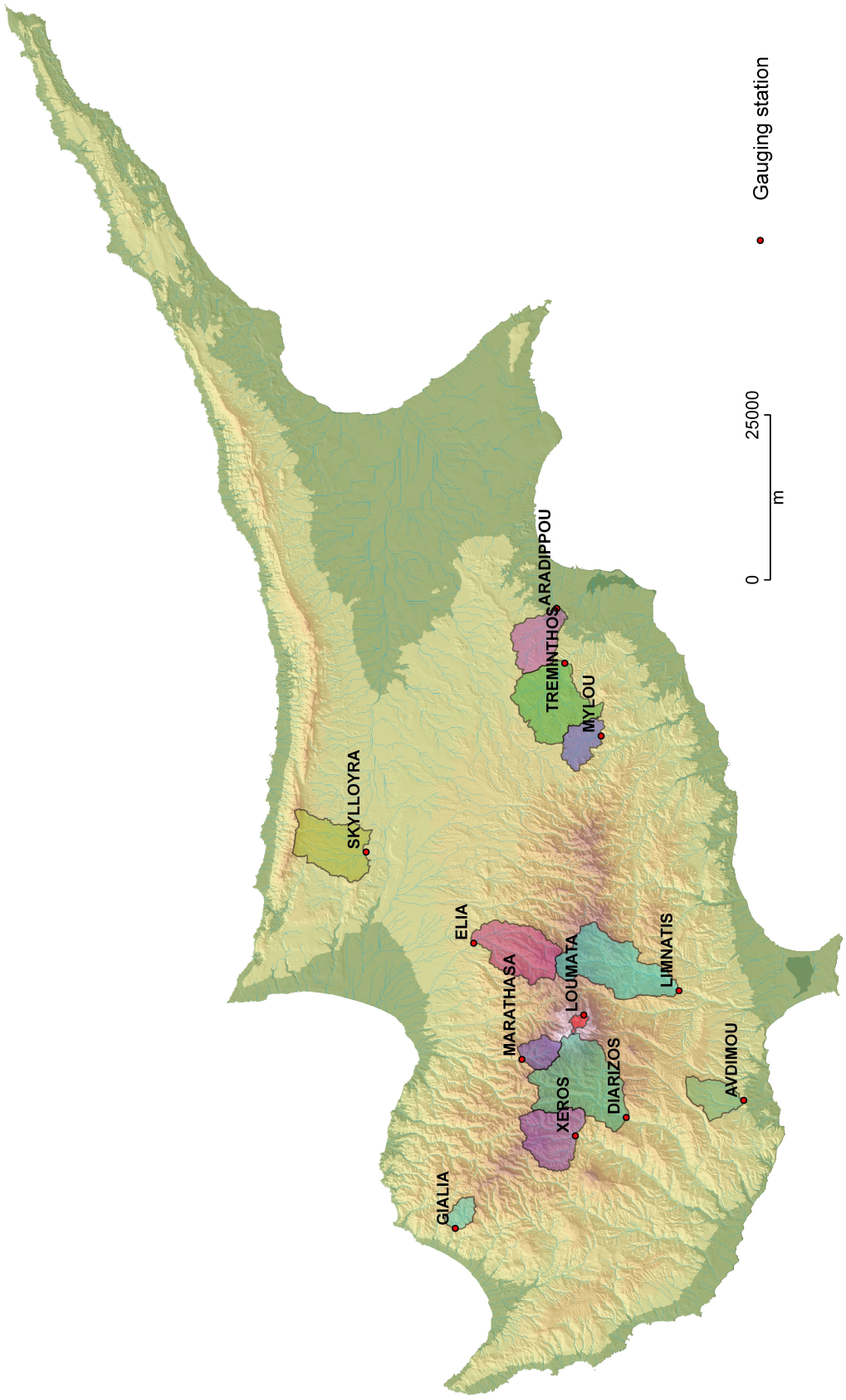

Figure 4.12: Catchment areas used for model calibration on the base of catchment response.

Table 4.5: Selected gauging stations for catchment calibration.

Number	Catchment	Time period	Area [km^2]	Hydrological unit
2-3-8-60	Gialia	10/1979–09/2003	15.3	C3
1-3-5-05	Xeros	10/1970–02/2005	67.5	C3
9-8-6-05	Avdimou	10/1967–09/1989	35.7	B2
3-2-1-85	Marathasa	11/1978–09/2002	22.6	C4, (C5)
9-6-3-15	Loumata	10/1990–09/2002	4.47	C6
3-7-7-85	Skylloyra	10/1967–09/1972	83.0	D2
8-7-3-60	Mylou	10/1965–09/1994	32.2	C1, (C2)
8-4-3-40	Treminthos	10/1965–09/2003	100.8	C1, (C2), (B3)
8-2-4-10	Aradippou	10/1984–02/2005	52.9	B3
1-2-4-95	Diarizos	10/1969–10/2004	128.7	C3, C2, C1, C5, C6, B3
9-6-7-70	Limnatis	10/1985–09/2002	114.7	C4, C3, C1, B3
3-5-4-40	Elia	10/1965–09/2003	80.9	C2, C3, C1, C4

() hydrological unit code in brackets indicates a small extension within the catchment area

records not being very representative. This is because of the fast discharge in karstic formations with complex water tables mostly below the river beds. The baseflow cannot be separated well from the stream discharge records and much of the southwestern and southeastern calcareous formations show subsurface discharge to the sea. Apart from those smaller and larger dams, deviations for irrigation, and pumping from wells influence natural discharge processes.

Chapter 5

Simulation of Actual Water Balances

5.1 Model Setup and Calibration

Preliminary model runs for specific calibration areas (see Table 4.5) are performed for the calibration of important parameters and the evaluation of the best model option settings. The applied raster resolution in the calibration areas is 50 x 50 m per cell. Thereafter, the final model is calculated with previously calibrated values and proven model settings and options. This final model for the whole island is based on a raster resolution of 100 x 100 m per cell.

Evaluation of available interpolation routines and their options, showed best results for the Inverse Distance Weighting (IDW) algorithm including the weighting of elevation (Eq. 3.1), as well as the embedded directional isolation (Eq. 3.4). The quality of interpolation results for Northern Cyprus is inferior because of the sparse data available for this area. Interpolation of relative humidity data based on transformed absolute humidity and temperature data, resulted in considerably better interpolation results with respect to topographical effects.

Regarding the different available equations for potential evapotranspiration, best results for Cyprus were retrieved with the original Penman-Monteith approach (3.46). For the subsequent derivation of actual evapotranspiration, the FAO approach by Allen et al. (1998) was selected in the model (Eq. 3.95).

The calibrated and applied physical parameters for land cover, soil and bedrocks are

Table 5.1: Mean meteorological conditions of Cyprus for the reference time period 1971-2000.

Parameter	Cyprus	Southern Cyprus	Troodos	Northern Cyprus
Annual precipitation [mm]	445.0	478.1	617.6	381.8
Maximum daily temperature [°C]	23.7	23.3	21.0	24.6
Mean temperature [°C]	18.2	17.7	15.8	19.1
Minimum daily temperature [°C]	12.7	12.2	10.6	13.6
Maximum daily rel. humidity [%]	66.7	64.9	63.6	70.1
Mean rel. humidity [%]	59.6	58.8	57.9	62.0
Minimum daily rel. humidity [%]	52.4	51.7	52.2	53.8
Mean rel. sunshine duration [%]	*	69.4	65.8	*

* = No values because of lack of data for Northern Cyprus

listed in Appendix A. Modelling results for different areas of the island are described and compiled in the following chapters and in Appendix B.

5.2 Precipitation

Precipitation of Cyprus is characterised by a distinctive seasonal cycle with rainy winters and dry summers (see Fig. 5.3). Typically, more than 70% of total annual rainfall occurs between November and mid-March.

Furthermore, precipitation is strongly related to terrain elevation. Annual mean averages range between 250 and 400 mm/a in the lowlands, and can reach up to 800 mm/a in the Kyrenia range, and up to 1100 mm/a in the highest crests of the Troodos mountains (see Fig. 5.1). Southern Cyprus benefits from precipitation amounts because the Troodos mountains extend mainly within the southern part of the island (see Table 5.1). The determined mean elevation gradient for Cyprus is approx. 42 mm/100 m (see Fig. 2.3).

Expositional effects are notable on both mountainous zones of the island. In the Troodos area, the southern and western slopes show higher precipitation sums than the northern and eastern slopes. In the Kyrenia range, the sea exposed northwestern slopes show wetter conditions than the southern slopes.

Snow occurs rarely in the low lying areas and the Kyrenia range. Only in the highest

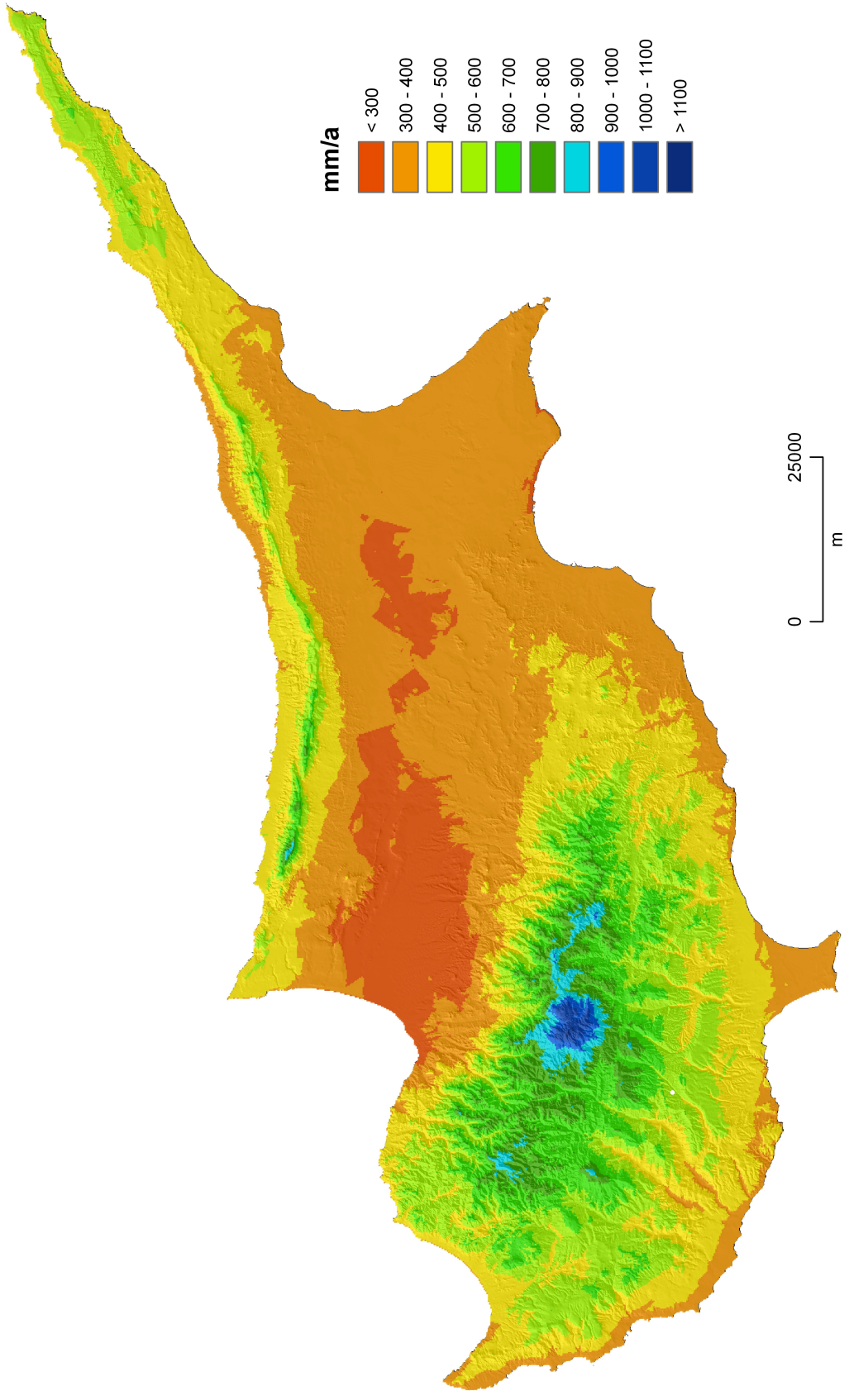

Figure 5.1: Mean annual precipitation of Cyprus for the reference time period 1971-2000.

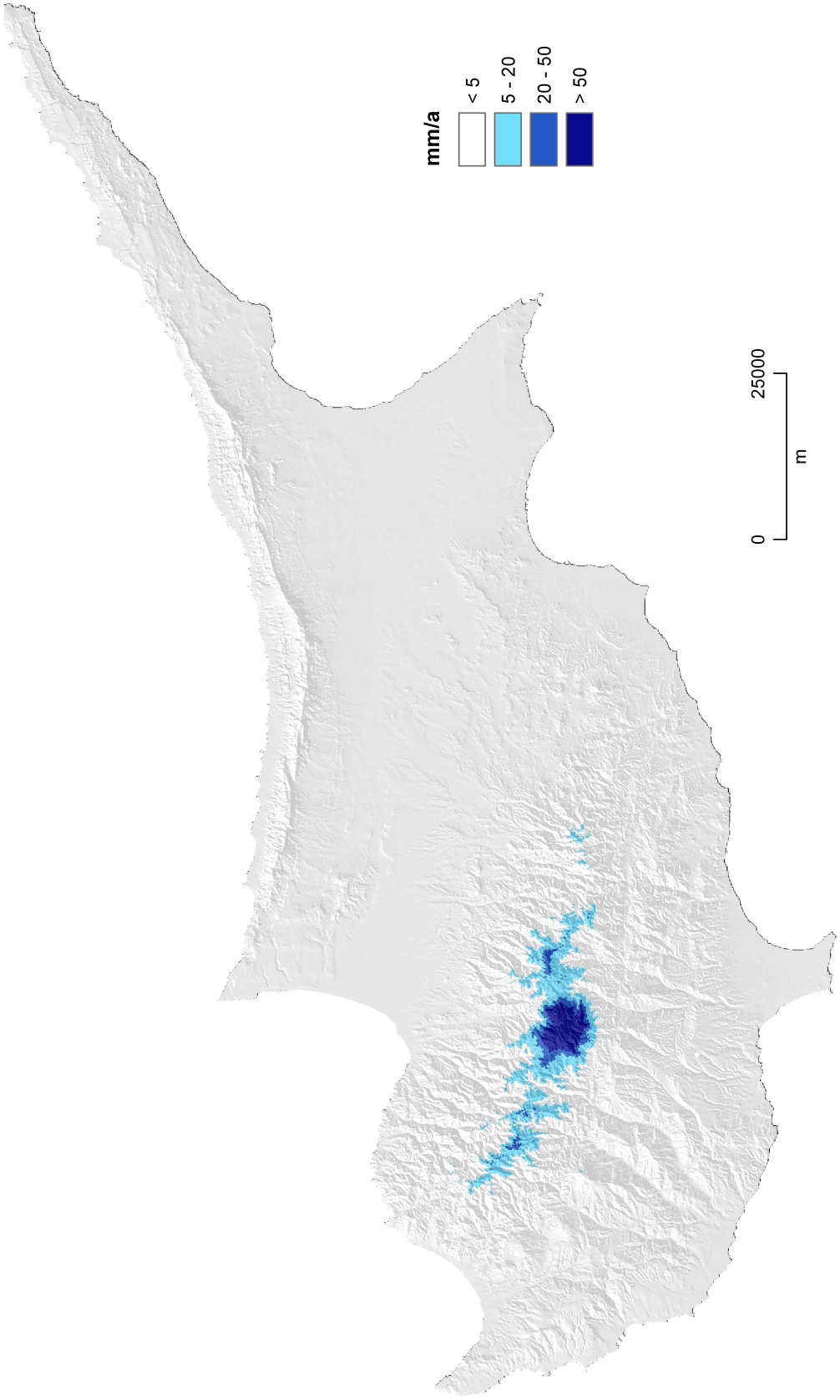

Figure 5.2: Mean annual snowfall of Cyprus for the reference time period 1971-2000.

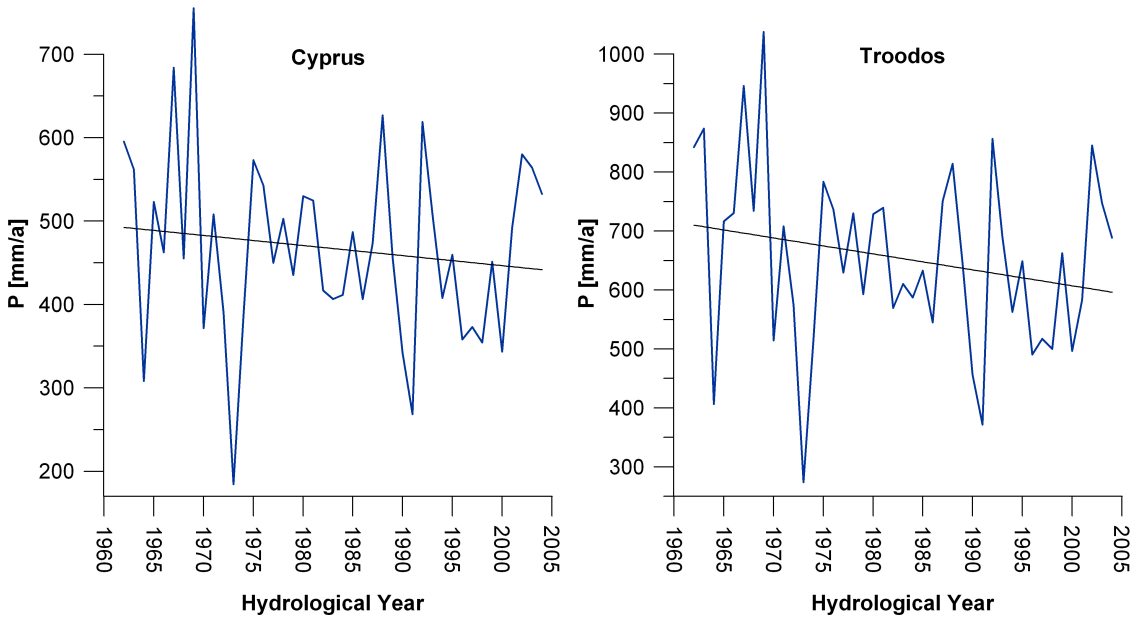

Figure 5.3: Mean areal precipitation of Cyprus (blue line) and its linear trend (black line) for the modelling period 1961-2004. The trends are not significant according to the Mann-Kendall trend test (Q = -0.99 | -1.39).

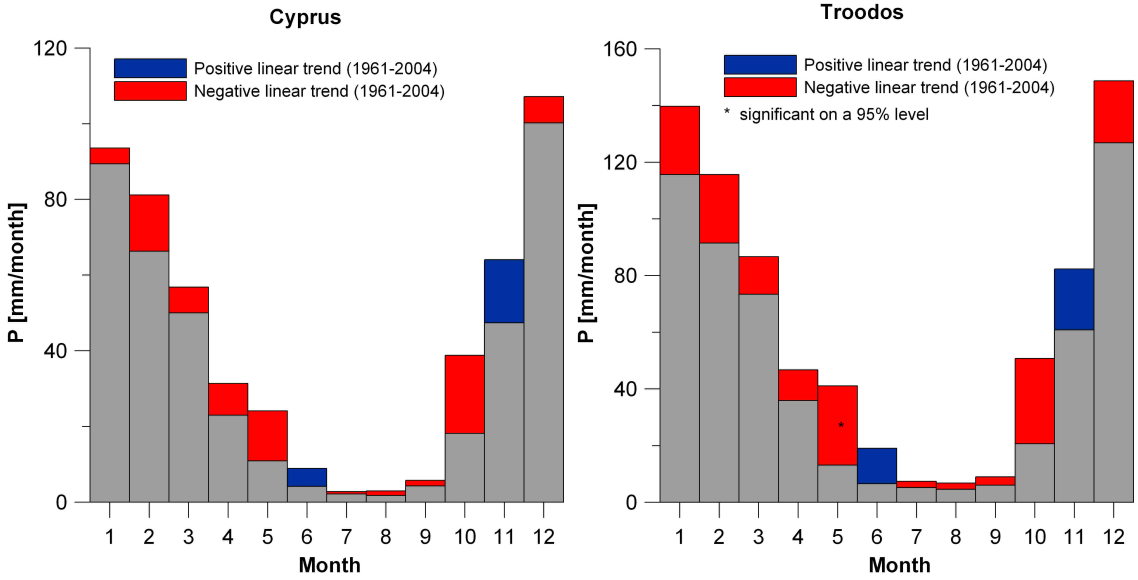

Figure 5.4: Monthly linear trends of the mean areal precipitation of Cyprus for the modelling period 1961-2004. Only the trend in May (Troodos) is significant according to the Mann-Kendall trend test on a 95% level.

areas of the Troodos range snowfall is registered frequently between December and April (see Fig. 5.2). The snow cover may lie for several weeks; especially in the northern slopes of high Troodos, but is not continuous for the winter months.

The interannual variability of the precipitation on Cyprus is very high. The mean areal precipitation for most years in the modelling period 1961-2004 varies between 300 and 600 mm/a (see Fig. 5.3). Standard deviation is about 110 mm, mean areal precipitation is calculated to 468 mm/a. The 1960s represent the wettest decade of the modelling period with a mean of 517 mm/a, the 1990s the driest decade with a mean 436 mm/a. The decreasing trend in the 20th century (see Fig. 2.4) is also notable (see Fig. 5.3) in the modelling period, but not significant (Mann-Kendall trend test, Q = -1.00) for this shorter period. The high interannual variability makes the detection of significant trends more difficult due to comparatively small absolute trends.

The monthly trend analysis (see 5.4) shows that there are also no significant trends for single months. Most months show insignificant decreasing precipitation trends, which appear most prominently in May and October. Only November and June show an insignificant increase.

5.3 Air Temperature

The temperature patterns show a close relationship to the terrain elevation of the island. Mean annual temperatures range between 18 and 20 °C in the coastal areas and plains, and decrease with increasing elevation (Fig. 5.6). In the highest areas of the Kyrenia range mean annual temperatures decrease to 14 °C, and in the uppermost areas around Mount Olympos down to 8.7 °C. The derived temperature gradient for Cyprus is approx. 0.5 K/100 m (see Fig. 2.2).

A more continental variant of the climate can be registered with increasing distance to the sea. This is explained by higher amplitudes between minimum and maximum temperatures. The highest daily temperatures are frequently registered in the central Mesaoria plain in the summer months; the lowest temperatures in the Troodos massif and its surroundings in the winter months. The distinctive seasonal cycle with hot summers and cool winters is less accentuated in coastal areas with moderate

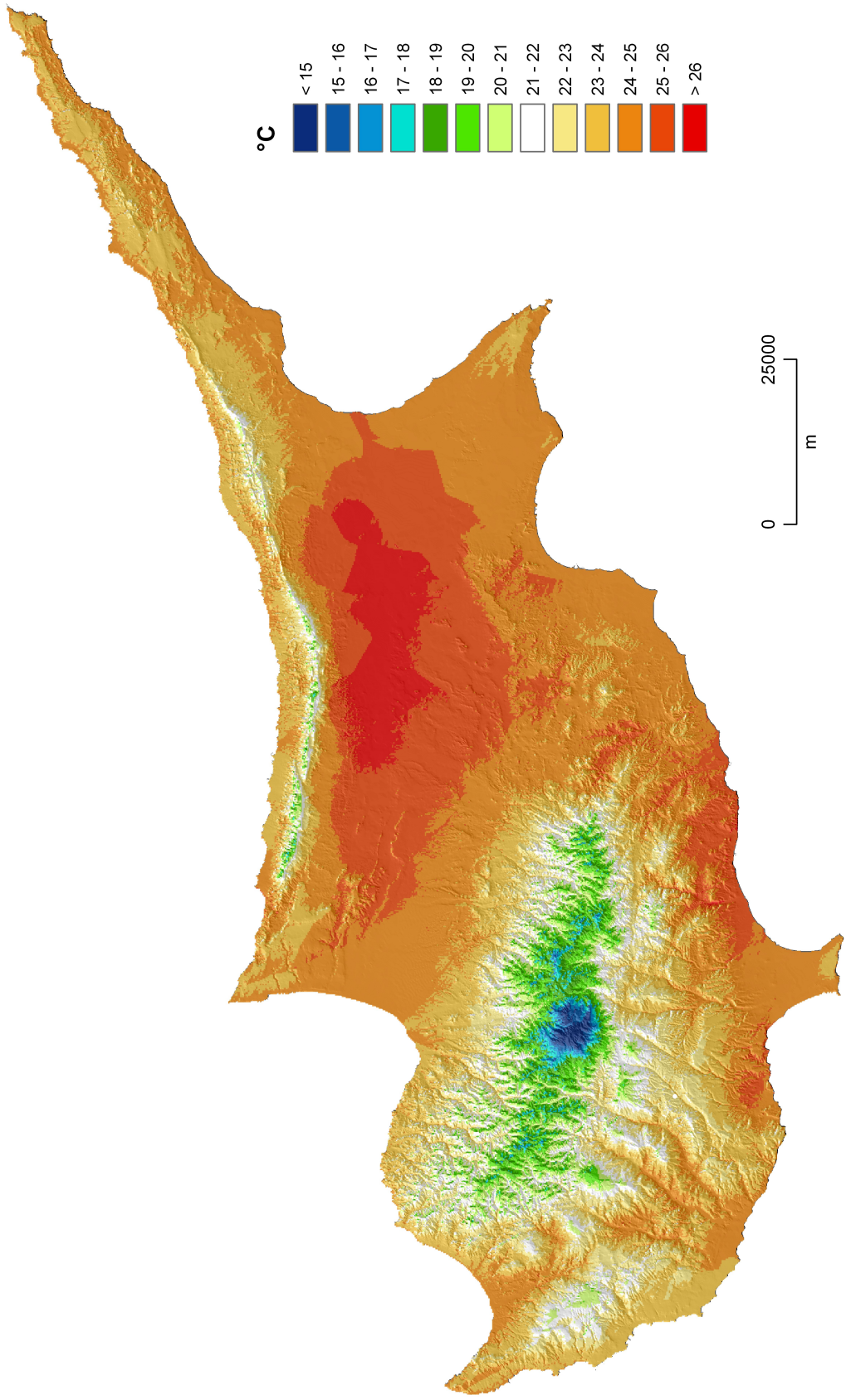

Figure 5.5: Mean daily maximum temperature of Cyprus for the reference time period 1971-2000.

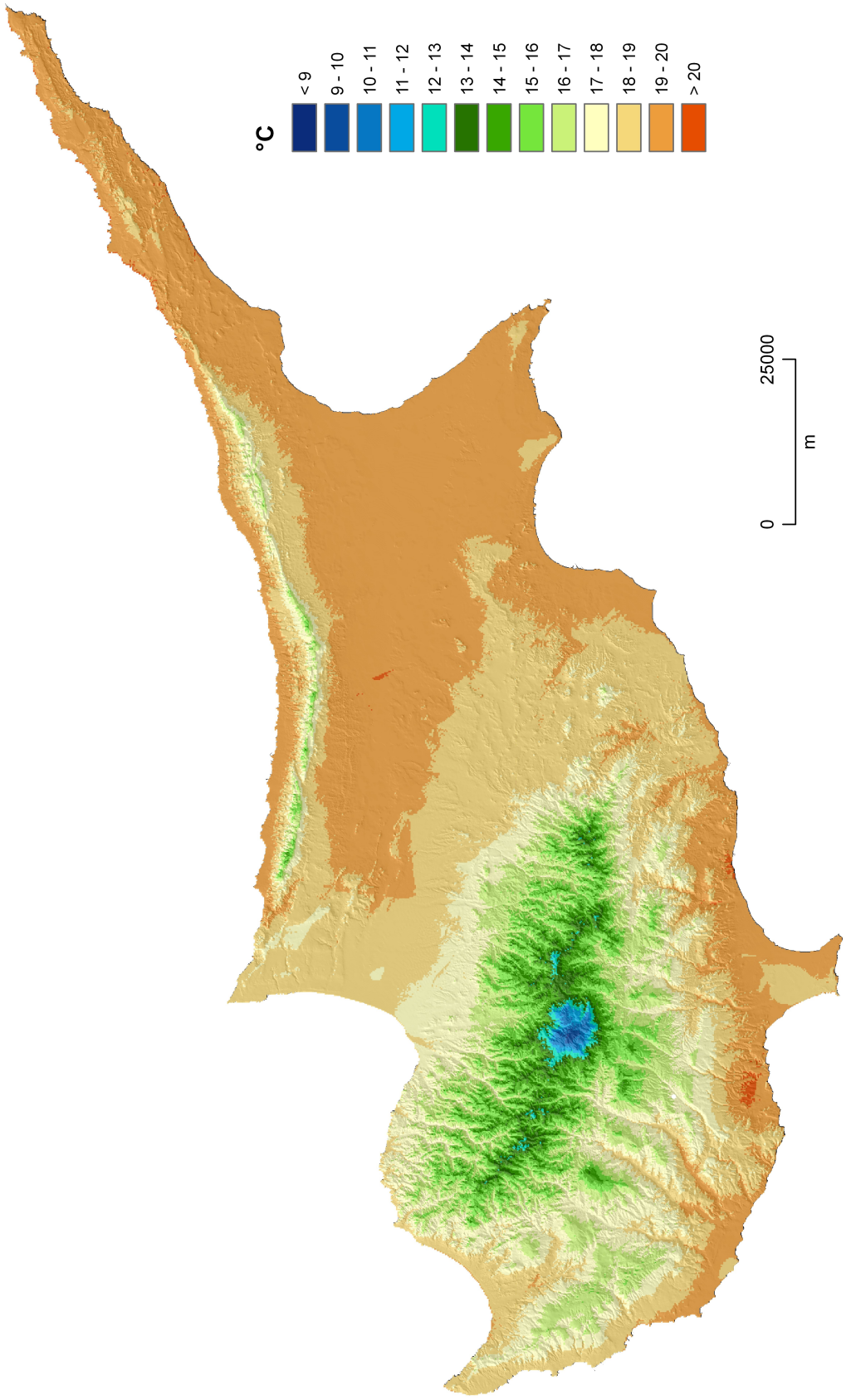

Figure 5.6: Mean temperature of Cyprus for the reference time period 1971-2000.

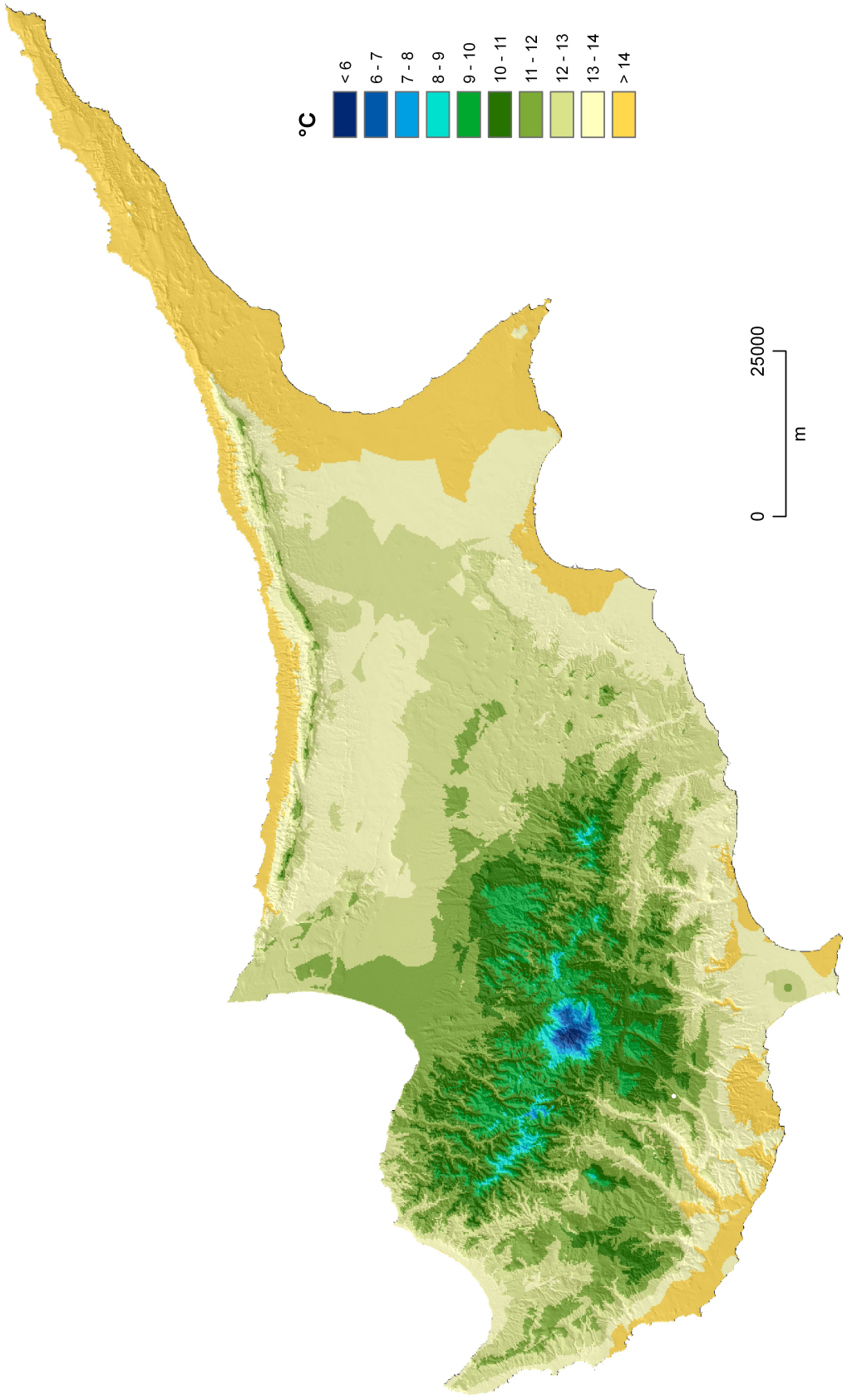

Figure 5.7: Mean daily minimum temperature of Cyprus for the reference time period 1971-2000.

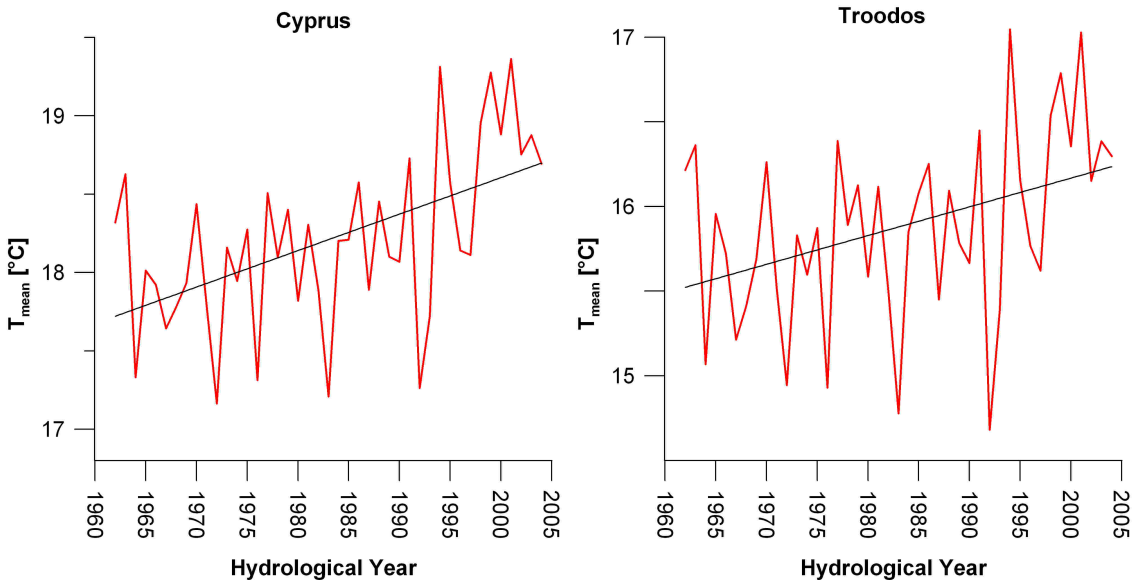

Figure 5.8: Mean areal annual temperature of Cyprus (red line) and its linear trend (black line) for the modelling period 1961-2004. Both trends are significant on a 99.9% | 95% level according to the Mann-Kendall test (Q = 3.4 | 2.3).

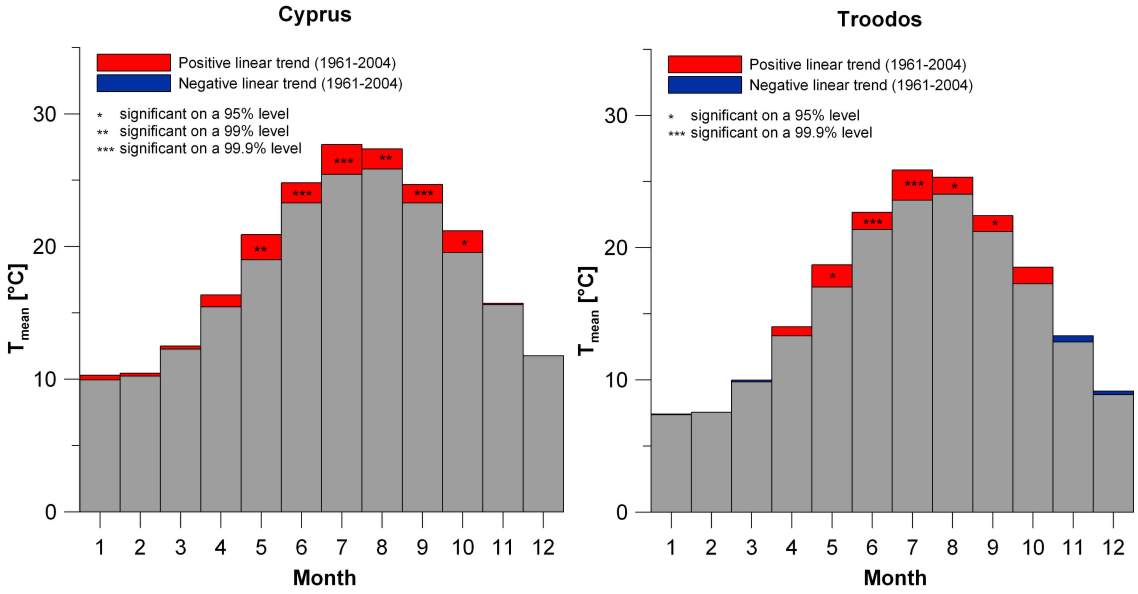

Figure 5.9: Monthly linear trends of the mean areal temperature of Cyprus for the modelling period 1961-2004. Months with significant trends according to the Mann-Kendall trend test are indicated.

temperature amplitudes balanced by the Mediterranean sea. This balancing effect appears most prominently at the eastern end of the isolated Karpas peninsula, which is less influenced by the heating and cooling of the large land masses on the island.

Expositional effects occur most prominently in the Kyrenia range and the Troodos mountains. The surplus of direct solar radiation on sunny days results in higher daily temperatures on the southern slopes. This also becomes evident on the southern coasts of Cyprus, which show higher mean and maximum temperatures than the coasts exposed north.

The interannual temperature variability is moderate because of the island's setting, with strong balancing effects by the Mediterranean Sea. A mean areal temperature of 18.2 °C and a standard deviation of 0.55 K was derived for the modelling period 1961-2004. The increasing temperature trend in the 20th century (see Fig. 2.5) can also be registered in the modelling period (see Fig. 5.8). The trend is highly significant on a >99.9% level (Mann-Kendall trend test; Q = 3.4) and can be detected within the mean daily maximum temperature time series (Mann-Kendall Q = 2.8, significance >99%), as well as mean daily minimum temperature time series (Mann-Kendall Q = 3.9, significance >99.9%).

A detailed monthly analysis shows that the trend is a result of a significant temperature rise in the summer half of the year, detected through the months May to October (Fig. 5.9). All those trends are significant on a 95% level or higher according to the Mann-Kendall trend test. In the winter half, some smaller non-significant increasing temperature trends can be detected.

5.4 Air Humidity

The patterns of relative humidity visualise the correlation of decreasing mean air humidity and increasing distance to the sea (Fig. 5.10 - 5.12). They also reveal the more continental character of the regional climate towards the centre of the island. The influence of elevation is also noticeable but not as distinctive as the influence by the sea. Some well exposed areas in the Kyrenia range and western and central Troodos especially, show favourable humidity conditions with increasing elevation. In contrast, the protected valleys of the Troodos show lower air humidity. The

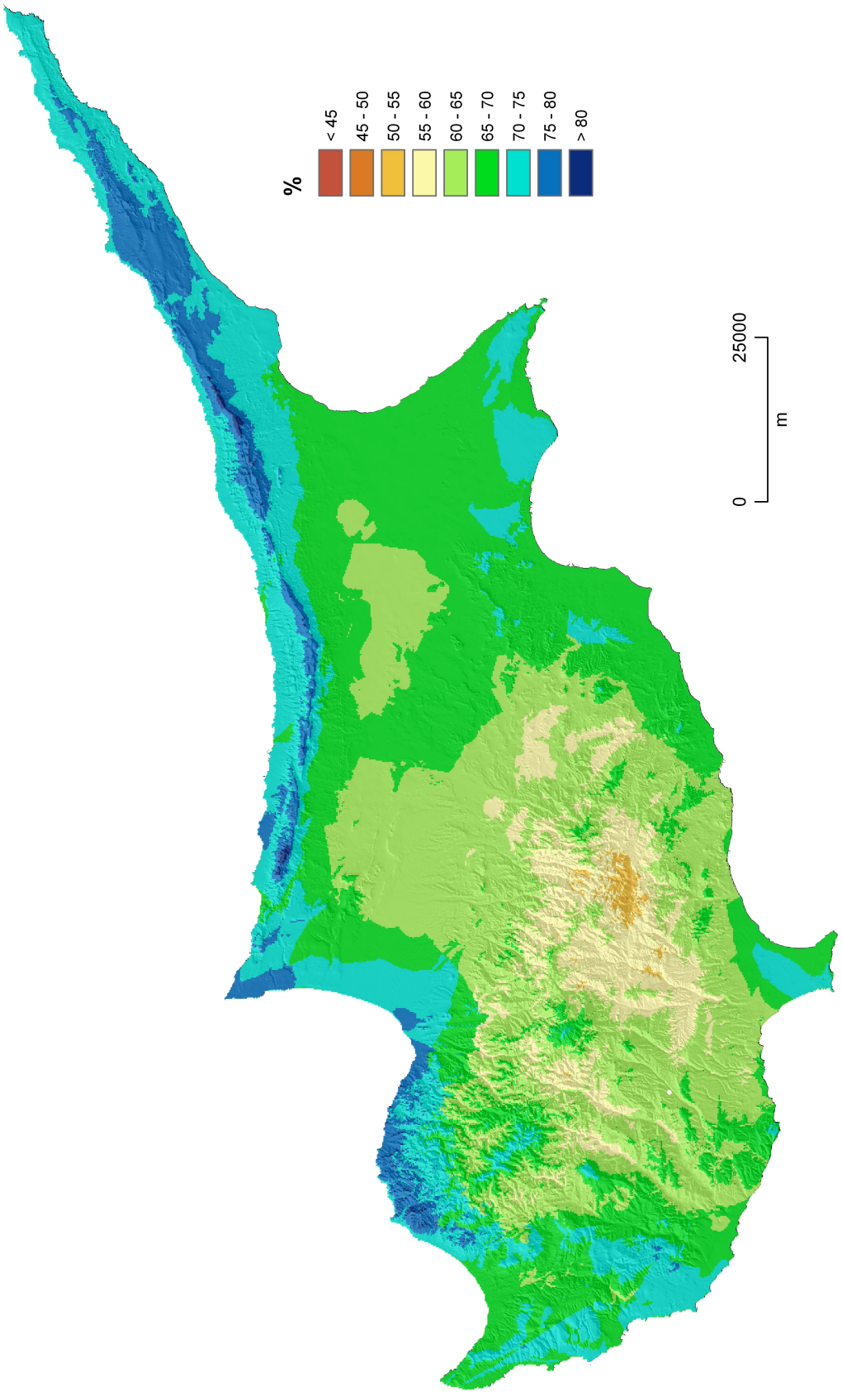

Figure 5.10: Mean maximum daily relative humidity of Cyprus for the reference time period 1971-2000.

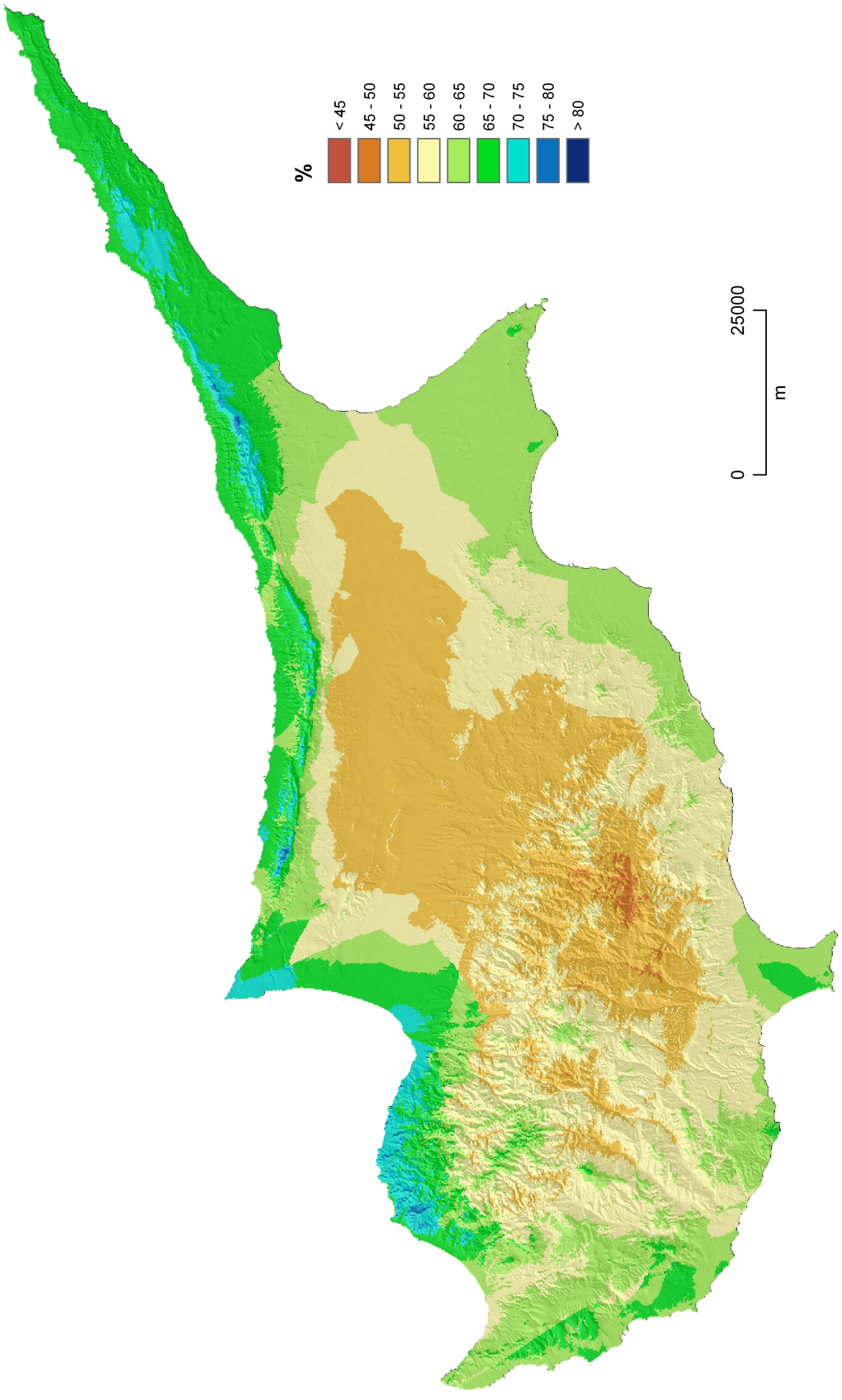

Figure 5.11: Mean relative humidity of Cyprus for the reference time period 1971-2000.

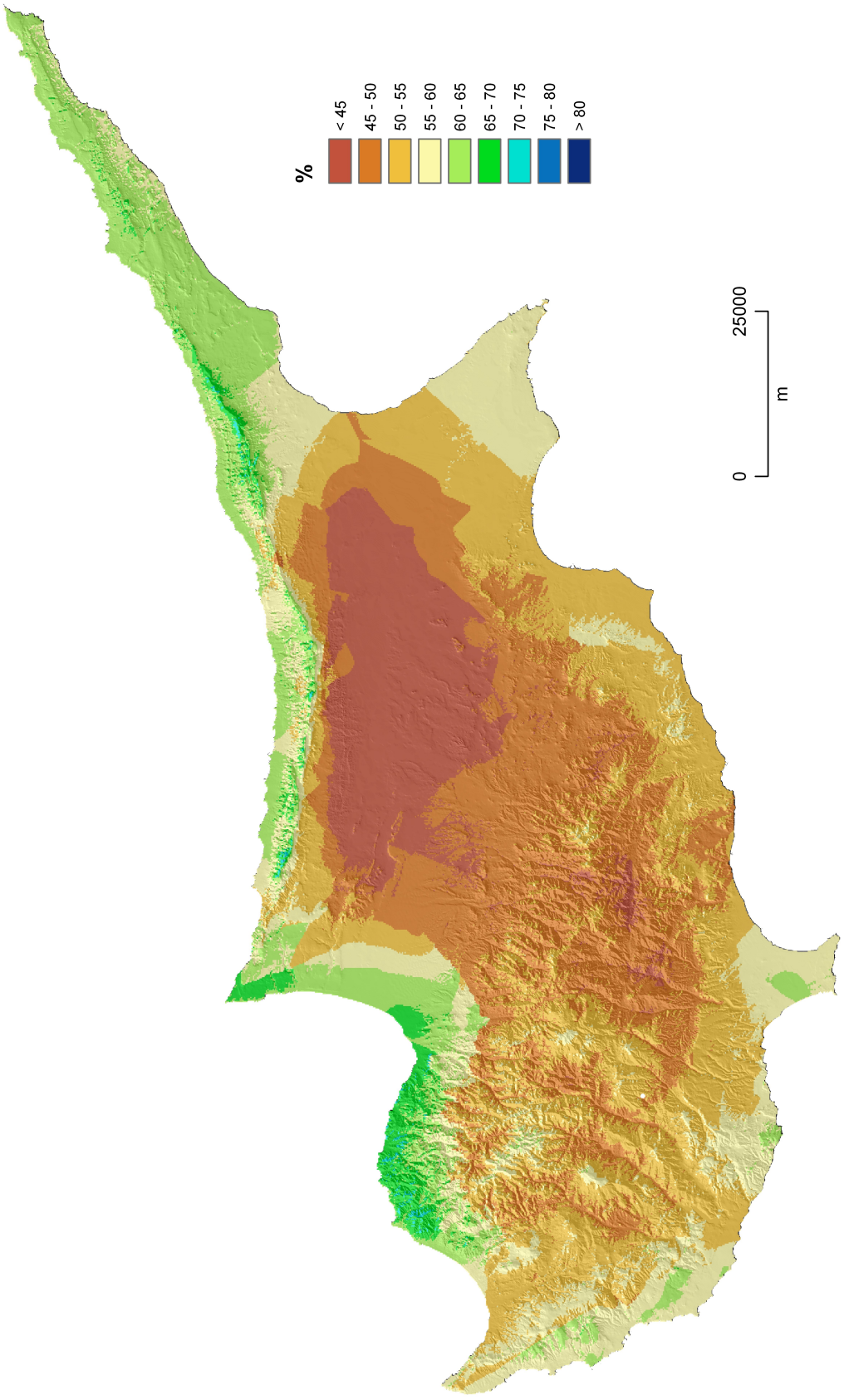

Figure 5.12: Mean minimum daily relative humidity of Cyprus for the reference time period 1971-2000.

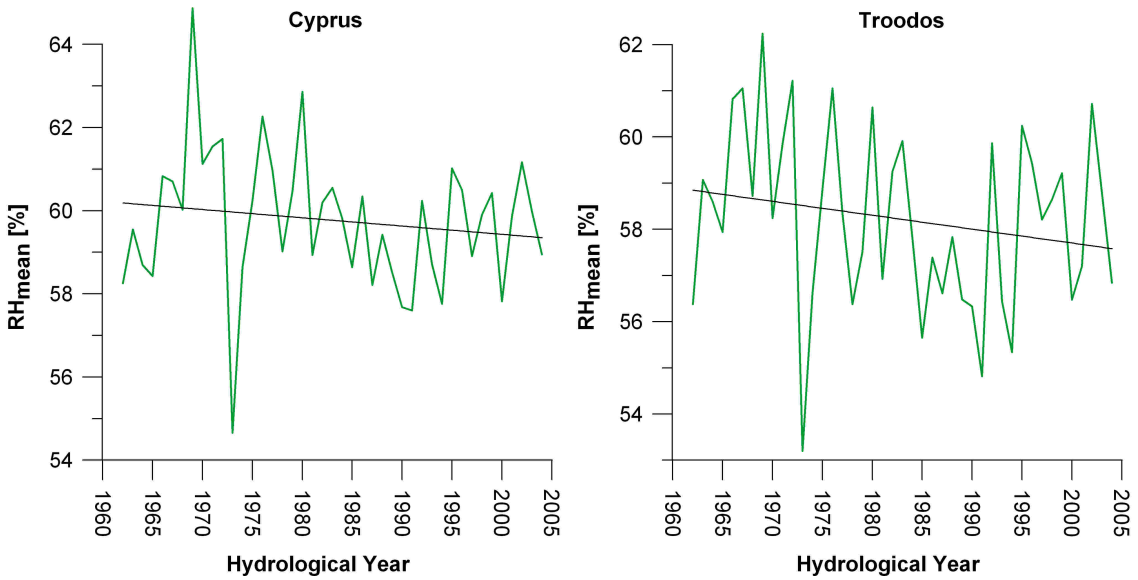

Figure 5.13: Mean areal relative humidity of Cyprus (green line) and its linear trend (black line) for the modelling period 1961-2004. The trends are not significant according to the Mann-Kendall test (Q = -0.81 | -1.37).

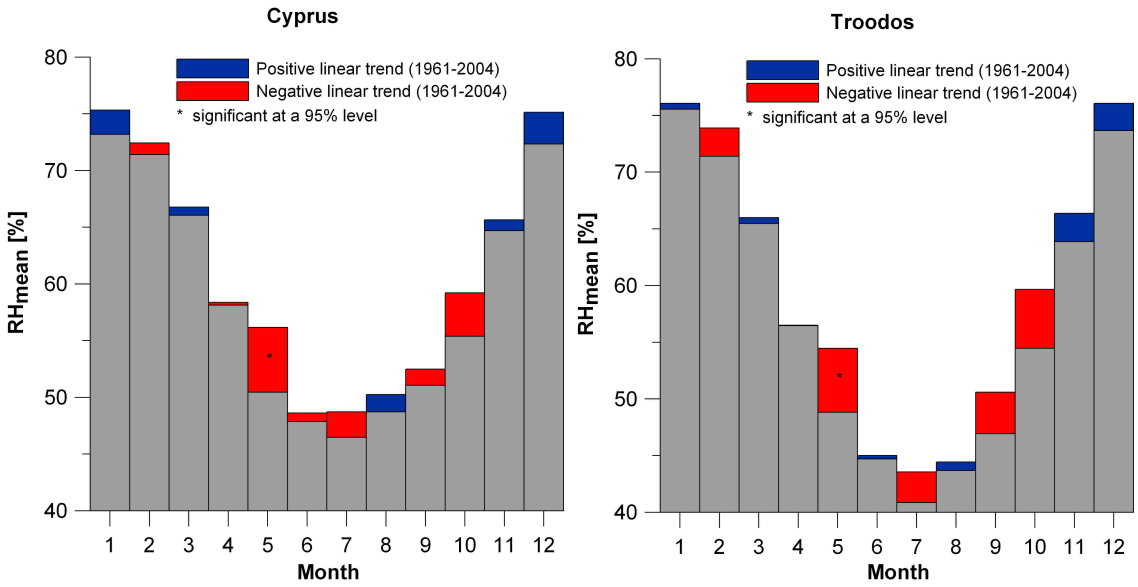

Figure 5.14: Monthly linear trends of mean areal relative humidity of Cyprus for the modelling period 1961-2004. Months with significant trends according to the Mann-Kendall trend test are indicated.

extreme minimum of daily relative humidity in the central Mesaoria plain (Fig. 5.12) is mainly a result of high daily temperatures in this area. The continental character of the climate in this area is supported by the ranges in the North (Kyrenia range) and South (Troodos range) suppressing direct air flow from the sea.

A mean areal relative humidity of 59.6% and a standard deviation of 1.6% was calculated for the modelling period 1961-2004. The plot of the interannual variability shows a notable correlation to the precipitation and temperature time series. Furthermore, decreasing trends can be detected for the whole of Cyprus. Although more distinctive for the Troodos area, the trends are not significant according to the Mann-Kendall trend test (Fig. 5.13). Also most of the monthly analyses do not show clear tendencies or trends, except for the relative humidity of May, which reveals a significant decreasing trend on a 95% level (Mann-Kendall trend test). In October, the decreasing trend narrowly missed the 95% significance level. This can be related to precipiation and temperature, which also show unfavourable trends for these transitional months (see Chap. 5.2, 5.3). Nonsignificant increases of relative humidity exist in the winter months November, December and January (see Fig. 5.13).

5.5 Sunshine Duration

Mean relative sunshine duration can be described as the fraction of daytime during which the sun casts an obvious shadow. Mean values for Cyprus are very high due to the setting of the island in the eastern Mediterranean. The mean interpolated pattern of the relative sunshine duration of Cyprus (not shown) does not appear very complex due to the small amount of available recorders (see Fig. 4.7). A close relationship to terrain elevation is dominant as a result of decreasing sunshine duration with increasing elevation. The long-term annual means for the Mesaoria plain and coastal areas range between 72-75%, and for the higher areas of the Troodos range between 59-62%. For Northern Cyprus no data is available, but a similar gradient of decrease with elevation can be assumed.

The pronounced seasonal cycle of Cyprus is also present in the seasonal averages of relative sunshine duration. In the winter months (D,J,F) the lowlands register about 57-60%, the higher Troodos areas only 40-43% of the possible sunshine duration. In

the summer months (J,J,A), the lowlands register about 85-90% and the higher Troodos area 75-80% of the possible sunshine duration.

The sparse and incomplete time series of the few recording stations were not considered to be suitable for a reliable trend analysis. For that reason, further statistical analyses of the data were not performed.

5.6 Wind Speed

Reliable daily spatial patterns of mean wind speeds for the modelling period could not be generated. The density of the station network available (Fig. 4.8) is not sufficient concerning standard interpolation techniques in this complex topographical island environment, where wind speed differs extremely within small areas. A special wind model would be required for a reasonable spatial interpolation. A further problem is that no time series are available for the whole period before 1976 in Southern Cyprus, and no time series for the complete modelling period in Northern Cyprus. The data also shows great quality differences due to varying types of operating recorders and incomplete time series.

For the current model, wind speed is reduced to a secondary parameter with less influence. Monthly mean conditions were derived for the time period before 1976. Stations with very high annual mean wind speeds were discarded, because their locations are presumably situated in one of the smaller corridors of strong winds. For the time period since 1976, mean wind speeds are derived for several sectors of the island.

The seasonal analysis of the mean data shows that the highest mean wind speeds typically occur in spring (3-7 m/s). April is usually the month with the highest mean on nearly all wind recorders. The calmest conditions (2-5.5 m/s) occur in the late summer months and in autumn (August-November), as a result of the relatively small pressure, air and sea temperature contrasts in that period.

5.7 Potential Evapotranspiration

The presented maps and graphs refer to the land cover specific potential evapotranspiration under hypothetical well-watered conditions (see Chap. 3.4.5). It is controlled by land cover properties and meteorological conditions. Forested areas with high transpiration and interception losses show higher values than areas with sparse vegetation. Meteorological influence is most prominent regarding the parameters for maximum daily temperature and minimum daily relative humidity. Topographic influences can be identified, especially in the mountainous areas where expositional effects lead towards a modification of the radiation conditions.

The mean annual pattern of Cyprus (Fig. 5.15) reveals a close relationship to land cover and meteorological factors. Despite lower temperatures, the Troodos range shows a relatively high potential evapotranspiration compared to other areas with sparse vegetation. Only the highest crests of the Troodos, with low mean temperatures, show reduced potential evaporation also in the forested areas. Generally, the meteorological influence appears most prominent towards the centre of the island, with a more continental climate. Higher maximum daily temperature and lower minimum daily relative humidity lead towards increasing values of potential evapotranspiration.

Overall, the highest potential evapotranspiration on the island appears in continental and forested areas of the island, like the central Mesaoria plain and the southern slopes of the Troodos range, where radiation effects also support higher evapotranspiration. In those areas, values of more than 1500 mm/a are common. In contrast, lowest values appear in areas with sparse or no vegetation, such as sealed areas. There, evapotranspiration is controlled by evaporation from surfaces and only little transpiration. The mean value assessed for the whole island is about 1340 mm/a for the reference time period 1971-2000.

The seasonal cycle of potential evapotranspiration is induced mainly by monthly meteorological conditions. A further influence is given by the variation of transpiration activity of the vegetation coverage, which is partially expressed by the bulk surface resistance, but of secondary importance compared to the meteorological influences. Highest rates occur in hot summer months with values up to 200 mm/month. In cool winter months, values lower than 50 mm/month are typical (see Fig. 5.17).

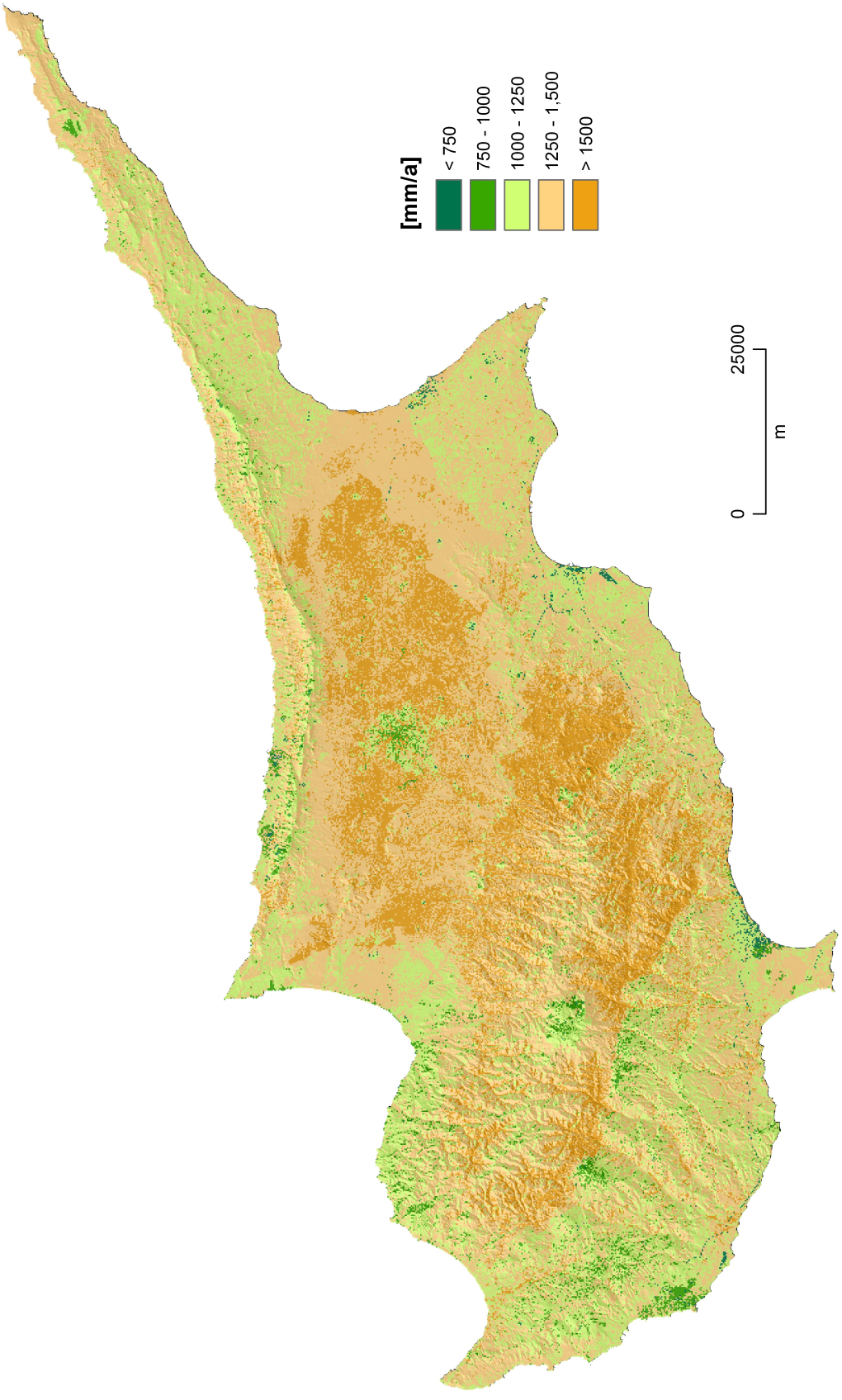

Figure 5.15: Land cover specific mean potential evapotranspiration of Cyprus for the reference time period 1971-2000.

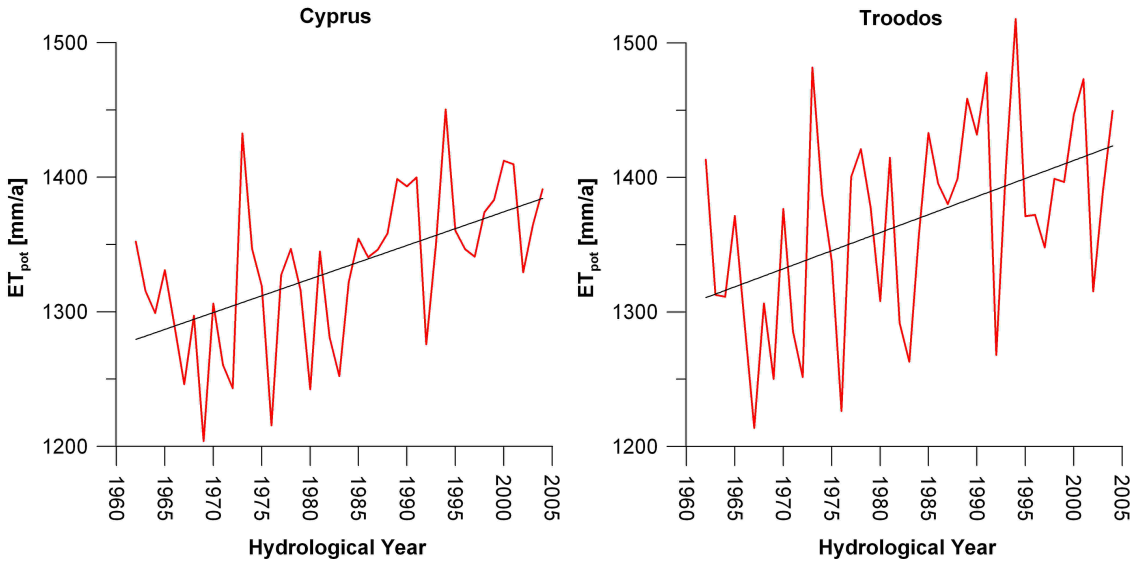

Figure 5.16: Mean areal potential (crop) evapotranspiration of Cyprus (red line) and its linear trend (black line) for the modelling period 1961-2004. Both trends are significant on a 99% level according to the Mann-Kendall test (Q = 2.85 | 3.91).

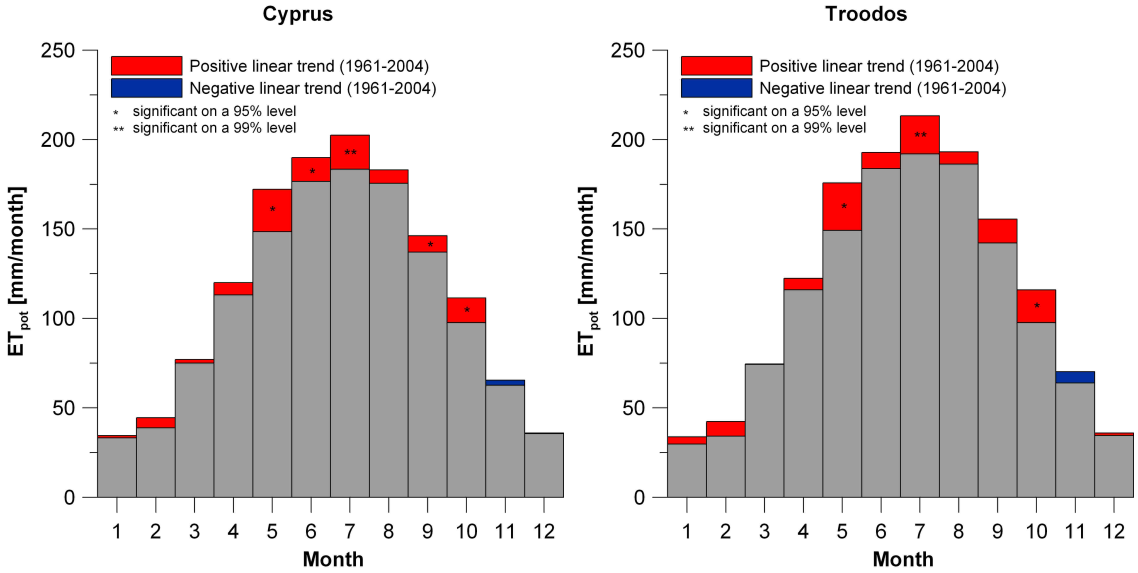

Figure 5.17: Monthly linear trends of mean areal potential (crop) evapotranspiration of Cyprus for the modelling period 1961-2004. Months with significant trends according to the Mann-Kendall test are indicated.

The trend analysis of the derived potential evapotranspiration time series for Troodos and the whole of Cyprus, shows significant positive trends in several summer months and the transitional months May and October (see Fig. 5.17). Most winter months show none or only minor increases. Variation and trends can be directly related to the important controlling meteorological factors: temperature and relative humidity, which show similar changes and trends. In case of temperature, the trends are more distinctive for the months May to October. In the case of relative humidity, the decreasing trend occurs especially in May and October, supporting the rise of potential evaporation in the transitional months.

5.8 Actual Evapotranspiration

The actual evapotranspiration is controlled by the potential evapotranspiration and local water availability (soil and interception storage). The mean annual pattern for the island (see Fig. 5.18) shows a strong dependence on the mean annual precipitation pattern, and indicates that water availability is the limiting factor for actual evapotranspiration on Cyprus. Therefore, areas with the lowest mean annual evapotranspiration rates correspond to areas with minimum annual precipitation on the island. In the driest areas of the island, such as the southwestern Mesaoria with rates of about 250 mm/a, nearly all water from precipitation is lost by evapotranspiration.

Highest values occur in forested areas of the Troodos mountains, where rates of more than 600 mm/a are possible. Still higher rates occur only in moist or irrigation areas, where additional water from other sources than direct precipitation is available (secondary evapotranspiration). If the additional water supply is kept throughout the whole year, then actual evapotranspiration rates can reach the level of potential evapotranspiration. On Cyprus, most natural moist areas exist on the valley floors of the Troodos rivers. Water from river flows compensate the water deficits in dry months and allow annual evapotranspiration rates of more than 1500 mm/a. Still higher actual evapotranspiration rates occur in artificial irrigation areas of the coastal and inner plains, where also more than 1500 mm/a are possible due to the still higher mean daily temperatures.

The particular seasonal cycle of mean actual evapotranspiration (see Fig. 5.20) is the result of the varying influence of two main controlling factors: water availability

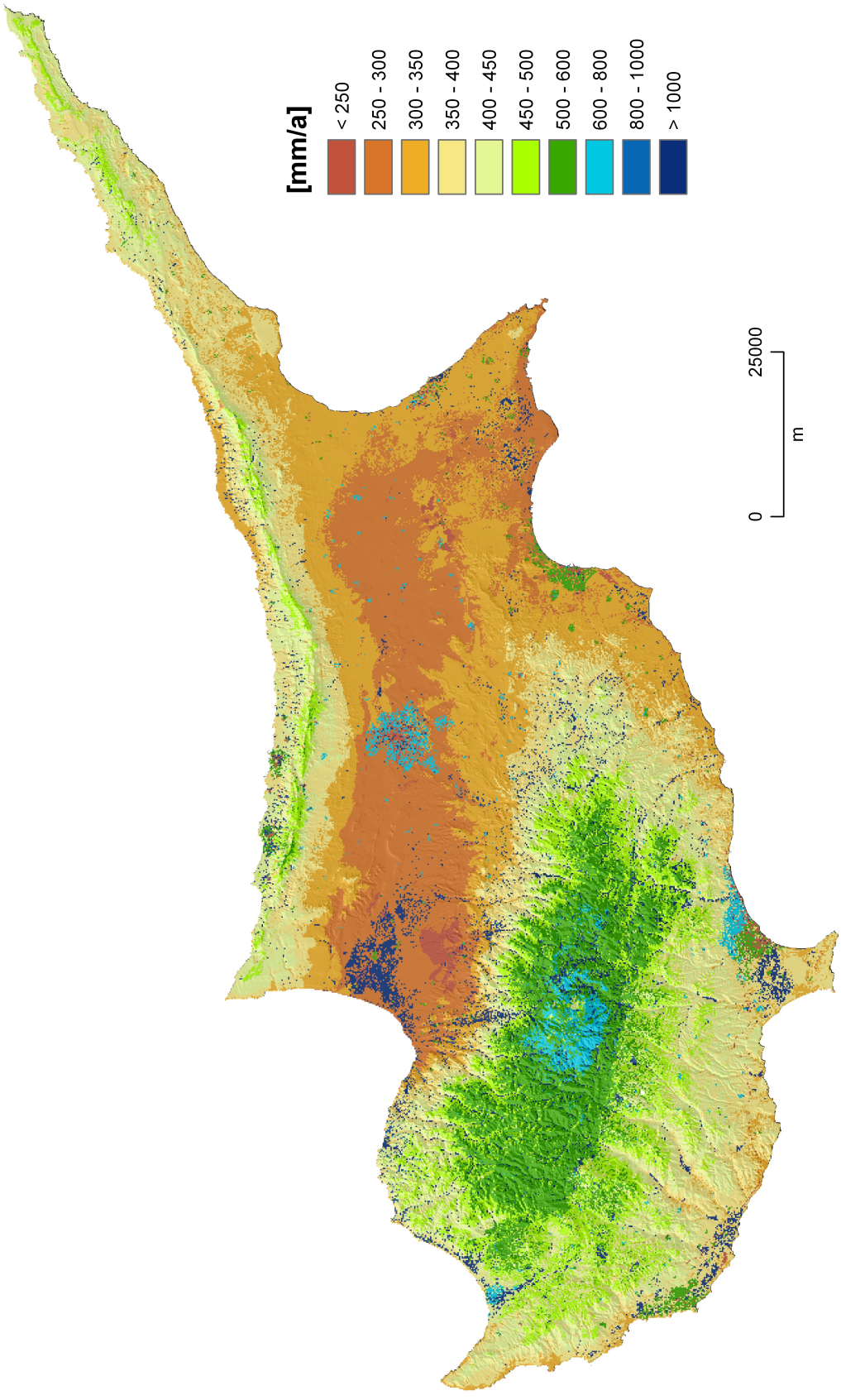

Figure 5.18: Mean actual evapotranspiration (incl. ET_{sec}) of Cyprus for the reference time period 1971-2000.

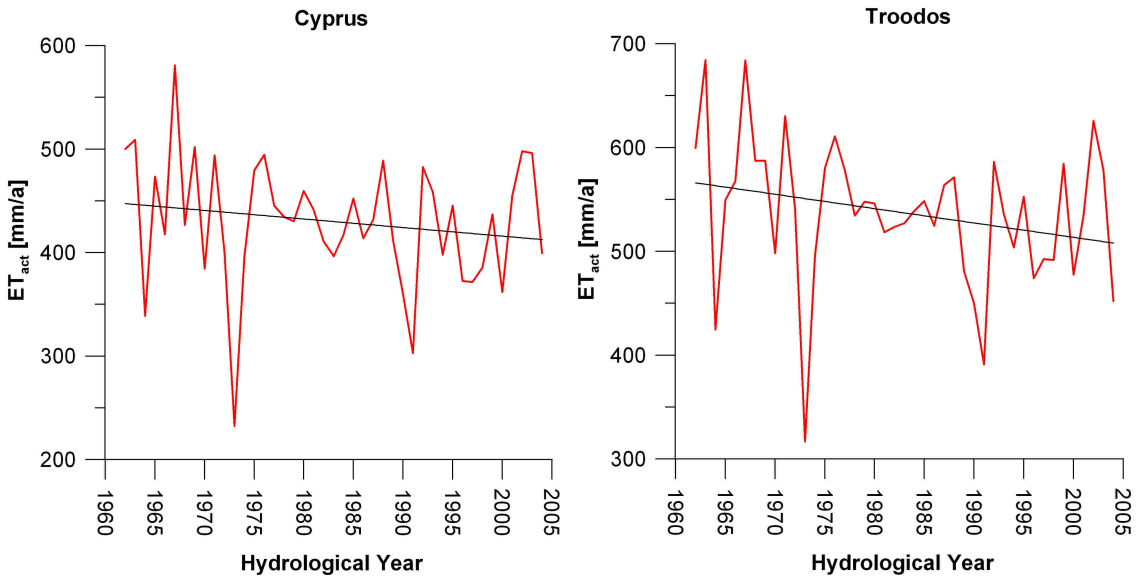

Figure 5.19: Mean areal actual evapotranspiration of Cyprus (red line) and its linear trend (black line) for the modelling period 1961-2004. Only the trend for Troodos area is significant on a 95% level according to the Mann-Kendall test (Q = -1.41 | -2.32).

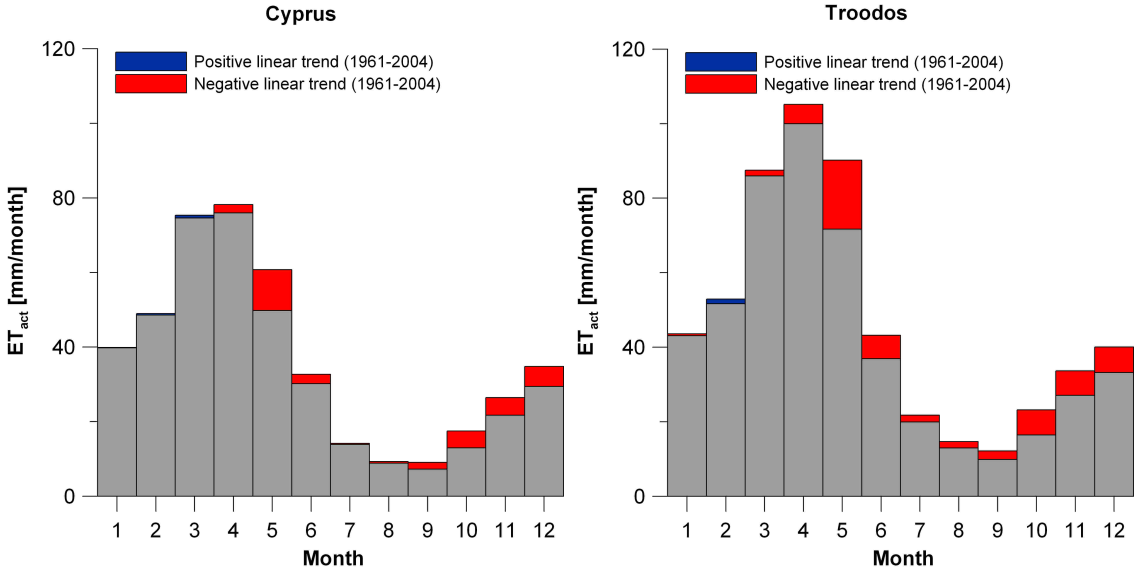

Figure 5.20: Monthly linear trends of the mean areal actual evapotranspiration of Cyprus for the modelling period 1961-2004. No months with significant trends exist according to the Mann-Kendall trend test.

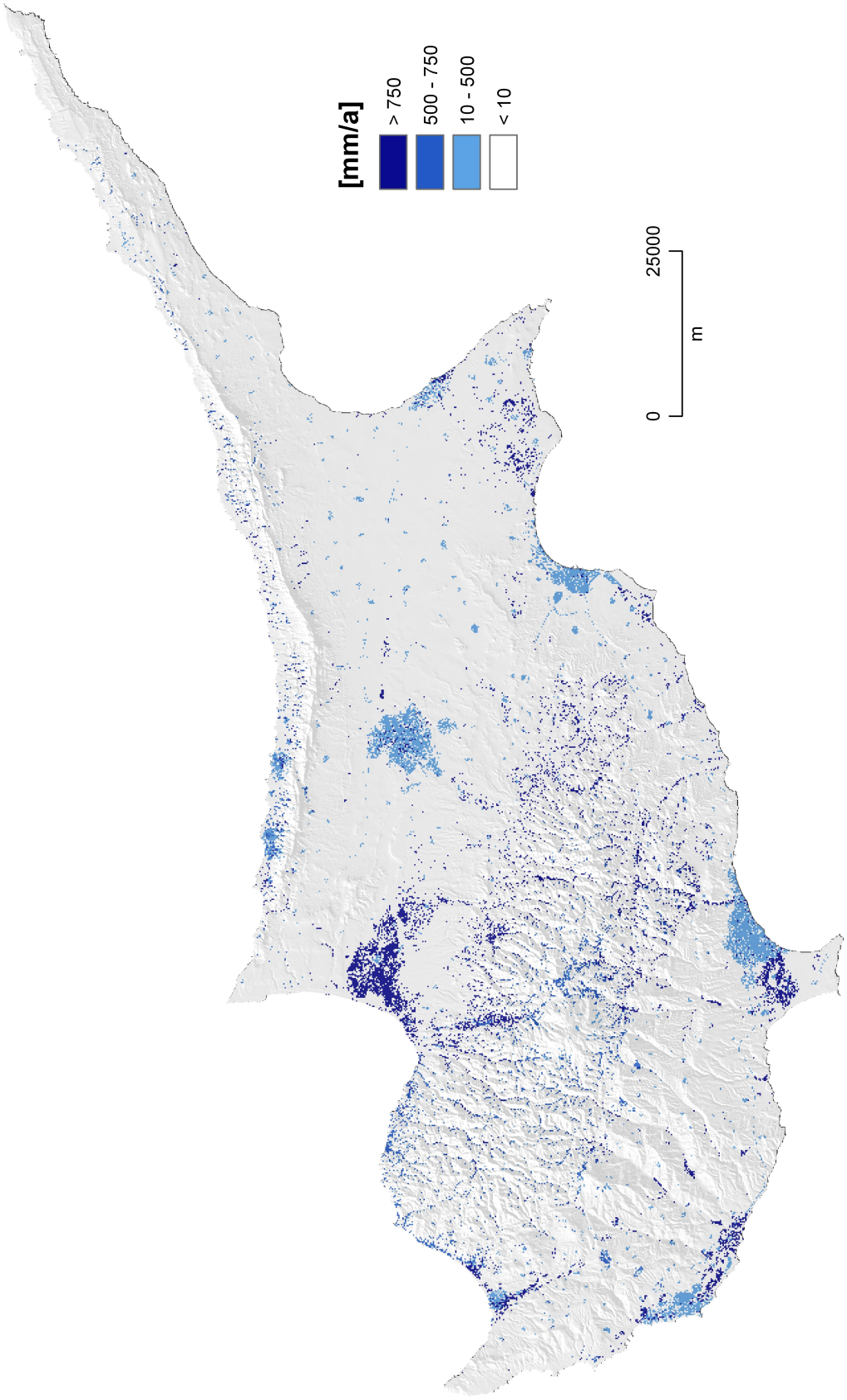

Figure 5.21: Mean secondary evapotranspiration of Cyprus for the reference time period 1971-2000.

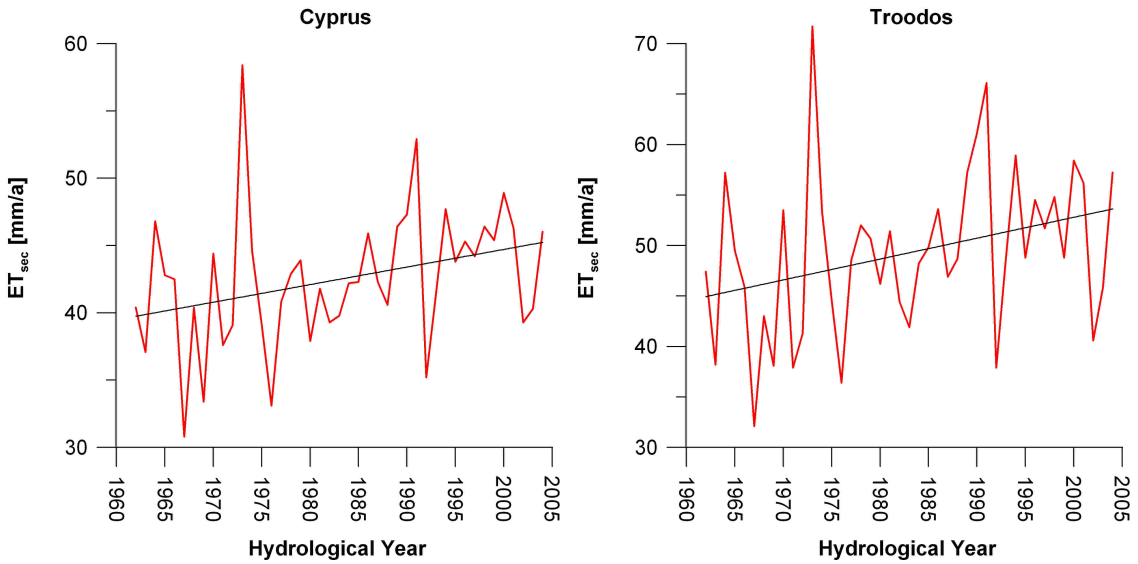

Figure 5.22: Mean areal secondary evapotranspiration of Cyprus (red line) and its linear trend (black line) for the modelling period 1961-2004. The detected trends are significant according to the Mann-Kendall test (Q = 2.69 | 2.41) on a 99% | 95% level.

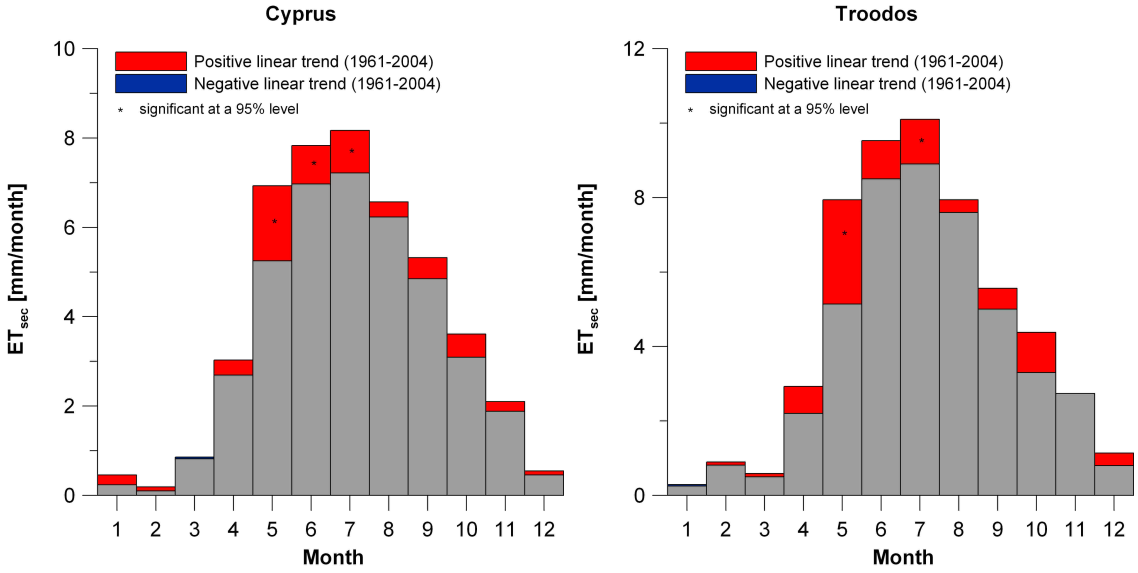

Figure 5.23: Monthly linear trends of the mean areal secondary evapotranspiration of Cyprus for the modelling period 1961-2004. Months with significant trends according to the Mann-Kendall trend test are indicated.

and potential evapotranspiration. Cool winter months with abundant rainfall do not coincide with the months of highest actual evapotranspiration. Potential evapotranspiration is too low and acts as a limiting factor. The surplus of water is either stored in the root zone or is lead away by direct runoff and groundwater recharge. In contrast, water availability becomes the limiting factor for actual evapotranspiration in summer and autumn months. Mean potential evapotranspiration is higher than the mean water available for evapotranspiration. As a consequence, the spring months (March, April, May) show the highest mean actual evapotranspiration rates throughout the year, as precipitation and water from soil storage are still available and potential evapotranspiration already increases during this season.

The trend analysis shows a decreasing trend of actual evapotranspiration (incl. ET_{sec}) for the Troodos area and the whole island, but significantly only for the Troodos area on a 95% level (Fig. 5.19). Since the potential evapotranspiration shows strong positive trends, it has to be the decreasing mean precipitation trends and the accompanied lower soil moisture state that cause the decrease of actual evapotranspiration. The monthly analysis (Fig. 5.20) confirms this assumption. The transitional and early winter months especially show (Fig. 5.4) decreases, which appear still higher after having excluded the influence of secondary evapotranspiration, because the secondary part of actual evapotranspiration shows significant positive trends. The latter is a result of the positive trends of potential evapotranspiration, as secondary evapotranspiration is not controlled by water availability (Fig. 5.22). The monthly analysis shows that the summer and transitional months are most affected (Fig. 5.23).

5.9 Direct Runoff

The mean pattern (Fig. 5.24) of direct runoff is one of the most important patterns concerning the investigation of renewable natural water resources of the island. A certain part of the annual direct runoff is caught in dams and used for domestic or agricultural use. The pattern for direct runoff reveals a strong dependence on topography and precipitation. In plains with a very smooth relief and low precipitation amounts, only very little runoff is simulated. In contrast, the areas with high precipitation amounts and very steep slopes in the Troodos and Kyrenia range

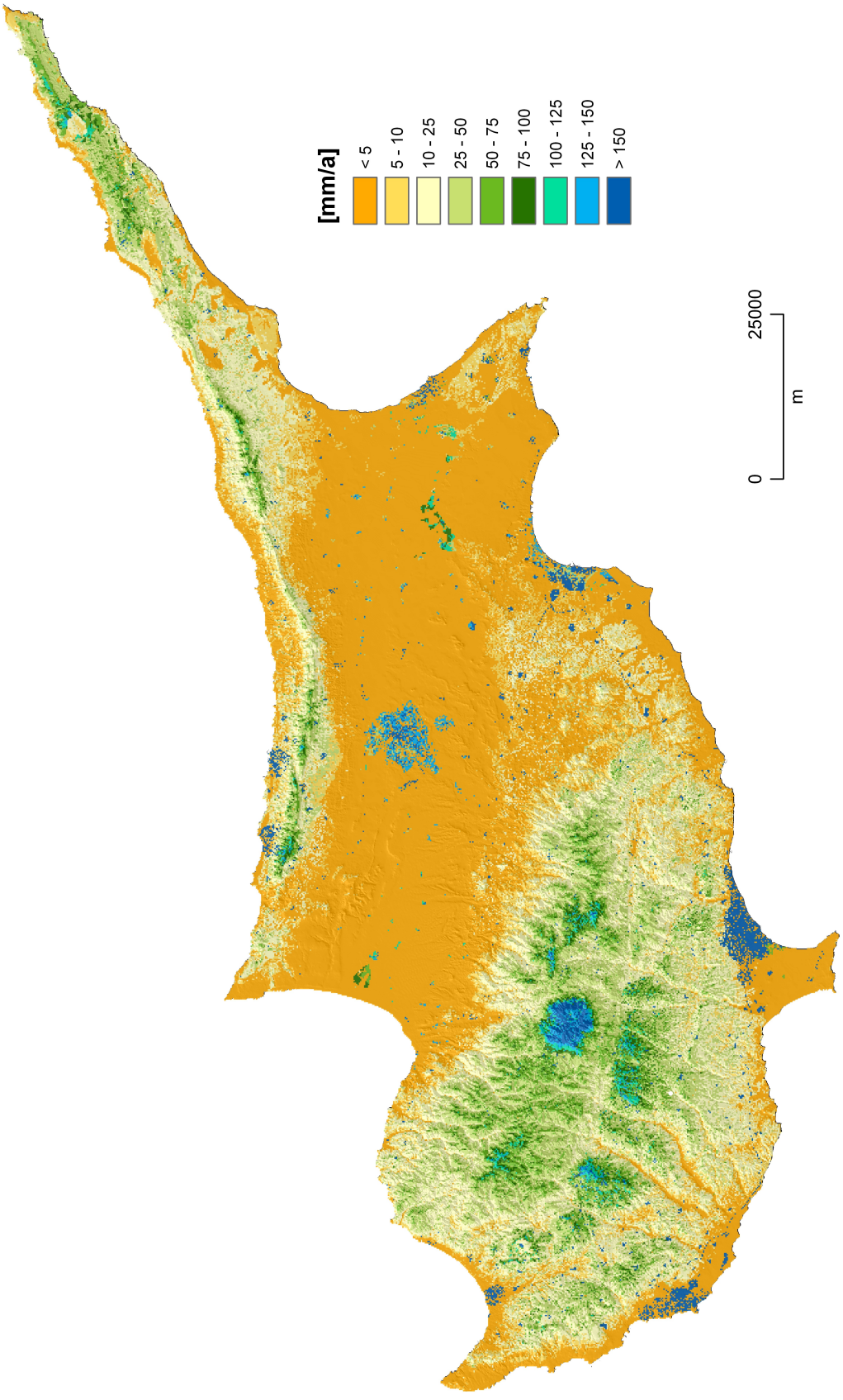

Figure 5.24: Mean direct runoff of Cyprus for the reference time period 1971-2000.

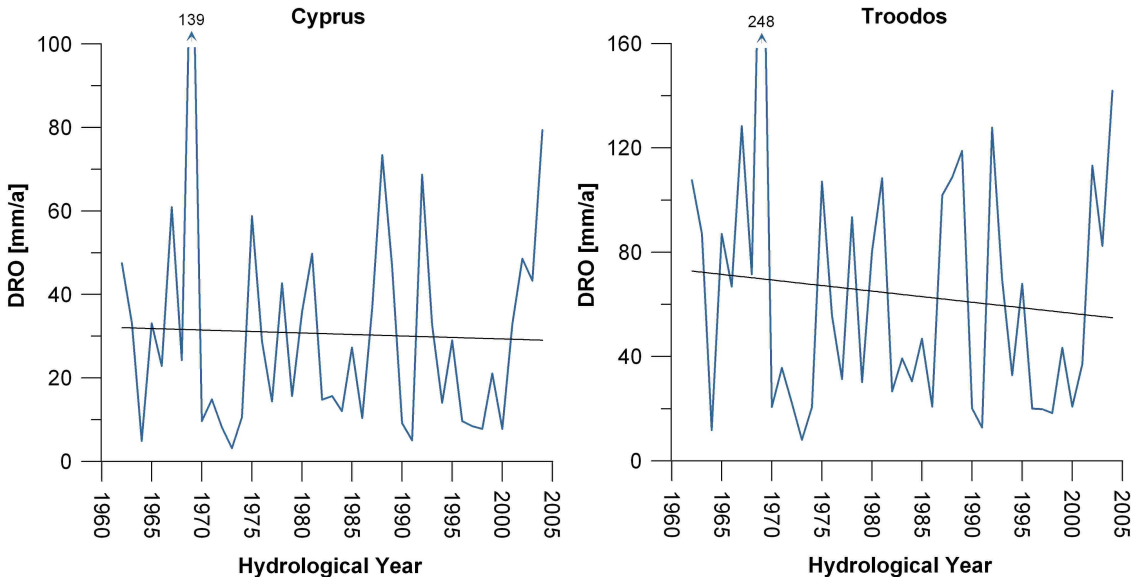

Figure 5.25: Mean areal direct runoff of Cyprus (blue line) and its linear trend (black line) for the modelling period 1961-2004. The trends are not significant according to the Mann-Kendall test (Q = -0.17 | -0.40).

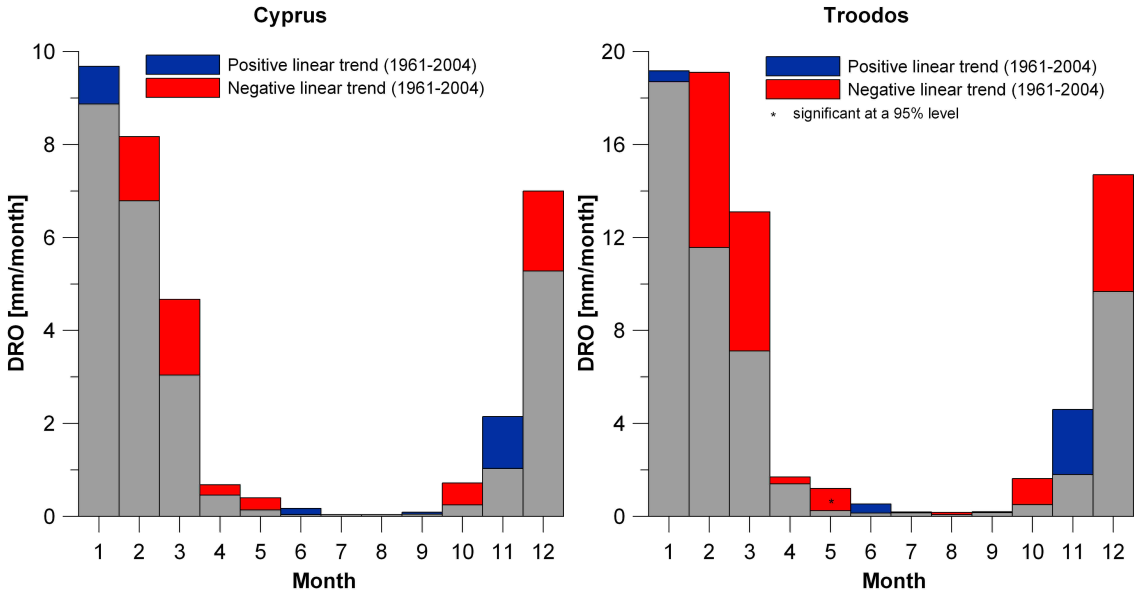

Figure 5.26: Monthly linear trends of mean areal direct runoff of Cyprus for the modelling period 1961-2004. Months with significant trends according to the Mann-Kendall trend test are indicated.

are areas of high direct runoff. Rates of more than 150 mm/a are common in the highest Troodos areas nearby Mount Olympos. Moreover, high runoff rates can also be found in settlements and industrial areas with a high fraction of sealed surfaces. Cities, larger settlements, airports and industrial areas can be well identified as spotted zones of high anomalies (Fig. 5.24). In these areas a considerable part of total precipitation is transferred to direct runoff.

The seasonal cycle is very distinctive (see Fig. 5.26). Most of the annual direct runoff is registered between the months November and March. The summer contribute little to the annual sum. The tendency for drier conditions in the transitional months May and October can also be detected for direct runoff.

The simulated direct runoff is furthermore characterised by a very strong interannual variability (see Fig. 5.25). From year to year, the values often vary strongly compared to the values from the previous year. For the whole of Cyprus a standard deviation of about 20 mm correspond to the mean direct runoff of 26.5 mm/a (time period 1961-2004). For the Troodos area, a similar situation exists with a standard deviation of more than 35 mm and a mean of 45.8 mm/a (modelling period 1961-2004). Due to high variability it is more difficult to detect trends owing to the low signal-to-noise-ratio. The graphs show a decreasing but not significant direct runoff, especially in the Troodos area. The comparison of monthly trends reveals that decreases occur most notably in the winter months December, February, March, and also during the transition months May and October (see 5.26).

5.10 Groundwater Recharge

The direct groundwater recharge pattern is the most important pattern for evaluating the renewability of natural water resources of the island. The pattern does not include secondary recharge processes like recharge by river-bed infiltration. The most prominent feature of the pattern is the strong dependency of groundwater recharge on the annual precipitation pattern. The hydrological properties of geological formations and land cover conditions contribute to a further differentiation of the pattern, but are of comparably smaller importance in the context of renewability.

This situation illustrates the outstanding importance of the Troodos massif. In large

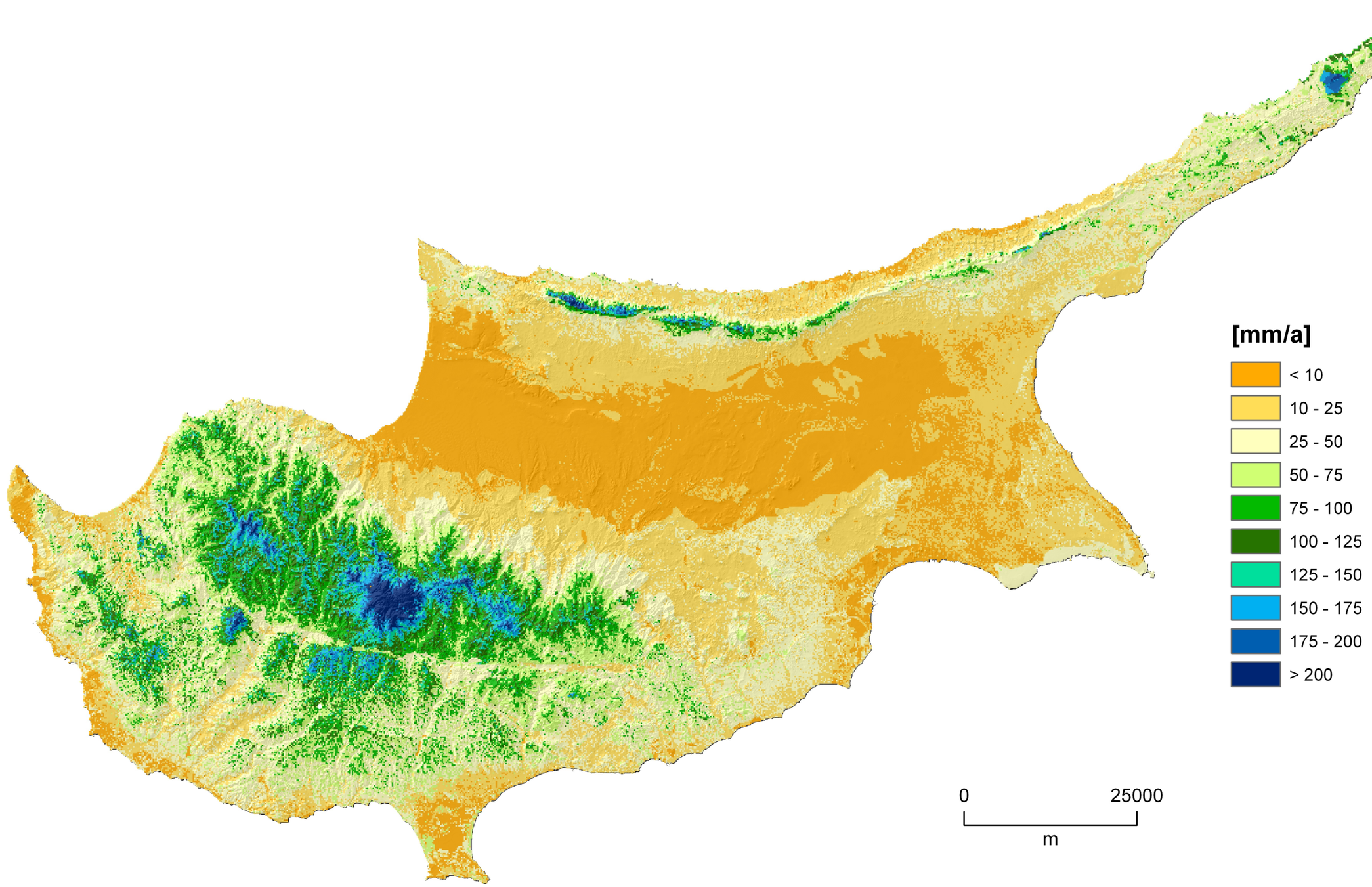

Figure 5.27: Mean direct groundwater recharge of Cyprus for the reference time period 1971-2000 (without secondary recharge like river-bed infiltration).

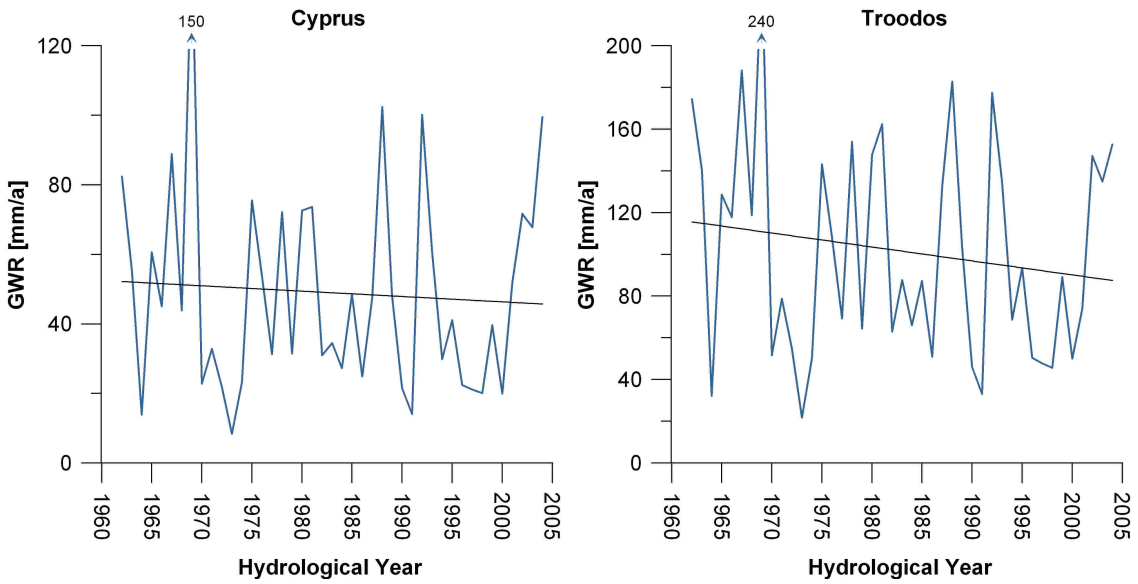

Figure 5.28: Mean areal direct groundwater recharge of Cyprus (blue line) and its linear trend (black line) for the modelling period 1961-2004. The trends are not significant according to the Mann-Kendall test (Q = -0.63 | -0.87).

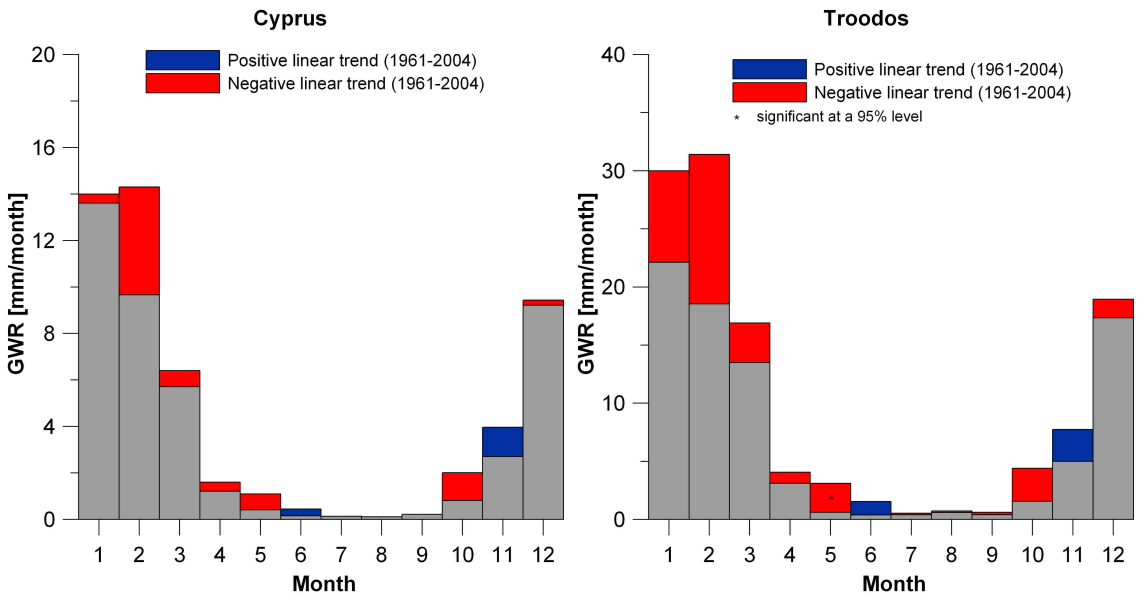

Figure 5.29: Monthly linear trends of mean areal direct groundwater recharge of Cyprus for the modelling period 1961-2004. Months with significant trends according to the Mann-Kendall trend test are indicated.

areas of the massif, average annual groundwater recharge rates above 100 mm/a are registered. Even 200 mm/a and more are common in the highest areas of the Troodos nearby Mount Olympos, where precipitation rates reach 1000 mm/a and more. In the Kyrenia Range and on the southern and western Troodos foothills, some smaller zones with medium recharge rates can be detected. Nevertheless, much of the areas of the inner and coastal plains are mostly zones with very low recharge rates (below 25 mm/a).

The seasonal cycle depends strongly on the monthly precipitation, evapotranspiration and soil water conditions (see Fig. 5.29), limiting the generation of recharge to the months December to March. Similar to the case of direct runoff, the interannual variability is extremely high (see Fig. 5.29). For the whole of Cyprus, a standard deviation of about 30 mm corresponds to the mean areal of 46.6 mm/a, in the Troodos area a standard deviation of more than 50 mm corresponds to a mean of 101.5 mm/a (modelling period 1961-2004).

Significant trends could not be detected for Cyprus and the Troodos area (Fig. 5.28). The determination is difficult owing to the high variability resulting in a low signal-to-noise-ratio. The decreasing is recognisable, but not a significant trend in the time series graph for the Troodos. It seems to be mainly a result of the decrease in the late winter months and early spring months (see Fig. 5.29). The transition months May and October, show also a noticeable, partially significant decrease, but on a very low absolute level.

5.11 Catchment Response

The simulation of discharge time series can be best performed for well-defined catchments, forming more or less closed systems. When the recorded discharge time series allows a good separation of direct runoff and base flow, then regional hydrological and hydrogeological factors can be calibrated by the comparison of recorded and simulated total discharge, direct runoff and baseflow (see also Chap. 3.9). The calibrated time series provide a detailed insight into regional dynamics of direct runoff, groundwater recharge and base flow; because of generation processes and their dynamics (discussed in Chap. 5.2-5.10, 5.12).

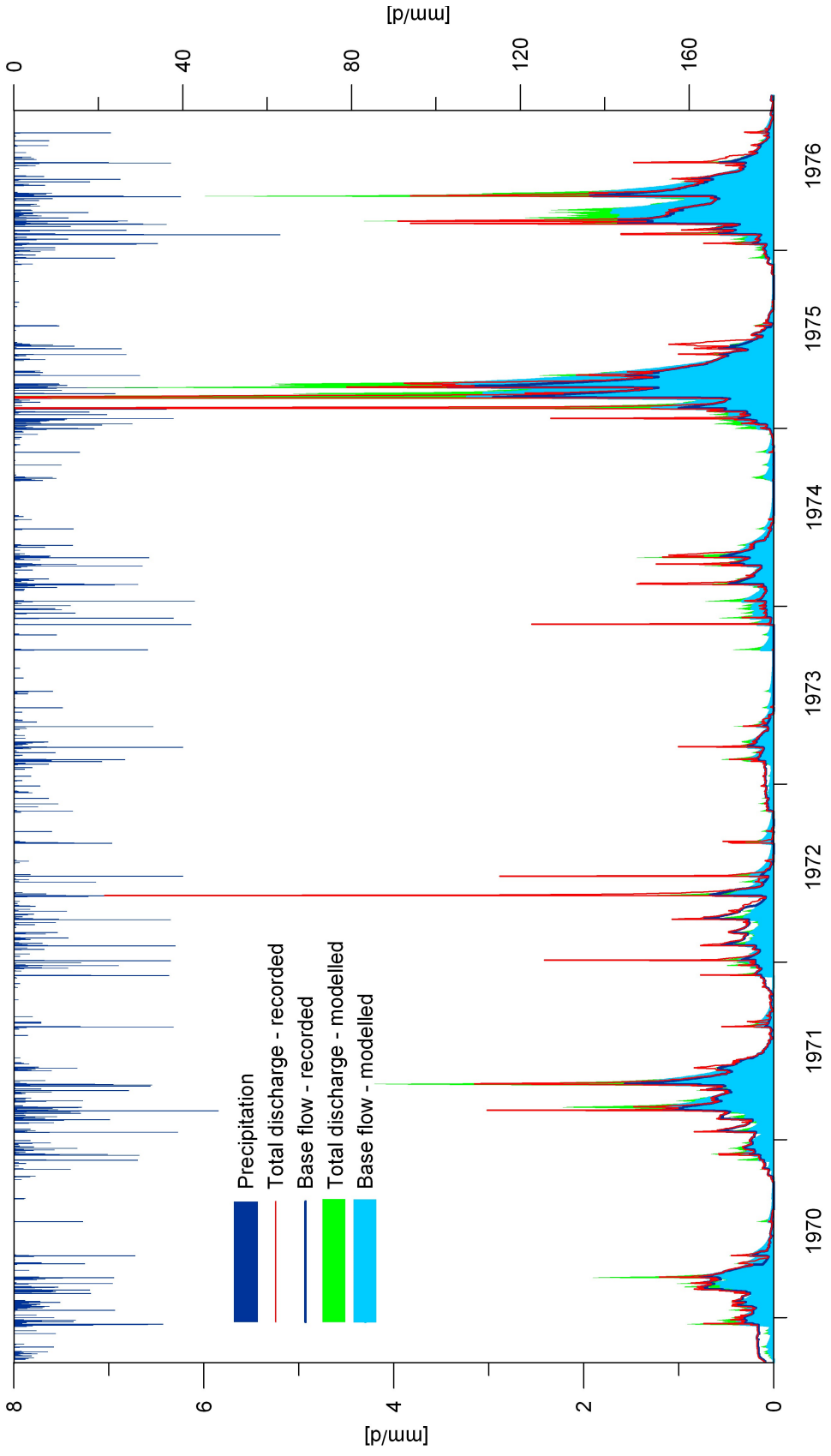

Figure 5.30: Recorded and modelled catchment discharge of the upper Diarizos valley 10/1969 - 09/1995.

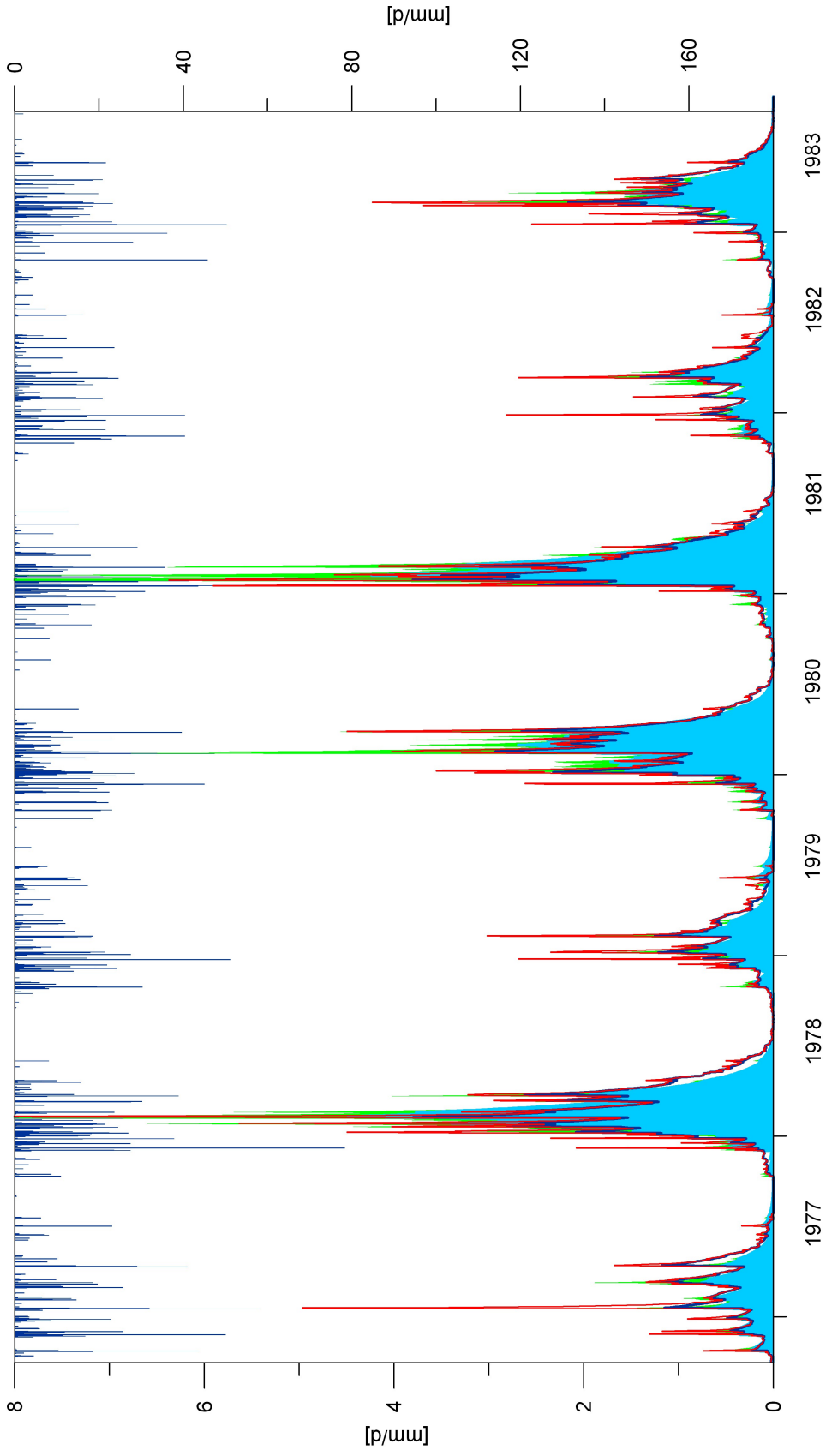

Figure 5.30 (Continued)

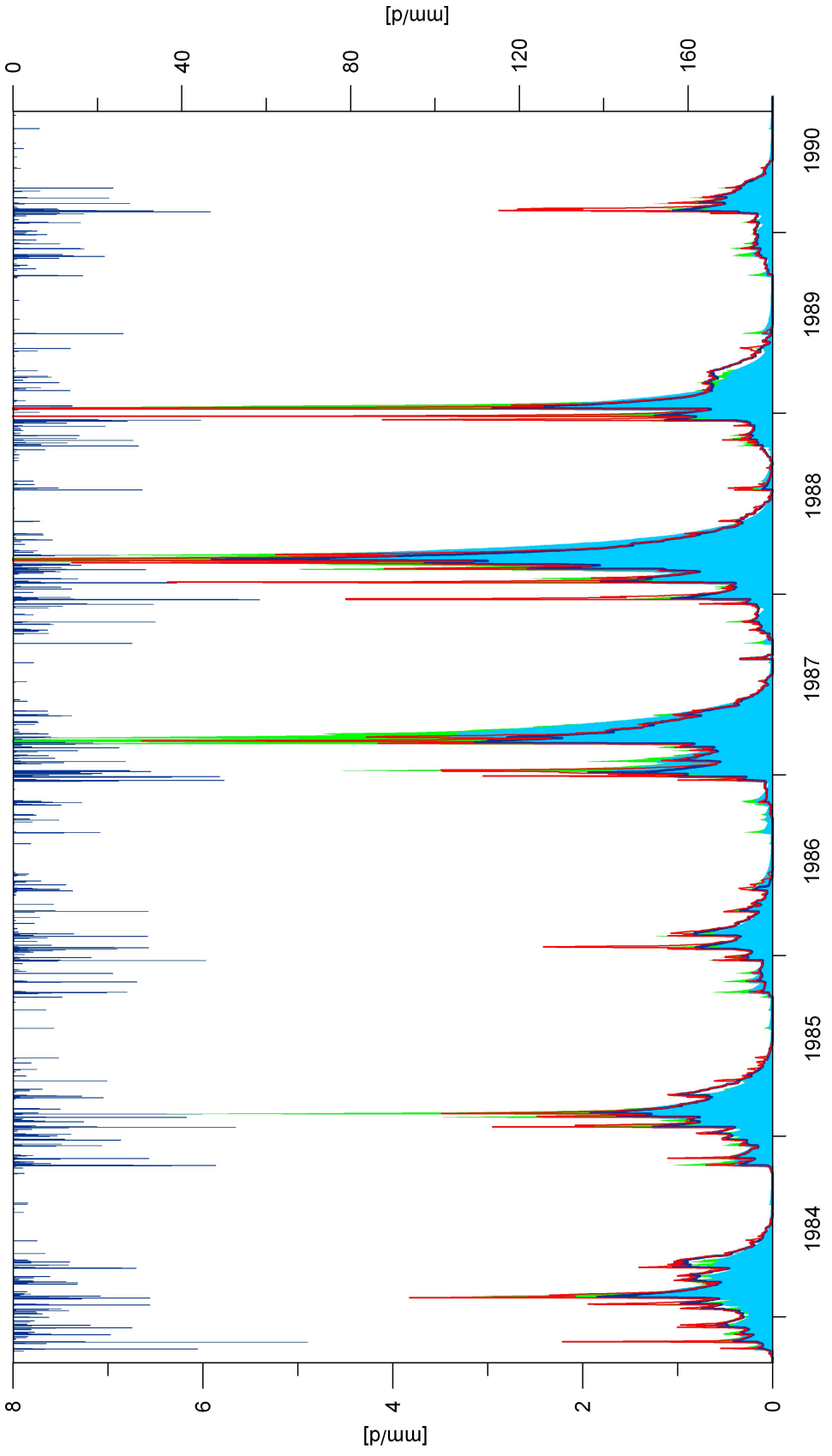

Figure 5.30 (Continued)

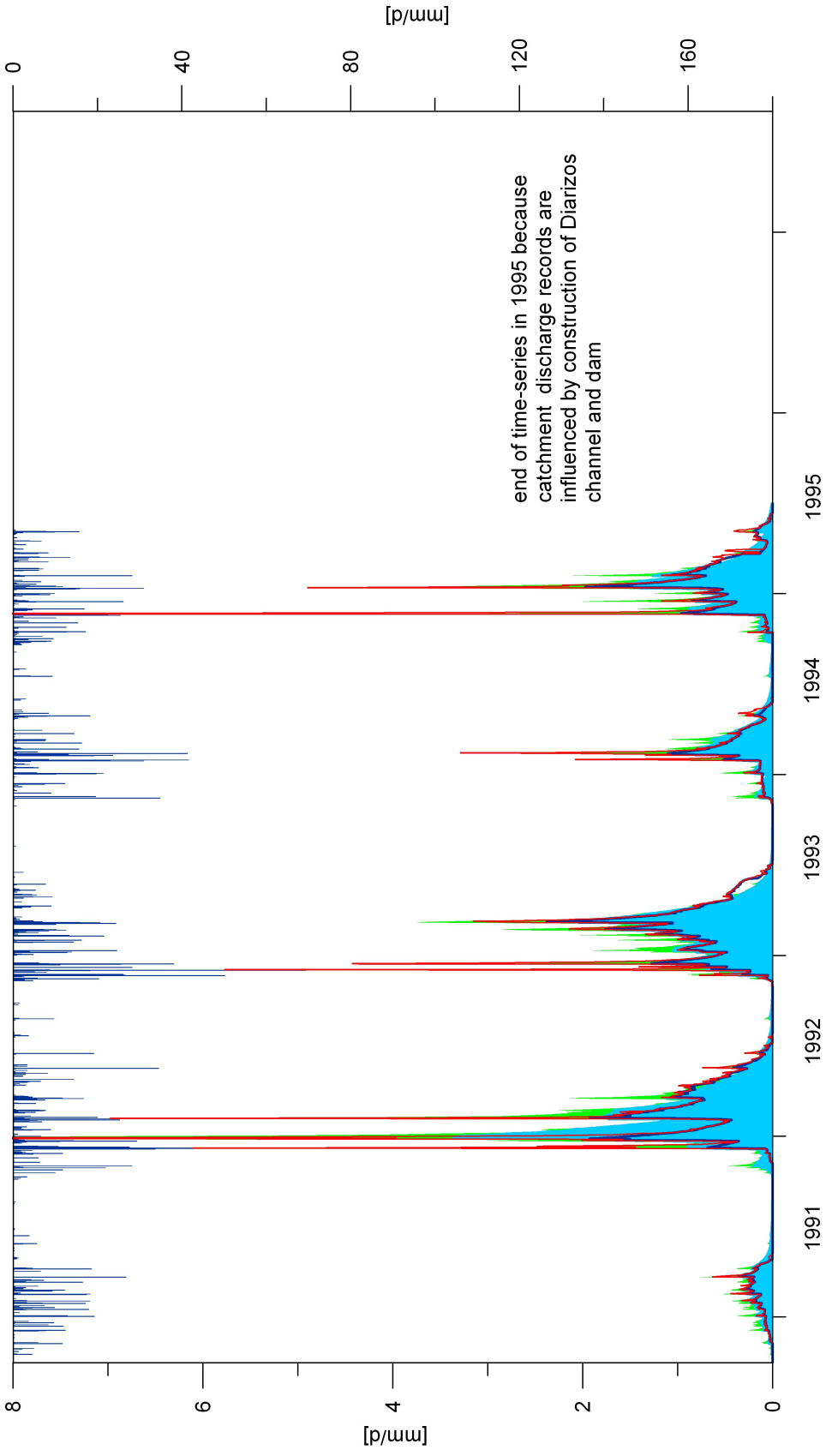

Figure 5.30 (Continued)

The upper Diarizos valley is one of the most important catchment areas for the understanding of the hydrological and hydrogeological system of the Troodos area. The construction of a calibrated regional water balance model for this area, is an important step within the development of the model for the whole island. The upper Diarizos valley is one of the biggest catchments in the central Troodos and integrates several important hydrological and land cover units. Important hydrological factors could be calibrated in this catchment and validated by modelling results from further catchments. Preliminary water balance studies on the upper Diarizos catchment (Dünkeloh 2005a, 2005b) were performed some years ago and considered in the present research.

The visualisation of recorded and modelled daily time series (Fig. 5.30) allows an evaluation of the model quality. It can be seen that the discharge recorded is reproduced very well by the simulated discharge. Especially the base flow shows an excellent concordance, which is one of the main goals of the model, allowing the evaluation of the renewability of natural water resources. Also, the interannual variability is reproduced very well, which is of crucial importance for further simulations of climate change scenarios.

The comparison of simulated and recorded direct runoff reveals that discrepancies occur especially in the case of extreme events. Several extreme discharge events were not registered by the local recorder, in other cases the recorder shows extreme events, which are not simulated by the model. These are presumably inaccuracies of the recorders regarding short and extreme discharge events. Furthermore, MODBIL is not optimised for the simulation of such extreme events, which require further routing algorithms and higher resolved meteorological data of time and space. Generally, it can be observed that in wet years with several extreme events, the model shows higher direct runoff than the recorders. In those cases it can be assumed that the recorder underestimates direct runoff, because during those periods, the soil water state is near field capacity, evapotranspiration is very low, and water can only be drained by direct runoff or groundwater recharge. The results show that an inaccurate simulation of extreme events is of limited importance for a good assessment of the total water balances in the present study areas.

The simulated discharge results simulated can be used for the detection of inconsistencies in the recorded time series. For several years, corrupted recordsets can be

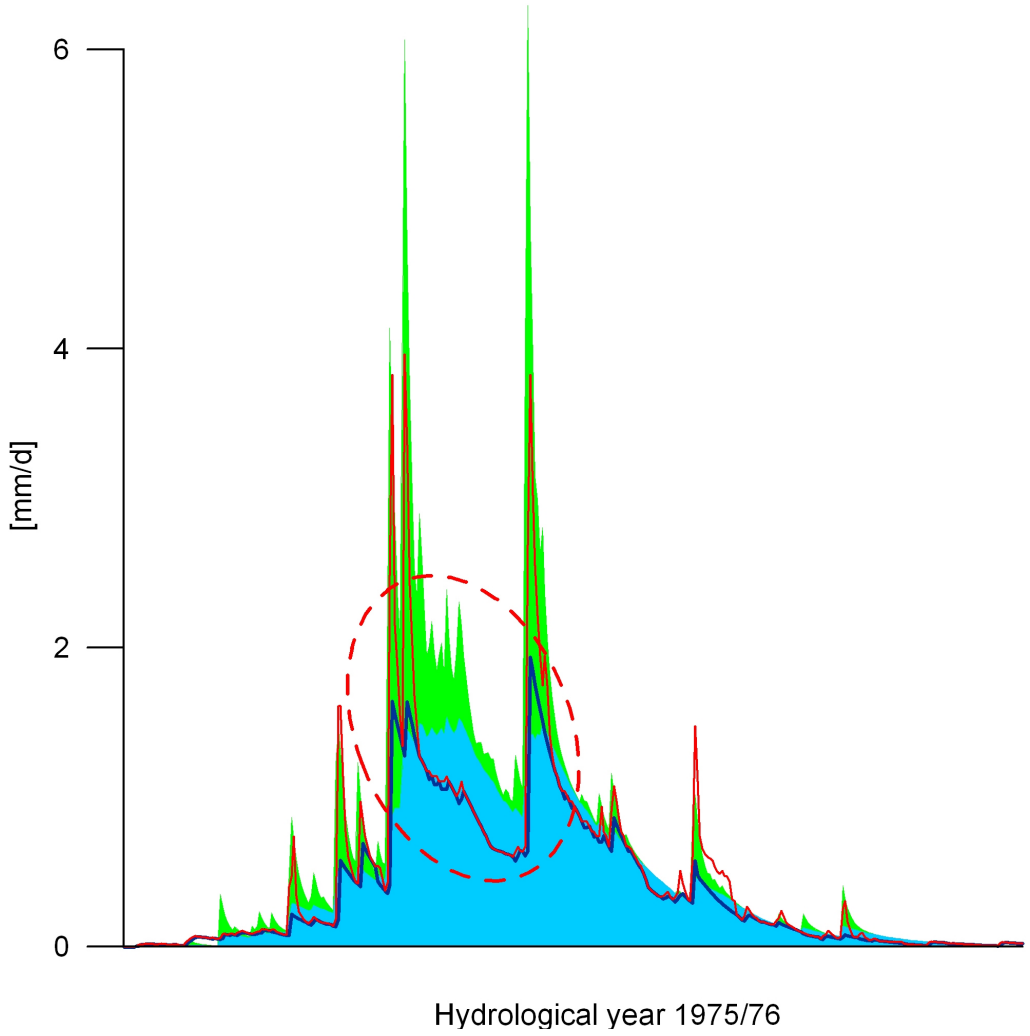

Figure 5.31: Corrupted recorder datasets detected by the comparison of simulated and recorded discharge. The figure shows an example of inconsistent recorder time series (marked with red, dashed circle) from the upper Diarizos valley in the hydrological year 1975/1976. Legend equal to Fig. 5.30.

determined by the comparison of modelled and recorded discharge. In most cases it can be assumed that sediments, boulders, wood and branches in the river bed hinder a correct operation of the recorder for several days or weeks. Then the recorded discharge usually appears lower than the real discharge. In many cases, the day of maintenance can also be recognised, according to the recorder having continued working correctly. For instance, in the upper Diarizos valley, an example of corrupted recordsets can be detected in the hydrological year 1975/76. The recorded discharge becomes too low in mid-winter after several extreme discharge events. The recorder seems to continue recording runoff events less sensitively (see Fig. 5.31). Some weeks later, the recording continues correctly. In this case overestimation of modelled discharge is hardly probable, because recorded and modelled discharge continue on the same level in the second half of the winter (see Fig. 5.31).

5.12 Complete Water Balances

A description of the particular water balance components is provided in the previous chapters. The synopsis of all components in this chapter, allows a comprehensive view of the hydrological system and its dynamics. The complete average water balances for Cyprus and several sub-regions are provided in Table 5.2. More detailed water balance results and their spatial distribution are also compiled in Appendix B.

The visualisation of the monthly (Fig. 5.32) and annual (Fig. 5.33) time series 1961-2004, show the progression of the water balances in the past decades. The analyses of the interseasonal and interannual variability allow the detection of dry and wet seasons and periods. The 1960s appear as a period of very high variability on a relatively high level, the 1990s as the driest period with consecutive dry years, especially between 1993/94 and 1999/2000. The driest hydrological years registered in the modelling period were in 1972/73 and 1990/91.

Figure 5.34 allows an enhanced view of the water balances by sorting all the hydrological years from wet to dry years on the base of the yearly precipitation amounts of Figure 5.33. It can be seen that precipitation equals actual evapotranspiration between 400-450 mm/a, revealing a critical threshold for the island (see also discussion in Chap. 7).

Table 5.2: Mean water balances for Cyprus and subareas for different time periods.

Period/parameter	Cyprus		Southern Cyprus		Troodos		Northern Cyprus	
	[mm/a]	[mcm/a]	[mm/a]	[mcm/a]	[mm/a]	[mcm/a]	[mm/a]	[mcm/a]
1961 - 1990								
Annual precipitation	472.1	4364.9	511.8	3068.4	667.0	1068.3	396.3	1288.2
Actual evapotransp. (excl. ET_{sec})	397.4	3674.2	417.8	2504.9	513.1	821.7	358.4	1165.0
Secondary evapotransp.	41.8	386.5	47.6	285.4	50.7	81.2	30.8	100.1
Actual evapotransp. (incl. ET_{sec})	439.2	4060.8	465.4	2790.3	563.8	903.0	389.2	1265.1
Direct runoff	27.1	250.6	33.9	203.2	48.1	77.0	14.1	45.8
Groundwater recharge	47.6	440.1	60.1	360.3	105.8	169.4	23.8	77.4
1971 - 2000								
Annual precipitation	445.0	4114.4	478.1	2866.4	617.6	989.2	381.8	1241.0
Actual evapotransp. (excl. ET_{sec})	384.5	3555.0	404.4	2424.5	492.3	788.5	346.1	1125.0
Secondary evapotransp.	43.4	401.3	49.7	298.0	53.2	85.2	31.5	102.4
Actual evapotransp. (incl. ET_{sec})	427.9	3956.3	454.1	2722.5	545.5	873.7	377.6	1227.4
Direct runoff	21.7	200.6	26.2	157.1	36.5	58.5	13.3	43.2
Groundwater recharge	39.6	366.1	48.7	292.0	87.1	139.5	22.3	72.5
1961 - 2004								
Annual precipitation	468.1	4328.0	504.1	3022.3	654.1	1047.7	399.3	1297.9
Actual evapotransp. (excl. ET_{sec})	395.0	3652.1	414.5	2485.1	506.8	811.7	357.2	1161.1
Secondary evapotransp.	42.6	393.9	48.6	291.4	51.8	83.0	31.0	100.8
Actual evapotransp. (incl. ET_{sec})	437.6	4046.0	463.1	2776.5	558.6	894.7	388.5	1262.8
Direct runoff	26.5	245.1	32.2	193.1	45.8	73.4	15.7	51.0
Groundwater recharge	46.6	430.9	57.4	344.1	101.5	162.6	26.1	84.8

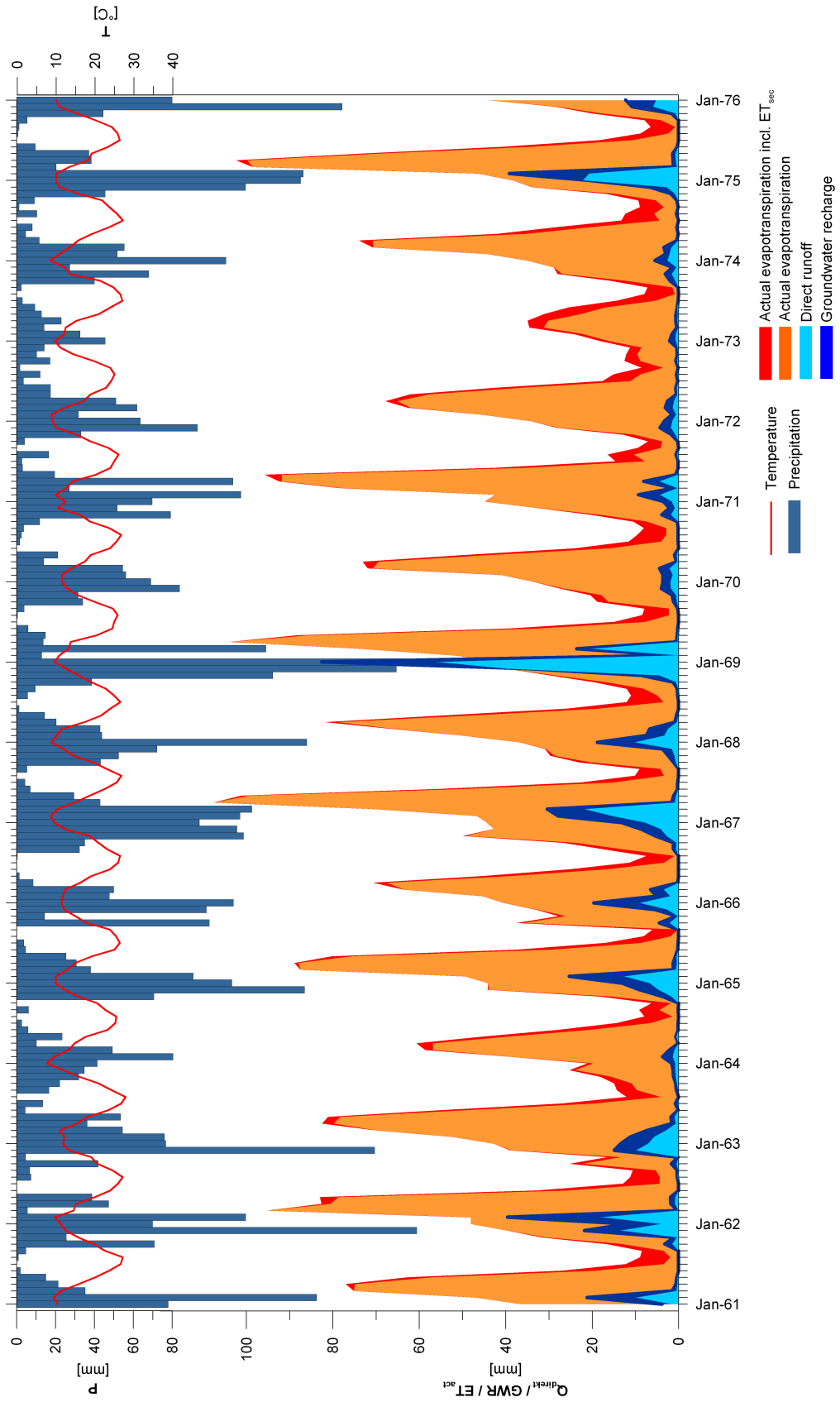

Figure 5.32: Monthly time-series of the water balance components of Cyprus for the modelling period 1961-2004.

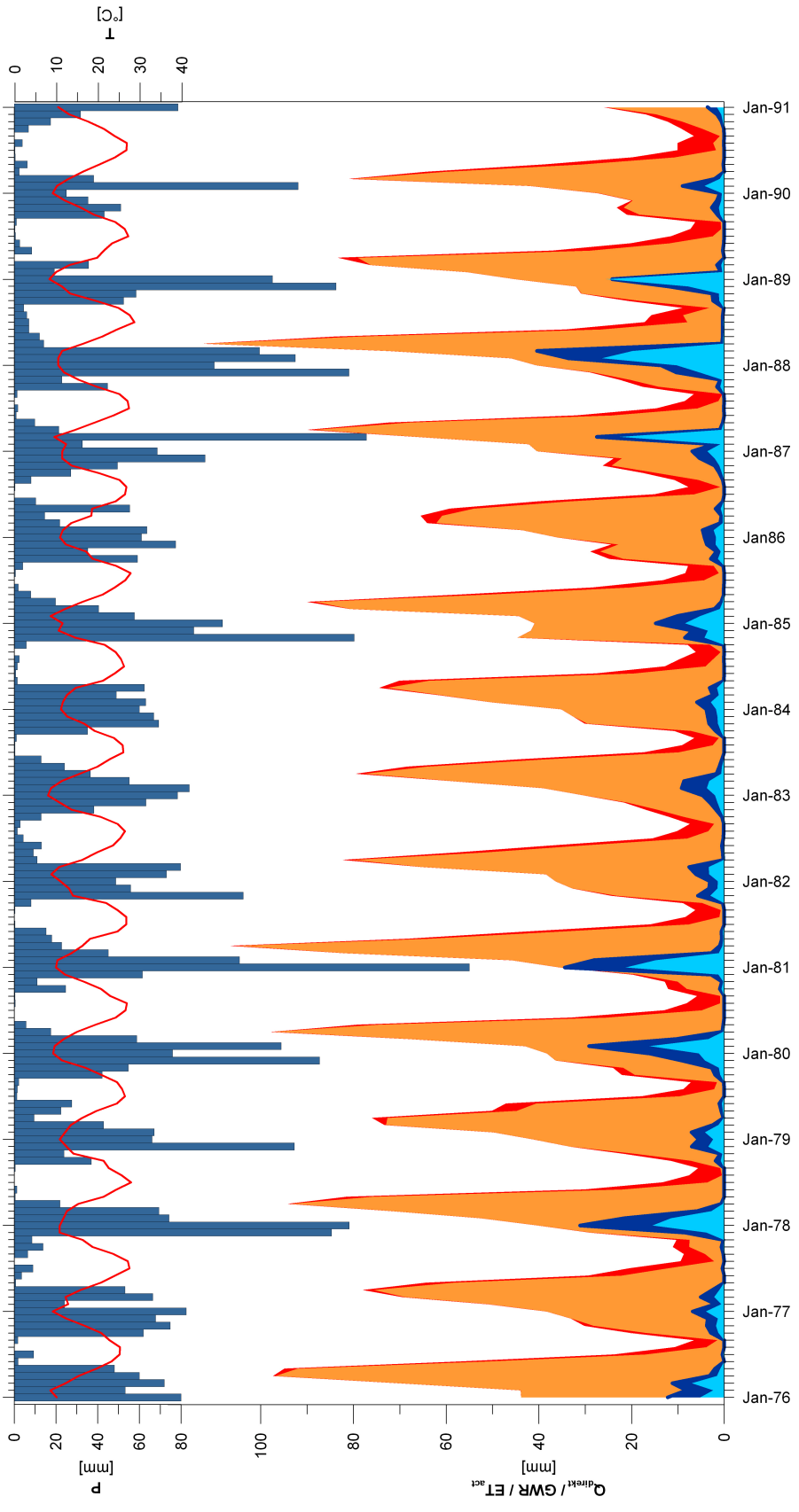

Figure 5.32 (Continued)

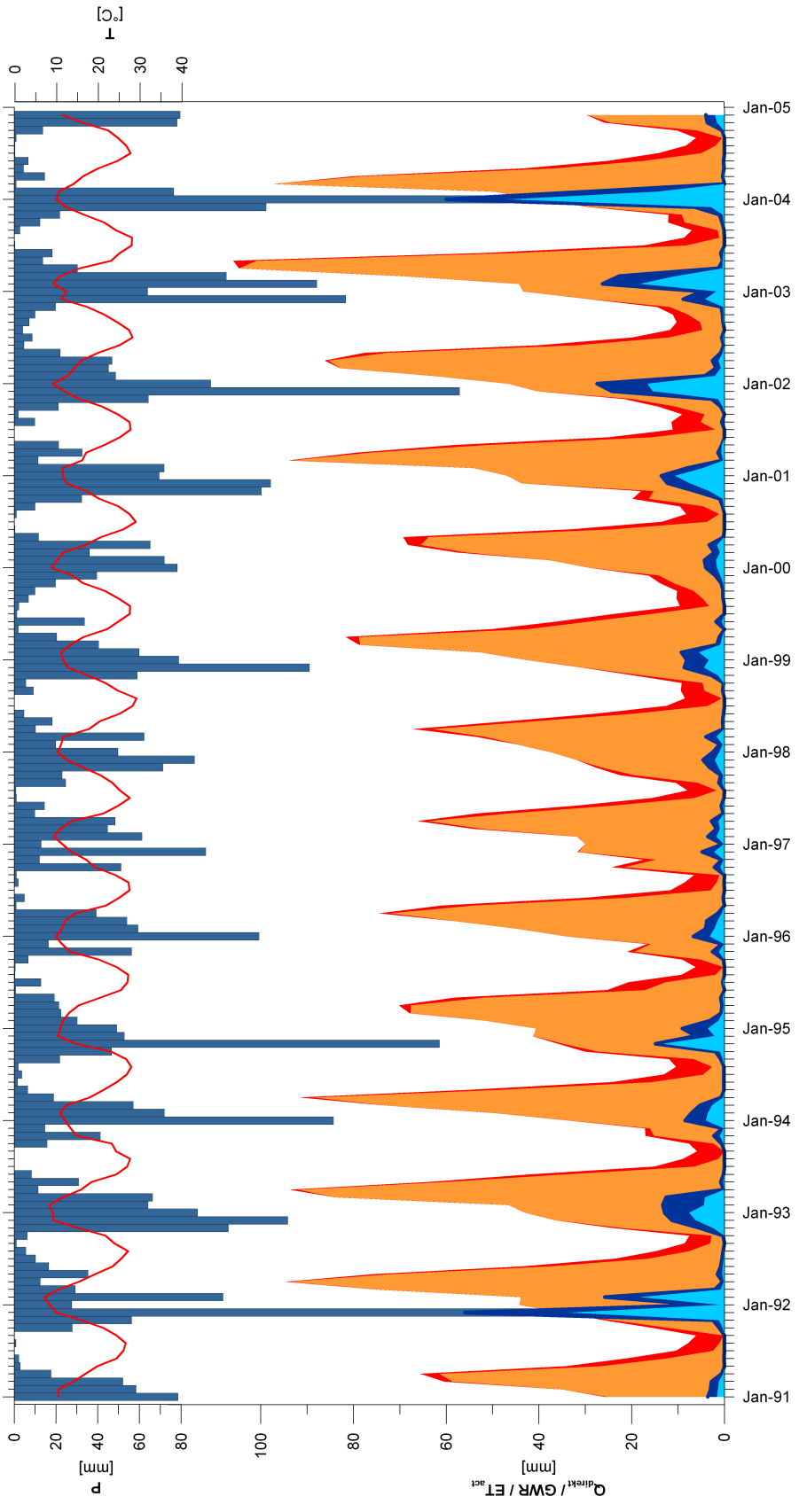

Figure 5.32 (Continued)

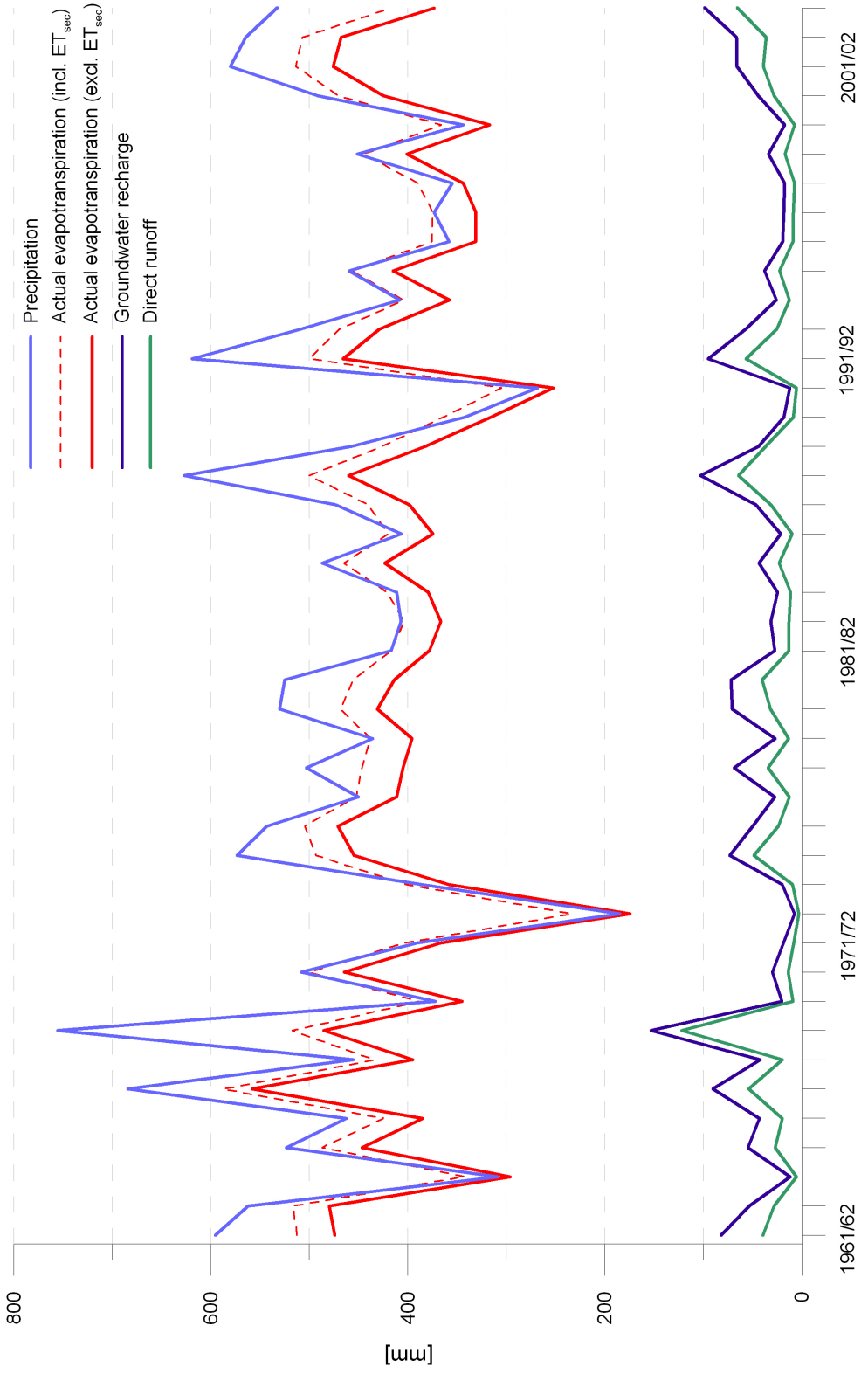

Figure 5.33: Mean annual water balance components of Cyprus for the hydrological years of the time period 1961-2004.

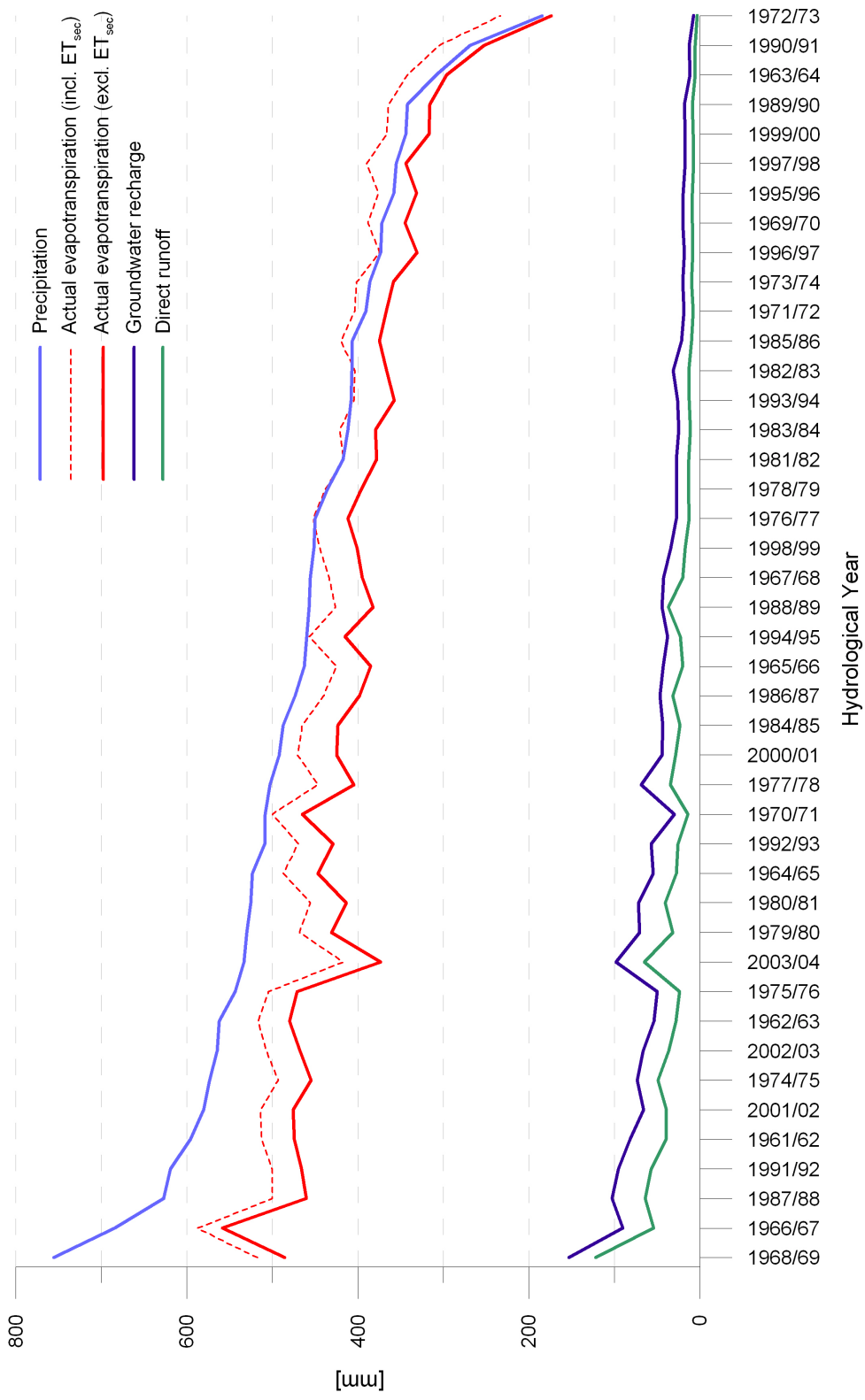

Figure 5.34: Mean annual water balance components of Cyprus sorted by annual precipitation of the hydrological years of the modelling period 1961-2004 in descending order.

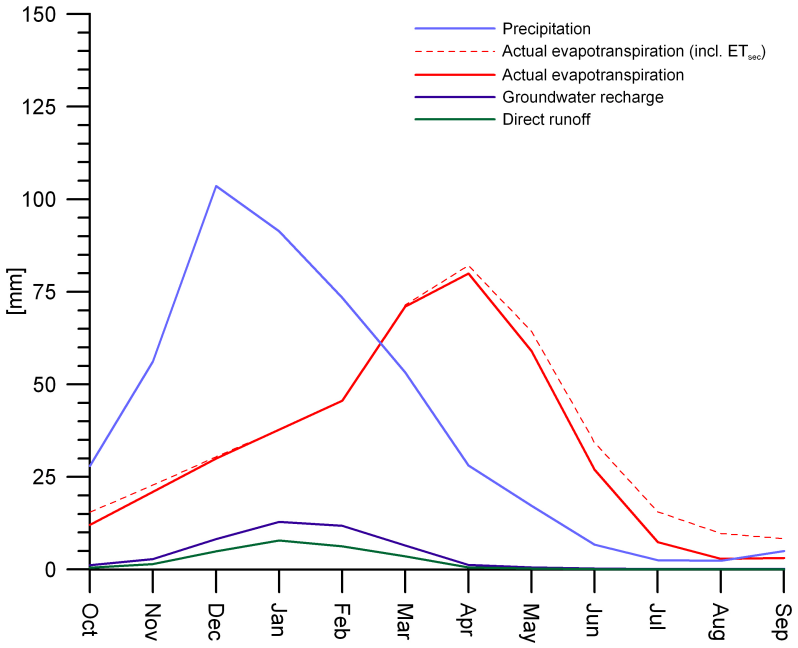

Figure 5.35: Areal monthly means (1961-2004) for Cyprus showing the seasonal interrelation of the water balance components.

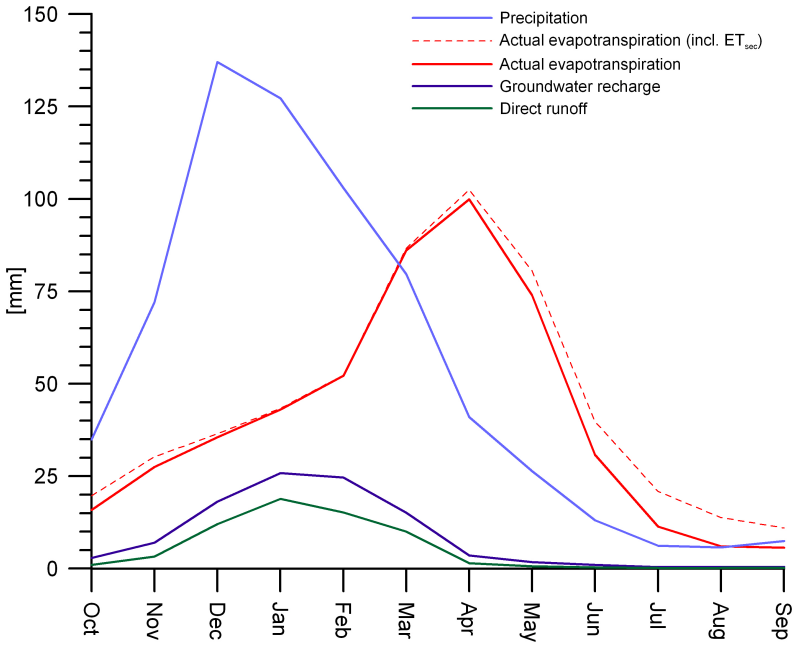

Figure 5.36: Areal monthly means (1961-2004) for Troodos showing the seasonal interrelation of the water balance components.

Fig. 5.35 and Fig. 5.36 show the typical average seasonal cycle of the particular water balance components revealing distinctive characteristics of their interaction. The seasonal cycle of precipitation shows the highest rainfall amounts in December and January; and groundwater recharge becomes retarded as a result of the soil water storage, which first has to be recharged before groundwater recharge processes become more effective. The actual evapotranspiration is characterised by a different cycle with a maximum in the spring months, when precipitation, soil moisture state and potential evapotranspiration are favourable. In the summer and autumn months, the low soil moisture state, and in the winter months the low potential evapotranspiration inhibit a higher actual evapotranspiration.

With respect to the values in Table 5.2, the ratio between direct runoff and direct groundwater recharge seems to be similar in the subregions. Considering the mean area values, the direct groundwater recharge assigns typically 60 to 70% of the whole water not lost by actual evapotranspiration (excl. ET_{sec}). The more detailed analysis shows that there are strong local and regional differences. The highest ratio can be found in the Mesaoria plain and the coastal plains. In these areas nearly no direct runoff is registered. In contrast, the lowest ratio can be found on sealed or partially sealed areas depending on the fraction of sealing. A particularly high fraction of direct runoff is also registerd in the Kyrenia range and the Mamonia complex, which in large parts consist of geological formations with low hydraulic conductivities. Especially in areas with higher precipitation rates and steep slopes, 50-70% of the non-evapotranspirating water is diverted to direct recharge. In contrast, large parts of the central Troodos register a fraction of around 70% for groundwater recharge, despite the steep slopes and the high precipitation rates.

Chapter 6

Climate Change Impact Assessment

6.1 Introduction

Beyond the understanding and quantification of actual water balance dynamics, water management requires the consideration of the impact of future climate change. The observed regional climate of Cyprus shows a tendency for drier and warmer conditions in the past century (e.g. Jacobeit 2000, Dünkeloh and Jacobeit 2003, Jacobeit et al. 2007), and suggests that the impact of climate change may have already been manifesting itself in the Mediterranean region (see Mariotti et al. 2008, IPCC 2007). The tendency is notable, especially with respect to a considerable precipitation decrease in the 20th century (see Fig. 2.4). It seems as if in the past four decades, changes have appeared mainly in the summer and transition months April and October. Until now, Cyprus has profited from the situation of the winter months, decisive for renewability of water resources, being less affected by the general tendency.

However, the future climate assessments by the Fourth Assessment Report of the Intergovernmental Panel on Climate Change (IPCC 2007), predicts unfavourable changes for the Mediterranean region in the 21st century. Extremely unfavourable conditions have been forecasted, especially for the wet season in the central and eastern Mediterranean (IPCC 2007, Mariotti et al. 2008).

The presented study focuses on the impacts of potential climate change on regional water balances, with special consideration of renewability of water resources. The

study is based on several runs of the physical water balance model (see Chapters 3-5) performed with adjusted meteorological datasets, considering different climate change scenarios. Firstly, the sensitivity of the hydrological system of Cyprus is analysed based on theoretical scenarios of precipitation decrease and increasing temperature (Chap. 6.2). Secondly, a first water balance scenario for Cyprus is developed based on the real changes expected for the 21st century, for this area under increased greenhouse warming conditions (see Chap. 6.3).

6.2 Potential Impacts of Climate Change

Physical water balance models are an excellent tool for the study of regional impacts expected under future climate change conditions. The separate modelling of theoretical precipitation and temperature changes, gives an insight into the sensitivity and behaviour of a hydrological system and the relevance of individual factors. The calibrated water balance model for the time period 1971-2000 (Chap. 5) serves as base and reference model for simulations.

The scenarios are designed as idealised models in which climate changes are assumed as a uniform impact on the whole study area. For comparison purposes, the extension of land cover units, irrigation areas and moist areas are kept fixed, implying that vegetation activity (transpiration) is only controlled by weather and soil water conditions. Furthermore, mean wind and sunshine duration remains unchanged for these simulations.

The computed results provide a quantitative assessment of impacts caused by temperature and precipitation changes. The scenarios (Table C.5 - C.13) reveal that the water balance impacts of temperature changes are largely an effect of provoked relative humidity changes. An increase of temperature usually causes a decrease of relative humidity and consequently an increase of the saturation deficit and potential evapotranspiration. Calculations confirm that a temperature decrease under unchanged relative humidity conditions, leads to comparably small changes (Table C.5 - C.13). Regarding the most important water balance components, direct runoff and groundwater recharge, the temperature increase of +1 K leads to a decrease of 2-3% under stable relative humidity conditions, and to a decrease of 8-9% under full adjustment of relative humidity (see Table 6.1).

Table 6.1: Direct runoff and direct groundwater recharge scenarios for theoretical mean air temperature and precipitation changes. Simulation based on the reference period 1971-2000.

Parameter/Scenario	Cyprus [%]	S. Cyprus [%]	Troodos [%]	N. Cyprus [%]	Table with full balance*
Change of direct runoff					
Scenario P -5%	−15.2	−14.5	−13.8	−17.2	C.1
Scenario P -10%	−28.5	−27.4	−26.3	−31.8	C.2
Scenario P -20%	−50.0	−48.7	−47.5	−55.0	C.3
Scenario P -30%	−65.2	−64.5	−63.1	−70.2	C.4
Scenario T +1 K, no RH adj.	−3.1	−2.6	−2.1	−3.3	C.5
Scenario T +1 K, mean RH adj.	−3.9	−3.5	−3.3	−4.6	C.6
Scenario T +1 K, full RH adj.	−9.8	−9.0	−9.2	−13.2	C.7
Scenario T +2 K, no RH adj.	−5.9	−5.5	−4.6	−7.3	C.8
Scenario T +2 K, mean RH adj.	−7.8	−7.4	−6.7	−9.3	C.9
Scenario T +2 K, full RH adj.	−18.4	−16.8	−17.7	−23.8	C.10
Scenario T +3 K, no RH adj.	−8.6	−8.1	−7.3	−9.9	C.11
Scenario T +3 K, mean RH adj.	−11.7	−11.0	−10.4	−13.9	C.12
Scenario T +3 K, full RH adj.	−25.4	−23.5	−25.0	−31.7	C.13
Change of groundwater recharge					
Scenario P -5%	−10.7	−10.3	−9.5	−12.7	C.1
Scenario P -10%	−20.9	−20.0	−18.5	−24.3	C.2
Scenario P -20%	−38.8	−37.6	−35.3	−44.2	C.3
Scenario P -30%	−53.5	−52.3	−50.0	−58.9	C.4
Scenario T +1 K, no RH adj.	−2.8	−2.7	−2.8	−3.2	C.5
Scenario T +1 K, mean RH adj.	−3.7	−3.6	−3.6	−4.0	C.6
Scenario T +1 K, full RH adj.	−8.4	−7.8	−8.1	−10.8	C.7
Scenario T +2 K, no RH adj.	−5.3	−5.2	−5.2	−6.0	C.8
Scenario T +2 K, mean RH adj.	−7.0	−6.7	−6.8	−7.2	C.9
Scenario T +2 K, full RH adj.	−15.1	−14.1	−14.8	−19.5	C.10
Scenario T +3 K, no RH adj.	−7.7	−7.4	−7.4	−8.4	C.11
Scenario T +3 K, mean RH adj.	−10.0	−9.5	−9.6	−11.6	C.12
Scenario T +3 K, full RH adj.	−20.5	−19.1	−20.1	−25.9	C.13

* = Tables in Appendix C

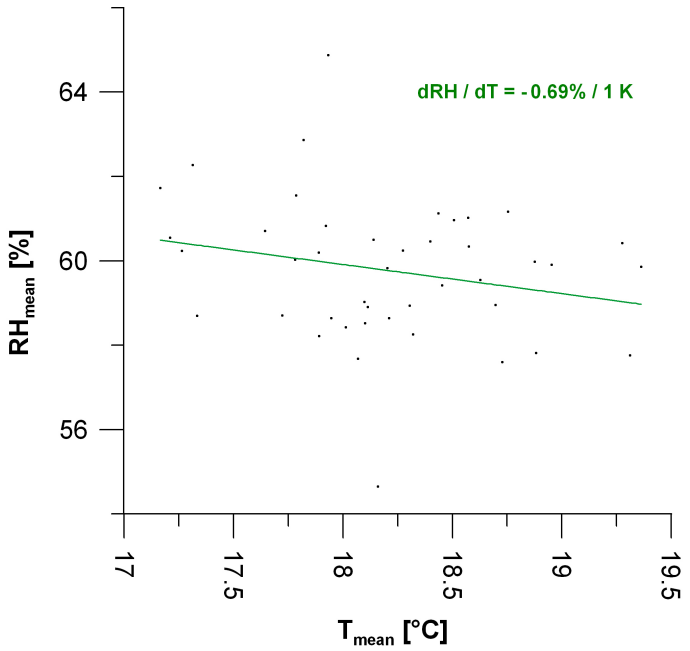

Figure 6.1: Relation between mean areal relative humidity and mean areal temperature of Cyprus. A mean temperature rise of 1 K causes an average decrease of mean areal relative humidity of 0.69%.

Both results are interesting in the context of a sensitivity analysis of the hydrological system, but do not represent realistic impacts of a temperature increase. Therefore, the last four decades were analysed with regard to the relationship between mean temperature and mean relative humidity (Fig. 6.1). A mean relative humidity decrease of 0.69% per 1 K could be derived for the island. This is a relatively small decrease compared to relative humidity changes appearing in a closed system. Cyprus profits from its island setting, enclosed by the Mediterranean Sea, which seems to compensate a part of the humidity deficit by higher air and sea surface temperatures, suggesting increasing evaporation over the sea. The simulation of temperature scenarios considering the mean relative humidity adjustment derived for Cyprus, according to Fig. 6.1, simulates a decrease of approx 3.5-4% of the annual usable and renewable water resources (direct runoff and groundwater recharge), for each Kelvin of mean annual temperature rise.

The precipitation scenarios (Table C.1-C.4) reveal substantially stronger impacts on water balances. Four runs were performed simulating the effects of precipitation decreases from 5 to 30% (Table 6.1). A reduction of the actual evapotranspiration can

be registered due to reduced soil water availability. This also leads to an increased secondary evapotranspiration, as additional water is needed for compensating the soil water deficit in moist and irrigated areas. With regard to renewable water balance components, a precipitation decrease of 10% of the annual sum results in approx. 20% less annual groundwater recharge. Direct runoff still seems to be more affected by a decrease of more than 25% of the annual sum. This value might by somewhat overestimated, because the strengthening of precipitation intensities related to a drying climate is not clear and could not fully be considered within these model runs. However, in the drier and warmer years of the past decades, no remarkable discrepancy between modelled and monitored direct runoff could be detected (see Fig. 5.30). Discrepancies occur mainly in the wettest years in which recorders may have faced problems in correctly registering extreme events. Furthermore, a detailed analysis of the model results show that surface runoff only contributes to a smaller degree of the total direct runoff. Interflow controls much of the direct runoff on Cyprus and is strongly affected by the lower soil water state. The consequence is that the necessary condititions for starting the interflow processes are often no longer fullfilled. Interflow decreases, especially when less events occur where the hydraulic conductivity of the bedrock is too low for the complete infiltration of the percolating water from the soil. The deep percolation (potential groundwater recharge) amounts are reduced, because soil water content exceeds field capacity less often under drier soil water conditions.

6.3 Scenario for the 21st Century

The simulation of the 21st century water balance conditions is based on studies performed by Hertig (2004) and Hertig and Jacobeit (2008a, 2008b). Statistical downscaling techniques were applied to assess regional precipitation and temperature changes in the Mediterranean for the period 1990-2100, under increased greenhouse warming conditions. Predictor output from global general circulation model runs (ECHAM4/OPYC3 for precipitation, HadCM3 for temperature) forced with B2 scenario assumptions (SRES - Special Report on Emission Scenarios) were used for the simulation of precipitation changes. The B2 emission scenarios are conservatively optimistic scenarios with an intermediary global energy demand. For a

detailed method and dataset description of this climate change assessment, the original study and related publications from Hertig (2004), Hertig and Jacobeit (2008a, 2008b) should be considered.

Differences between the 30-year means of the model periods 1990-2019 and 2071-2100 are extracted for Cyprus and compiled in Table 6.2. These values give a benchmark for the changes, which are expected between the beginning and end of the 21st century. The results show much drier conditions for all transitional and most winter months. Only the core winter months December and January do not seem to be affected by the changes. The drying is accompanied by a temperature increase of about 2 K, which is predicted for all seasons.

On the basis of the predicted changes (see Table 6.2), a first principal scenario was calculated for the future water balances of Cyprus at the end of the 21st century (Table 6.3). The simulation concept is equal to the scenarios described in Chap. 6.2 and also based on the calibrated water balance model for the time period 1971-2000 (Chap. 5).

The simulations show severe impacts on future water balances with a mean predicted loss of roughly 50% of renewable resources. From the theoretical senarios, (Chap. 6.2) it can be seen that this is mainly a result of the precipitation decrease. The temperature increase contributes only a comparatively small fraction to the total changes. The results should only be regarded as a first principal assessment of the impacts expected for the 21st century. A more detailed research on the basis of coupled large-scale scenarios, regional climate models, and the regional water balance model, is required for superior assessments. Furthermore, the impacts of several secondary factors, such as changes of vegetation or adaptation of precipitation intensities, have to be revealed in future studies and considered in integrated modelling concepts.

Table 6.2: Future climate change assessments for Cyprus by Hertig (2004), Hertig and Jacobeit (2008a, 2008b). Cyprus is represented by eleven grid points of the Mediterranean dataset. The changes are given as two-month means.

	Month							
	O,N	N,D	D,J	J,F	F,M	A,M	J,J	A,S
Precipitation change [%]	−24.1	−54.0	−5.5	−32.6	−33.3	*	*	*
Temperature change [K]	+2.8		+2.4		+1.6	+2.0	+2.2	+2.2

* = Precipitation amounts are too small in the summer half year

Table 6.3: Mean annual water balance changes for Cyprus simulated on the base of a future climate change scenario described in Hertig (2004), Hertig and Jacobeit (2008a, 2008b) (see Table 6.2). The simulation is based on the reference period 1971-2000.

Parameter	Cyprus	Southern Cyprus	Troodos	Northern Cyprus
Precipitation				
P change [%]	−26.5	−26.5	−26.5	−26.5
Actual evapotranspiration				
ET_{act} (excl. ET_{sec}) change [%]	−21.1	−20.5	−18.7	−22.4
ET_{sec} change [%]	+22.4	+22.5	+27.8	+20.7
ET_{act} (incl. ET_{sec}) change [%]	−16.5	−15.6	−14.1	−18.8
Direct runoff				
DRO change [%]	−62.5	−61.3	−60.0	−66.9
Groundwater recharge				
GWR change [%]	−51.9	−50.6	−48.7	−56.9

Chapter 7

Discussion and Conclusions

7.1 Mean Water Balances

The results of the physical water balance modelling give a detailed insight into the hydrological system and the water balance dynamics of Cyprus. They provide a quantitative review and allow an evaluation of the sensitivity and renewability of the island's natural water resources. Furthermore, the model's results are suitable for planning and evaluating water management with regard to sustainability.

The water balances simulated for Cyprus reveal the outstanding importance of the Troodos massif for the island's natural water resources and their renewability (see Fig. 5.27). It was shown that the precipitation amount is the most important factor for the generation of direct groundwater recharge and still more decisive than the properties of most hydrogeological units. In the Troodos area, the modelled mean annual groundwater recharge rates lie at about 100 mm/a. In the highest areas, rates of 200 mm/a and more are common. Further zones of limited extension, but with considerable recharge rates are located in the Kyrenia range and in the southern and western Troodos foothills. All other areas on the island can be considered as areas of secondary importance with low to very low direct recharge rates. The latter also comprise the areas where the most important aquifers of unconsolidated and semiconsolidated rocks are located, particularly the Mesaoria plain and several coastal areas. Less than 25 mm/a are usually detected for these areas, implying a very low renewability of natural groundwater resources by direct recharge.

Besides the groundwater recharge, direct runoff is also of importance for the renewal of natural water resources. Considerable amounts of direct runoff are generated in the Troodos and partly in the Kyrenia range. The most important factors for direct runoff generation are high precipitation rates, steep slopes and bedrocks with low hydraulic conductivities. In the Troodos range, a total mean of about 45 mm/a could be assessed for direct runoff. Part of the runoff contributes to the groundwater resources by secondary recharge through river bed infiltration. Especially rivers with major alluvial deposits (e.g Ezusa, Xeros, Chrysochou valley), rivers (e.g. Peristerona, Pediaios or the Treminthos river) crossing the Mesaoria and coastal plains with unconsolidated and semiconsolidated rocks, benefit from secondary recharge. Furthermore, the runoff from most large valleys, especially on the southern Troodos foothills, is retained in dams and contribute to the water supply of the island. Otherwise the damming of rivers and diverting discharge without an integrated surface-groundwater management can result in a serious impact on the groundwater resources of the affected aquifers, which is discussed below.

To summarise, the comparison of the total water balances for different areas (see Fig. 5.2) points out that most of the island contributes scarcely to the renewability of water resources. A large part of the annual precipitation is lost by evapotranspiration. Only the upper areas of the mountain ranges show a clear positive balance with a considerable generation of groundwater recharge and direct runoff under mean meteorological conditions. This is why the Troodos has recently often been called the 'water tower' of Cyprus. Furthermore, the comparison of the water balances of Northern and Southern Cyprus reveals that the mean renewability of natural resources in Northern Cyprus, on the basis of mean groundwater recharge and direct runoff, is only about half per unit area, therefore emphasising the severity of the situation for the northern part.

7.2 Seasonal Cycle

The model reveals the interaction of different meteorological and hydrological factors, and its relevance for the generation of direct runoff and groundwater recharge, crucial for the renewability of the natural water resources. One aspect is the importance of Cyprus' typical seasonal cycle regarding groundwater recharge and direct

runoff. The coincidence of the wet and the cool seasons characterised by a high precipitation rate, a high soil water state and low evapotranspiration results in a surplus of water in the months November to March, therefore supporting the generation of considerable amounts of groundwater recharge and direct runoff (see Fig. 5.26, 5.29), especially in the mountainous areas. The results illustrate the outstanding importance of these few winter months, as all other months hardly contribute to the renewability of natural water resources at all. In this context, the hydrogeological conditions of the formations also become relevant as they act as natural detention reservoirs. The discharge characteristics of the Troodos catchments, such as the upper Diarizos valley (see Fig. 5.30), show the limited storage capability of the Troodos formations, which consist mainly of fractured aquifers in igneous rocks. After a recharge event, most of the percolated water is registered as base flow in the Troodos valleys within the subsequent two months. Part of the base flow contributes to secondary groundwater recharge through river bed infiltration, particularly in the river beds of the Troodos foothills or the Mesaoria plain. In most Troodos rivers, discharge decreases to very small rates in the late summer months and often dries up in the upper reaches. In recent decades, especially in summertime, many streams disappeared completely as a result of the drawdown of groundwater levels by pumping and the artificial deviation of river water.

7.3 Interannual Variability

The distinctive interannual climate variability shows strong influences on the yearly renewability of natural water resources and water supply of the island. The model results allow the quantification of the impacts on the decisive factors groundwater recharge and direct runoff (see Fig. 5.25, 5.28). From year to year, the quantities can fluctuate strongly making water management much more difficult. Periods with consecutive dry years result in a continuous water shortage on the island as it occurred in the years 1993-2000.

The strong interannual variability is typical for the eastern Mediterranean and demonstrates the high sensitivity of the small zone of the Mediterranean climate with its alternating regimes in this intermediate position. The water balance analysis of past decades (Fig. 5.33, 5.34) show that the renewability in dry years with

a mean island precipitation below 400 mm/a becomes critical, because actual evapotranspiration (incl. secondary evapotranspiration) becomes higher than the total precipitation rate. Amounts of more than 450 mm/a at least are required for a surplus of water to support the renewability of water resources. If precipitation amounts decrease to less than 300 mm/a, then nearly the whole precipitation is consumed by direct actual evapotranspiration. Hardly any groundwater recharge and direct runoff are available for feeding moist, irrigated and settlement areas (secondary evapotranspiration). On this level, the hydrological system would change to semi-desert conditions.

This elucidates the precarious situation in Cyprus because the registered areal means of the past decades vary around the critical threshold of 450 mm/a. Small shifts within the climate system would provoke considerable effects on the whole water balance system of the island. The number of years, which contribute enough precipitation for the renewability of the water resources, could decrease significantly.

7.4 Annual Trends

Besides the detailed data available for the modelling period (1961-2004), there are also few precipitation and temperature time series covering the whole 20th century. This data allows a certain evaluation of the long-term changes of the climate of Cyprus and the northeastern Mediterranean. The datasets show unfavourable changes for the regional water balances with a significant precipitation decrease and a significant temperature increase in the 20th century (see Fig. 2.4, 2.5).

Within the modelling period the same trends can be registered, but are kept statistically significant for temperature only (see Fig 5.4, 5.8). Further available parameters for the modelling period, like air humidity, also show unfavourable but insignificant decreasing trends (see Fig. 5.13).

All important water balance parameters depend strongly on the main meteorological parameters precipitation, temperature and air humidity. The generally unfavourable tendencies of all parameters in the last four decades lead towards an increase of potential evapotranspiration, which is strongly significant (see Fig. 5.16). Actual evapotranspiration also includes the secondary evapotranspiration and is therefore

affected by two opposite trends. Secondary evapotranspiration depends directly on potential evapotranspiration and shows the same significant positive trend. Actual evapotranspiration without secondary evapotranspiration is limited mainly by soil water availability and interception storage, which are showing a decreasing trend due to the decreasing precipitation rates in the last decades.

Direct runoff and groundwater recharge show complex connections to variability and trends of several parameters in the water balance system. Notable but insignificant decreases can be seen for direct runoff and groundwater recharge. The comparison of the monthly analysis reveals that variability and trends are mostly influenced by precipitation, which also shows an insignificant decrease, especially in the late winter and early spring months (see Fig. 5.4). The high variability of the time series cause a low signal-to-noise-ratio, which makes a determination of trends much more difficult. For all parameters the trends occur most prominently in the Troodos area.

7.5 Seasonal Trends

The monthly analyses of the parameters reveal a more detailed view on the types of change controlling the annual tendencies and trends of the last decades. The most prominent trend occurs in the time series of air temperature. The monthly analysis shows that significant increases, especially in the summer months, which induce a highly significant increase in the annual means. The trend can be evaluated as reliable owing to the large amount of temperature stations included into the calculation of the mean areal temperature time series. This significant summer trend is also found in other meteorological datasets and is detected for great parts of the Mediterranean. Discussions are given in several publications such as Jacobeit (2000) or Dünkeloh and Jacobeit (2003).

Regarding precipitation data, the summer months June to September are too dry for the detection of any relevant tendency or trend. However, relative humidity is slightly affected by temperature rise in the summer months, but decreases do not become statistically significant. Air humidity seems to be balanced and the deficits are partly compensated by the nearby sea. The mean relationship between air temperature and air humidity on Cyprus is also analysed in Chap. 6.2. The results confirm that the impacts of temperature changes on air humidity are substantially

lower than in a closed system.

The renewability of annual water resources is hardly affected by the changes described in the summer months. These months barely contribute to the annual sum of direct runoff and groundwater recharge. Important impacts can only be registered for moist and irrigation areas by a markable increase of potential evaporation due to higher temperatures and slightly lower relative humidities.

The monthly analyses of the winter half-year (November to March) reveal few significant changes in the last decades for precipitation, temperature and humidity. Expectedly, the simulated water balance components as potential and actual evapotranspiration, direct runoff and groundwater recharge also show few statistically significant trends. Although the low signal-to-noise-ratio due to the high variability should be kept in mind. Under the given conditions, the determination of changes based on trends and significance is difficult. The detailed examination of precipitation shows a (statistically insignificant) decreasing tendency for nearly all winter months (except for November), which is most prominent in the Troodos area. Direct runoff and groundwater recharge seem to respond to the small precipitation decreases. Accordingly, decreases can be detected for many winter months, most prominently for the late winter months (Fig. 5.26, 5.29). The decreases are also responsible for the decreasing tendency of annual means, which are most evident for the Troodos area, as in the case of precipitation (Fig. 5.25, 5.28).

On Cyprus, predominantly the months April, May and October cover the comparably short spring and autumn season in form of a transitional period between the wet and cool winter, and hot and dry summer conditions. Strong changes of precipitation, temperature and relative humidity with unfavourable impacts on water balances are documented, especially for transitional months May and October. As expected, many of the water balance parameters show statistically significant changes, which are strongest in May. In general, climate change in the last decades on Cyprus seems to manifest itself in form of a prolonged summer period on account of a successive drying in the transitional months. This is documented by the noticeable shift to summer conditions in these months, which can be detected for important meteorological parameters (Fig. 5.4, 5.9, 5.14).

Severe impacts on the eco-system must be expected as a result of the shortening of the wet period. Notable influences are also registered concerning the renewability of

natural water resources (see Fig. 5.26, 5.29), but currently the impacts occur mainly in the months which are contributing only little to the annual sum of direct runoff and groundwater recharge. Some influences are given, for instance, by a retarded rise of soil water content at the beginning of the winter periods. However, it can generally be observed that the smaller, statistically insignificant precipitation changes in the winter months provoke stronger impacts on Cyprus' water balances than the changes in the transitional and summer months. This elucidates the vulnerability of natural water resources, especially regarding the winter months, which up to now were fortunately less affected by the registered climate changes of the past decades.

7.6 Sensitivity and Potential Impacts of Climate Change

Temperature and precipitation scenarios (Chap. 6.2) reveal the high sensitivity of the water balance dynamics of Cyprus. Even small precipitation changes provoke strong impacts on the renewability of water resources that can be detected by analysing the interannual variability of the past decades (see 5.25, 5.28). The scenarios show that a decrease of 10% of the mean island precipitation provokes a mean loss of about 20% of the renewable resources (direct groundwater recharge and direct runoff). The influences from air temperature changes are smaller but also notable. A mean temperature rise of 1 K with a typical relative humidity adjustment for Cyprus, causes losses of about 3.5 to 4% of the renewable water resources. The impacts of air temperature rise on the water balance changes are especially controlled by the induced relative humidity decrease, leading to higher potential evapotranspiration. In Cyprus, the effect seems to be reduced because a considerable part of the expected relative humidity decrease seems to be compensated by the nearby Mediterranean sea, where higher air and sea surface temperatures contribute to higher evaporation rates.

Based on climate assessments for the 21st century performed by Hertig (2004), Hertig and Jacobeit (2008a, 2008b), a first principal scenario for future water balances of Cyprus was developed (Table 6.3). The results state a first benchmark for the expected changes under an increase of green-house gasses (optimistic prediction)

until the end of the 21st century. A proceeding of mean temperature rise and a further shortening of the wet winter season are predicted (see Table 6.2). These tendencies could already be observed in the past decades on Cyprus (see Chap. 5). All transitional and winter months will become considerably drier, except for the core winter months December and January. These results reveal severe impacts on the future water balances with a mean predicted loss of roughly 50% of renewable resources. The analysis shows that this is mainly provoked by precipitation decreases. Mean air temperature increase and relative humidity changes show only a secondary influence.

The simulation under static land cover conditions of the island also reveals that the annual water demand for moist, irrigated and partly settled areas (indicated by secondary evapotranspiration) becomes higher than the annual renewable resources. The natural water resources become even more over-exploited. Substantial changes in future water management, especially regarding irrigation plants, will be inevitable under the predicted water balance conditions.

The presented results have to be regarded as a first principal assessment, but further research on the base of coupled large-scale scenarios and the enhancement of the regional water balance model are recommended. Furthermore, dynamic factors should be considered in those models such as land cover changes and vegetation scenarios.

7.7 Water Management Perspectives

The results outline the importance of the Troodos mountains for the renewability of the water resources of the island, although the massif is not an excellent aquifer considering its limited storage capacity and its comparable fast turnover. In contrast, the large aquifers of unconsolidated and semiconsolidated rocks with high storage capacities, are located in the inner and coastal plains and suffered a strong over-exploitation over the last decades. Renewability of groundwater in these aquifers is small and depends strongly on riverbed infiltration of water originating from the mountain ranges. The decrease of direct runoff and base flow in the adjacent ranges as well as the construction of dams lead towards an aggravation of the situation. Already today, many coastal aquifers are damaged or partly damaged by sea water

intrusion caused by falling groundwater levels from excessive exploitation. In the western Mesaoria, sea water intruded just several kilometers inland due to overexploitation for irrigated agricultural areas. Year to year, large quantities of natural groundwater are lost in these badly managed aquifers.

The trends of the last decades and future climate scenarios reveal a successive shortening of the wet period for the whole Mediterranean with severe impacts on water balances. On Cyprus, a considerable improvement of water management is necessary for compensating at least parts of the decreasing resources. Furthermore, a re-evaluation of the water consumption for agricultural use is inevitable. For instance, several irrigated crops - like bananas - should no be longer supported due to their high water demand. Water could also be saved by funding innovations for a more efficient domestic water use. From a global point of view, efforts must continue to diminish the progress of climate change with all its unfavourable changes for many sensitive regions like Cyprus.

From a hydrogeological point of view, an improved water management on Cyprus has to include the rehabilitation of damaged aquifers to reduce the loss of groundwater resources. The further development of integrated dam-aquifer concepts is necessary to obtain an optimal use and rehabilitation of the plain (Mesaoria), coastal and riverbed aquifers. However, dams are important for the retention of water, which otherwise would be lost to sea, and to facilitate controlled aquifer recharge by riverbed infiltration. The coastal plains are an important sedimentary belt, which could act as a transitional storage and buffer zone for the retention of river bed losses and supplying flow connections between aquifers.

A sustainable water management demands abstractions being optimised for guaranteeing a zero recharge-abstraction balance on a long term perspective. An important tool for this purpose is the continuous quantification of the annual renewability of natural water resources based on a physical water balance model like MODBIL. The management of single aquifers can be combined with the additional application of a coupled groundwater model. Further research is recommended for a better understanding of the connections between the regional climate and the global climate system and future impacts of climate change. The monitoring survey has to be extended to all important aquifer and recharge regions on the island. Uncontrolled abstractions should be reduced, and a system of rules and supervision

is recommended to guarantee the preservation and sustainable use of the natural groundwater resources of Cyprus in the future.

Bibliography

Afrodisis, S., Avraamides, C., Fischbach, P., Hahn, J., Udluft, P., Wagner, W., 1986. Hydrogeological and hydrochemical studies in the Troodos region. Technical Report N6 in Cyprus - German Geological and Pedological Project No. 81.2224.4, Ministry of Agriculture and Natural Resources, Geological Survey Department, Nicosia.

Afrodisis, S., Fischbach, P., 1988. Mineral waters in the Troodos region. In: Ministry of Agriculture and Natural Resources Cyprus (Ed.), Proceedings, workshop on conservation and development of natural resources in Cyprus - case studies, 13th - 18th October 1986, Nicosia, pp. 185-186.

AG Boden, 1994. Bodenkundliche Kartieranleitung. 4th Ed., Hannover.

Al-Alami, H., 1999. Watershed Management In Wadi Hadi (Jordan). Hydrogeologie und Umwelt 18, University of Würzburg, pp. 1-160.

Al-Farajat, M., 2003. Hydrogeo-Eco-Systems in Aquaba/Jordan - Coasts and Region. Hydrogeologie und Umwelt 30, University of Würzburg.

Albert, K., 1994. Hydrogeologische Untersuchungen in den Einzugsgebieten des Grünbaches, Gerchsheimer Grabens und Rödersteingrabens auf Blatt 6324 Tauberbischofsheim-Ost. Hydrogeologie und Umwelt 8, University of Würzburg.

Albrecht, F., 1962. Die Berechnung der natürlichen Verdunstung (Evapotranspiration) der Erdoberfläche aus klimatischen Daten. Berichte des Deutschen Wetterdienstes 83(11).

Allen, R.G., 1986. A Penman for all Seasons. Journal of the Irrigation and Drainage Division ASCE 112, 348-369.

Allen, R.G., 1996. Nongrowing season evaporation in North Utah. http://www.kimb

erly.uidaho.edu/water/papers/evapotranspiration/Allen_1996_nongrowing _season_Evaporation_anaheim_2.3.pdf [Status: March 2009].

Allen, R.G., Jensen, M.E., Wright, J.L., Burman, R.D., 1989. Operational Estimates of Reference Evapotranspiration. Agronomy Journal 81, 650-662.

Allen, R.G., Pereira, L.S., Raes, D., Smith, M., 1998. Crop evapotranspiration: guidelines for computing crop water requirements. Irrigation and Drainage Paper 56, FAO, Rome.

Allen, R.G., Smith, M., Pereira, L.S., Perrier, A., 1994. An update for the calculation of reference evapotranspiration. ICID bulletin 43(2), 35-92.

Anderson, E.A., 1973. National Weather Service River Forecast System - Snow Accumulation and Ablation Model, NOAA Technical Memorandum NWS HYDRO-17, US Department of Commerce, Silver Spring, MD.

Angström, A., 1924. Solar and terrestrial radiation. Quarterly Journal of the Royal Meteorological Society 50, 121-125.

ASCE [American Society of Civil Engineers], 1996. Hydrology Handbook. ASCE Manuals and Reports of Engineering Practice 28.

Bear, L.M., 1963. Geological map of Cyprus. Scale: 1:250 000. Cyprus Geological Survey Department, Nicosia.

Beisecker, R., 1994. Einfluß langjährig unterschiedlicher Bodenbearbeitungssysteme auf das Bodengefüge, die Wasserinfiltration und die Stoffverlagerung eines Löß- und eines Sandbodens. In: Bork, H.R. et al. (Eds.), Bodenökologie und Bodengenese 12, Technische Universität Berlin.

Bellamy, C.V., Jukes-Browne, A.J., 1905. The Geology of Cyprus. Plymouth.

Ben-Mehrez, M., Taconet, O., Vidal-Madjar, D., Valencogne, C., 1992. Estimation of stomatal resistance and canopy evaporation during the HAPEX-MOBILHY experiment. Agricultural and Forest Meteorology 58, 285-313.

Beven, K., Germann, P., 1981. Water flow in soil macropores. II. A combined flow model. Journal of Soil Science 32, 15-29.

Beven, K., Germann, P., 1982. Macropores and water flows in soils. Water Resources Research 18(5), 1311-1325.

Beyazgül, M., Kayam, Y., Engelsmann, F., 2000. Estimation Methods of Crop Water Requirements in the Gediz Basin of Western Turkey. Journal of Hydrology 229, 19-26.

Blaney, H.F., Criddle, W.D., 1950. Determinating water requirements in irrigated areas from climatological and irrigation data. US Dep. Abr. Div. Irrigation and Water Conservation, SCS TP 96.

Boje-Klein, G., 1982. Entstehung, Klassifikation und Bewertung von Böden einer Toposequenz vom Troodos-Massiv nach Nicosia (Zypern). Ph.D. Thesis, Rheinische Friedrich-Wilhelms-Universität Bonn.

Booltink, H.W.G., Bouma, J., 1993. Sensitivity analysis on processes affecting by-pass flow. Hydrological Processes 7, 33-43.

Booltink, H.W.G., Hatano, R., Bouma, J., 1993. Measurement and simulation of bypass flow in a structured clay soil: a physicomorphological approach. Journal of Hydrology 148, 149-168.

Borgstedt, A., 2004. Grundwasserneubildung im Einzugsbereich des Ouham, Zentralafrikanische Republik. Hydrogeologie und Umwelt 32, University of Würzburg.

Boronina, A., 2004. Application of numerical modelling, isotope studies and streamflow observations for quantitative description of hydrogeology of the Kouris catchment (Cyprus). Ph.D. Thesis, Eidgenössische Technische Hochschule Zürich.

Boronina, A., Renard, P., Balderer, W., Christodoulides, A., 2003. Groundwater resources in the Kouris catchment (Cyprus): Data analysis and numerical modelling. Journal of Hydrology 271, 130-149.

Bouman, B.A.M., van Kasteren, H.W.J., Uenk, D., 1992. Standard Relations to Estimate Ground Cover and LAI of Agricultural Crops from Reflectance Measurements. European Journal of Agronomy 4, 249-262.

Brakensiek, D.L., Rawls, W.J., Stephenson, G.R., 1984. Modifying SCS hydrologic soil groups and curve numbers for rangeland soils. ASAE Paper No. PNR-84-203, St. Joseph/Michigan.

Braun, F.J., 2002. Mesoskalige Modellierung der Bodenhydrologie. Wissenschaftliche Berichte des Instituts für Meteorologie und Klimaforschung 30, Universität Karl-

sruhe.

Braun, L.N., 1985. Simulation of snowmelt-runoff in lowland and lower alpine regions of Switzerland. Züricher Geographische Schriften 21, Eidgenössische Technische Hochschule Zürich, Switzerland.

Breuer, L., Eckhardt, K., Frede, H.G., 2003. Plant parameter values for models in temperate climates. Ecological Modelling 169, 237-293.

Bronstert, A., 1994. Modellierung der Abflußbildung und der Bodenwasserdynamik in Hängen. Mitteilungen des Instituts für Hydrologie und Wasserwirtschaft 46, Universität Karlsruhe.

Brown, R.V., McGinty, J., 1946. Geological map of Cyprus. Scale: 4 miles to one inch. 42nd Geological Section, S.A.E.C., G.H.Q., M.E.F.

Burdon, D.J., 1952. Hydrogeological characteristics of the water bearing formations of Cyprus. In: Report of the 19th Session - International Geological Congress, Algiers, 50 pp.

Burdon, D.J., 1953. The underground water resources of Cyprus. In: Water Supply and Irrigation Department, Nicosia, 49 pp.

Burman, R.D., Nixon, P.R., Kimberly, I.D., Pruitt, W.O., 1980. Water requirements. In: Jensen, M.E. (Ed.), Design and operation of farm irrigation systems, ASAE monograph 3, 189-232.

Cabral, M.C., Garrote, L., Bras, R.L., Entekhabi, D., 1992. A kinematic model of infiltration and runoff generation in layered and sloped soils. Advances in Water Resources 15, 311-324.

Chen, C., Wagenet, R.J., 1992. Simulation of water and chemicals in macropore soils, Parts I and II. Journal of Hydrology 130, 105-149.

Choudhury, B.J., Reginato, R.J., Idso, S.B., 1986. An analysis of infrared temperature observations over wheat and calculation of latent heat flux. Agricultural and Forest Meteorology 37, 75-88.

Clevers, J.G.P.W., 1989. The Application of a Weighted Infrared-Red Vegetation Index for Estimating Leaf Area Index by Correcting for Soil Moisture. Remote Sensing of Environment 29, 25-37.

Clevers, J.G.P.W., Büker, C., van Leeuwen, H.J.C., Bouman, B.A.M., 1994. A Framework for Monitoring Crop Growth by Combining Directional and Spectral Remote Sensing Information. Remote Sensing of Environment 50, 161-170.

Constantinou, G., 1995. Geological map of Cyprus. Scale: 1:250 000. Cyprus Geological Survey Department, Nicosia.

Cosby, B.J., Hornberger, G.M., Clapp, R.B., Ginn, T.R., 1984. A statistical exploration of the relationships of soil moisture characteristics to the physical properties of soils. Water Resources Research 20, 682-690.

Dijon, R., 1977. Groundwater investigation through United Nations projects in karstic areas. In: Doyle, F.L. (Ed.), IAH-Congress, Huntsville, Alabama: Karst Hydrogeology, New York, 43 pp.

DIN [Deutsche Institut für Normung], 1997/2002. Datenblatt - DIN 19685 Klimatologische Standortuntersuchungen. 7th Ed., August 2002, Beuth Verlag GmbH, Berlin.

Dommermuth, H., Trampf, W., 1990/91. Die Verdunstung in der Bundesrepublik Deutschland Zeitraum 1951 - 1980, Teil I-III. Selbstverlag des Deutschen Wetterdienstes, Offenbach am Main.

Doorenbos, J., Kassam, A.H., 1979. Yield response to water. FAO Irrigation Drainage Paper 33, FAO, Rome.

Doorenbos, J., Pruitt, W.O., 1977. Guideline for Predicting Crop Water Requirements. FAO Irrigation Drainage Paper 24, FAO, Rome.

Ducloz, C., 1972. The geology of the Bellapais-Kythrea area of the central Kyrenia Range. Cyprus Geological Survey Department Bulletin 6.

Dünkeloh, A., 2004. Hydrogeological Map of Cyprus. In: Udluft, P., Dünkeloh, A., Mederer, J., Kuells, C., Schaller, J., Re-evaluation of the Groundwater Resources of Cyprus, GRC-Project Final Report, Nicosia, Geological Survey Department of Cyprus, Chap. 5.2.2 and Fig. 58.

Dünkeloh, A., 2005a. Geologie und Wasserhaushalt des oberen Diarizos-Einzugsgebiets (Troodos-Gebirge, Zypern). Diploma Thesis, Institute of Geology, University of Würzburg, 142 pp.

Dünkeloh, A., 2005b. Water budget of the upper Diarizos catchment, Troodos, Cyprus. Hydrogeologie und Umwelt 33(15), 1-24.

Dünkeloh, A., Hertig, E., Jacobeit, J., 2003. Circulation Dynamics of Mediterranean Temperature Variability. Terra Nostra 2003/6, 112-116.

Dünkeloh, A., Jacobeit, J., 2003. Circulation dynamics of Mediterranean precipitation variability 1948-1998. International Journal of Climatology 23, 1843-1866.

Dünkeloh, A., Udluft, P., 2004a. Water balance dynamics of Cyprus - Part 2: Model application for the assessment of the natural groundwater resources and the construction of scenario models, 5th International Symposium on Eastern Mediterranean Geology Thessaloniki, Greece, 14-20 April 2004.

Dünkeloh, A., Udluft, P., 2004b. Anwendung physikalischer Wasserhaushaltsmodellierung auf Zypern - Teil 2: Modelleinsatz zur Abschätzung natürlicher Wasserressourcen und die Entwicklung von Szenarien. In: Schiedek, T., Kaufmann-Knoke, R. (Eds.), Hydrogeologie regionaler Aquifersysteme, Schriftenreihe der Deutschen Geologischen Gesellschaft 32, pp. 175.

Dünkeloh, A., Udluft, P., 2009. MODBIL - A numerical water balance model. Software package and manual. Version V49/2009, Hydrogeological Section, University of Würzburg.

Dünkeloh, A., Udluft, P., Jacobeit, J., 2003. Physikalische Wasserhaushaltsmodellierung für ein typisches Einzugsgebiet des Troodos-Gebirges (Zypern). 22. Jahrestagung des AK Klima der Deutschen Gesellschaft für Geographie (DGfG), Delemont, pp. 62.

Dünkeloh, A., Udluft, P., Jacobeit, J., 2004. Modellierung der Wasserhaushaltsdynamik von Zypern. In: Tagungsband der 23. Jahrestagung des AK Klima der DGfG in Eltville/Rhein, pp. 42.

DVWK [Deutscher Verband für Wasserwirtschaft und Kulturbau], 1986. Ermittlung des Interzeptionsverlustes in Waldbeständen bei Regen. DVWK Merkblatt 211, Hamburg, Berlin, Parey.

DVWK [Deutscher Verband für Wasserwirtschaft und Kulturbau], 1996. Ermittlung der Verdunstung von Land- und Wasserflächen. DVWK Merkblatt 238, Bonn.

Dyck, S., Peschke, G., 1995. Grundlagen der Hydrologie. Verlag für Bauwesen, 3rd Ed., Berlin.

Eckert, S., Kneubühler, M., 2004. Application of Hyperion data to agricultural land classification and vegetation properties estimation in Switzerland, XXth ISPRS Congress, Commission 7, Istanbul, Turkey, ISPRS vol. XXXV, Part B7.

Ergil, M.E., 2000. The salination problem of the Guzelyurt aquifer Cyprus. Water Research 34(4), 1202-1214.

FAO [Food and Agriculture Organization of the United Nations], 1998. World Reference Base for Soil Resources. World Soil Resources Report 84, FAO, Rome, 88 pp.

Fritsch, U., Katzenmaier, D., 2001. Wasser, Trinkwasser und Gewässerschutz: Quantifizierung des Einflusses der Landnutzung und -bedeckung auf den Hochwasserabfluss in Flussgebieten. Bundesministeriums für Umwelt, Naturschutz und Reaktorsicherheit. Abschlussbericht Förderkennzeichen 297 24 508. Available online: http://www.umweltbundesamt.de/wasser/veroeffentlich/kurzfassungen/29724508.htm [Status: 11.08.2008].

Fröhlich, K., Fröhlich, W., Wittenberg, H., 1994. Determination of groundwater recharge by baseflow separation: regional analysis in northeast China. FRIEND: Flow Regimes from International Experimental and Network Data, Proceedings of Braunschweig Conference, October 1993, IAHS Publ. No 221.

Garnier, B.J., Ohmura, A., 1968. A Method of Calculating the Direct Shortwave Radiation Income of Slopes. Journal of Applied Meteorology 7, 796-800.

Gash J.H.C., Morton, A.J., 1978. An application of the Rutter model to the estimation of the interception loss from Thetford Forest. Journal of Hydrology 38, 49-58.

Gass, I.G., MacLeod, C.J., Murton, B.J., Panayiotou, A., Simonian, K.O., Xenophontos, C., 1994. The geology of the Southern Troodos transform fault zone. Memoir No. 9, Ministry of Agriculture, Natural Resources and Environment, Cyprus Geological Survey Department, Nicosia, 218 pp.

Gaudry, A., 1862. Géologie de l'Île de Chypre. Extrait des Mémoires de la Société géologique de France, Série 2, Vol. VII, 269 pp.

Germann, P.F., 1990. Preferential flow and the generation of runoff 1. Boundary layer theory. Water Resources Research 26(12), 3055-3063.

Germann, P.F., Beven, K.J., 1981. Water flow in soil macropores 1. An experimental approach. European Journal of Soil Science 32, 1-13.

Ghodrati, M., Jury, W.A., 1990. A field study using dyes to characterize preferential flow of water. Soil Science Society of America Journal 54, 1558-1563.

Gish, T.J., Shirmohammadi, A. (Eds.), 1991. Preferential Flow. Proceedings of the National Symposium 1991, Chicago, Illinois, American Society of Agricultural Engineers.

Green, W.H., Ampt, G.A., 1911. Studies on soil physics. 1. The flow of air and water through soils. Journal of Agricultural Science 4(1), 1-24.

Grivas, G.C., 1969. Report on the soils of the Morphou Watershed. Ministry of Agriculture and Natural Resources, Department of Agriculture, Nicosia, 42 pp.

Hadjistavrinou, Y., 1972. Groundwater resources of the karstic regions of Cyprus. Bulletin of the Geological Survey Department of Cyprus 5, 1-21.

Hadjistavrinou, Y., Afrodisis, S., 1977. Geology and Hydrogeology of the Paphos region. Bulletin of the Geological Survey Department of Cyprus 7, 1-44.

Hadjistavrinou, Y., Constantinou, C., 1977. Hydrogeology of the Akrotiri Peninsula. Bulletin of the Geological Survey Department of Cyprus 7, 45-74.

Hargreaves, G.H., Samani, Z.A., 1982. Estimation of potential evapotranspiration. Journal of Irrigation and Drainage Division, Proceedings of the American Society of Civil Engineers 108, 223-230.

Hargreaves, G.H., Samani, Z.A., 1985. Reference crop evapotranspiration from temperature. Applied Engineering in Agriculture 1, 96-99.

Hartmann, G., 2007. Investigation of Evapotranspiration Concepts in Hydrological Modelling for Climate Change Impact Assessment. Mitteilungshefte des Instituts für Wasserbau 161, Universität Stuttgart.

Haude, W., 1955. Zur Bestimmung der Verdunstung auf möglichst einfache Weise. Mitteilungen des Deutschen Wetterdienstes 2(11).

Haude, W., 1959. Über die Verwendung verschiedener Klimafaktoren zur Berechnung potentieller Evaporation und Evapotranspiration. Meteorologische Rundschau 12, 11-17.

Henson, S., Vermon, R., McGinty, J., 1949. A Synopsis of the Stratigraphy and Geological History of Cyprus. Quarterly Journal of the Geological Society of London 417(105), 1-41.

Hertig, E., 2004. Niederschlags- und Temperaturabschätzungen für den Mittelmeerraum unter anthropogen verstärktem Treibhauseffekt. Ph.D. Thesis, University of Würzburg, published online at http://opus.bibliothek.uniwuerzburg.de/opus/volltexte/2004/874/.

Hertig, E., Jacobeit, J., 2008a. Assessments of Mediterranean precipitation changes for the 21st century using statistical downscaling techniques. International Journal of Climatology 28, 1025-1045.

Hertig, E., Jacobeit, J., 2008b. Downscaling Future Climate Change: Temperature Scenarios for the Mediterranean area. Special Issue of Global and Planetary Change, pp. 127-131.

Hock, R., 2003. Temperature index melt modelling in mountain areas. Journal of Hydrology 282, 104-115.

Hoogmoed, W.B., Bouma, J., 1980. A simulation model for predicting infiltration into cracked clay soil. Soil Science Society of America Journal 44, 458-462.

Hörmann, G., 2005. SIMPEL - Speichermodelle zum Bodenwasserhaushalt. http://www.hydrology.uni-kiel.de/simpel/.

Hoyningen-Huene, J.V., 1983. Die Interzeption des Niederschlags in landwirtschaftlichen Pflanzenbeständen. In: Einfluss der Landnutzung auf den Gebietswasserhaushalt, DVWK Schriften 57.

Iacovides, S.J., 1997. Artificial groundwater recharge practice in Cyprus. In: Simmers, I. (Ed.), Recharge of phreatic aquifers in (semi-)arid areas. Rotterdam (Balkema), pp. 200-213.

IPCC [Intergovernmental Panel on Climate Change], 2007. Climate Change 2007: The Physical Science Basis. Contribution of Working Group I to the Fourth As-

sessment Report of the Intergovernmental Panel on Climate Change, Cambridge University Press, 996 pp.

Jacobeit, J., 2000. Rezente Klimaentwicklung im Mittelmeerraum. Petermanns Geographische Mitteilungen 144, 26-37.

Jacobeit, J., Dünkeloh, A., Hertig, E., 2007. Mediterranean rainfall changes and their causes. In Global Change: Enough Water for All? Lozan, J.L., Graßl, H., Hupfer, P., Menzel, L., Schönwiese, C.D. (Eds.), Wissenschaftliche Auswertungen: Hamburg, pp. 195-199.

Jarvis, N.J., Jansson, P.E., Dik, P.E., Messing, I., 1991. Modeling water and solute transport in macroporous soil. I. Model description and sensitivity analysis. European Journal of Soil Science 42, 59-70.

Jensen, M.E., Burman, R.D., Allen, R.G., 1990. Evapotranspiration and Irrigation Water Requirements. Manual of Practice 70, ASCE, New York.

Jensen, M.E., Haise, H.R., 1963. Estimating evapotranspiration from solar radiation. ASCE Journal of Irrigation and Drainage Engineering 89 IR4, 15-41.

Kambanellas, C.A., 1998. Recycling of Grey Water in Cyprus. Water Development Department of Cyprus, Nicosia.

Kane, D.L., Gieck, R.E., Hinzman, L.D., 1997. Snowmelt Modeling at small Alaskan Arctic watershed. Journal of Hydrologic Engeneering 2(4), 204-210.

Kitching, R., 1975. A mathematical model of the Akrotiri Plio-Pleistocene gravel aquifer, Cyprus. Natural Environment Research Council, Institute of Geological Sciences, U.K., Report 75-2, 32 pp.

Kitching, R., Edmunds, W.M., Shearer, T.R., Walton, N.R.G., Jacovides, J., 1980. Assessment of recharge to aquifers. Bulletin des Sciences Hydrologiques 25(3), 217-235.

Klock, H., 2002 Hydrogeologie der Kalahari in NE-Namibia. Hydrogeologie und Umwelt 31, University of Würzburg.

König, R., 1993. Quantifizierung der Bodenwasserbewegungen im Hinblick auf die Grundwasserneubildung mit Hilfe deckschichtenphysikalischer Kenngrößen. Hydrogeologie und Umwelt 6, University of Würzburg.

Konteatis, C.A.C., 1987. Groundwater recharge studies (Cyprus, Oman). University of Nottingham, Nottingham, 780 pp.

Koumis, C.I., 1970. Report on the soils of the Pissouri-Paramali watershed. Ministry of Agriculture and Natural Resources, Department of Agriculture, Nicosia, 59 pp.

Kramvis, S.C., 1987. Application of electrical resistivity in groundwater exploration in Cyprus. Ph.D. Thesis, University of Leicester.

Krause, P., 2001. Das hydrologische Modellsystem J2000. Beschreibung und Anwendung in grossen Flussgebieten. Schriften des Forschungszentrums Jülich - Reihe Umwelt 29.

Kuells, C., 2003. Groundwater of the north-western Kalahari, Namibia - Estimation of recharge and quantification of the flow system. Hydrogeologie und Umwelt 28, University of Würzburg.

Kuells, C., Constantinou, C., Petrides, G., Udluft, P., 2000a. Dynamics of groundwater recharge in natural environments and mining areas: Case studies from Cyprus. Proceedings of the 3rd Mineral Wealth Conference 2000, Athens.

Kuells, C., Constantinou, C., Udluft, P., 2000b. Mapping the availability and dynamics of groundwater recharge - II: Case studies from Mediterranean Basins. Proceedings of the Third Congress on Regional Geological Cartography and Information Systems, München 2000, pp. 163-168.

Kuells, C., Zagana, E., Udluft, P., 1998. Integrated evaluation of quantitative and qualitative groundwater potential in the Eastern Mediterranean Region. In: Weaver, T.R., Lawrence, C.R. (Eds.), Groundwater Sustainable Solutions, pp. 683-688.

Kuusisto, E., 1984. Snow accumulation and snowmelt in Finland. In: Publ. Water Research Institute 151 N55.

Kuusisto, E., 1986. The energy balance of a melting snow cover in different environments. International Association of Hydrological Sciences Publication 155, 37-45.

Liermann, R., 1999. Makroporenkartierung und Freilandtracerstudien als methodisches Konzept zum qualitativen Nachweis potentieller Transportpfade. Leipziger Geowissenschaften Band 11.

Linsley, R.K. Jr., 1943. A simple procedure for the daily forecasting of runoff from

snowmelt. Transaction of the American Geophysical Union, Part III, 62-67.

Lippard, S.J., Shelton, A.W., Gass, I.G., 1986. The ophiolite of northern Oman. Geological Society of London's Memoirs 11, 178 pp.

Liu, S., Mao, D., Lu, L., 2006. Measurement and estimation of the aerodynamic resistance. Hydrology and Earth Systems Sciences Discussions 3, 681-705.

Löpmeier, F.J., 1994. Berechnung der Bodenfeuchte und Verdunstung mittels agrarmeteorologischer Modelle. Zeitschrift für Bewässerungswirtschaft 29, 157-167.

Ludwig, R., Gerke, H.H., Wendroth, O., 1999. Describing water flow in macroporous field soils using the modified MACRO model. Journal of Hydrology 215, 135-152.

Lüken, H., 1988. Calcareous soils of Cyprus - Land classification, mapping examples. In: Pedology, hydrochemistry and non-metallic mineral resources Vol. IV. Technical cooperation project no. 81.2224.4, Bundesanstalt für Geowissenschaften und Rohstoffe, Hannover.

Maillet, E., 1905. Mécanique et physique du globe. Essais d´hydraulique souterraine et fluviatile. Hermann, Paris, 218 pp.

Mainardy, H., 1999. Grundwasserneubildung in der Übergangszone zwischen Festgesteinsrücken und Kalahari-Lockersedimentüberdeckung (Namibia). Hydrogeologie und Umwelt 17, University of Würzburg.

Malpas, J., Moores, E.M., Panayiotou, A., Xenophontos, C. (Eds.), 1990. Ophiolites. Oceanic Crustal Analogues. Proceeding of the 'Troodos 87' Symposium, Geological Survey Department, Nicosia.

Mariotti, A., Zeng, N., Yoon, J.H., Artale, V., Navarra, A., Alpert, P., Li, L.Z.X., 2008. Mediterranean water cycle changes: transition to drier 21st century conditions in observations and CMIP3 simulations. Environmental Research Letters 3, 044001, 8 pp, doi:10.1088/1748-9326/3/4/044001.

Markides, L., 1973. Soils memoirs of Polemi. Soil Series Report 2. Sheet no. 44 & 45, Department of Agriculture, Ministry of Agriculture and Natural Resources, Nicosia, 138 pp.

Markides, L., 1999. Soil Map of Cyprus 1:250 000. Department of Agriculture, Ministry of Agriculture natural Resources and Environment, Nicosia.

Mederer, J., 2003. Hydrogeologische, hydrochemische und bodenphysikalische Untersuchungen im Einzugsgebiet des Limnatis, Troodos-Gebirge, Zypern. Diploma Thesis, Institute of Geology of the University of Würzburg, 98 pp.

Mederer, J., 2005. Groundwater resources of the Limnatis catchment in Cyprus: Application of the water balance modelling program MODBIL in an area of irrigation. In: Hydrogeologie und Umwelt 33, University of Würzburg.

Mederer, J., 2009. Water Resources and Dynamics of the Troodos Igneous Aquifersystem, Cyprus - Balanced Groundwater Modelling. Ph.D. Thesis, University of Würzburg, published online: http://www.opus-bayern.de/uni-wuerzburg/volltexte/2009/3730/.

Menzel, L., 1997. Modellierung der Evapotranspiration im System Boden-Pflanze-Atmosphäre. Zürcher Geographische Schriften 67, Geographisches Institut, ETH Zürich.

Merz, B., 1996. Modellierung des Niederschlag-Abfluß-Vorgangs in kleinen Einzugsgebieten unter Berücksichtigung der natürlichen Variabilität. Mitteilungen des Instituts für Hydrologie und Wasserwirtschaft 56, Universität Karlsruhe.

Meteorological Service, 1984. Local climates of Cyprus. Meteorological Paper 6 (second edition), Meteorological Service, Nicosia.

Meteorological Service, 1985a. Some Studies of the Amounts of Precipitation on Cyprus. Meteorological Paper 1 (second edition), Meteorological Service, Nicosia.

Meteorological Service, 1985b. Rainfall Intensity Over Short Periods in Cyprus. Meteorological Paper 2 (second edition), Meteorological Service, Nicosia.

Meteorological Service, 1985c. Surface Air Temperature in Cyprus. Meteorological Paper 3 (second edition), Meteorological Service, Nicosia.

Meteorological Service, 1987. The Climate of Cyprus: Past and Present. Meteorological Note 3, Meteorological Service, Nicosia.

Meteorological Service, 1989. The Distribution of Raindays in Cyprus. Meteorological Note 6, Meteorological Service, Nicosia.

Monteith, J.L., 1965. Evaporation and environment. Proceedings of the Symposium of the Society for Experimental Biology 19, Cambridge University Press, pp. 205-

234.

Monteith, J.L., 1973. Principles 5 of Environmental Physics. Arnold, Paris.

Moores, E., Vine, F.J., 1971. The Troodos massif, Cyprus and other ophiolites as oceanic crust: evaluation and implications. Philosophical Transactions of the Royal Society A 268, 443-466.

Myneni, R.B., Williams, D.L., 1994. On the relationship between FAPAR and NDVI. Remote Sensing of Environment 49, 200-211.

Nathan, R.J., McMahon, T.A., 1990. Evaluation of automated techniques for baseflow and recession analysis. Water Resources Research 26(7), 1465-1473.

Obeidat, M., 2001. Hydrochemistry and Isotope Hydrology of Groundwater Resources in the Hammad Basin (Jordan). Hydrogeologie und Umwelt 26, University of Würzburg.

Oke, T.R., 1987. Boundary Layer Climates. Routledge, New York.

Paltineanu, C., Mihailescu, I.F., Torica, V., Albu, A.N., 2002. Correlation between sunshine duration and global solar radiation in south-eastern Romania. International Agrophysics 16, 139-145.

Panayides, I., Xenophontos, C., Malpas, J. (Eds.), 2000. Proceedings of the Third international conference on the Geology of the eastern Mediterranean. Ministry of Agriculture, Natural Resources and Environment, Geological Survey Department, Nicosia, 376 pp.

Panayiotou, A. (Ed.), 1980. Ophiolites. Proceedings, International ophiolite symposium. Ministry of Agriculture and Natural Resources, Geological Survey Department of Cyprus, Nicosia, 781 pp.

Panayiotou, A., 1987. An overview of the geology of Cyprus. In: Xenophontos, C., Malpas, J.G. (Eds.), Field Excursion Guidebook, Symposium 'Troodos 87', Geological Survey Department, Nicosia, Cyprus.

Pasig, R., 2005. Origen y Dinámica del Agua Subterránea en el noroeste del Chaco Sudamericano. Hydrogeologie und Umwelt 34, University of Würzburg.

Penman, H.L., 1948. Natural evaporation from open water, bare soil and grass. Proceedings of the Royal Society of London A 193, 120-146.

Penman, H.L., 1953. The physical basis of irrigation control. Report 13th International Horticultural Congress 2, 913-914.

Penman, H.L., 1956. Estimating evaporation. Transactions - American Geophysical Union 37(1), 43-50.

Peschke, G., 1977. Ein zweistufiges Modell der Infiltration von Regen in geschichtete Böden. Acta Hydrophysica XXII, H 1, 39-48.

Peschke, G., Gurtz, J., 1987. The role of infiltration in rainfall-runoff relationship. Acta Hydrophysica, Berlin 31 3/4, 207-223.

Prasad, R., 1967. A nonlinear hydrologic system response model. Proceedings of the American Society of Civil Engineers, 93(HY4), 201-221.

Price, C., Michaelides, S., Pashiardis, S., Alpert, P., 1999. Long term changes in diurnal temperature ranges in Cyprus. Atmospheric Research 51(2), 85-98.

Raeburn, C., 1945. Water supply in Cyprus: a general report. Department of Water Development, Nicosia, 53 pp.

Rasmussen, T.M., 2005. Konzeption und Erprobung eines Moduls zur horizontdifferenzierten Simulation von Bodenwasserbewegungen im hydrologischen Modellsystem J2000. Diploma Thesis, Institute of Geography, University of Jena.

Reger, B., 2004. Land-use units and the description, characteristics and hydrological properties. In: Udluft, P., Dünkeloh, A., Mederer, J., Kuells, C., Schaller, J., 2004. Data Collection and Collation - GRC-Project Report T 3, Geological Survey Department of Cyprus, Nicosia, 213 pp.

Renger, M., Voigt, A., Strebel, O., Giesel, W., 1974. Beurteilung bodenkundlicher, kulturtechnischer und hydrologischer Fragen mit Hilfe von klimatischer Wasserbilanz und bodenphysikalischen Kennwerten. Zeitschrift für Kulturtechnik und Flurbereinigung 15, 206-221.

Rijtema, P.E., 1965. Analysis of actual evapotranspiration. Agricultural Research Report 69, Centre for Agricultural Publications and Documentation, Wageningen, 111 pp.

Robertson, A.H.F., 1990. Tectonic evolution of Cyprus. In: Malpas, J., Moores, E.M., Panayiotou, A., Xenophontos, C. (Eds.), Ophiolites - oceanic crustal ana-

logues, Proceedings of the symposium 'Troodos 1987', Ministry of Agriculture, Natural Resources and Environment, Nicosia, pp. 235-250.

Robertson, A.H.F., 2000. Tectonic evolution of Cyprus in its easternmost Mediterranean setting. In: Panayides, I., Xenophontos, C., Malpas, J. (Eds.), Proceedings of the Third international conference on the Geology of the eastern Mediterranean, Ministry of Agriculture, Natural Resources and Environment, Geological Survey Department, Nicosia.

Robertson, A.H.F., Xenophontos, C., 1997. Cyprus. In: Moores, E.M., Fairbridge, R.W. (Eds.), Encyclopedia of European and Asian regional geology, Chapman & Hall, London, pp. 160-171.

Robertson, A.H.F., Dixon, J.E., et al., 2003. Edinburgh University School of GeoSciences Honours Geology and GPG excursion to Cyprus Field Guide. Edinburgh University School of GeoSciences, Edinburgh.

Rosa Filho, E.F., 1991. Umweltgeologische Untersuchungen und Hydrogeologische Modellrechnungen im Einzugsgebiet der Trinkwassertalsperre Passaúna (Curitiba, Paraná, Brasilien). Ph.D. Thesis, Institute of Geology, University of Würzburg.

Roth, D., Günther, R., 1992. Vergleich von Meß- und Schätzwerten der potentiellen Evapotranspiration. Zeitschrift für Kulturtechnik und Landentwicklung 33, 13-22.

Rutter, A.J., Morton, A.J., 1977. A predictive model of rainfall interception in forest. 3. Sensitivity of the model to stand parameters and meteorological variables. Journal of Applied Ecology 14, 567-588.

Saxton, K.E., 2007. Soil Water Characteristics - Hydraulic Properties Calculator. Software. http://hydrolab.arsusda.gov/soilwater/Index.htm [Status: March 2009].

Saxton, K.E., Rawls, W.J., Romberger, J.S., Papendick, R.I., 1986. Estimating generalized soil-water characteristics from texture. Soil Science Society of America Journal 50(4), 1031-1036.

Schaap, M.G., Leij, F.J., van Genuchten, M.T., 2001. ROSETTA: a computer program for estimating soil hydraulic parameters with hierarchical pedotransfer functions. Journal of Hydrology 251, 163-176.

Schmidt, G., Avraamides, C., Plothner, D., Wagner, W., Zomenis, S., 1988. Techni-

cal cooperation Cyprus-German Geological and Pedological Project, Groundwater Model Investigation on the Kiti Aquifer. Bundestanstalt für Geowissenschaften und Rohstoffe, Hannover.

Schulla, J., 1997. Hydrologische Modellierung von Flussgebieten zur Abschätzung der Folgen von Klimaänderungen. Zürcher Geographische Schriften 69.

Schulla, J., Jasper, K., 1999. Modellbeschreibung WaSiM-ETH. Zürich.

Schwarze, R., Dröge, W., Opherden, K., 1997. Regional analysis and modelling of groundwater runoff components from small catchments in solid rock areas. Landschaftsökologische Umweltforschung 25, 59-62.

Scurlock, J.M.O., Asner, G.P., Gower, S.T., 2001. Worldwide Historical Estimates and Bibliography of Leaf Area Index, 1932-2000. ORNL Technical Memorandum TM-2001/268, Oak Ridge National Laboratory, Oak Ridge, Tennessee, U.S.A.

Sellers, P.J., Tucker, P.J., Collatz, G.J., Los, S.O., Justice, C.O., Dazlich, D.A., Randall, D.A., 1994. A global 1degree by 1 degree NDVI data set for climate studies. Part 2: the generation of global fields of terrestrial biophysical parameters from NDVI. International Journal of Remote Sensing 15(17), 3519-3545.

Shepard, D., 1968. A two-dimensional interpolation function for irregularly-spaced data. Proceedings of the 1968 ACM National Conference, pp. 517-524.

Shepard, D., 1984. Computer mapping: The SYMAP interpolation algorythm. In: Gaile, G.L., Willmott, C.J. (Eds.), Spatial Statistics and Models, pp. 133-145.

Sonntag, D., 1994. Advancements in the field of hygrometry. Meteorologische Zeitschrift NF 3, 51-66.

Soteriades, C.G., Grivas, G.C., 1970. General soil map of Cyprus. Scale: 1:200 000. FAO/UNESCO, Rome.

Soteriades, C.G., Koudounas, C., 1968. Soils Memoirs of Paphos. Soil Series Report 1. Sheet no. 51 (+ 2 maps, scale 1: 25,000). Ministry of Agriculture and Natural Resources, Department of Agriculture, Nicosia, 96 pp.

Sponagel, H., 1980. Zur Bestimmung der realen Evapotranspiration landwirtschaftlicher Kulturpflanzen. Geologisches Jahrbuch F9, Hannover, pp. 3-87.

Thiessen, A.H., 1911. Precipitation averages for large areas. Monthly Weather Review 39(7), 1082-1084.

Thom, A.S., 1975. Momentum, mass and heat exchange of plant communities. In: Monteith, J.L. (Ed.), Vegetation and the Atmosphere. Academic Press, London, pp. 57-109.

Thom, A.S., Oliver, H.R., 1977. On Penman's equation for estimating regional evaporation. Quarterly Journal of the Royal Meteorological Society 103, 345-357.

Thornthwaite, C.W., 1948. An approach toward a rational classification of climate. Geographical Rev. 38, 55-93.

Tietje, O., Hennings, V., 1996. Accuracy of the saturated hydraulic conductivity prediction by pedo-transfer functions compared to the variability within FAO textural classes. Geoderma 69, 71-84.

Tullström, N.H.O., 1970. Hydrogeological map of Cyprus. Scale 1:250000. Geological Survey Department of Cyprus, Nicosia.

Turc, L., 1961. Evaluation de besoins en eau d'irrigation, evapotranspiration potentielle. Annales agronomiques 12, 13-49.

Udluft, P., 2002. Groundwater Recharge in the Eastern Meditaerranea (GREM) - A comparative study on Intergrated Evaluation Techniques for Groundwater Resources: Final Report. Science Research Development, European Comission, Office for Official Publications, Luxembourg.

Udluft, P., Dünkeloh, A., 2004a. Water balance dynamics of Cyprus - Part 1: Modelling techniques. 5th International Symposium on Eastern Mediterranean Geology Thessaloniki, Greece, 14-20 April 2004.

Udluft, P., Dünkeloh, A., 2004b. Anwendung physikalischer Wasserhaushaltsmodellierung auf Zypern - Teil 1: Modelliertechnik. In: Schiedek, T., Kaufmann-Knoke, R. (Eds.), Hydrogeologie regionaler Aquifersysteme, Schriftenreihe der Deutschen Geologischen Gesellschaft 32, pp. 54.

Udluft, P., Dünkeloh, A., Mederer, J., Kuells, C., Schaller, J., 2004a. Water balances for catchments and the whole island - GRC-Project Report T 6/7. Geological Survey Department of Cyprus, Nicosia, 363 pp.

Udluft, P., Dünkeloh, A., Mederer, J., Kuells, C., Schaller, J., 2004b. Re-evaluation of the Groundwater Resources of Cyprus - GRC-Project Final Report. Geological Survey Department of Cyprus, Nicosia, 181 pp.

Udluft, P., Kuells, C., 2000. Mapping the availability and dynamics of groundwater recharge - I: Modelling techniques. Proceedings of the Third Congress on Regional Geological Cartography and Information Systems, München 2000, pp. 337-340.

Udluft, P., Zagana, E., 1994. Calculation of the Water Budget of the Venetikos Catchment Area. Bulletin of the Geological Society of Greece XXX/4, 267-274.

Uenk, D., Bouman, B.A.M., van Kasteren, H.W.J., 1992. Reflectiemetingen aan landbouwgewassen. CABO Verslag 156, CABO-DLO, Wageningen, The Netherlands, 56 pp.

Uhlenbrook, S., Leibundgut, C., 1997. Abflußbildung bei Hochwasser in verschiedenen Raumskalen. Wasser & Boden 49, pp. 13-21.

UNDP [United Nations Development Programme], 1970. UNDP - Survey of groundwater and mineral resources. New York, 231 pp.

Unger, F.J., Kotschy, T., 1865. Die Insel Zypern, ihrer physischen und organischen Natur nach mit Rücksicht auf ihre frühere Geschichte. Braumüller, Wien, 598 pp.

USACE [U.S. Army Corps of Engineers], 1994. Engineering and Design: Flood-Runoff Analysis. EM 1110-2-1417, Washington, D.C.

van Genuchten, M.T., Rolston, D.E., Germann, P.F. (Eds.), 1990. Transport of water and solutes in macropores. Geoderma 46(1-3), 1-297.

Vereecken, H., Maes, J., Feyen, J., 1990. Estimating unsaturated hydraulic conductivity from easily measured soil properties. Soil Science 149, 1-12.

Verma, S.B., Rosenberg, N.J., Blad, B.L., Baradas, M.W., 1976. Resistance-energy balance method for predicting evapotranspiration: Determination of boundary layer resistance and evaluation of error effects. Agronomy Journal 68, 776-782.

Vörösmarty, C.J., Federer, C.A., Schloss, A.L., 1998. Potential Evaporation Functions Compared on US Watersheds: Possible implications for global-scale water balance and terrestrial ecosystem modeling. Journal of Hydrology 207, 147-169.

Wagner, W., Zomenis, S., Ploethner, D., 1990. Groundwater quality in the region

between Nicosia, Larnaca and Limassol. In: Bundesanstalt für Geowissenschaften und Rohstoffe (Ed.), Geologisches Jahrbuch C 54, Hannover, pp. 3-56.

Walter, E.E., 2010. Konventionelle mineralische Stickstoff- und N-Injektionsdüngung in Feldversuchen 1991 bis 2005 - Einfluss auf Nitratauswaschung und Getreideproduktion. Ph.D. Thesis, Institut für Pflanzenbau und Grünland, Universität Hohenheim.

Wanke, H., Beyer, U., Dünkeloh, A., Udluft, P., 2007. A water balance approach to indicate effects of man-made enhanced greenhouse warming on groundwater recharge in the Kalahari. IAHS Publication 315, 310-319.

Wanke, H., Dünkeloh, A., Udluft, P., 2008. Groundwater Recharge Assessment for the Kalahari Catchment of North-eastern Namibia and North-western Botswana with a Regional-scale Water Balance Model. Water Resources Management 22, 1143-1158.

Waterloo Hydrogeologic, 2002. AquiferTest software package (Version 2002). http://www.waterloohydrogeologic.com/software/aquifertest/aquifertest_ov.htm.

WDD/FAO [Water Development Department of Cyprus / Food and Agriculture Organization of the United Nations], 2002. Re-Assessment of the Water Resources and Demand of the Island of Cyprus. Volume I, II, III and synthesis report, Ministry of Agriculture, Natural Resources and Environment, Nicosia, ISBN 9963-1-7003-X.

Weigand, S., 2001. Entwicklung und Validierung des Computerprogramms MODTRANS - Ein Computerprogramm zur Berechnung des Stofftransports in der ungesättigten Bodenzone. Hydrogeologie und Umwelt 25, University of Würzburg.

Weiler, M., Naef, F., 2003. Simulating surface and subsurface initiation of macropore flow. Journal of Hydrology 273(1-4), 139-154.

Wijnen, J., 2002. A groundwater flow and particle tracking model for the Iraíbasin, Paraná, Brazil. Ph.D. Thesis, University of Würzburg, OPUS [Online Publikation University of Würzburg], http://opus.bibliothek.uni-wuerzburg.de/opus/volltexte/2002/53/

Willmott, C.J., Rowe, C.M., Philpot, W.D., 1985. Small-scale climate maps: a sensitivity analysis of some common assumptions associated with grid point interpolation and contouring. American Cartographer 12, 5-16.

Wittenberg, H., 1999. Baseflow recession and recharge as nonlinear storage processes. Hydrological Processes 13, 715-726.

WMO [World Meteorological Organization], 1986. Intercomparison of models for snowmelt runoff. Operational Hydrology Report 23, WMO No. 646.

WMO [World Meteorological Organization], 1994. Guide to hydrological practices, data acquisition and processing, an-alysing forecasting and other applications, fifth edition, WMO report No 168, WMO, Geneva, 286 pp.

Wood, E.F., Lettenmaier, D.P., Zartarian, V.G., 1992. A land-surface hydrology parameterization with subgrid variability for general circulation models. Journal of Geophysical Research 97, 2717-2728.

Wright, J.L., 1982. New evapotranspiration crop coefficients. Journal of the Irrigation and Drainage Division 108, 57-74.

Zagana, E., 2001. Wasserhaushalt und Stofftransport im Aliakmonasgebiet (Nordwest-Griechenland). Hydrogeologie und Umwelt 24, University of Würzburg.

Zagana, E., Kuells, C., Udluft, P., 1999. Hydrochemie und Wasserhaushalt des Aliakmonas, Nordgriechenland. Vom Wasser 94, 29-39.

Zagana, E., Kuells, C., Udluft, P., Constantinou, C., 2007. Methods of groundwater recharge estimation in eastern Mediterranean - a water balance model application in Greece, Cyprus and Jordan. Hydrological Processes 21(18), 2405-2414.

Zagana, E., Udluft, P., 1999. Wasserhaushalt im Aliakmonas-Gebiet (Griechenland); Bilanzierung und Modellierung. Hydrogeologie und Umwelt 18, University of Würzburg, pp. 258-288.

Zhangshi, Y., Williams, T.H.L., 1997. Obtaining spatial and temporal vegetation data from landsat MSS and AVHRR/NOAA satellite images for a hydrologic model. Photogrammetric Engineering & Remote Sensing 63(1), 69-77.

Zomenis, S., 1972. Stratigraphy and hydrogeology of the neogene rocks in the northern foothills of the Troodos massif Cyprus. Cyprus Geological Survey Department Bulletin 6, 22-90.

Zomenis, S., 1977. Hydrogeology of central Mesaoria (Cyprus). Ph.D. Thesis, University of London.

Zomenis, S.L., Wagner, W., Ploethner, D., 1988. Groundwater Quality Investigations in Cyprus - Main Results of a Project of Technical Cooperation in Applied Sciences. Cyprus Geological Survey Department Bulletin 8.

Zuidema, P.K., 1985. Hydraulik der Abflussbildung während Starkniederschlägen. Eine Untersuchung mit Hilfe numerischer Modelle unter Verwendung plausibler Bodenkennwerte. Mitteilung der Versuchsanstalt für Wasserbau, Hydrologie und Glaziologie 79.

Appendix A

Land Cover Coefficients

Table A.1: Albedo, vegetation cover, sealed surface, secondary evapotranspiration.

No	Land cover class	Albedo α [-]	Vegetation cover (Frac. of area) vc [-]	Sealed surface (Frac. of area) vs [-]
1	Coniferous forest	0.15	0.95	0
2	Deciduous forest	0.17	0.95	0
3	Scrubland, few higher trees (Maquis)	0.20	0.95	0
4	Low scrubland, grassland, fields (Garrigue)	0.20	0.85	0
5	Sparse vegetation, rocks, boulders, bare soils	0.15	0.70	0
6	Fields, fallow land	0.25	0.95	0
7	Vine yards	0.25	0.80	0
8	Irrigated areas (plantations, fields, green areas, parks)	0.17	0.95	0
9	Wetlands, moist areas	0.17	0.95	0
10	Open water bodies	0.05	1.00	0
11	Salt lake pans	0.20	1.00	0
12	Settlements	0.15	0.60	0.4
13	Settlements (sealing >70%), aiports, highways	0.10	0.30	0.7

Table A.2: Effective plant height for aerodynamic roughness length in [m].

No	Land cover class	Month											
		1	2	3	4	5	6	7	8	9	10	11	12
1	Coniferous forest	2.0	2.0	2.1	2.3	2.3	2.1	2.0	2.0	2.0	2.0	2.0	2.0
2	Deciduous forest	1.6	1.6	1.7	1.8	1.8	1.7	1.6	1.6	1.6	1.6	1.6	1.6
3	Scrubland, few higher trees (Maquis)	1.2	1.2	1.3	1.4	1.4	1.3	1.2	1.2	1.2	1.2	1.2	1.2
4	Low scrubland, grassland, fields (Garrigue)	0.7	0.7	0.7	0.8	0.8	0.7	0.7	0.7	0.7	0.7	0.7	0.7
5	Sparse vegetation, rocks, boulders, bare soils	0.2	0.2	0.2	0.3	0.3	0.2	0.2	0.2	0.2	0.2	0.2	0.2
6	Fields, fallow land	0.1	0.1	0.3	0.5	0.5	0.5	0.4	0.4	0.3	0.2	0.1	0.1
7	Vine yards	0.3	0.3	0.4	0.5	0.5	0.5	0.4	0.4	0.4	0.4	0.4	0.3
8	Irrigated areas (plantations, fields, green areas, parks)	0.7	0.7	0.8	1.0	1.0	1.0	0.9	0.8	0.8	0.8	0.8	0.7
9	Wetlands, moist areas	1.5	1.5	1.8	2.0	2.0	1.8	1.7	1.6	1.6	1.5	1.5	1.5
10	Open water bodies	0.002	0.002	0.002	0.002	0.002	0.002	0.002	0.002	0.002	0.002	0.002	0.002
11	Salt lake pans	0.04	0.04	0.04	0.04	0.04	0.04	0.04	0.04	0.04	0.04	0.04	0.04
12	Settlements	1.2	1.2	1.2	1.2	1.2	1.2	1.2	1.2	1.2	1.2	1.2	1.2
13	Settlements (sealing >70%), aiports, highways	1.2	1.2	1.2	1.2	1.2	1.2	1.2	1.2	1.2	1.2	1.2	1.2

Table A.3: Effective rooting depth in [m].

No	Land cover class	Month											
		1	2	3	4	5	6	7	8	9	10	11	12
1	Coniferous forest	2.1											
2	Deciduous forest	2.0											
3	Scrubland, few higher trees (Maquis)	1.8											
4	Low scrubland, grassland, fields (Garrigue)	1.5											
5	Sparse vegetation, rocks, boulders, bare soils	1.0											
6	Fields, fallow land	0.8	0.8	0.9	1.0	1.1	1.3	1.3	1.1	0.9	0.8	0.8	0.8
7	Vine yards	1.6											
8	Irrigated areas (plantations, fields, green areas, parks)	2.0											
9	Wetlands, moist areas	2.1											
10	Open water bodies	(10)											
11	Salt lake pans	(10)											
12	Settlements	1.6											
13	Settlements (sealing >70%), aiports, highways	1.6											

Table A.4: Minimum stomatal resistance in [s/m].

No	Land cover class	Month											
		1	2	3	4	5	6	7	8	9	10	11	12
1	Coniferous forest	80	80	75	65	65	70	80	85	85	85	80	80
2	Deciduous forest	80	80	75	65	65	70	80	85	85	85	80	80
3	Scrubland, few higher trees (Maquis)	80	80	75	65	65	70	80	85	85	85	80	80
4	Low scrubland, grassland, fields (Garrigue)	85	85	80	70	70	75	85	90	90	90	85	85
5	Sparse vegetation, rocks, boulders, bare soils	90	90	85	75	75	80	90	95	95	95	90	90
6	Fields, fallow land	85	85	75	65	65	70	80	90	90	90	85	85
7	Vine yards	85	85	80	70	70	70	75	80	80	85	85	85
8	Irrigated areas (plantations, fields, green areas, parks)	80	80	75	65	65	70	75	75	75	75	80	80
9	Wetlands, moist areas	80	80	75	65	65	70	75	75	75	75	80	80
10	Open water bodies	20											
11	Salt lake pans	50											
12	Settlements	100											
13	Settlements (sealing >70%), aiports, highways	100											

Table A.5: Secondary evapotranspiration (defined as fraction of potential crop evapotranspiration ET_{pot} [-]).

No	Land cover class	Month											
		1	2	3	4	5	6	7	8	9	10	11	12
1	Coniferous forest	0											
2	Deciduous forest	0											
3	Scrubland, few higher trees (Maquis)	0											
4	Low scrubland, grassland, fields (Garrigue)	0											
5	Sparse vegetation, rocks, boulders, bare soils	0											
6	Fields, fallow land	0											
7	Vine yards	0											
8	Irrigated areas (plantations, fields, green areas, parks)	0.6	0.6	1.0	1.0	1.0	0.8	0.7	0.6	0.6	0.6	0.6	0.6
9	Wetlands, moist areas	1.0	1.0	1.0	0.9	0.8	0.7	0.6	0.5	0.4	0.5	0.8	1.0
10	Open water bodies	1.0											
11	Salt lake pans	0											
12	Settlements	0.6											
13	Settlements (sealing >70%), aiports, highways	0.3											

Table A.6: Interception storage (for all intercepting surfaces) [mm].

No	Land cover class	Month											
		1	2	3	4	5	6	7	8	9	10	11	12
1	Coniferous forest	3.5	3.5	3.5	4.0	4.0	3.5	3.5	3.5	3.5	3.5	3.5	3.5
2	Deciduous forest	3.0	3.0	3.0	3.5	3.5	3.0	3.0	3.0	3.0	3.0	3.0	3.0
3	Scrubland, few higher trees (Maquis)	3.0	3.0	3.0	3.5	3.5	3.0	3.0	3.0	3.0	3.0	3.0	3.0
4	Low scrubland, grassland, fields (Garrigue)	2.0	2.0	2.0	2.5	2.5	2.0	2.0	2.0	2.0	2.0	2.0	2.0
5	Sparse vegetation, rocks, boulders, bare soils	1.5											
6	Fields, fallow land	1.5	1.5	2.0	2.5	3.0	3.0	2.5	2.0	1.5	1.5	1.5	1.5
7	Vine yards	1.5	1.5	2.0	2.5	2.5	2.5	2.5	2.5	2.5	2.0	1.5	1.5
8	Irrigated areas (plantations, fields, green areas, parks)	2.5	2.5	2.5	3.0	3.0	3.0	3.0	3.0	3.0	2.5	2.5	2.5
9	Wetlands, moist areas	3.0	3.0	3.5	4.0	4.0	4.0	3.5	3.5	3.5	3.0	3.0	3.0
10	Open water bodies	0.0											
11	Salt lake pans	1.0											
12	Settlements	1.2	1.2	1.5	1.5	1.5	1.5	1.5	1.5	1.5	1.5	1.2	1.2
13	Settlements (sealing >70%), aiports, highways	1.0											

Table A.7: Leaf Area Index [-].

No	Land cover class	Month											
		1	2	3	4	5	6	7	8	9	10	11	12
1	Coniferous forest	4.0	4.0	4.0	4.5	4.5	4.0	4.0	4.0	4.0	4.0	4.0	4.0
2	Deciduous forest	3.5	3.5	3.5	4.0	4.0	3.5	3.5	3.5	3.5	3.5	3.5	3.5
3	Scrubland, few higher trees (Maquis)	3.0	3.0	3.0	3.5	3.5	3.0	3.0	3.0	3.0	3.0	3.0	3.0
4	Low scrubland, grassland, fields (Garrigue)	2.0	2.0	2.5	2.5	2.0	2.0	2.0	2.0	2.0	2.0	2.0	
5	Sparse vegetation, rocks, boulders, bare soils							1.0					
6	Fields, fallow land	1.5	1.5	3.0	4.0	4.0	4.0	3.5	3.0	2.5	2.0	1.5	1.5
7	Vine yards	1.5	1.5	2.0	2.5	2.5	2.5	2.5	2.5	2.5	2.0	1.5	1.5
8	Irrigated areas (plantations, fields, green areas, parks)	2.0	2.0	2.5	3.5	3.5	3.5	3.5	3.5	3.0	3.0	2.0	2.0
9	Wetlands, moist areas	2.5	2.5	3.5	5.0	5.0	4.5	4.5	4.5	4.5	3.5	2.5	2.5
10	Open water bodies							0.0					
11	Salt lake pans							1.0					
12	Settlements	1.5	1.5	2.0	2.0	2.0	2.0	2.0	2.0	2.0	2.0	1.5	1.5
13	Settlements (sealing >70%), aiports, highways	1.5	1.5	2.0	2.0	2.0	2.0	2.0	2.0	2.0	2.0	1.5	1.5

Appendix B

Actual Water Balances

Table B.1: Mean annual precipitation for several periods and areas of Cyprus.

Parameter	Cyprus [mm]	Southern Cyprus [mm]	Troodos [mm]	Northern Cyprus [mm]
1961 - 1990				
Max. in the area	1197.8	1197.8	1197.8	912.8
Areal mean	472.1	511.8	667.0	396.3
Min. in the area	256.1	256.1	277.8	257.8
1971 - 2000				
Max. in the area	1117.7	1117.7	1117.7	859.0
Areal mean	445.0	478.1	617.6	381.8
Min. in the area	237.6	237.6	261.5	241.5
1961 - 2004				
Max. in the area	1170.7	1170.7	1170.7	901.8
Areal mean	468.1	504.1	654.1	399.3
Min. in the area	255.3	255.3	276.5	253.1

Table B.2: Means of daily maximum temperatures for several periods and areas of Cyprus.

Parameter	Cyprus [°C]	Southern Cyprus [°C]	Troodos [°C]	Northern Cyprus [°C]
1961 - 1990				
Max. in the area	26.2	26.0	25.3	26.2
Areal mean	23.6	23.1	20.9	24.4
Min. in the area	11.9	11.9	11.9	17.0
1971 - 2000				
Max. in the area	26.5	26.4	25.6	26.5
Areal mean	23.7	23.3	21.0	24.6
Min. in the area	12.0	12.0	12.0	17.0
1961 - 2004				
Max. in the area	26.4	26.3	25.6	26.4
Areal mean	23.7	23.3	21.1	24.6
Min. in the area	12.1	12.1	12.1	17.1

Table B.3: Mean annual temperatures for several periods and areas of Cyprus.

Parameter	Cyprus [°C]	Southern Cyprus [°C]	Troodos [°C]	Northern Cyprus [°C]
1961 - 1990				
Max. in the area	20.2	20.2	19.0	20.1
Areal mean	18.0	17.6	15.7	18.9
Min. in the area	8.6	8.6	8.6	13.9
1971 - 2000				
Max. in the area	20.4	20.4	19.1	20.4
Areal mean	18.2	17.7	15.8	19.1
Min. in the area	8.7	8.7	8.7	14.0
1961 - 2004				
Max. in the area	20.4	20.4	19.1	20.3
Areal mean	18.2	17.7	15.9	19.1
Min. in the area	8.7	8.7	8.7	14.0

Table B.4: Means of daily minimum temperatures for several periods and areas of Cyprus.

Parameter	Cyprus [°C]	Southern Cyprus [°C]	Troodos [°C]	Northern Cyprus [°C]
1961 - 1990				
Max. in the area	15.3	15.4	13.6	15.5
Areal mean	12.5	12.0	10.5	13.3
Min. in the area	5.1	5.1	5.1	10.4
1971 - 2000				
Max. in the area	15.8	15.6	13.8	16.0
Areal mean	12.7	12.2	10.6	13.6
Min. in the area	5.2	5.2	5.2	10.5
1961 - 2004				
Max. in the area	15.8	15.6	13.8	15.8
Areal mean	12.7	12.2	10.7	13.6
Min. in the area	5.3	5.3	5.3	10.5

Table B.5: Means of daily maximum rel. humidity for several periods and areas of Cyprus.

Parameter	Cyprus [%]	Southern Cyprus [%]	Troodos [%]	Northern Cyprus [%]
1961 - 1990				
Max. in the area	86.0	84.3	84.3	86.0
Areal mean	66.7	65.2	63.8	69.5
Min. in the area	50.0	50.0	50.4	61.5
1971 - 2000				
Max. in the area	85.7	84.8	84.8	85.7
Areal mean	66.7	64.9	63.6	70.1
Min. in the area	50.0	50.0	50.5	61.3
1961 - 2004				
Max. in the area	86.2	85.1	85.1	86.2
Areal mean	66.7	65.1	63.8	69.8
Min. in the area	50.1	50.1	50.6	61.3

Table B.6: Means of rel. humidity for several periods and areas of Cyprus.

Parameter	Cyprus [%]	Southern Cyprus [%]	Troodos [%]	Northern Cyprus [%]
1961 - 1990				
Max. in the area	81.3	79.4	79.4	81.3
Areal mean	59.8	58.8	58.2	61.7
Min. in the area	45.9	45.9	46.2	52.7
1971 - 2000				
Max. in the area	81.6	80.0	80.0	81.6
Areal mean	59.6	58.8	57.9	62.0
Min. in the area	45.8	45.8	46.0	51.9
1961 - 2004				
Max. in the area	81.8	80.1	80.1	81.8
Areal mean	59.7	58.6	58.2	61.9
Min. in the area	45.9	45.9	46.2	52.3

Table B.7: Means of daily minimum rel. humidity for several periods and areas of Cyprus.

Parameter	Cyprus [%]	Southern Cyprus [%]	Troodos [%]	Northern Cyprus [%]
1961 - 1990				
Max. in the area	76.5	74.4	74.4	76.5
Areal mean	52.9	52.4	52.5	53.8
Min. in the area	40.6	41.1	41.9	40.6
1971 - 2000				
Max. in the area	77.4	75.1	75.1	77.4
Areal mean	52.4	51.7	52.2	53.8
Min. in the area	39.4	39.9	41.5	39.4
1961 - 2004				
Max. in the area	77.3	75.1	75.1	77.3
Areal mean	52.7	52.1	52.5	53.9
Min. in the area	40.0	40.5	41.8	40.0

Table B.8: Mean rel. sunshine duration for several periods and areas of Cyprus.

Parameter	Cyprus [%]	Southern Cyprus [%]	Troodos [%]	Northern Cyprus [%]
1961 - 1990				
Max. in the area	*	74.4	71.6	*
Areal mean	*	68.5	65.2	*
Min. in the area	*	60.5	60.5	*
1971 - 2000				
Max. in the area	*	75.6	72.8	*
Areal mean	*	69.4	65.8	*
Min. in the area	*	60.5	60.5	*
1961 - 2004				
Max. in the area	*	75.1	72.4	*
Areal mean	*	69.1	65.7	*
Min. in the area	*	60.6	60.6	*

* = no value because of lack of data for Northern Cyprus

Table B.9: Mean actual evapotranspiration (incl. ET_{sec})for several periods and areas of Cyprus.

Parameter	Cyprus [mm]	Southern Cyprus [mm]	Troodos [mm]	Northern Cyprus [mm]
1961 - 1990				
Max. in the area	1681.8	1681.8	1671.8	1635.0
Areal mean	439.2	465.4	563.8	389.2
Min. in the area	172.1	172.1	267.0	176.7
1971 - 2000				
Max. in the area	1696.8	1696.8	1696.8	1660.8
Areal mean	427.9	454.1	545.5	377.6
Min. in the area	169.3	169.3	188.6	174.7
1961 - 2004				
Max. in the area	1698.7	1698.7	1687.8	1656.4
Areal mean	438.2	464.5	557.8	388.0
Min. in the area	173.9	173.9	263.5	178.7

Table B.10: Mean secondary evapotranspiration for several periods and areas of Cyprus.

Parameter	Cyprus [mm]	Southern Cyprus [mm]	Troodos [mm]	Northern Cyprus [mm]
1961 - 1990				
Max. in the area	1271.0	1271.0	1222.7	1256.6
Areal mean	41.8	47.6	50.7	30.8
Min. in the area	0	0	0	0
1971 - 2000				
Max. in the area	1307.8	1307.8	1271.7	1301.5
Areal mean	43.4	49.7	53.2	31.5
Min. in the area	0	0	0	0
1961 - 2004				
Max. in the area	1288.8	1288.8	1241.4	1276.2
Areal mean	42.6	48.6	51.8	31.0
Min. in the area	0	0	0	0

Table B.11: Mean annual direct runoff for several periods and areas of Cyprus.

Parameter	Cyprus [mm]	Southern Cyprus [mm]	Troodos [mm]	Northern Cyprus [mm]
1961 - 1990				
Max. in the area	812.2	812.2	745.7	648.0
Areal mean	27.1	33.9	48.1	14.1
Min. in the area	0	0	0	0
1971 - 2000				
Max. in the area	728.7	728.7	670.6	612.3
Areal mean	21.7	26.2	36.5	13.3
Min. in the area	0	0	0	0
1961 - 2004				
Max. in the area	775.4	775.4	719.3	646.8
Areal mean	26.5	32.2	45.8	15.7
Min. in the area	0	0	0	0

Table B.12: Mean annual groundwater recharge for several periods and areas of Cyprus.

Parameter	Cyprus [mm]	Southern Cyprus [mm]	Troodos [mm]	Northern Cyprus [mm]
1961 - 1990				
Max. in the area	522.0	522.0	522.0	350.3
Areal mean	47.6	60.1	105.8	23.8
Min. in the area	0	0	0	0
1971 - 2000				
Max. in the area	439.3	439.3	439.3	320.5
Areal mean	39.6	48.7	87.1	22.3
Min. in the area	0	0	0	0
1961 - 2004				
Max. in the area	495.4	495.4	495.4	340.5
Areal mean	46.6	57.4	101.5	26.1
Min. in the area	0	0	0	0

Table B.13: Water balances for several periods and areas of Cyprus.

Parameter	Cyprus [mm]	Southern Cyprus [mm]	Troodos [mm]	Northern Cyprus [mm]
1961 - 1990				
Annual precipitation	472.1	511.8	667.0	396.3
Actual evapotransp. (excl. ET_{sec})	397.4	417.8	513.1	358.4
Secondary evapotransp.	41.8	47.6	50.7	30.8
Actual evapotransp. (incl. ET_{sec})	439.2	465.4	563.8	389.2
Direct runoff	27.1	33.9	48.1	14.1
Groundwater recharge	47.6	60.1	105.8	23.8
1971 - 2000				
Annual precipitation	445.0	478.1	617.6	381.8
Actual evapotransp. (excl. ET_{sec})	384.5	404.4	492.3	346.1
Secondary evapotransp.	43.4	49.7	53.2	31.5
Actual evapotransp. (incl. ET_{sec})	427.9	454.1	545.5	377.6
Direct runoff	21.7	26.2	36.5	13.3
Groundwater recharge	39.6	48.7	87.1	22.3
1961 - 2004				
Annual precipitation	468.1	504.1	654.1	399.3
Actual evapotransp. (excl. ET_{sec})	395.0	414.5	506.8	357.2
Secondary evapotransp.	42.6	48.6	51.8	31.0
Actual evapotransp. (incl. ET_{sec})	437.6	463.1	558.6	388.5
Direct runoff	26.5	32.2	45.8	15.7
Groundwater recharge	46.6	57.4	101.5	26.1

Appendix C

Water Balance Scenarios

Table C.1: Scenario for the mean annual water balance under a theoretical precipitation decrease of 5%. Simulation based on the reference period 1971-2000.

Parameter	Cyprus	Southern Cyprus	Troodos	Northern Cyprus
Precipitation				
P change [%]	−5.0	−5.0	−5.0	−5.0
Actual evapotranspiration				
ET_{act} (excl. ET_{sec}) change [%]	−3.6	−4.1	−3.2	−3.9
ET_{sec} change [%]	+1.8	+1.6	+1.9	+1.6
ET_{act} (incl. ET_{sec}) change [%]	−3.1	−3.4	−2.7	−3.4
Direct runoff				
DRO change [%]	−15.2	−14.5	−13.8	−17.2
Groundwater recharge				
GWR change [%]	−10.7	−10.3	−9.5	−12.7

Table C.2: Scenario for the mean annual water balance under a theoretical precipitation decrease of 10%. Simulation based on the reference period 1971-2000.

Parameter	Cyprus	Southern Cyprus	Troodos	Northern Cyprus
Precipitation				
P change [%]	−10.0	−10.0	−10.0	−10.0
Actual evapotranspiration				
ET_{act} (excl. ET_{sec}) change [%]	−7.5	−7.3	−6.6	−8.0
ET_{sec} change [%]	+3.4	+3.3	+4.3	+3.2
ET_{act} (incl. ET_{sec}) change [%]	−6.3	−6.1	−5.6	−7.0
Direct runoff				
DRO change [%]	−28.5	−27.4	−26.3	−31.8
Groundwater recharge				
GWR change [%]	−20.9	−20.0	−18.5	−24.3

Table C.3: Scenario for the mean annual water balance under a theoretical precipitation decrease of 20%. Simulation based on the reference period 1971-2000.

Parameter	Cyprus	Southern Cyprus	Troodos	Northern Cyprus
Precipitation				
P change [%]	−20.0	−20.0	−20.0	−20.0
Actual evapotranspiration				
ET_{act} (excl. ET_{sec}) change [%]	−15.8	−15.4	−14.1	−16.7
ET_{sec} change [%]	+7.0	+7.1	+9.1	+6.1
ET_{act} (incl. ET_{sec}) change [%]	−13.4	−12.8	−11.8	−14.8
Direct runoff				
DRO change [%]	−50.0	−48.7	−47.5	−55.0
Groundwater recharge				
GWR change [%]	−38.8	−37.6	−35.3	−44.2

Table C.4: Scenario for the mean annual water balance under a theoretical precipitation decrease of 30%. Simulation based on the reference period 1971-2000.

Parameter	Cyprus	Southern Cyprus	Troodos	Northern Cyprus
Precipitation				
P change [%]	−30.0	−30.0	−30.0	−30.0
Actual evapotranspiration				
ET_{act} (excl. ET_{sec}) change [%]	−24.9	−24.3	−22.6	−26.1
ET_{sec} change [%]	+10.9	+11.0	+14.5	+10.8
ET_{act} (incl. ET_{sec}) change [%]	−21.2	−20.3	−19.0	−23.1
Direct runoff				
DRO change [%]	−65.2	−64.5	−63.1	−70.2
Groundwater recharge				
GWR change [%]	−53.5	−52.3	−50.0	−58.9

Table C.5: Scenario for the mean annual water balance under a theoretical air temperature rise of +1 K (without adjustment of relative humidity) based on the reference period 1971-2000.

Parameter	Cyprus	Southern Cyprus	Troodos	Northern Cyprus
Precipitation				
P change [%]	–	–	–	–
Actual evapotranspiration				
ET_{act} (excl. ET_{sec}) change [%]	+0.5	+0.4	+0.8	+0.4
ET_{sec} change [%]	+5.0	+5.0	+5.6	+4.8
ET_{act} (incl. ET_{sec}) change [%]	+1.0	+0.9	+1.2	+0.8
Direct runoff				
DRO change [%]	−3.1	−2.6	−2.1	−3.3
Groundwater recharge				
GWR change [%]	−2.8	−2.7	−2.8	−3.2

Table C.6: Scenario for the mean annual water balance under a theoretical air temperature rise of +1 K (with mean adjustment of relative humidity according to Fig. 6.1) based on the reference period 1971-2000.

Parameter	Cyprus	Southern Cyprus	Troodos	Northern Cyprus
Precipitation				
P change [%]	–	–	–	–
Actual evapotranspiration				
ET_{act} (excl. ET_{sec}) change [%]	+0.7	+0.8	+1.0	+1.0
ET_{sec} change [%]	+5.9	+5.9	+6.8	+5.7
ET_{act} (incl. ET_{sec}) change [%]	+1.2	+1.3	+1.6	+1.0
Direct runoff				
DRO change [%]	−3.9	−3.5	−3.3	−4.6
Groundwater recharge				
GWR change [%]	−3.7	−3.6	−3.6	−4.0

Table C.7: Scenario for the mean annual water balance under a theoretical air temperature rise of +1 K (with full adjustment of relative humidity [closed system]) based on the reference period 1971-2000.

Parameter	Cyprus	Southern Cyprus	Troodos	Northern Cyprus
Precipitation				
P change [%]	–	–	–	–
Actual evapotranspiration				
ET_{act} (excl. ET_{sec}) change [%]	+1.6	+1.7	+2.5	+1.4
ET_{sec} change [%]	+10.0	+9.6	+10.1	+10.5
ET_{act} (incl. ET_{sec}) change [%]	+2.5	+2.6	+3.4	+2.1
Direct runoff				
DRO change [%]	−9.8	−9.0	−9.2	−13.2
Groundwater recharge				
GWR change [%]	−8.4	−7.8	−8.1	−10.8

Table C.8: Scenario for the mean annual water balance under a theoretical air temperature rise of +2 K (without adjustment of relative humidity) based on the reference period 1971-2000.

Parameter	Cyprus	Southern Cyprus	Troodos	Northern Cyprus
Precipitation				
P change [%]	–	–	–	–
Actual evapotranspiration				
ET_{act} (excl. ET_{sec}) change [%]	+1.0	+1.1	+1.5	+0.8
ET_{sec} change [%]	+10.0	+9.8	+11.3	+9.6
ET_{act} (incl. ET_{sec}) change [%]	+1.9	+2.1	+2.4	+1.5
Direct runoff				
DRO change [%]	−5.9	−5.5	−4.6	−7.3
Groundwater recharge				
GWR change [%]	−5.3	−5.2	−5.2	−6.0

Table C.9: Scenario for the mean annual water balance under a theoretical air temperature rise of +2 K (with mean adjustment of relative humidity according to Fig. 6.1) based on the reference period 1971-2000.

Parameter	Cyprus	Southern Cyprus	Troodos	Northern Cyprus
Precipitation				
P change [%]	–	–	–	–
Actual evapotranspiration				
ET_{act} (excl. ET_{sec}) change [%]	+1.3	+1.5	+2.0	+0.9
ET_{sec} change [%]	+12.0	+12.0	+14.0	+11.8
ET_{act} (incl. ET_{sec}) change [%]	+2.4	+2.7	+3.2	+1.8
Direct runoff				
DRO change [%]	−7.8	−7.4	−6.7	−9.3
Groundwater recharge				
GWR change [%]	−7.0	−6.7	−6.8	−7.2

Table C.10: Scenario for the mean annual water balance under a theoretical air temperature rise of +2 K (with full adjustment of relative humidity [closed system]) based on the reference period 1971-2000.

Parameter	Cyprus	Southern Cyprus	Troodos	Northern Cyprus
Precipitation				
P change [%]	–	–	–	–
Actual evapotranspiration				
ET_{act} (excl. ET_{sec}) change [%]	+3.0	+3.2	+4.7	+2.5
ET_{sec} change [%]	+19.9	+19.4	+22.7	+20.7
ET_{act} (incl. ET_{sec}) change [%]	+4.8	+4.8	+6.5	+4.0
Direct runoff				
DRO change [%]	−18.4	−16.8	−17.7	−23.8
Groundwater recharge				
GWR change [%]	−15.1	−14.1	−14.8	−19.5

Table C.11: Scenario for the mean annual water balance under a theoretical air temperature rise of +3 K (without adjustment of relative humidity) based on the reference period 1971-2000.

Parameter	Cyprus	Southern Cyprus	Troodos	Northern Cyprus
Precipitation				
P change [%]	–	–	–	–
Actual evapotranspiration				
ET_{act} (excl. ET_{sec}) change [%]	+1.5	+1.6	+2.2	+1.1
ET_{sec} change [%]	+14.9	+14.9	+17.1	+14.3
ET_{act} (incl. ET_{sec}) change [%]	+2.9	+3.1	+3.6	+2.2
Direct runoff				
DRO change [%]	−8.6	−8.1	−7.3	−9.9
Groundwater recharge				
GWR change [%]	−7.7	−7.4	−7.4	−8.4

Table C.12: Scenario for the mean annual water balance under a theoretical air temperature rise of +3 K (with mean adjustment of relative humidity according to Fig. 6.1) based on the reference period 1971-2000.

Parameter	Cyprus	Southern Cyprus	Troodos	Northern Cyprus
Precipitation				
P change [%]	–	–	–	–
Actual evapotranspiration				
ET_{act} (excl. ET_{sec}) change [%]	+1.9	+2.1	+2.9	+1.5
ET_{sec} change [%]	+18.3	+18.2	+21.7	+17.8
ET_{act} (incl. ET_{sec}) change [%]	+3.7	+4.0	+4.7	+2.8
Direct runoff				
DRO change [%]	−11.7	−11.0	−10.4	−13.9
Groundwater recharge				
GWR change [%]	−10.0	−9.5	−9.6	−11.6

Table C.13: Scenario for the mean annual water balance under a theoretical air temperature rise of +3 K (with full adjustment of relative humidity [closed system]) based on the reference period 1971-2000.

Parameter	Cyprus	Southern Cyprus	Troodos	Northern Cyprus
Precipitation				
P change [%]	–	–	–	–
Actual evapotranspiration				
ET_{act} (excl. ET_{sec}) change [%]	+4.1	+4.4	+6.5	+3.3
ET_{sec} change [%]	+29.9	+29.2	+34.5	+31.2
ET_{act} (incl. ET_{sec}) change [%]	+6.8	+7.2	+9.2	+5.7
Direct runoff				
DRO change [%]	−25.4	−23.5	−25.0	−31.7
Groundwater recharge				
GWR change [%]	−20.5	−19.1	−20.1	−25.9

Eidesstattliche Erklärung

Hiermit erkläre ich, dass ich die vorliegende Dissertation selbständig angefertigt und keine anderen als die angegebenen Quellen und Hilfsmittel benutzt habe.

Armin Dünkeloh